This electronic thesis or dissertation has been downloaded from the King's Research Portal at https://kclpure.kcl.ac.uk/portal/

Non-apical progenitors in the embryonic zebrafish neural tube Characterising their origin and spatial distribution

McIntosh, Rebecca Louise Lord

Awarding institution:
King's College London

The copyright of this thesis rests with the author and no quotation from it or information derived from it may be published without proper acknowledgement.

END USER LICENCE AGREEMENT

This work is licensed under a Creative Commons Attribution-NonCommercial-NoDerivatives 4.0 International licence. https://creativecommons.org/licenses/by-nc-nd/4.0/

You are free to:

- Share: to copy, distribute and transmit the work

Under the following conditions:

- Attribution: You must attribute the work in the manner specified by the author (but not in any way that suggests that they endorse you or your use of the work).
- Non Commercial: You may not use this work for commercial purposes.
- No Derivative Works - You may not alter, transform, or build upon this work.

Any of these conditions can be waived if you receive permission from the author. Your fair dealings and other rights are in no way affected by the above.

Take down policy

If you believe that this document breaches copyright please contact librarypure@kcl.ac.uk providing details, and we will remove access to the work immediately and investigate your claim.

Download date: 06. Nov. 2017

Non-apical progenitors in the embryonic zebrafish neural tube

Characterising their origin and spatial distribution

Rebecca Louise Lord McIntosh

Submitted for the degree of PhD
August 2016
King's College London

TABLE OF CONTENTS

TABLE OF FIGURES

TABLE OF TABLES

TABLE OF MOVIES

ACKNOWLEDGEMENTS

First and foremost I would like to thank my supervisors, Prof Jon Clarke and Dr Paula Alexandre, for giving me the opportunity to carry out my PhD as a collaboration between their labs. Thank you both for your patience, encouragement and advice. I am extremely grateful for everything you have taught me over the past three and a half years.

Next, to the wonderful members of the Clarke lab: Andy Symonds, Rachel Moore, Chris Rookyard, Vineetha Vijakumar, Claire Bromley, Sean Hourihane, Klairy Arkoudi, Charlie Williams, Laura Ward, and Clare Buckley. The continual supply of (excellent) baked goods, crosswords and punny jokes made working on this project a joy. On top of all that, you are always available for a question or a favour. I am very grateful to you all.

I would also like to thank my colleagues at both the MRC Centre for Developmental Neurobiology, KCL and the Developmental Biology of Birth Defects unit, UCL-ICH, for their help and advice. I'd particularly like to thank Tiago Martins, Anna Janue, Jordana Peake, Paul Hunter, Dale Moulding, Andrew Lowe, Matteo Mole and Zena Hadjivasiliou.

Thanks to Oli for providing distractions, entertainment and moral support – the 'novel' is finally finished!

Finally, to Mom, John and Steph, I would not have been able to complete this thesis without your endless encouragement and support. Thank you.

ABSTRACT

Non-apical neuronal progenitors divide at a distance from the ventricle and are thought to be responsible for the expansion of the cerebral cortex during mammalian evolution. Non-apical progenitors are also present in non-cortical regions and non-mammalian species, but their function in these regions is less well understood. Non-apical progenitors have not been widely studied in zebrafish. The aim of this thesis is to characterize non-apical neuronal progenitors during zebrafish embryonic development and investigate the mechanisms regulating their generation and distribution.

We have identified a varied population of non-apical divisions using immunohistochemical analysis of mitotic cells throughout early zebrafish development. In the spinal cord, non-apical divisions appear to be highly spatially restricted and express either *vsx1* or *olig2*. In the hindbrain, these non-apical divisions are seen in different spatial compartments and the majority express *vsx1*. We have also observed a small number of non-apical divisions in the telencephalon, the analogous structure to the mammalian cortex, although coexpression with *vsx1* in this region is rare. Therefore, similar to mammalian brains, our data shows that diverse subpopulations of non-apical neuronal progenitors are generated during zebrafish embryonic development. Our data also suggest that non-apical progenitors share features of their differentiation with neurons; they express the early neuronal marker HuC/D, they require aPKC to differentiate (Alexandre et al. 2010) and are regulated by Notch signalling. These findings might provide insights into the evolution of non-apical progenitors in the zebrafish neural tube as well as mammalian species.

To further understand the development of *vsx1* non-apical progenitors I carried out a time-lapse analysis of neuronal differentiation in the Tg(*vsx1*:GFP) line. This revealed that initial *vsx1* progenitors appear in a long-distance spacing pattern and subsequent *vsx1* progenitors differentiate in the intervening space. This pattern forms independently of mesoderm-derived signals. By quantifying the spatiotemporal dynamics of this pattern as it forms, I found that two progenitors are unlikely to differentiate close in time and space. High-resolution imaging of non-apical progenitors during the differentiation process revealed that they extend transient processes along the basal surface (basal arms) that retract before division. We propose that these transient basal arms deliver long-distance inhibitory signals to self-organise the differentiation of *vsx1* progenitors, similar to a mechanism known to pattern neuronal cells in *Drosophila* (Cohen et al. 2010; De Joussineau et al. 2003). I have tested and refined this hypothesis by generating a simple model using quantitative data regarding the pattern formation and the dynamics of basal arms. These data provide the first detailed insight into spatiotemporal dynamics of neurogenesis in the zebrafish spinal cord.

CHAPTER 1
GENERAL INTRODUCTION

1 General Introduction

Diverse populations of neural progenitors give rise to the vertebrate brain. These progenitors can vary in terms of their proliferative and neurogenic capacities as well as the neuronal types that they generate. Therefore, the behaviour and daughter cell fate of neural progenitors has to be tightly controlled to regulate brain growth and development. In the vertebrate neural tube, the primary location of neurogenesis is the ventricular, or apical, surface. However, in the developing mammalian cortex progenitors that divide at a distance from the apical surface (referred to in the literature as basal progenitors, but in this thesis as non-apical progenitors) are common and are thought to play a key role in the evolutionary expansion of the forebrain. Non-apical progenitors are found in non-mammalian and non-cortical regions, although in smaller numbers, and the role of these cells here is less well understood. In this thesis, I have studied the distribution and regulation of non-apical progenitors during embryonic neurogenesis in the teleost model organism, *Danio rerio* (zebrafish).

In this chapter, I give an overview of the current knowledge of the contribution of different subtypes of neuronal progenitors to neurogenesis and how the production of neuronal progenitors is regulated in time and space. This review focuses on the neurogenesis in the mammalian cortex and zebrafish neural tube.

1.1 Early brain development

1.1.1 Neural induction

The vertebrate central nervous system arises from the neuroectoderm, which is specified from the ectodermal layer from the beginning of gastrulation by BMP antagonists, including Noggin, Follistatin and Chordin (reviewed in Stern 2005, Gaspard & Vanderhaeghen 2010 and Schmidt et al. 2013). These molecules are secreted by the dorsal lip of the blastopore, called Spemann's organiser in *Xenopus* (reviewed in Streit & Stern 1999; Stern 2005), Hensen's node in birds and mammals (Anderson et al. 2002) and the shield organiser in zebrafish and other teleosts (Oppenheimer 1936; Shih & Fraser 1996; Saúde et al. 2000). This process of specifying neural tissue by the inhibition of BMP signalling is referred to as the default model of neural induction (**Figure 1-1**A and B). Spemann's organiser is sufficient to induce the whole neuraxis n *Xenopus*, however in mammals, birds and zebrafish neural induction by BMP inhibition only generates primitive neural tissue with rostral characteristics (Stern 2005; Gaspard & Vanderhaeghen 2010). The mechanisms that act to induce posterior identity in the tissue are less well understood but roles have been suggested for retinoic acid (RA), FGF, TGF-β and Wnt signalling (Kim et al. 2000; Kiecker & Niehrs 2001; Houart et al. 2002; Kudoh et al. 2002;

Nordström et al. 2002; Dorsky 2003; Ciani & Salinas 2005; Price et al. 2011). The signalling molecules involved in these pathways are expressed in caudal regions and rostral tissue identities are protected by expression of antagonists (Bouwmeester et al. 1996; Piccolo et al. 1999; Kiecker & Niehrs 2001; Houart et al. 2002; Diez del Corral & Storey 2004; Hernandez et al. 2007; Schmidt et al. 2013). Therefore, the complex interaction between a number of signalling pathways is required to 'induce' the pre-neuronal tissue. Similar conditions can be used to generate the full range of neuronal stem cells *in vitro* (reviewed in Gaspard & Vanderhaeghen 2010).

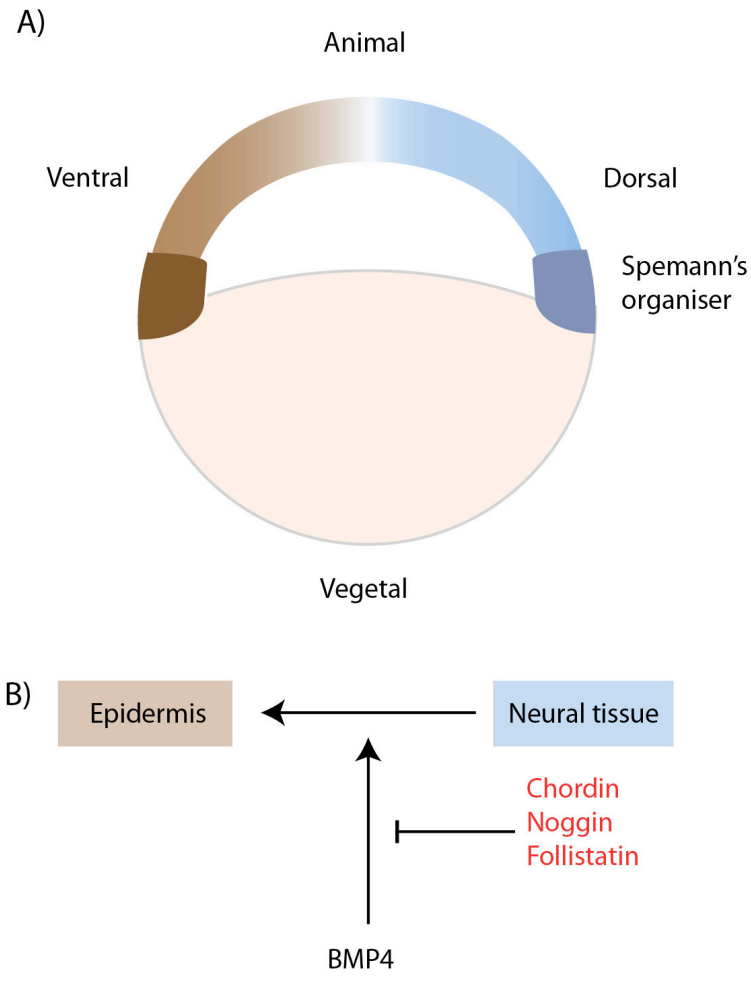

Figure 1-1: Neural induction: The default model. **A**) A blastula stage Xenopus embryo showing Spemann's' organiser, and the prospective neural tissue (blue) and epidermis (brown). The yolky endoderm is shown in beige. **B**) The genetic interactions proposed by the model. Ectodermal cells have an autonomous tendency to differentiate into neural tissue, but are inhibited from doing so by BMP4 and are specified as epidermis instead. The organiser secretes BMP antagonists (red), which allow cells to develop according to their 'default' fate. (Adapted from: Stern 2005; Streit & Stern 1999.)

1.1.2 Neurulation in amniotes and teleosts

After the process of specifying the neural plate (a dorsal epithelial sheet that forms the neural primordium) the neuroepithelial tissue undergoes drastic morphological changes. In the majority of vertebrates, the neural plate undergoes neurulation in one of two ways to form a neural tube. Primary neurulation involves the lateral edges of the neural plate folding to fuse dorsally, sometimes via one or more hinge points (Copp & Greene 2009). In secondary neurulation, a mesenchymal population first forms a solid rod of cells that then cavitates to form a neural tube.

Teleost neurulation occurs via an independent process (reviewed in Lowery & Sive 2004). First, the neural plate condenses medially and sinks into the embryo to form the neural keel. The neuroepithelial cells then interdigitate across the midline forming a solid neural rod and establish mirror-symmetric microtubule network about the plane of the presumptive midline (Buckley et al. 2013). Apicobasal polarity is obvious at neural plate stages in avian and mammalian embryos however, in the zebrafish neural tube apicobasal polarity is not established until late neural rod stages, (Buckley et al. 2013; Geldmacher-Voss et al. 2003). The cells in the neural rod then undergo a midline crossing division (C-division) during which apical polarity proteins accumulate at the presumptive midline (Tawk et al. 2007; Geldmacher-Voss et al. 2003; Papan & Campos-Ortega 1994; Buckley & Clarke 2014). This generates a polarised tissue with daughters from C-divisions connected at the apical surface and stretching to contact both basal sides of the tube (Clarke 2009; Buckley et al. 2013). C-divisions are involved in instructing the location of the midline and have been shown to increase the efficiency of lumen opening, but are not required for the development of apicobasal polarity in the tissue (Buckley et al. 2013; Buckley & Clarke 2014). Instead, signalling from extracellular matrix components of the basal lamina is thought to direct the polarisation of cells within the neural rod (Buckley et al. 2013; L. Ward et al, in preparation).

In both amniotes and teleosts, these morphological events result in a tube structure composed of a single layer of epithelial cells (neural tube).

1.1.3 Patterning the dorsoventral axis of the neural tube

The suite of signalling molecules that induce the full neuraxis (i.e. RA, FGF, TGF-β and Wnt) are also involved in regionalisation of the neural tube along the anteroposterior axis (reviewed in Kiecker & Lumsden 2005). The most relevant patterning event for this thesis is how the progenitor domains of the ventral spinal cord are established. The ventral progenitor domains (p3, pMN, p0, p1 and p2, from ventral to dorsal; **Figure 1-2**C) predominantly give rise to the motor and proprioceptive circuitry of the vertebrate spinal cord (Jessell 2000). These domains

are induced and patterned by graded sonic hedgehog (Shh) signals originating from the notochord and floor plate (**Figure 1-2**B; reviewed in Jessell 2000; Wilson & Maden 2005; Briscoe & Thérond 2013). Two classes of transcription factors are activated in response to Shh signals: (1) the expression of Class I (Pax6, Irx3, Dbx1 and Dbx2) genes is repressed by specific levels of Shh activity; while (2) the expression of Class II genes (Nkx6, Nkx2.2) is activated at specific Shh signalling levels (**Figure 1-2**A). Cross repression between Class I and Class II genes generates a transcriptional code that then specifies postmitotic cell types in discrete dorsoventral domains of the spinal cord (**Figure 1-2**D; reviewed in Jessell 2000; Wilson & Maden 2005). The final identity of the neuronal cell types generated within a domain is further refined by intercellular signalling (Jessell 2000; Le Dréau & Martí 2012).

There is data from across vertebrate species that suggests Shh signalling alone is insufficient to induce the whole range of ventral progenitor domains (Litingtung & Chiang 2000; Persson et al. 2002; Novitch et al. 2003; Diez del Corral & Storey 2004; Wilson & Maden 2005; England et al. 2011). RA and Wnt signalling have been implicated in generating this pattern (reviewed in Ciani & Salinas 2005), however additional signalling mechanisms might also be required to

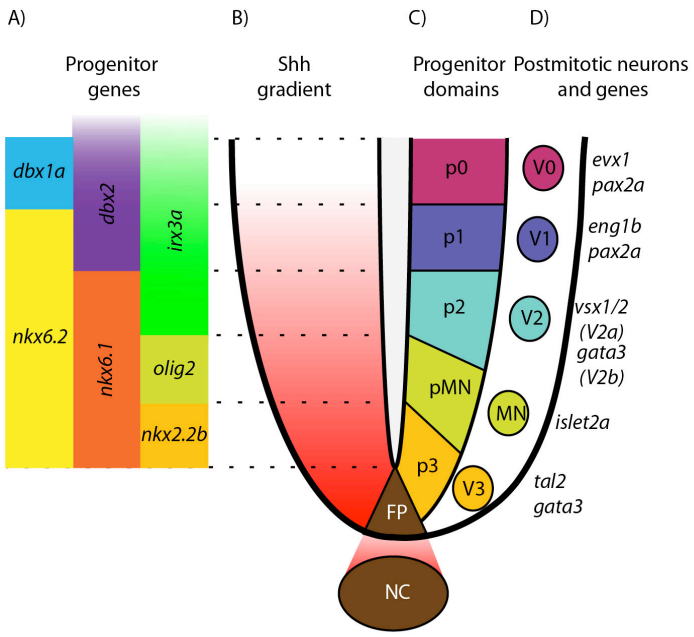

Figure 1-2: Patterning the ventral spinal cord. Schematic of a transverse section of the zebrafish ventral spinal cord. The notochord (NC) and floor plate (FP) generate a gradient of sonic hedgehog (Shh; shown in red; **B**). A number of genes are induced at different points along this gradient (**A**). These genes form a code that specifies the ventral progenitor domains (p0-1, pMN and p3; **C**). The individual progenitor domains each give rise to a specific population of neurons that express unique combinations of post-mitotic genes (**D**; Adapted from: Ribes & Briscoe 2009; England et al. 2011).

form this pattern. Currently, a key question in this field is how the concentration and duration of Shh signalling can be quantitatively converted into transcriptional changes and the production of different progenitor domains (Balaskas et al. 2012; Cohen et al. 2014; Briscoe & Thérond 2013; Cohen et al. 2013).

1.2 Neural progenitors

The process of neural induction specifies neuroepithelial cells (NE cells), which are the neural progenitor cells that generate all of the neuronal and glial cell types that form the adult nervous system. NE cells need to strike a balance between the generation of newborn neurons and the maintenance of the progenitor population so that the appropriate numbers of neurons are produced and growth can be regulated.

In order to balance the opposing need for growth and differentiation progenitors utilize different modes of division to produce different combinations of differentiating and proliferating daughter cells types. The first mode of division is symmetric division in which progenitors generate equivalent daughters. Symmetric proliferative divisions, where both the daughters are progenitors (p – p; **Figure 1-3**A), are a mechanism for rapid growth, as they expand the progenitor population. Symmetric terminal divisions produce two differentiated daughters (n – n; **Figure 1-3**B) and provide a fast way to increase neuronal production. An alternate mode of division is canonical asymmetric division, where the progenitor divides to regenerate itself and produce a differentiated daughter (n – p; **Figure 1-3**), thereby maintaining the progenitor population while allowing neurogenesis. Finally, neural progenitors that are able to generate two progenitors with different fates (e.g. one self-renewing progenitor and one neuron-producing progenitor) produce an increased number of neurons with each apical progenitor division (**Figure 1-3**D). It is likely that the regulation of growth and differentiation is region and species specific.

The majority of our understanding of vertebrate neurogenesis comes from studies of the mammalian neocortex, particularly rats, mice and ferrets (revieved in Paridaen & Huttner 2014), although recent studies have used macaque and human tissue (Hansen et al. 2010; Fietz et al. 2010; Betizeau et al. 2013; Florio et al. 2015; Johnson et al. 2015). Mammalian evolution has caused a disproportionate increase in the size of cortical regions (neocorticalisation; Florio & Huttner 2014), culminating in humans where the neocortex represents 80% of the brain's mass (Stephan et al. 1981; Azevedo et al. 2009). The neocortex is a six-layered structure that forms the cerebral hemispheres in mammals and has expanded radially from a three layered structure seen in reptiles (**Figure 1-4**; Tarabykin et al. 2001; Martínez-Cerdeño et al. 2006). The cortex of mammalian species show one of two gross structures: A) smooth, or lissencephalic, cortex

which is seen in rodents; or B) folded, or gyrencephalic, cortex seen in primates and ferrets. The generation of gyri, or folded bulges, increases the surface area of the cortex allowing increased numbers of neurons to be accommodated within the tissue, thereby increasing the processing power of this region of the brain (Fietz & Huttner 2011; Lui et al. 2011; Kelava et al. 2013; reviewed in Borrell & Götz 2014). Gyrification is thought to be genetically encoded as the gyrification pattern is stable between individuals and because gyrification pattern disorders exist (Kelava et al. 2013).

The laminar structure of the neocortex develops in an inside-out manner, where early-born neurons form the deep cortical layers (VI-IV) and late-born neurons migrate through the deep layers to form the superficial laminae (layers III-I; Götz & Huttner 2005; Molyneaux et al. 2007; Dehay & Kennedy 2007; Leone et al. 2008). Evidence suggests that mammalian neuronal progenitors change competency through time to specify neurons destined for each layer (Desai & McConnell 2000; Shen et al. 2006). This temporal pattern of neuronal subtype birth and their self-organisation into layers has also been shown *in vitro* (reviewed in Gaspard & Vanderhaeghen 2010; Gaspard et al. 2008; Eiraku et al. 2008; Lancaster et al. 2013), however a bias exists towards the production of pyramidal cells with a deep layer identity (Gaspard et al. 2008; Eiraku et al. 2008). This suggests that some aspects of cortical cytoarchitecture can be specified *in vitro*, however this 'brain in a dish' environment is missing cues involved in regulating the balance of cell types produced (reviewed in Gaspard & Vanderhaeghen 2010).

In this region a number of different subgroups of neural progenitors have been characterised based on their morphology, location of mitosis, behaviour, neurogenic potential and expression profile (**Figure 1-3**E and **Table 1-1**; reviewed in Borrell & Götz 2014; Florio & Huttner 2014)[1]. How these different populations are generated and how they contribute to neurogenesis and the regulation of tissue size and shape is outlined here.

1.2.1 Apical progenitors

The region of the neural tube adjacent to the ventricle is the canonical location of vertebrate neurogenesis. This apical proliferative zone, or ventricular zone (VZ), is initially populated by a single layer of neuroepithelial cells (NE cells; **Figure 1-3**E and **Table 1-1**). NE cells are a polarised cell type with thin radial processes extending to the apical and pial (basal) surfaces of the neural tube (**Figure 1-3**E). The apical process of NE cells contacts the ventricle lumen via their 'apical footprint', which is the site of accumulation of apical proteins like the Par complex

[1] The nomenclature used to describe different populations of neural progenitors in vertebrates is currently a matter of debate and is complicated by the growing knowledge of these cells (Martínez-Cerdeño & Noctor 2016). In this thesis, I will use the terms from a recent review from the lab of Weiland Huttner (Florio & Huttner 2014) to describe different types of mammalian neural progenitors.

(Par-3, Par6 and αPKC), prominin-1 (CD133), ZO-1 as well as adherens and tight junctions (Alexandre et al. 2010; and reviewed in Wodarz & Huttner 2003). The basal process extends to the basal lamina, which contains extracellular matrix components including integrin α6, laminin and fibronectin (reviewed in Götz & Huttner 2005). *In vivo*, the basal processes of the apical progenitors maintain contact with the basal surface and extend as the cortical plate thickens. These long radial processes play an important role as scaffolding during radial migration of newborn neurons from the ventricular zone to the cortical plate (Poluch & Juliano 2007). In this axis, perpendicular to the ventricular surface, pyramidal cells and interneurons are stereotypically arranged into columns (Rakic 2008). Each column shares functional properties and are thought to form the computational units of the cortex (Per 2010). The neocortex is then subdivided into areas each with a functional specialization (e.g. motor cortex, visual cortex, etc.).

At the onset of neurogenesis NE cells convert to a related but more restricted cell type called apical radial glial (aRG) cells, which are able to divide asymmetrically to self-renew and generate differentiating daughter cells (**Figure 1-3**E and **Table 1-1**; reviewed in Götz & Huttner 2005; Kowalczyk et al. 2009). The neuronal daughter cell then migrates to the basal, or pial, surface to form the cortical plate (mantlezone) where they differentiate. One of the signals that regulates the transition from proliferative NE cells to neurogenic aRG cells is the expression of Fgf10 (Sahara & O'Leary 2009). aRG cells share many characteristics with NE cells, including apicobasal polarity and the expression of some markers. However, aRG cells also express Pax6 (Englund et al. 2005), GFAP (an astroglial marker) and show loss of apical proteins (reviewed in Götz & Huttner 2005). Collectively, NE cells and aRG cells are called apical progenitors (AP) as both cell types undergo mitosis at the apical surface. Apical progenitors also undergo interkinetic nuclear migration (INM) in time with their cell cycle (reviewed in Del Bene 2011). This asynchronous movement of cells within the epithelium gives the tissue a pseudostratified appearance (Taverna & Huttner 2010; Spear & Erickson 2012). Single cell gene expression profiling has shown that apical progenitor cells express genes involved in cell cycle regulation, DNA replication, extracellular matrix components and growth factor pathways critical for aRG cell maintenance, all 'stem cell' markers (Fietz et al. 2012; Johnson et al. 2015; Florio et al. 2015).

A number of studies suggest that the VZ contains two classes of apical progenitor; one that is biased towards proliferative divisions and the other biased towards differentiative divisions (Haubensak et al. 2004; Noctor et al. 2004; Pinto et al. 2008; Stahl et al. 2013). In mice, the expression of the transcription factors AP2γ and Trnp1 can be used to discriminate between these two populations, as AP2γ is highly expressed in aRGs that generate basal progenitors

(Pinto et al. 2008) and Trnp1 is enriched in self-amplifying AP (Stahl et al. 2013). Further studies are needed to fully understand the molecular control of the proliferative to neurogenic shift in the whole tissue and in single cells.

1.2.1.1 Apical intermediate progenitors and subapical progenitors

NE and aRG cells, as described above, represent the majority of the progenitors in the VZ of the embryonic cortex, however two minor populations of progenitors have also been described. The first population displays a truncated basal process terminating in the intermediate zone at mitosis (Gal et al. 2006; Kowalczyk et al. 2009; Tyler & Haydar 2013). These apical intermediate progenitors (aIPs; also referred to as short neuronal precursors; SNPs) downregulate astroglial markers, express the neuronal marker tubulin α-1 (Tα1; Gal et al. 2006), retract their basal process before division and undergo a single differentiating division (Gal et al. 2006; Stancik et al. 2010; Tyler & Haydar 2013). The other minor population maintains contact with the apical surface but divides away from it, in the VZ or SVZ (Pilz et al. 2013). These cells are referred to as subapical progenitors but much less is known about the cell biology and expression profile of this cell type (Florio & Huttner 2014). Subapical progenitors are relatively rare in the developing neocortex but represent a significant proportion of the mitotic cells in the ganglionic eminences (Pilz et al. 2013). The developmental role of these subtypes of apical progenitors is currently unknown.

1.2.1.2 Expansion of the apical progenitor pool and neocorticalisation

Rakic described the cortex as 'radial units' (Rakic 1995), where neurons generated from a single apical progenitor form an 'ontogenetic column' of radially aligned, clonally related cells (reviewed in Florio & Huttner 2014). According to his radial unit hypothesis, the number of units (or founder aRG cells) determines the surface area of the tissue while the number of neurons in each radial unit determines the thickness (Rakic 1995; reviewed by Götz & Huttner 2005 and Borrell & Götz 2014). Therefore, the size of the apical progenitor pool at the onset of neurogenesis and its neurogenic capacity both influence the final number of neurons in the cortex.

Control over the time of the onset of neurogenesis has been shown to be particularly important in controlling the size of the tissue in the brain. Premature differentiation of apical progenitors *in vitro* has been shown to lead to microcephaly (Lancaster et al. 2013). On the other hand, loss of Fgf10 in mouse embryos inhibits the NE to aRG cell switch, maintaining the proliferative apical progenitor pool (Sahara & O'Leary 2009). The cortex of these specimen show increased neuron and basal progenitor production as well as radial thickening of the tissue but these

specimen do not form gyri (Sahara & O'Leary 2009). It has also been shown that a human-accelerated regulatory enhancer (HARE) of Frizzled8 expands the apical progenitor population resulting in increased cortical area and neural density in mice (Lomax Boyd et al. 2015). Again, this larger cortex did not form any gyri.

Taken together these data show that the size of the apical progenitor pool is influential in controlling the final size of the cortex. However, increasing the number of neurons is insufficient to induce folding of the cortex. Furthermore, manipulations that expand the apical progenitor pool often also result in increased ventricular surface and increased ventricle size (Chenn & Walsh 2002; Lomax Boyd et al. 2015) which is not seen in mammalian evolution (Rakic 2009). This data suggest that there is a biological limit placed on the expansion of the apical progenitor pool. Therefore, alternative methods must exist to generate the increased numbers of neurons seen in mammalian evolution.

1.2.2 Basal progenitors

From early stages of neurogenesis the mammalian cortex contains two mitotically active zones (Smart 1973); the VZ, where apical progenitors are located, and the subventricular zone (SVZ) (Haubensak et al. 2004; reviewed in Götz & Huttner 2005 and Kriegstein et al. 2006). The SVZ has been shown to arise shortly after the formation of the VZ in the mammalian cortex (Haubensak et al. 2004; Martínez-Cerdeño et al. 2006) and can be morphologically distinguished from other layers from E13 in mice. The SVZ of gyrencephalic species is expanded along the apicobasal axis and can be split into the inner and outer SVZ (iSVZ and oSVZ, respectively). The SVZ contains mitotically active cells that can be distinguished from apical progenitors by the absence of apical processes at mitosis and, most importantly, division away from the ventricular surface (**Figure 1-3**E and **Table 1-1**). Progenitors that undergo mitosis at a distance from the apical surface are collectively known as basal progenitors in mammals.

The SVZ was originally thought to contribute solely to gliogenesis, however dividing basal progenitors in the SVZ have been shown to produce daughter cells with cortical neuronal identities (Tarabykin et al. 2001; Haubensak et al. 2004; Noctor et al. 2004; Attardo et al. 2008; Kowalczyk et al. 2009). These data confirmed that basal progenitors are cortical neuron progenitors during embryonic neurogenesis and further data has shown that by mid-stages of neurogenesis the SVZ has overtaken the VZ as the main source of newborn cortical neurons (Haubensak et al. 2004; Martínez-Cerdeño et al. 2006; Kowalczyk et al. 2009). Further investigation has identified two class of basal progenitor in the developing neocortex: basal intermediate neuronal progenitors and basal radial glia.

1.2.2.1 Basal intermediate neuronal progenitors

Basal intermediate neuronal progenitors (bIP) were first identified in the SVZ of lissencephalic mammals (Noctor et al. 2004; reviewed in Florio & Huttner 2014). These neural progenitors lack apicobasal polarity at division (Attardo et al. 2008). The majority of bIP divisions (~90%) in the murine neocortex generate two daughter neurons and, therefore, are referred to as neurogenic bIP (**Figure 1-3**E and **Table 1-1**; Noctor et al. 2004; Haubensak et al. 2004; Miyata et al. 2004; Kowalczyk et al. 2009; Mizutani et al. 2007; Attardo et al. 2008; Sessa et al. 2008; Vasistha et al. 2015; and reviewed in Florio & Huttner 2014). This population of basal progenitors transiently express the T-box transcription factor Tbr2 (Englund et al. 2005; Sessa et al. 2008; Arnold et al. 2008), which is required for production of bIP from aRG (Arnold et al. 2008), and higher levels of the neurogenic bHLH transcription factor Ngn2 (Miyata et al. 2004). bIPs do not express the apical progenitor marker Pax6 nor Hes transcription factors (Englund et al. 2005; Cappello et al. 2006). It has been suggested that the loss of apicobasal polarity and loss of progenitor gene expression might explain the limited self-renewal potential of this population of progenitors, suggesting that bIPs are a more restricted subtype of neuronal progenitors compared to apical progenitors (reviewed in Florio et al. 2015 and Johnson et al. 2015).

In gyrencephalic species, the iSVZ contains Tbr2-expressing bIPs as well as a number of non-polar basal progenitors that are able to undergo multiple rounds of self-amplifying divisions (Hansen et al. 2010; Lui et al. 2011; Fietz et al. 2012; Stenzel et al. 2014). These progenitors are called proliferative bIP (Florio & Huttner 2014).

The mechanisms that regulate the production of basal progenitors in the mammalian neocortex are currently unknown. It is also not yet clear what in regulatory mechanisms lead to the differences between proliferative and neurogenic bIP.

1.2.2.2 Basal radial glia

The outer SVZ of gyrencephalic species contains a population of dividing cells that do not contact the apical surface at mitosis and, unlike bIP, show cell polarity (Lukaszewicz et al. 2005; Dehay & Kennedy 2007; Hansen et al. 2010; Fietz et al. 2010; Reillo & Borrell 2012; Betizeau et al. 2013). These progenitors are capable of undergoing multiple rounds of cell division to self-renew and produce differentiated cell types (Hansen et al. 2010; Betizeau et al. 2013). These progenitors also express Sox2, Pax6, nestin and GFAP (all markers of aRG cells) but not Tbr2 (Fietz et al. 2010; Hansen et al. 2010; Fietz & Huttner 2011; Reillo & Borrell 2012). Therefore, this population of cells share a number of characteristics with aRG cells and, as such, is referred to as basal radial glia (bRG; previously known as oSVZ radial glia-like (oRG) cells; Hansen et al. 2010; Fietz et al. 2010; Betizeau et al. 2013; **Figure 1-3**E and **Table**

1-1). Analysis of the transcriptome of aRG and bRG showed that both cell types express similar sets of genes and that both have transcriptional profiles that are distinct from that of neurons (Florio et al. 2015; Johnson et al. 2015). In the embryonic murine cortex a small population of bRG are present however, the bRG have a diminished proliferative potential and their transcriptome most closely resembles that of neurons (Florio et al. 2015; Johnson et al. 2015).

Initially, bRG were reported to possess a basal process and to be in contact with the basal laminae, however recent data from macaque embryos showed variations in morphology within the population of bRG, with examples of cells possessing apically and/or basally-directed processes (Betizeau et al. 2013). Therefore, bRG can be categorised based on their morphology as bRG-basal-P (process), bRG-both-P or bRG-apical-P and a complex lineage relationship exists between the classes (Betizeau et al. 2013; reviewed in Florio & Huttner 2014). bRG have been shown to undergo asymmetric divisions, generating a self-renewing bRG cell and either a neuron or bIP (both neurogenic and proliferative; Hansen et al. 2010; X. Wang et al. 2011; Betizeau et al. 2013). Further work is required to understand the functional significance of the morphological varieties of bRG.

In summary, due to their high proliferative capacity bRG are capable of drastically increasing neuronal output. The ability to expand the neuronal population is thought to be particularly important in the evolution and development of the human brain (Lui et al. 2011). This is discussed in detail below.

1.2.2.3 Role of basal progenitors in the expansion of the mammalian neocortex

In order to overcome the limitations to expansion of the VZ (see section 1.2.1.2), a secondary germinal zone, the SVZ, containing basally dividing progenitors is generated in mammals (reviewed in Kriegstein et al. 2006; Borrell & Götz 2014; Florio & Huttner 2014). The ability to produce a second type of progenitor ensures the maintenance of the apical progenitor pool, allowing an extended period of neurogenesis and growth, while still increasing production of neurons (reviewed in Lui et al. 2011). The neuronal output can be greatly increased if the basal progenitor undergoes self-amplifying divisions (reviewed in Lui et al. 2011).

Interestingly, radial expansion of the ancestral mammalian cortex to a 6 layered structure arose along side the generation of the SVZ, containing bIP (Martínez-Cerdeño et al. 2006). Furthermore, in gyrencephalic mammals, including humans, macaques and ferrets (Hansen et al. 2010; Fietz et al. 2010; Betizeau et al. 2013), the SVZ is substantially larger than in the mouse and is further divided into the inner iSVZ and the outer oSVZ around midgestation (Smart 2002). From these correlations it has been hypothesised that basal progenitors produce the large

numbers of neurons that drove the evolutionary expansions that led to 1) the 6-layered cortex and 2) gyrencephaly (reviewed in Florio & Huttner 2014; Borrell & Götz 2014).

Two hypotheses have been put forward to explain how basal progenitors might underlie gyrification. First, it has long been known that regions of the developing cortex that go on to form gyri contain larger numbers of basal divisions (Smart 1972a; Smart 1972b). This observation led to the intermediate progenitor hypothesis which states that folding of the pial surface can be generated by locally altering the numbers of IP (Kriegstein et al. 2006); a region with a high density of basal progenitors will form a gyri and the adjacent region with lower levels of basal divisions will form a sulcus. Nonaka-Kinoshita and colleagues tested this idea by overexpressing the Cdk4/cyclinD1 complex to force bIP cells in the mouse cortex to re-enter the cell cycle. The cortex of these animals showed lateral expansion but the radial thickness of the tissue did not change, nor did the manipulation lead to the generation of gyri. This result suggests that the number and proliferative capacity of bIP does impact the size of the cortical tissue but does not play a role in gyrification.

The second hypothesis, known as either the tangential divergence hypothesis (Borrell & Götz 2014) or the radial cone hypothesis (Florio & Huttner 2014) is based on the identification of bRG as the major population of basal progenitors in gyrencephalic brains. bRG are characterised by their high proliferative capacity and the maintenance of their basal process and basal attachment (Fietz et al. 2010; Hansen et al. 2010; Reillo et al. 2011; Betizeau et al. 2013). The radial cone hypothesis proposes that the basal processes of bRG cells in the oSVZ add radial fibres to the pre-existing scaffolds, allowing a fanlike tangential expansion of the basal surface (**Figure 1-4**C; Lui et al. 2011; Reillo et al. 2011; Reillo & Borrell 2012; Kelava et al. 2013; Lewitus et al. 2013). This suggests that the radial unit in gyrencephalic species is not a column, but a cone. This hypothesis is strongly supported by work from the Gotz lab, which shows that that folding of the basal surface of the cortical plate can be achieved in the mouse neocortex through the shRNA-induced silencing of the transcription factor Trnp1, which increases the population of Tbr2-expressing bIP and bRG (Stahl et al. 2013). This study strongly implicates bRG specifically in the formation of a folded neocortex. Evidence for the role of bRG in the evolution of the human cortex has also been reported by the Huttner lab, which identified a human-specific gene that is enriched in aRG and bRG, ARHGAPIIB (Florio et al. 2015). The molecular function of this gene is not yet understood, but its overexpression in mouse cortical progenitors promotes basal progenitor production and self-amplification, thickening the SVZ and resulting in the formation of folds in the cortical surface (Florio et al. 2015). Taken together these data show that bRG are capable of high levels of neuron production

as well as providing a scaffolding to support neuronal migration and enable tangential growth of the cortical tissue, leading to gyrification.

In summary, basal progenitors in the mammalian cortex are able to generate large numbers of neurons, which ultimately leads to a radial thickening of the tissue. Current data suggests that bRG provide extra radial glial scaffolding to support the tangential expansion of the cortical plate. Therefore, basal progenitors were fundamental to the evolutionary expansion of the mammalian neocortex.

Table 1-1: Comparison of the cell biological features of neural progenitors in the mammalian neocortex. (Adapted from Florio & Huttner 2014). Brackets indicate a minor population that express that gene. NE: neuroepithelial cell; aRG: apical radial glial cell; aIP: apical intermediate progenitor; bIP: basal intermediate progenitor (N: neurogenic; P: proliferative); bRG: basal radial glia; P: directed process (see Betizeau et al. 2013).

	Apical progenitors			**Basal progenitors**				
	NE	**aRG**	**aIP**	**bIP**	**bRG**			
					Basal-P	**Apical-P**	**Both-P**	
Location of mitosis	Apical surface			SVZ/iSVZ	oSVZ			
Apical domain at mitosis	Yes			No	No			
Basal contact at mitosis	Yes		No	No	Yes/No	No	Yes/No	
Process retention at mitosis	Basal		No	No	Basal	Apically directed	Basal and apically directed	
Cell polarity at mitosis	Apical and basal		Apical	No	Basal	Pseudo-apical	Basal and pseudo-apical	
Pax6/Tbr2 expression	Pax6			Tbr2 (Pax6)	Pax6 (Tbr2)			
Astroglial markers	No	Yes	No	No	Yes			
Proliferative potential	Yes		No	N bIP No	P bIP Yes	Yes		

Figure 1-3: Modes of division and progenitor cells in the mammalian cortex.**A-D**) Schematic of the different modes of division. Neuronal progenitors (green cells) can divide symmetrically to generate two progenitors (p – p; **A**) or two neurons (n – n; blue cells, **B**). Alternatively, the progenitor can undergo an asymmetric division to produce a self-renewed progenitor and a differentiating neuron (p – n; **C**). It is also know that neuronal progenitors can divide asymmetrically to generate differently fated progenitors, one that is characteristically similar to the mother cell and another with more limited proliferative potential (p1 – p2; **D**). In **D**, the second type of progenitor (orange cell) undergoes a single round of division, generating two neurons. **E**) Simplified overview of the subtypes of neural progenitor cells in the developing mammalian neocortex. Prior to the onset of neurogenesis the neural tube is composed of NE cells, which mostly undergo proliferative divisions. When neurogenesis begins, NE cells convert into aRG cells, which are capable of self-renewal, neurogenesis and producing basal progenitors. NE cells and aRG cells are collectively called apical progenitors because they divide at the apical surface in the VZ. There are two classes of basal progenitors in the developing neocortex: bIP and bRG. bIP are located in the SVZ of lissencephalic species and the inner SVZ of gyrencephalic species. They mostly undergo symmetrical divisions generating two neuronal daughters, but some can undergo self-renewing divisions. bRG are mostly found in the outer SVZ of gyrencephalic species. bRG are a highly proliferative population and can give rise to more bRG, bIP cells as well as neurons. Newborn neurons migrate basally to the CP where they differentiate. During late stages of neurogenesis, aRG cells begin to generate glial cell types. NE: neuroepithelial cell; aRG: apical radial glial cell; bIP: basal intermediate progenitor; bRG: basal radial glia; VZ: ventricular zone; SVZ: subventricular zone; CP: cortical plate; IZ: intermediate zone. Green cells represent apical progenitor cells (NE and aRG cells); orange cells present basal progenitor cells (bIP and bRG); newborn neurons are shown in dark blue and astrocytes in light blue (adapted from (Tiberi et al. 2012).

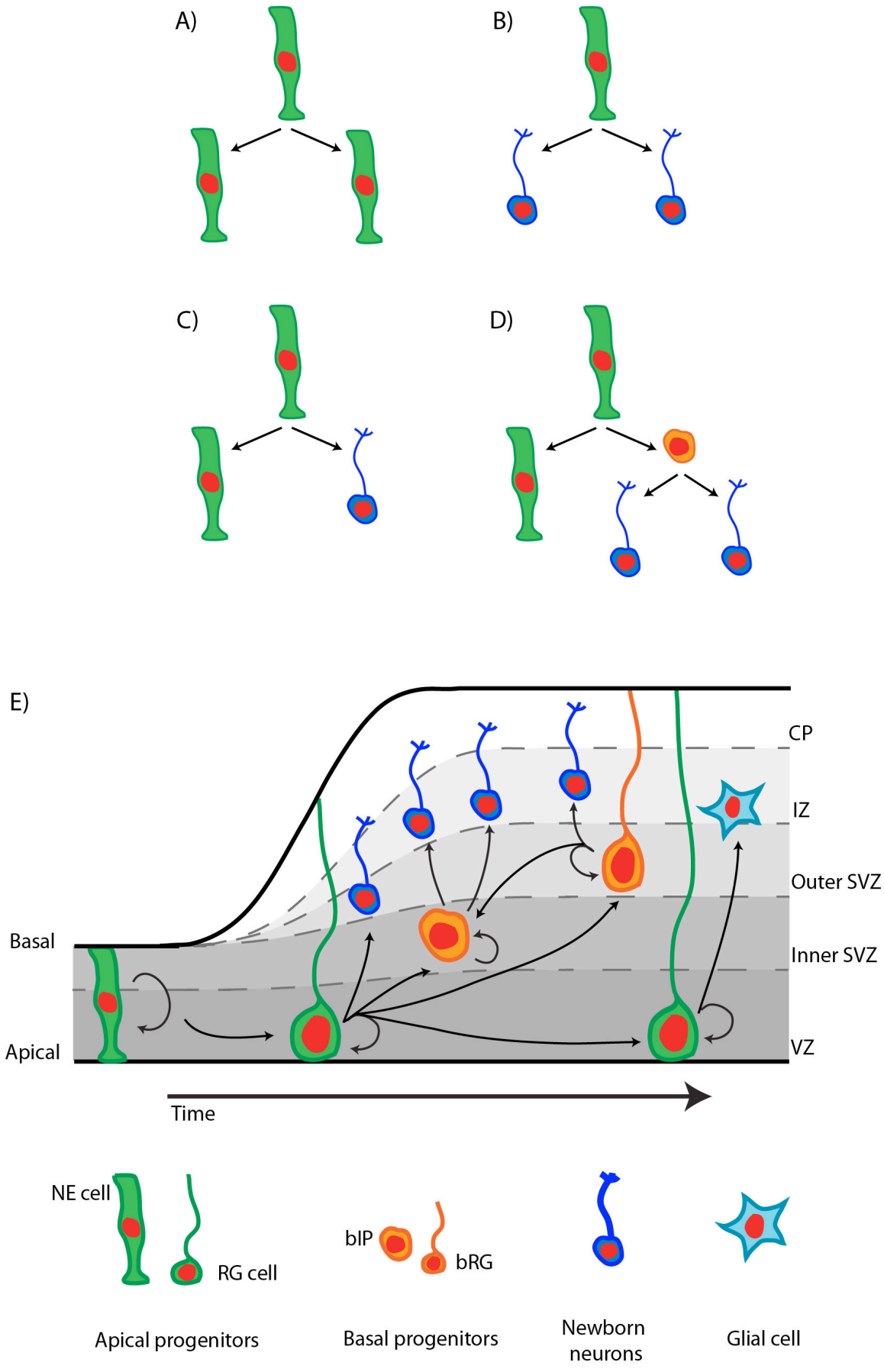
A)
B)
C)
D)
E)
CP
IZ
Outer SVZ
Inner SVZ
VZ
Basal
Apical
Time
NE cell
RG cell
bIP
bRG
Apical progenitors
Basal progenitors
Newborn neurons
Glial cell

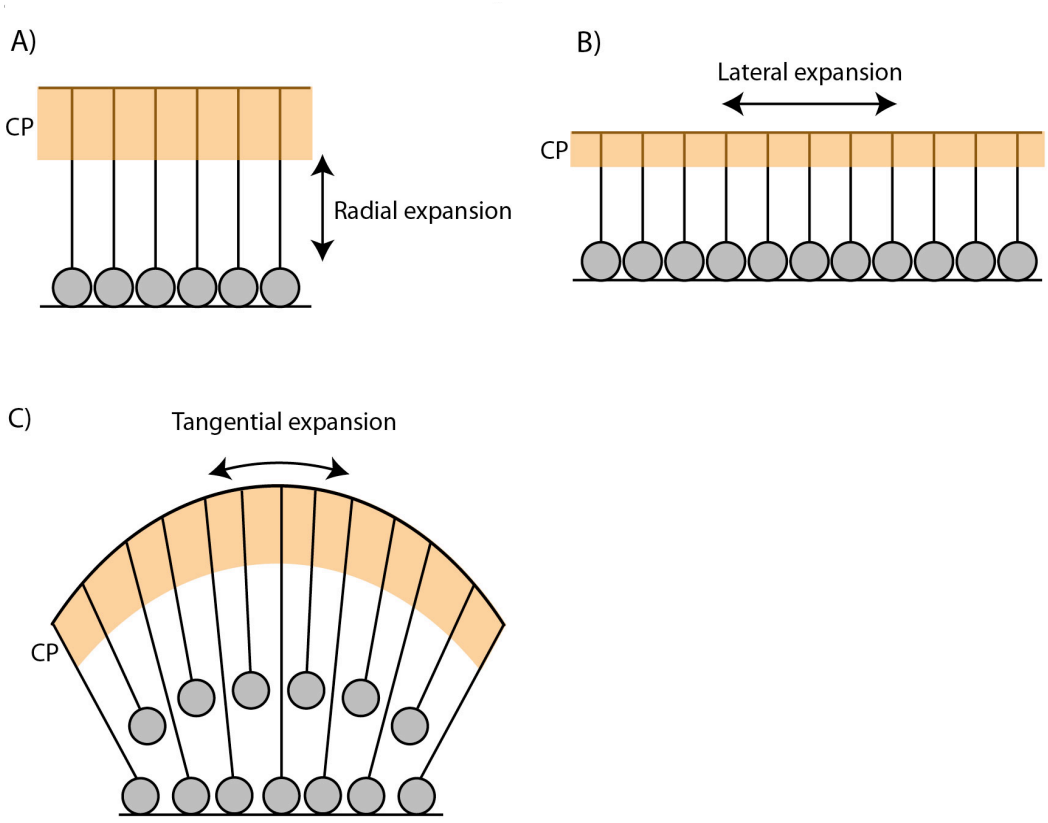

Figure 1-4: Axes of expansion. The cortical tissue can grow on a number of axes. **A**) Growth along the apicobasal axis is referred to as radial expansion. **B**) Growth perpendicular to the apicobasal axis, i.e. in the plane of the neuroepithelium, is referred to as lateral expansion. **C**) Differentiatial growth of the basal surface, compared to the apical surface is called tangential expansion. Neuroepithelial cells are shown in grey, with a radial process contacting the basal surface. The cortical plate is shown in orange.

1.2.3 Neural progenitors in zebrafish embryonic development

In zebrafish embryonic development, neuroepithelial cells expressing proneural genes are present from late gastrulation stages, when the neural plate first forms (reviewed in Schmidt et al. 2013). At this stage the neural tissue does not display apicobasal polarity and the progenitor cells mostly undergo symmetrical proliferative divisions (p – p; Kressmann et al. 2015). After the tissue has become polarised and neural tube has formed, zebrafish neuroepithelial undergo interkinetic nuclear migration, and transform into GFAP-expressing aRG cells that undergo mostly asymmetric divisions (Lyons et al. 2003; Bernardos & Raymond 2006; Kim et al. 2008; Esain et al. 2010; Alexandre et al. 2010; Kressmann et al. 2015). Previous work by the Clarke lab and others has shown that zebrafish apical progenitors in the spinal cord and hindbrain are able to divide either to produce two progenitors (p – p), a neuron and a progenitor (p – n) or two neurons (n – n; Lyons et al. 2003; Alexandre et al. 2010; Kressmann et al. 2015). In late embryonic stages these progenitors begin to generate glial cells (Park et al. 2002; Park et al.

2004; Lee et al. 2010) as known in mammals (Campbell & Götz 2002), while some NE cells are maintained in specific regions to contribute to adult neurogenesis (Schmidt et al. 2013; Furutachi et al. 2015).

In summary, the apical neural progenitor cells that comprise the zebrafish neural tube share many characteristics with those found in the mammalian species (see section 1.2.1). This suggests that the characteristics of apical progenitors are conserved across vertebrate species.

1.2.3.1 Non-apical progenitors in the zebrafish neural tube

Like the developing mammalian neocortex, the zebrafish neural tube is functionally polarised along the apicobasal axis with the apical VZ acting as the location of progenitor divisions and the basal marginal zone specialised for neuronal differentiation. The VZ of the zebrafish neural tube appears as a one cell thick structure that is tightly packed with nuclei. The rest of the tissue does not have obvious cytoarchitectural subdivisions as is seen in the mammalian neocortex. Specifically, zebrafish and other non-mammalian species do not contain a morphological SVZ (Martínez-Cerdeño et al. 2006). However, small numbers of non-apically dividing cells have been seen in the developing nervous system of non-mammalian species, including turtles (Martínez-Cerdeño et al. 2006), chicken (Nomura et al. 2016) and zebrafish (Kimura et al. 2008; Lee et al. 2010) embryos. In the embryonic zebrafish spinal cord neuronal progenitors have been observed dividing at a distance from the apical surface from early developmental stages (17 hpf; Kimura et al. 2008) and non-ventricular dividing progenitors are seen again during gliogenesis (Lee et al. 2010).

Divisions that occur at a distance from the apical surface in the mammalian neocortex are often referred to as basal progenitors. This is not the most accurate description of these cells as they undergo mitosis at a distance from both the apical and basal surfaces. For this reason this divisions are sometimes referred to as abventricular or non-surface progenitors in the mammalian literature (Noctor et al. 2004; Miyata et al. 2004). However, as some non-apical divisions in the zebrafish neural tube divide near or at the basal surface (see Chapter 3), this term is not accurate in the zebrafish neural tube. Therefore, I will refer to all divisions in the zebrafish neural tube that do not divide at the apical surface as non-apical divisions and progenitors.

Currently, the only characterised population of neurogenic non-apical progenitors in the zebrafish spinal cord express *vsx1* and have been shown to undergo terminal divisions to generate differentially fated daughter cells, V2a and V2b neurons (Kimura et al. 2008; Okigawa et al. 2014). These data suggest that *vsx1*-expressing non-apical progenitors are similar to

terminally dividing bIPs in the mammalian brain (Kimura et al. 2008). Mammalian bIPs are known to express Tbr2 and, although there is a Tbr2 orthologue in the zebrafish (Tbr2/eomesa), the expression of this gene is largely limited to post-mitotic neurons in a small frontal region of the telencephalon (olfactory bulb; K. Arkoudi and J. Clarke, unpublished; Mione et al. 2001; Mueller et al. 2008; Ganz et al. 2014). Non-apical glial progenitors (oligodendrocyte precursor cells; OPCs) are also known to exist in zebrafish neural tube and divide in a dorsal region of the neural tube from approximately 60 hpf (Lee et al. 2010).

It is not known if other populations of neurogenic basal progenitors exist in the developing zebrafish central nervous system.

1.3 Regulating the spacing of neurons and neurogenesis

It is known that a large variety of mechanisms pattern and space neurogenesis during development. Here I give an overview of the mechanisms most relevant to this thesis.

1.3.1 Delta Notch signalling

Delta Notch signalling is a fundamental mechanism for regulating the production of neurons within the neuroepithelium. This system was first described in *Drosophila* and homologues have since been identified in vertebrates, including mice (Chenn & McConnell 1995), chicken (Henrique et al. 1995), *Xenopus* (Chitnis et al. 1995) and zebrafish (Dornseifer et al. 1997; Appel et al. 2001). Activated Notch signalling inhibits neurogenesis and allows the neuroepithelium to maintain a population of dividing neuronal progenitor cells. The Delta Notch pathway is now known to play multiple roles in neurogenesis by regulating progenitor proliferation, differentiation as well as specifying neuronal cell fate.

Delta and its receptor Notch are both membrane bound proteins and the interaction between Delta on one cell and Notch on its neighbour results in the cleavage of Notch intracellular domain (NICD; **Figure 1-5**). NICD is then transported into the nucleus of the signal-receiving cell where it interacts with a complex of co-activators, including CSL (named after CBF1/RBPjκ in mammals, *Drosophila* suppressor of hairless (Su(H) and Lag-1 from *Caenorhabditis elegans*; Johnson & Macdonald 2011; Hori et al. 2013; D'Souza et al. 2008; Louvi & Artavanis-Tsakonas 2006; Bray 2006) and Mastermind (Mam; Hori et al. 2013; Louvi & Artavanis-Tsakonas 2006; Bray 2006; **Figure 1-5**). This complex then acts to promote the expression of basic Helix-Loop-Helix (bHLH) transcription factors, for example, genes in the enhancer of split complex (E(Spl)-C; Wettstein et al. 1997) in *Drosophila* or the hairy and enhancer of split (HES) and HES-related (HER) family of genes in vertebrates. These bHLH transcription factors inhibit the transcription of proneural genes in the achaete scute, neurogenin

and atonal families (Campos-Ortega & Jan 1991; **Figure 1-5**). In this way, Delta applies an inhibitory signal to the neighbouring cell, suppressing it from developing into a neuron. This signalling pathway is known as lateral inhibition.

This pathway is self-reinforcing as activated Notch also down regulates Delta, impeding the signal-receiving cell from signalling back to its neighbours (Artavanis-Tsakonas 1999). In *Drosophila,* where Delta and Notch are expressed uniformly throughout the neuroepithelium, it is thought that neurons escape from lateral inhibition though a positive feedback loop amplifying transcriptional differences between neighbouring cells, selecting one as a nascent neuroblast. This eventually results in the nascent neuroblast expressing higher levels of Delta compared to surrounding cells, thereby supplying increased inhibition to its neighbours while itself receiving reduced inhibition (**Figure 1-5**; Haddon et al. 1998). This process results in a signal-sending cell inhibiting its direct neighbours from adopting the same cell fate and generates a salt-and-pepper pattern of neuroblasts within the neuroepithelium.

The core elements of the Notch signalling pathway are conserved through evolution (Hori et al. 2013; D'Souza et al. 2008; Louvi & Artavanis-Tsakonas 2006; Bray 2006). Activated Notch signalling has been shown to inhibit neurogenesis, in favour of progenitor cell maintenance in the retina of *Xenopus Laevis* (Coffman et al. 1993; Dorsky et al. 1995), the murine forebrain (Chenn & McConnell 1995; Ishibashi et al. 1994; Ohtsuka et al. 2001; Sakamoto et al. 2003; Kawaguchi et al. 2008) and the zebrafish neural tube (Appel et al. 2001; reviewed in Pierfelice et al. 2011). This suggests the Notch signalling pathway is also functionally conserved.

Delta Notch signalling is known to impact multiple events during development and can act in a context dependent manner (Schwanbeck 2015). One example of this comes from the zebrafish spinal cord where deltaA and deltaD are required to maintain the p2 progenitor pool and deltaA and deltaC are required for the correct cell fate assignment within V2 interneurons (Okigawa et al. 2014). In the latter case, it is thought that Delta Notch signalling occurs within a lineage to induce distinct neuronal fates in the daughters of *vsx1* non-apical progenitors in zebrafish (Kimura et al. 2008; Okigawa et al. 2014). Similar intralineage Delta Notch signalling has been implicated in the regulation of daughter cell fates after progenitor divisions in the mouse (Mizutani et al. 2007), chicken (Vilas-Boas et al. 2011) and zebrafish (Dong et al. 2012; Kressmann et al. 2015).

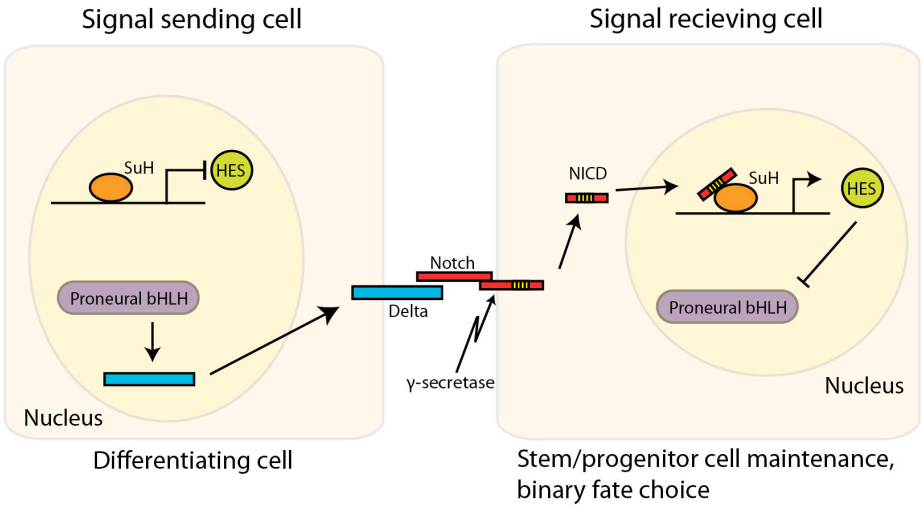

Figure 1-5: Delta-Notch mediated lateral inhibition. The interaction between Delta on one cell and Notch on its neighbour results in the cleavage of the Notch Intracellular Domain (NICD) in the signal-receiving cell. NICD then acts with coactivators (including suppressor of hairless (Su(H)) to activate the expression of target genes. Key targets include basic helix-loop-helix Hes proteins. Hes proteins then inhibit transcription of proneural bHLH genes. The activation of Notch signalling in the signal-receiving cell inhibits neuronal differentiation. In the signal-sending cell, lack of Notch signalling allows the expression of proneural bHLH genes and the activation of the differentiation process in these cells. (Adapted from Chen et al. 2014.)

1.3.1.1 Long distance lateral inhibition

Traditionally it was thought that Delta Notch lateral inhibition could only occur between immediately adjacent cells, as the signalling pathway requires cell-to-cell contact. However, studies in the *Drosophila* notum suggest that differentiating neuronal cells might be able to send inhibitory signals to cells at a distance from its own cell body. The notum is a neuroectodermal tissue from which sensory organ precursors (SOP) are specified. SOPs go on to generate bristles and associated mechanosensory organs. In normal tissue, SOPs are induced in a pattern spread and isolated throughout the tissue (**Figure 1-6**A). Cells that are destined to become SOPs have been shown to extend a web of Delta-rich filopodia into the surrounding tissue and activate Notch signalling in cells as far as 5 cell diameters away (**Figure 1-6**B'; De Joussineau et al. 2003; Cohen et al. 2010; Doe 2008). These filopodia are actin-based, requiring the action of Rac and the SCAR complex to form (De Joussineau et al. 2003; Cohen et al. 2010). Furthermore, if you interfere with the formation or elongation of filopodia from SOPs or ameliorate Notch signalling in these cells, the normal spacing and patterning of SOPs within the notum ectoderm is lost (**Figure 1-6**C and D, respectively; De Joussineau et al. 2003; Cohen et al. 2013). Therefore, in this system, differentiating neuronal cells are able to use basal filopodia to deliver long-range Delta Notch-mediated lateral inhibition to refine a self-organised pattern of bristles (De Joussineau et al. 2003; Cohen et al. 2010).

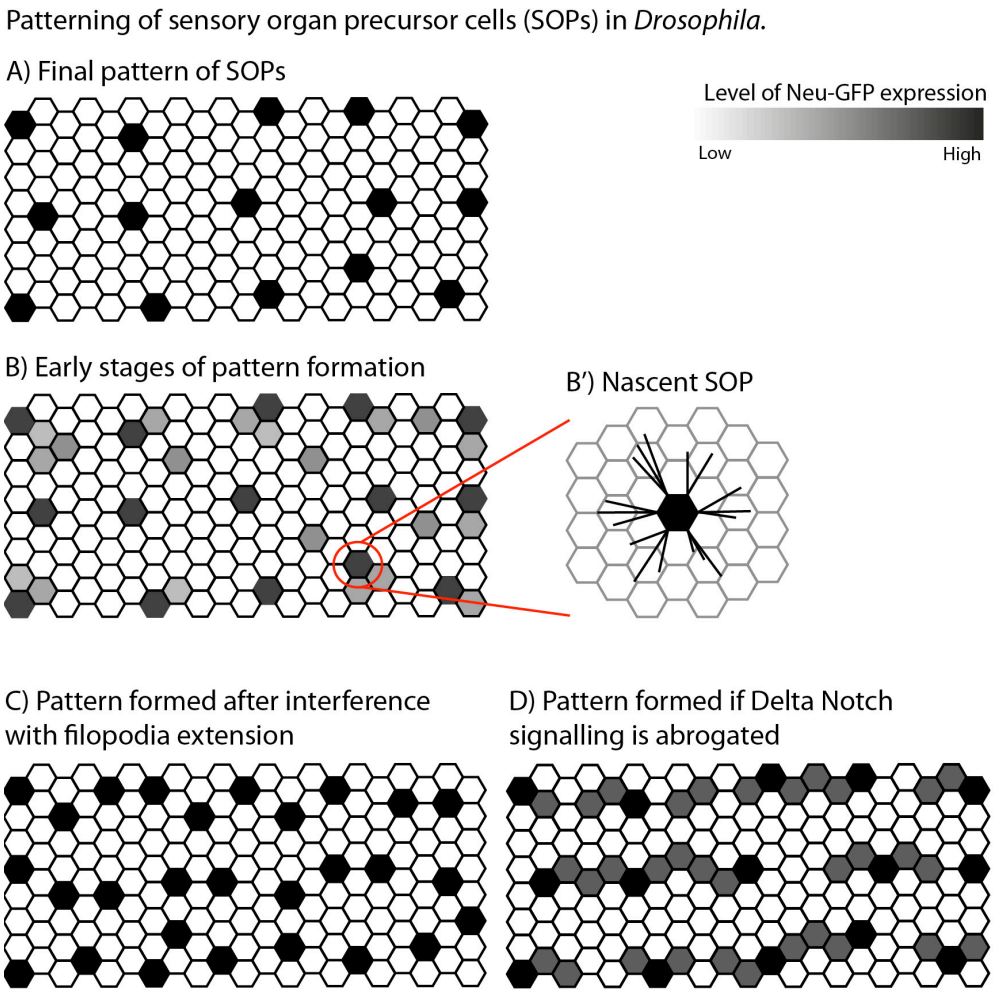

Figure 1-6: Patterning of SOP cells in *Drosophila*. Adapted from Cohen et al. 2010. Neuronal cells express Neu-GFP (Neuralized-GAL4, UAS Moesin-GFP; grey scale; the darker the colour the higher the expression level) and the outlines of the cells in the tissue are labelled with E-Cadherin-GFP. **A**) The final pattern of SOP cells is ordered and shows regular spacing between individual precursor cells (adapted from Figure 1 in Cohen et al. 2010). **B**) In early stages of pattern formation an excess number of cells expressing Neu-GFP appear in the notum, generating an overcrowded and poorly organised arrangement of precursor cells (Figure 4 in Cohen et al. 2010). **B'**) The nascent SOP cells in this tissue extend membrane protrusions into the surrounding tissue (Figure 7 in Cohen et al. 2010). **C**) Expression of dominant negative Rac or a mutant form of *scar* (regulators of filopodia formation in the notum) in Neu-expressing cells results in a disordered final pattern of SOP cells (Figure 7 in Cohen et al. 2010). **D**) Inhibiting Notch signalling while the pattern is being refined results in rows of Neu-GFP-expressing SOPs (adapted from Figure 2 in Cohen et al. 2010).

1.3.1.2 Specialised signalling filopodia (cytonemes) in *Drosophila* and vertebrates

It is not known whether membrane extensions deliver long-range lateral inhibition in other species to pattern neurogenesis. However, there is a growing literature from *Drosophila* development and the vertebrate immune system regarding signalling events that require the delivery of molecules over long distances by specialised filopodia.

Long, dynamic, actin-based filopodia (known as cytonemes, tubulovesicular extension (TVEs) or membrane tethers) are a common feature of patterning in the *Drosophila* wing imaginal disc (reviewed in Kornberg & Roy 2014). Directed trafficking of proteins along the cytonemes has been shown to contribute to the generation of gradients of the *Drosophila* signalling protein decapentaplegic (Dpp; Ramírez-Weber & Kornberg 1999; Kornberg & Roy 2014) as well as hedgehog signalling (Hh; Bischoff et al. 2013). Delta proteins have also been observed in the cytonemes produced by myoblast cells in the wing imaginal disc. Delivery of Delta by these cytonemes is required for the activation of Notch signalling in the air sac primordium and controls growth of the tissue (Huang & Kornberg 2015). In the case of Dpp signalling, the cytonemes of signal-sending and -receiving cells directly interact with each other and form relatively stable contacts that resemble neuronal synapses and allow the direct transfer of Dpp (Roy et al. 2014; Kornberg & Roy 2014). These data show that specialised signalling filopodia are commonly used during *Drosophila* development.

There is a growing field of evidence that cytonemes are also found in vertebrate species. A number of *in vitro* studies have observed cytonemes on immune system cells following antigenic or chemical stimulation, including B cells (Gupta & DeFranco 2003), mast cells (Fifadara et al. 2010) and neutrophils (Galkina et al. 2009; Corriden et al. 2013). The cytonemes generated by these cells can reach multiple cell diameters in length (Gupta & DeFranco 2003; Galkina et al. 2009; Corriden et al. 2013). The signalling function of these processes is currently unknown but it has been suggested that they are involved in targeted, long-range capture of bacteria (Corriden et al. 2013). Outside of the immune system, signal-sending processes have been reported to traffick Wnt ligands in fibroblastic *Xenopus* tissue culture (Holzer et al. 2012). In this system there is some evidence that Xwnt2b is released from the membrane and taken up by surrounding cells but the role of this long distance trafficking in Wnt signal transduction has not yet been shown (Holzer et al. 2012). Finally, cytonemes have also been observed *in vivo* in the chick limb bud. Both Shh signal-sending cells and signal-receiving cells extend several long filopodia which traffic either the signalling molecule or its receptors (Sanders et al. 2013). The cytonemes from signalling-sending and -receiving cells form stable long-range connections, which are thought to allow targeted Shh signalling (Sanders et al. 2013).

In summary, there is a growing field of evidence that membrane extensions are used to transmit a variety of signals over long distances in vertebrate species. However, the exact role these extensions play in signal delivery and transduction is still unclear (Kornberg & Roy 2014) and it is unknown whether long distance lateral inhibition operates in vertebrate neurogenesis (Pierfelice et al. 2011).

1.3.2 Overt tissue segmentation and the spacing of neurogenesis in the zebrafish hindbrain

The zebrafish hindbrain is a good example of overt tissue segmentation, which is otherwise rare in the vertebrate neural tube. The tissue is composed of a series of segments (rhombomeres) that are visible as repeated swellings along the anteroposterior axis in early development and each show individual molecular and neurogenic characteristics (Lumsden & Krumlauf 1996). Specialised boundary cells exist between each rhombomere (Guthrie et al. 1991; Trevarrow et al. 1990) and within each rhombomere neurogenesis is restricted to a region adjacent to the boundary cells and is excluded from the segment centres (Gonzalez-Quevedo et al. 2010). The pattern of neurogenesis is gradually formed and refined through the first two days of development by interactions between boundary cells and differentiated neurons (Gonzalez-Quevedo et al. 2010).

The inhibition of neurogenesis within boundary cells is most likely due to the expression of radical fringe in these cells, which is a known activator of Notch signalling (Cheng et al. 2004; Qiu et al. 2004; Qiu et al. 2009). A separate mechanism has been found to pattern neurogenesis within non-boundary cells. A population of early born neurons are found in the segment centres and express fgf20a, which inhibits neurogenesis through the localised activation of FGF signalling in the neuroepithelial cells adjacent to the fgf20a-expressing neurons (Gonzalez-Quevedo et al. 2010). In the hindbrain of fgf20a mutant zebrafish neurogenesis is increased in the segment centres, showing the requirement of this signalling pathway to pattern neurogenesis within each segment (Gonzalez-Quevedo et al. 2010). This pattern of neurogenesis therefore requires the correct placement of neurons in the segment centres. This has been shown to be dependent on signals from boundary cells as if the formation of the segment boundaries is disrupted, the fgf20a neurons are spread along the anteroposterior axis of the hindbrain (Terriente et al. 2012). The boundary cells have been shown to express Sema family proteins, which activate the neuropilin receptor Nrp2a expressed by fgf20a neurons thereby chemorepel fgf20a neurons away from the segment boundaries and causes them to accumulate in the segment centres (Terriente et al. 2012). Neurogenesis in the hindbrain increases if Sema/Nrp signalling is abrogated.

From this work, a two-step model has been generated to explain how neurogenesis in the zebrafish hindbrain is patterned: Sema signalling by the boundary cells drives fgf20a-expressing neurons to cluster in the centre of each segment. These neurons then activate FGF signalling in surrounding cells to inhibit neurogenesis in the segment centres. This model demonstrates how the pattern of neurogenesis in the segmented hindbrain is generated through the complex

interaction of multiple signalling pathways. This is also a clear example of a mechanism by which the gross patterning of a tissue can in turn pattern neurogenesis.

1.3.3 Spatial patterning of primary neurons

Primary motor neurons arise from the ventral pMN progenitor domain early in neurogenesis in the zebrafish spinal cord (9-14 hpf), and are characterised into three subtypes based on their soma location relative to the paraxial mesoderm (somites): rostral primary (RoP); middle primary (MiP); and caudal primary (CaP; Myers 1985; Eisen et al. 1986; Lewis & Eisen 2003)[2]. These motor neurons are found repeated along the anteroposterior axis of the spinal cord so that one motor neuron of each subtype is found per spinal hemisegment. Specifically, MiP and CaP neurons are found in a regularly spaced and alternating pattern that is symmetrical across the midline. The development of this pattern has been shown to be dependent on mesoderm-derived signals (Lewis & Eisen 2004; Eisen & Pike 1991; Sato-Maeda et al. 2008). Zebrafish mutants which lack paraxial mesoderm (for example, *no tail* or *spadetail*) show irregular spacing between primary motor neurons and also show examples of clusters of these cells (Lewis & Eisen 2004; Eisen & Pike 1991). Furthermore, in convergent extension mutants (for example, *trilobite* or *knypek*) a decrease is seen in the spacing between the primary motor neurons which correlates with the decreased somite size in these mutants (Lewis & Eisen 2004). Double mutants of these genes, which display severe convergent extension phenotypes, contain primary motor neurons that appear in continuous clumps (Lewis & Eisen 2004). These effects were shown to be generated by cell non-autonomous mechanisms through transplantation experiments (Lewis & Eisen 2004). Therefore, the correct patterning of the somites is required to generate the normal pattern of primary motor neurons.

The molecular mechanism that underlies the patterning of the CaP class of motor neurons has been elucidated (Sato-Maeda et al. 2006; Sato-Maeda et al. 2008). CaP neurons are initially irregularly spaced in the spinal cord and their distribution is refined prior to axonogeneis so that each CaP primary motor neuron is located at the midpoint of the overlying somite (Sato-Maeda et al. 2008). This refinement has been shown to require Sema3ab/Neuropilin1a signalling. Sema3ab expression is restricted to the posterior half of the somite (Bernhardt et al. 1998) while Neurophilin1a is specifically expressed in CaP primary motor neurons (Sato-Maeda et al. 2006). Sema3ab acts as a chemorepellent and by binding to Neuropilin1a is able to adjust the position of CaP neurons (Sato-Maeda et al. 2008).

[2] Primary motor neurons have recently been reclassified to reflect the patterns of their axonal projections (Bagnall & McLean 2014; Menelaou & McLean 2012). Here, I will use the names of the subtypes based on their soma location, as is used in the literature on how the motor neurons are patterned relative to the somites (Lewis & Eisen 2004; Eisen & Pike 1991; Sato-Maeda et al. 2008).

It is unknown whether mesoderm-derived signals are required for the correct spacing of other neuron cell types in the developing spinal cord during primary or secondary neurogenesis. Other potential mechanisms (if any) by which mesodermal signals influence neuronal spacing have not yet been elucidated.

1.4 Specific aims

In the current view of mammalian neurogenesis, basal progenitors are thought to produce the large numbers of neurons that are required to generate a large and complex cortex. However, there are reports that both non-cortical regions and non-mammalian species contain populations of non-apically diving neuronal progenitors (Martínez-Cerdeño et al. 2006; Kimura et al. 2008; Nomura et al. 2016). These data suggest that non-apical progenitors may play alternate or additional roles in neurogenesis. To increase our knowledge of non-apical progenitors in non-cortical tissues, I have studied them in the zebrafish embryonic central nervous system.

In this thesis, I address the following questions:

- To what extent do non-apical neuronal progenitors contribute to zebrafish embryonic neural development?
- How are non-apical progenitor divisions regulated in developmental time and space?
- What mechanisms control the production of non-apical progenitors?

CHAPTER 2
GENERAL MATERIALS AND METHODS

2 General Materials and Methods

2.1 Animals

Wild type, transgenic and mutant zebrafish were maintained under standard conditions (Westerfield, 2000) on a 14-hour photoperiod in the King's College London Fish Facility. Embryos were obtained from timed matings.

2.1.1 Wild-type strains

King's College Wild-type, Ekkwill, AB Tubingen and Tupfel Long fin.

2.1.2 Transgenic zebrafish lines

The following zebrafish transgenic lines were used in this thesis:

- **Tg(*vsx1*:GFP)** – (Kimura et al. 2008). Obtained from the Harris lab, University of Cambridge. This reporter line was generated using a bacterial artificial chromosome (BAC) containing promoter and enhancer elements for the zebrafish *vsx1* gene (Kimura et al. 2006) with enhanced GFP (eGFP) inserted at the transcription start site. GFP is expressed in the cytoplasm of any cell that expresses *vsx1*.
- **Tg(*olig2*:eGFP)** – (Shin et al. 2003). Obtained from Houart Lab, KCL. This line was generated using a BAC containing promoter and enhancer elements for the zebrafish *olig2* gene (Shin et al. 2003) with eGFP inserted at the start of transcription of the *olig2* gene. GFP is expressed in the cytoplasm of any cell that expresses *olig2*.
- **Tg(*tbr2a*:dsRed)** – (Miyasaka et al. 2009) Obtained from the Wilson Lab, UCL. This transgenic line contains a cassette composed of a 5kb genomic region upstream of the zebrafish *tbr2* gene driving expression of the fluorophore dsRed. dsRed is expressed in the cytoplasm of cells that express *tbr2*.
- **Et(g*ata2*:GFP)^{bi105}** – (Folgueira et al. 2012). Obtained from the Wilson Lab, UCL. This enhancer trap line uses endogenous *gata2* enhancer elements to drive expression of GFP. GFP expression is seen in the cytoplasm of pallial neurons from 30 hpf (Folgueira et al. 2012).
- **Tg(*deltaD*-GFP)** – (unpublished). Obtained from the Oates lab, UCL. A BAC containing promoter and enhancer regions for zebrafish *deltaD* gene was used to create a *deltaD-GFP* fusion protein. This line contains seven insertions of this BAC construct.

2.1.3 Mutant zebrafish line

The following zebrafish mutant line was used in this thesis:

- *Fused somites (fss)*^{te314a} (van Eeden et al. 1996). Obtained from the Oates lab, UCL. Mutants were identified by morphological phenotype.

2.1.4 Embryo culture

Wild type, transgenic and mutant adult zebrafish were maintained under standard conditions (Westerfield, 2000) on a 14-hour photoperiod in the King's College London Fish Facility. Embryos were obtained from timed matings and raised at 28.5°C in fish water with methylene blue (Sigma Aldrich) or embryo medium (E2) (Westerfield, 2000). Reducing incubation temperature to 23°C from five hours post-fertilisation caused development to proceed at a slower rate, enabling early embryonic stages to be visualised at an appropriate time. Embryos were staged according to published criteria (Kimmel et al., 1995) and stages are given in terms of hours post fertilisation (hpf). After 20-24 hpf embryos were maintained in fish water or E2 medium containing 0.003% 1-Phenyl-3-(2-thiazolyl)-2-thiourea (PTU; Sigma) to prevent pigment formation.

2.2 Molecular biology

2.2.1 Plasmid preparation

One Shot® TOP10 Chemically Competent (Invitrogen) or Z-Competent™ 5α (Zymo Research) *Eschericha coli* cells and Qiagen plasmid preparation kits were used for general cloning and plasmid preparation.

2.2.2 mRNA synthesis

PCS2+ expression vectors were linearised with various restriction enzymes (Promega) for 2 hours at 37°C and precipitated at -20°C overnight in 70% ethanol and 0.05M sodium acetate. DNA was then washed in 70% ethanol and resuspended in nuclease-free dH_20 (Ambion). Sense strand capped mRNA was transcribed using the mMESSAGE SP6 Kit (Ambion) and purified through a column (Roche). Resulting RNA concentration was measured using a spectrophotometer or nanodrop (ThermoFisher Scientific).

2.3 Microinjection

All injections were carried out under a dissecting microscope using a glass slide and petri dish. Injections were delivered using a glass micropipette with filament (Harvard Apparatus) mounted on a micromanipulator and attached to a Picospritzer® (General Valve Corporation).

2.3.1 mRNA Injections

Various mRNAs were injected either at the one-cell stage for ubiquitous expression or into one blastomere between the 16 and at 64-cell stages for mosaic labelling of neuroprogenitor cells. mRNA was injected at 10-150 pg per embryo and did not exceed half the volume of a cell.

2.3.2 Anti-sense Morpholino Injections

Anti-sense morpholino oligonucleotides (Gene Tools) were stored as 4mM stocks at -20 °C and diluted as required in sterile water. For ubiquitous knockdown of the protein of interest, various morpholinos were injected at the one to two-cell stage. A standard control morpholino (Gene Tools) was injected at equivalent concentrations and control morpholino injected siblings were raised alongside morpholino-injected animals.

2.4 Immunohistochemistry

Wholemount immunohistochemistry was carried out as previously described (Westerfield, 2000), with some modifications.

- Embryos were fixed in 4% paraformaldehyde (PFA; Sigma) in PBS, shaking for 2 hours at room temperature (RT) or overnight at 4°C.
- Embryos were dehydrated through a methanol series (25%, 50%, 75%, 100%, in PBS, with 5 min washes each) and stored at -20 °C in 100% MeOh for at least 12 hrs.
- Embryos were rehydrated through a decreasing methanol series (75%, 50%, 25%, in PBS; 5 min washes each) and then washed 2 x 5 mins in PBS.
- Embryos were treated to increase permeabilisation.
    - For embryos 36 hpf or younger - cryogenic treatment:
        - Incubate the embryos in cryogenic buffer (8% sucrose, 5% goat serum, 0.2% Gelatin, 1% triton in PBS), shaking, at RT for an hour.
        - Replace the buffer and freeze at -20°C for 3 mins or until the solution goes cloudy. Repeat this step.
        - Wash 2 x 5 mins in blocking solution (10% goat serum, 5% DMSO in PBT; PBS + 0.1-1% Triton-X-100).
    - For embryos older than 36 hpf - protein kinase K (PK) treatment:
        - Incubate embryos in 1000 µl PBS + PK (48 hpf, 1:1000; 72 hpf, 1:500) for 30 mins
        - Wash 2 x 5 mins in PBS
- Incubate in blocking solution for 1 hr, shaking at room temperature
- Incubate embryos in primary antibody at 4°C, shaking for up to a week
- Wash in PBT initially with 3 x 5 mins washes followed by longer 30 min washes.
- Incubate embryos in secondary antibody at 4°C, shaking for 2-3 days
- Wash in PBT initially with 3 x 5 mins washes followed by longer 30 min washes.

2.4.1 Antibodies

Various primary antibodies were used in combination with Alexa® Fluor (405, 488, 568, 633, 647) conjugated secondary antibodies (1:500; Invitrogen).

Table 2-1: Primary antibodies used in this thesis.

Protein Target	Source	Catalogue number	Host species	Storage	Dilution
aPKC (λ and ζ)	Santa Cruz	SC-216	Rabbit polyclonal	4°C	1/350
GFP	Abcam	Ab-13970	Chicken polyclonal	-20°C	1/300
HuC/D	Invitrogen	A21271	Mouse monoclonal IgG2b	-20°C	1/300
Phospho-Histone H3	Upstate Biotech	06-570	Rabbit polyclonal	-20°C	1/500
ZO-1	Invitrogen	339111	Mouse monoclonal IgG	-20°C	1/300

Counterstains were added during incubation with secondary antibody to visualize nuclei. The following counterstains were used (all ThermoFisher Scientific Molecular Probes; all 1:10,000):

- Hoechst (H3570)
- Sytox Green (S7020)
- Sytox Orange (S11368)

2.5 In situ hybridisation

Vectors were linearised and purified as described. Anti-sense probes were synthesised using a Dig NTP mix and RNA Polymerase kit (Roche).

The following probe was used:
vsx1 (He et al. 2014), a gift from Dr Chen Lou, Zangjiang University, China.

- Embryos were fixed in 4% PFA overnight at 4°C.
- Embryos were dehydrated through a methanol series (25%, 50%, 75%, 100%, in PBS, with 5 min washes each) and stored at -20°C in 100% MeOh for at least 12 hrs.
- Embryos were rehydrated through a decreasing methanol series (75%, 50%, 25%, in PBS, with 5 min washes each) and then washed 2 x 5 mins in PBS.

- Embryos were subsequently incubated in hybridization buffer (Hyb; 50% Formamide, 25% SSC 20X, 10% Tween 20, 25 mg mRNA Torula, 25 mg Heparin in ddH_2O) for 30 mins at RT and then in fresh Hyb in a heat block at 65°C for at least 2 hrs.
- Probes were diluted to approximately 150 µg/ml and placed at 80°C for 5 mins.
- Diluted probes were added to the embryos and left overnight in at 65°C.
- The next day the embryos were washed as follows at 65°C:
    - 2 x 30 mins in Hyb.
    - Through a decreasing Hyb/2X SSC (Sigma) + 0.1% Tween20 series (75%, 50%, 25%), 20 mins each.
    - 2 x 30 mins in 2X SSC + 0.1% Tween20.
    - 2 x 30 mins in 0.2X SSC + 0.1% Tween20.
    - 1 x 10 min in MABT (0.1M Maleic acid pH7.5, 150mM NaCl, 0.1% Triton) at RT.
- Embryos were incubated in blocking solution (MABT + 10% Bovine Serum Albumin; Sigma) for 2 hours at RT, shaking.
- Anti-DIG antibody was diluted 1:2000 in blocking solution and added to the embryos, which were then left overnight at 4°C, with gentle shaking.
- Wash 6 x 30 mins at RT with MABT.
- Incubate embryos in alkaline phosphatase buffer (100mM NaCl, 100 mM Tris pH 9.5, 50 mM MgCl2, 1% Tween20) for NBT/BCIP colouration or fast red buffer (pH 8.2: 100 mM Tris-HCl (pH 9.5), 150 mM NaCl, 0.1% Tween in ddH2O) for fast red colouration.
- The colour reaction was done using NBT/BCIP (5µg/ml; Roche) or Fast red (Roche; 1 tablet/3ml buffer) in the dark.
- The reaction was stopped by washing in 3 x 5 mins in PBST (0.1%)

2.6 Microscopy

2.6.1 Mounting

Embryos were mounted in 1.5% low-melting point agarose (A9414, Sigma) and supported in a wax or glue chamber in a petri dish filled with fish water (for live imaging) or PBS (fixed specimens; see **Figure 2-1**A). From 16hpf, embryos were anaesthetised in 0.016% tricaine methane sulfonate (MSS-222, E102521, Sigma). Embryos were mounted so that they could be imaged from a dorsal view of the hindbrain or spinal cord or frontally for forebrain (**Figure 2-1**B), unless otherwise specified.

2.6.2 Imaging

Embryos were imaged on either an SP5 Laser Scanning (Leica), Spinning disk (PerkinElmer) or LSM 880 Laser Scanning (Zeiss) Confocal Microscope, using a 20x water immersion objective with a numerical aperture (NA) of 0.95 or higher. Brightfield images were acquired with a

QImaging Micropublisher camera mounted on a Nikon SMZ1500 dissecting microscope. For live imaging, a heated environmental chamber at 28.5°C was used.

2.7 Data analysis

2.7.1 Image processing

Raw confocal data was exported to ImageJ (http://rsbweb.nih.gov/ij/), Volocity® (PerkinElmer) or IMARIS® (Bitplane) for analysis. Images were processed in ImageJ or IMARIS® to adjust brightness and contrast. Figures and schematics were constructed using Adobe Illustrator CS4.

2.7.1.1 Drift correction

In IMARIS®, the 'Spots' function was used to identify and track landmark cells in a time-lapse movie. This track was then used to correct drift, using IMARIS®' algorithms.

2.7.1.2 Quantification

In cases where large numbers of cells needed to be counted, the automatic 'Spots' function in IMARIS® was used. In these cases, the average size of the cell (usually labelled by PH3) was estimated and this size was used to identify PH3-expressing cells as objects. Alternatively, this function was used to aid in manual counting.

2.7.2 Statistical Analysis

Microsoft Excel and Prism 6 (Graphpad) were used for numerical and accompanying statistical analysis. Graphs were created in Prism 6.

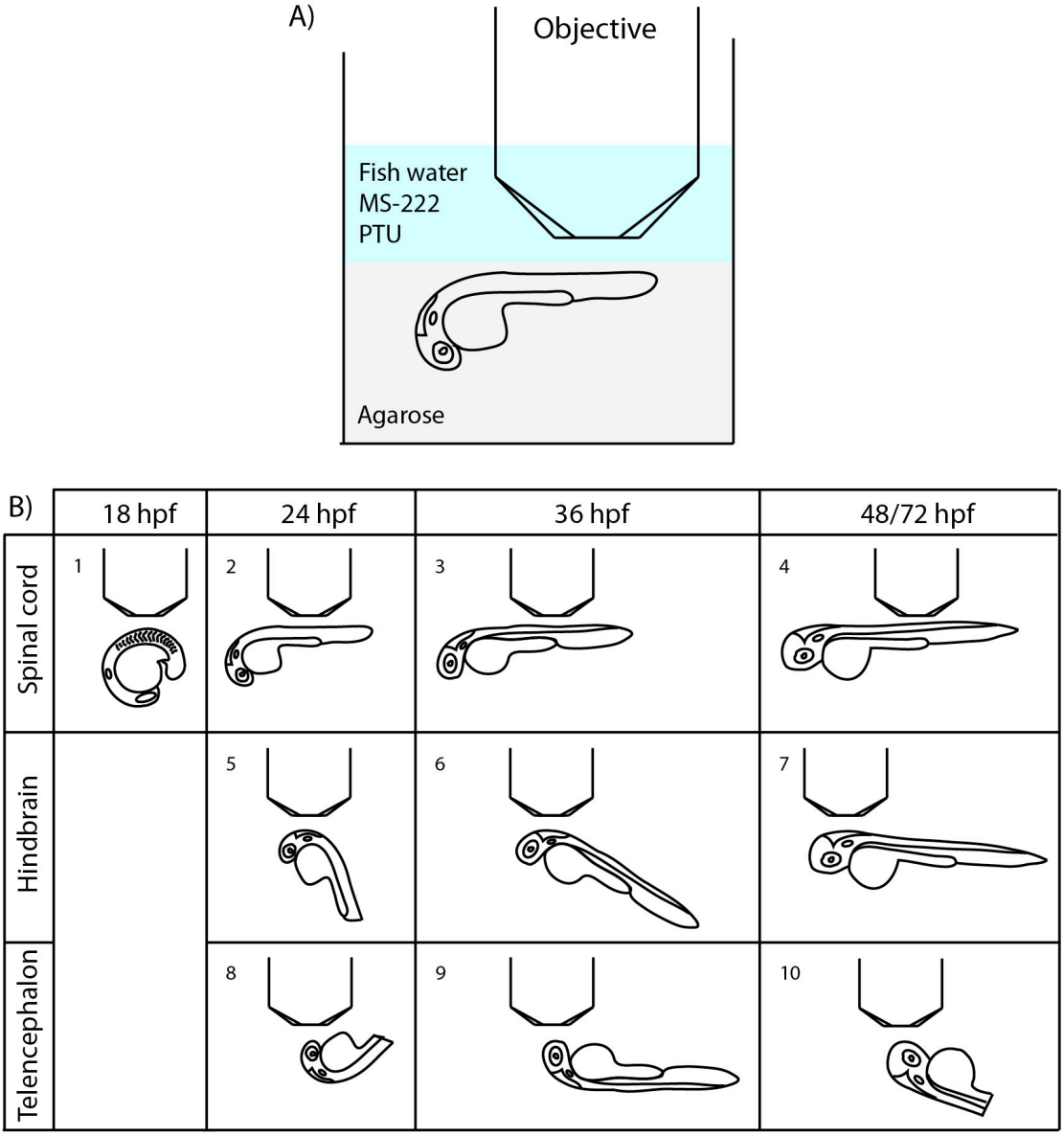

Figure 2-1: Mounting procedures and Imaging set up. **A**) Embryos were mounted in 1.5% low melting point agarose (grey) in a petri dish. For live imaging, embryos were maintained in fish water containing MS-222 (anaesthetic) and 0.003% PTU to prevent pigmentation. To image fixed samples, the specimen where maintained in PBS. **B**) The spinal cord (**1-4**) and hindbrain (**5-7**) were imaged dorsally and the forebrain (**8-10**) was imaged frontally. The tail of the embryo was occasionally removed to aide mounting. Not to scale.

CHAPTER 3
CHARACTERISATION OF NON-APICAL DIVISIONS DURING ZEBRAFISH EMBRYONIC NEURAL TUBE DEVELOPMENT

3 Characterisation of non-apical divisions during zebrafish embryonic neural tube development

3.1 Introduction

The mammalian neocortex is currently the main model used to study the contribution of different subtypes of neural progenitors to brain growth and differentiation. In early vertebrate neurodevelopment, the neuroepithelial cells that make up the neural tube divide at the apical surface in a region known as the ventricular zone (VZ). In all vertebrate species at first these apical progenitors divide symmetrically to increase their population.As neurogenesis begins the apical progenitors being to divide asymmetrically to generate one neuron while self-renewing the apical progenitor population (for example: Miyata et al. 2004; Alexandre et al. 2010; Kressmann et al. 2015). As development progresses mitoses also appear in non-apical locations in the mammalian cortex, and are collectively referred to as basal progenitors (reviewed in Florio & Huttner 2014; see section 1.2.2 for full discussion). Multiple subpopulations of basal progenitors with varying self-renewal and neurogenic properties contribute to mammalian neocorticogenesis (see **Table 1-1**). Basal progenitors are thought to drive an expansion in the number of neurons produced during neurogenesis and generate the relatively large and complex cortical structure that is a defining feature of the mammalian forebrain (reviewed in Florio & Huttner 2014 and see section 1.2.2). These ideas imply an important role for non-apically dividing neuronal progenitors in the evolution of the structurally and functionally complex primate and human brain.

Perhaps contrary to the notion that basal progenitors act to expand neuronal tissue and increase its sophistication, non-apically located progenitors have been observed in the embryonic zebrafish spinal cord. As these abventricular divisions are not necessarily located on the basal surface I will refer to them as non-apical divisions and progenitors. Kimura and colleagues described a non-apical interneuron progenitor that expresses *vsx1* in the zebrafish spinal cord (Kimura et al. 2008; discussed in detail in section 3.1.1). This is currently the only known non-apical neuronal progenitor in the spinal cord of any species. However, there is a known gliogenic non-apical progenitor population in the zebrafish spinal cord, oligodendrocyte precursor cells (OPCs) that express *olig2* (Kirby et al. 2006). OPCs generate a myelinating glial cell type and are typically specified from 60 hpf, towards the end and after embryonic neurogenesis in the zebrafish neural tube (Lee et al. 2010).

To my knowledge, no other information regarding populations of non-apical divisions in the developing embryonic zebrafish neural tube has been published to date. In fact, in the

telencephalon, Dong et al reported that they did not observe any non-apical divisions in live imaging experiments between 28 hpf and 60 hpf (Dong et al. 2012). However, during late stages of zebrafish retinogenesis three populations of non-apical neuronal progenitors have been identified, one of which expresses *vsx1* and generates two daughter cells that differentiate as bipolar cells (Weber et al. 2014). These *vsx1*-expressing non-apical progenitors appear to have lost apical attachment by mitosis, but are still in contact with the basal surface via a basal process (Weber et al. 2014). It has been speculated that non-apical progenitors in the retina act to overcome limited space at the apical surface as well as difficulties accessing the apical surface as the different photoreceptor laminae develop (Weber et al. 2014).

These data and others show that non-apical progenitors are present during the development of relatively simple and compact regions of developing nervous systems, both in non-cortical regions and non-mammalian species (e.g. murine thalamus (L. Wang et al. 2011) and ventral telencephalon (Pilz et al. 2013) and the chick retina (Boije et al. 2009)). The role played by non-apical neuronal progenitors during neurogenesis in the neural tube, when the tissue does not go through dramatic expansion such as seen in the cortex, is still unknown. A thorough characterisation of non-apical progenitors in wild type zebrafish embryos may be informative with regards to this question. To this end, in this chapter I describe experiments to characterise the spatial distribution and molecular identity of non-apical progenitors in the spinal cord, hindbrain and telencephalon of zebrafish embryos during the first three days of development.

3.1.1 Non-apical p2 progenitors in the zebrafish neural tube

Non-apically dividing neuronal progenitors were first observed in the zebrafish transgenic line Tg(*vsx1:*GFP) (Kimura et al. 2008). In the embryonic zebrafish spinal cord *vsx1* mRNA and Tg(*vsx1:*GFP) expression can be observed from as early as 16 hpf, the stage where the neural rod has just been formed (Kimura et al. 2008). *Vsx1* is expressed in p2 progenitors in the ventral spinal cord (**Figure 3-1**A) and *vsx1*:GFP expression is initiated in cells located near the basal surface shortly before they undergo a terminal division, generating pairs of V2a/V2b interneuron daughter cells (Kimura et al. 2008; **Figure 3-1**B). The expression of *vsx1* is maintained in the V2a daughter but is lost in the V2b cell as it differentiates (Kimura et al. 2008; **Figure 3-1**B). These data suggest that p2 progenitors expressing *vsx1* represent a subtype of zebrafish progenitors that are committed to neurogenic divisions, similar to what has been shown for non-apical progenitors in the mammalian telencephalon (e.g. Haubensak et al. 2004; Noctor et al. 2004). This data was the first indication that the developing zebrafish nervous system contained neuronal progenitors that divided at a distance from the apical surface.

The p2 progenitor domain is unique in the ventral spinal cord as it produces two intermingled subtypes of V2 interneurons at the same time of development, in rodents, chicken as well as zebrafish (Karunaratne et al. 2002; Al-Mosawie et al. 2007; Kimura et al. 2008; Panayi et al. 2010). V2 interneurons diversify into V2a and V2b subtypes which have similar morphologies (ipsilateral descending axonal trajectories) but disparate function and expression profiles in zebrafish (Kimura et al. 2006; Batista et al. 2008; Kimura et al. 2008), chicken (Karunaratne et al. 2002; Li et al. 2010; Kang et al. 2013) and mammalian (Li et al. 2005) spinal cords. In zebrafish, V2a interneurons are glutamatergic (excitatory) circumferential descending (CiD) interneurons and express *vsx2* (previously a*lx*; Kimura et al. 2006), a zebrafish homolog of *Chx10* in mice (Passini et al. 1998; **Figure 3-1**C). V2b interneurons are ventral lateral descending (VeLD) GABAergic (inhibitory) interneurons and express Scl, Gata2 and Gata3 (Batista et al. 2008). It is thought that V2 cells in mice also develop into approximately equal in number inhibitory and excitatory interneurons with ipsilateral descending axon trajectories (Al-Mosawie et al. 2007; Lundfald et al. 2007). However, in the mouse it has recently been shown that the V2b lineage can diversify to contain two cell types V2b (Gata3-expressing) and V2c (Sox1-expressing; Li et al. 2010; Panayi et al. 2010; **Figure 3-1**C). There is no evidence that V2 interneurons are generated by non-apical progenitors in either the chicken or the mouse spinal cord.

Currently, it remains unknown whether *vsx1*:GFP-expressing V2 intermediate progenitors are the only non-apical progenitor population in the zebrafish neural tube.

3.1.2 Markers of non-apical progenitors

In the literature on mammalian and zebrafish non-apical progenitors there are three genes that are associated with this progenitor subtype; *vsx1*, *olig2* and *tbr2*. Below I summarise what is known about the cells that express these genes in the context of neural development.

3.1.2.1 Non-apical neural progenitors in the zebrafish spinal cord express the *vsx1*

Visual system homeobox-1 (*vsx1*) encodes a transcription factor containing a paired-type homeodomain and a CVC domain (Passini et al. 1998). It was first identified from the goldfish retina (Levine et al. 1994) and then cloned in zebrafish (Passini et al. 1998) where expression in the developing hindbrain and spinal cord was observed alongside retinal expression. This expression pattern is recapitulated in the zebrafish transgenic reporter line Tg(*vsx1:*GFP) (Kimura et al. 2008). *Vsx1* plays a role in the regulation of a number of processes during development. Maternally deposited *vsx1* has been shown to act as a transcriptional repressor during the initiation of axial-paraxial mesodermal patterning in zebrafish embryos (He et al.

2014). During vertebrate eye development, *vsx1* is required for retinal progenitor cell proliferation and neuron specification (Shi et al. 2011). *Vsx1*-expressing retinal progenitors undergo division in subapical positions and give rise to a type of retinal interneurons known as bipolar cells (Weber et al. 2014). *Vsx1* non-apical progenitors maintain contact with the basal surface at mitosis but lack any apical attachment or process (Weber et al. 2014). The function of the *vsx1* gene in the biology of non-apical progenitors in the spinal cord is currently unknown.

3.1.3 *Olig2* is expressed in the pMN progenitor domain

Olig genes are basic helix-loop-helix (bHLH) transcription factors that are expressed in the pMN domain (**Figure 3-1**A). This dorsal progenitor domain gives rise to motor neurons, interneurons and oligodendrocytes in the spinal cord of mammals (Zhou et al. 2000; Masahira et al. 2006), chicken (Lee 2005; Liu et al. 2007) and zebrafish (Park et al. 2002; Park et al. 2004; Park et al. 2007; Zannino & Appel 2009). In zebrafish a single Olig gene, *olig2* is expressed in the embryonic spinal cord and hindbrain (Park et al. 2002; Park et al. 2007; Zannino & Appel 2009). *Olig2*+ progenitors generate motor neurons and interneurons until approximately 36 hpf, after which *olig2*-expressing progenitors start to produce OPCs. *Olig2*-expressing OPCs then translocate to the basal surface of the ventral pMN progenitor domain before migrating dorsally and ventrally, where they divide at later stages of neurogenesis (± 60 hpf) and the daughter cells differentiate as oligodendrocytes (Lee et al. 2010).

In summary, *olig2*-expressing glial progenitors from the pMN domain divide at a distance from the apical surface during gliogenesis. It is not known if *olig2*-expressing cells undergo division in non-apical locations during neurogenic stages to produce motor neurons or interneuron cell types.

3.1.4 *Tbr2* is a marker of intermediate neuronal progenitors in the mammalian neocortex

The T-box transcription factor Tbr2 (Eomesa) is a known marker of mammalian basal intermediate progenitors (bIPs; Englund et al. 2005; Mizutani et al. 2007; Hansen et al. 2010; see section 1.2.2 and **Table 1-1**), which typically undergo self-consuming divisions generating two neurons. Tbr2 has been shown to be required for the production of bIPs from apical radial glial (aRG) cells and is downregulated in newborn neurons (Arnold et al. 2008). In contrast, Tbr2 is expressed in differentiated neuron cells in the forebrain of chicken embryos (Nomura et al. 2016). Similarly, in the forebrain of zebrafish embryos, Tbr2 is expressed in a subset of pallial neurons (Mueller & Wullimann 2003; Thisse et al. 2005). Tbr2 expression has also been reported in non-apical progenitors in the spinal cord of 30 hpf zebrafish embryos (Ohata et al.

2011). However, this was observed using an antibody against the human protein and I have been unable to repeat this observation (discussed fully in section 3.3.3.2).

In summary, different cell populations express Tbr2 in the mammalian (basal progenitors) and zebrafish and avian (neurons) pallium. It is currently unclear whether *tbr2* is expressed in non-apically dividing cells in the zebrafish.

3.1.5 Aim of chapter

In order to understand the role non-apical progenitors may play in the development of the zebrafish nervous system my first aim is to characterize the non-apical progenitor population in the early zebrafish neural tube.

In this chapter, I address the following questions, focusing specifically on the zebrafish hindbrain, spinal cord and dorsal telencephalon:

1. How many non-apical progenitors are present in these regions?
2. What is the spatial distribution of non-apical progenitors in these regions?
3. Do non-apical progenitors express *vsx1*, *olig2* or *tbr2*?
4. Does the distribution and characterisation of non-apical progenitors change during early zebrafish neural tube development?

Figure 3-1: The cell types generated by the p2 progenitor domain in the ventral teleost and murine spinal cord. **A**) Schematic of the progenitor domains of the ventral zebrafish spinal cord, p0 – p3, the neurons each domain gives rise to and the genes expressed in each neuronal type. (Adapted from: Ribes & Briscoe 2009; England et al. 2011.) **B**) The lineage of the p2 progenitor domain. V2 intermediate progenitor cells divide to generate V2a and V2b interneuron pairs (adapted from Kimura et al. 2008). **C**) In rodents the p2 progenitor lineage includes a third neuronal type, V2c, which arises through the diversification of the V2b lineage (adapted from: Panayi et al. 2010).

Figure 3-1

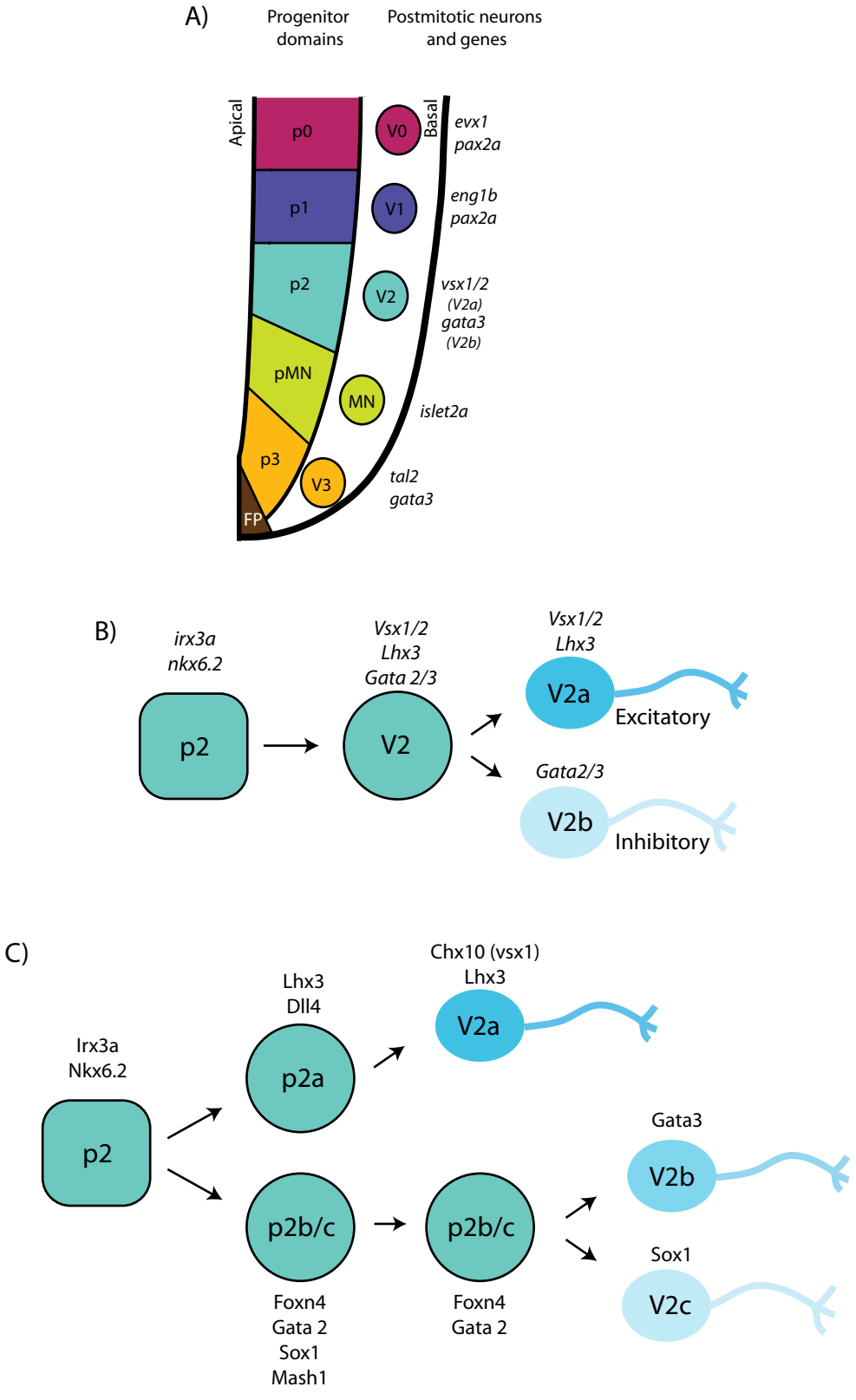
A)
Progenitor domains
Postmitotic neurons and genes
Apical
Basal
p0
p1
p2
pMN
p3
FP
V0
V1
V2
MN
V3
evx1
pax2a
eng1b
pax2a
vsx1/2
(V2a)
gata3
(V2b)
islet2a
tal2
gata3
B)
irx3a
nkx6.2
p2
Vsx1/2
Lhx3
Gata 2/3
V2
Vsx1/2
Lhx3
V2a
Excitatory
Gata2/3
V2b
Inhibitory
C)
Irx3a
Nkx6.2
p2
Lhx3
Dll4
p2a
Chx10 (vsx1)
Lhx3
V2a
p2b/c
Foxn4
Gata 2
Sox1
Mash1
p2b/c
Foxn4
Gata 2
Gata3
V2b
Sox1
V2c

3.2 Materials and Methods

3.2.1 Transgenic zebrafish lines

The transgenic zebrafish lines used in this chapter are described in the General Materials and Methods.

3.2.2 Immunohistochemistry

Primary antibodies, secondary antibodies and counterstains used in this chapter are listed in the General Materials and Methods.

3.2.3 mRNA constructs

Following mRNA constructs were used in this chapter. Synthesis of mRNA is described in the General Materials and Methods.

Construct	Referred to as:	Stage used	Source	Amount injected	Reference
***GFP-CAAX* (from human)**	Membrane - GFP	8-32 cell	(Alexandre et al. 2010)	0.25-0.5 nl of 0.1 µg/µl	(Alexandre et al. 2010)
***mCherry-CAAX* (from human)**	Membrane - RFP	8-32 cell	(Alexandre et al. 2010)	0.25-0.5 nl of 0.1 µg/µl	(Alexandre et al. 2010)
***Histone H_2B (H_2b)-RFP* (from human)**	Nuclear-RPF	8-32 cell	(Alexandre et al. 2010)	0.25-0.5 nl of 0.1 µg/µl	(Alexandre et al. 2010)

3.2.4 Imaging

The hindbrain and spinal cord of fixed embryos were imaged dorsally and the telencephalon was imaged frontally, ensuring that the entire Sytox counterstained region is captured (**Figure 2-1**). A z-step size of 0.35-0.5 µm was used to allow digital transverse reconstructions of the neural tube to be made (see 3.2.5.1, below). Live imaging was performed with 2-3 µm z-step sizes to ensure that nuclei and divisions could be visualized. Z-stacks were captured every 5 mins.

3.2.5 Image analysis

Apical divisions were defined as PH3-positive cells in contact with the apical surface, visible as a gap in the nuclear counterstain. Non-apical divisions were defined as PH3-positive cells at least one cell diameter from the apical surface, which can be determined by the presence of a Sytox counterstained nucleus in between PH3 signal and the apical surface.

3.2.5.1 Generating transverse reconstructions

Confocal z-stacks where digitally resliced to generate transverse views referred to as ‘transverse reconstructions’ using the ‘Orthoslicer’ function in IMARIS®.

3.2.5.2 Drift correction

Drift in x, y and z in live imaging movies was corrected using the drift correction option within the ‘spots’ function in IMARIS®.

3.3 Results

It has previously been shown by Kimura and colleagues that the Tg(*vsx1*:GFP) line labels a population of non-apical neuronal progenitors in the spinal cord (Kimura et al. 2008). This was the first indication that the developing zebrafish central nervous system contained non-apical progenitors. However, it remains unknown what the size of the non-apical progenitor population is, whether or not *vsx1* marks the whole population of non-apical progenitors in the zebrafish neural tube, or what the contribution of non-apical progenitors might be to neurogenesis.

To further characterise non-apical divisions throughout zebrafish embryonic development, wild type and transgenic embryos were fixed at 24, 36, 48 and 72 hpf and mitoses were visualised using the anti-phospho histone H3 (PH3) antibody. High z-resolution confocal z-stacks were obtained of the hindbrain, spinal cord (both dorsal views) and telencephalon (frontal view) of these embryos. A nuclear counterstain (Sytox) was used to reveal the general morphology of the neural tube, allowing clear identification of the apical surface and basal edge of the tissue. From these images it is possible to visualise where cells are entering mitosis within the tissue. Mitotic cells were considered non-apical if they were at least one cell diameter away from the apical surface (discernable by the presence of a nuclei in between the division and the ventricle). Furthermore, quantification of the total number of PH3-positive cells was used as a proxy for overall proliferation in the regions we have analysed.

This approach, analysing mitoses in fixed embryos, allowed me to carry out an unbiased search for all non-apical divisions in the hindbrain, spinal cord and dorsal telencephalon at multiple stages throughout embryonic development. I specifically looked at:

- The number of non-apical progenitors in the tissue.
- Spatial distribution of cells along the dorsoventral and apicobasal axis.
- Co-expression of non-apical PH3 and our genes of interest (*vsx1*, *olig2* and *tbr2*).

3.3.1 Spinal cord

The spinal cord remains a small and relatively simple structure throughout embryonic development. At 24 hpf it is an elliptically shaped primitive neural tube with a lumen located at the midline of the tissue, visible as a distinctive gap in the nuclear counterstain (**Figure 3-2**). At this stage neuroepithelial cells constitute the majority of the tissue and they all maintain connection to the apical surface. As neurogenesis progresses and neuroepithelial cells differentiate, the VZ shrinks. This causes the lumen to change shape, starting around 48 hpf, converting the lumen into the central canal, which is located in the ventral portion of the spinal cord (dotted line **Figure 3-2**G and H; Salta et al. 2014). This process continues until approximately 52 hpf.

3.3.1.1 Non-apical divisions are found in the ventral spinal cord during early neurogenesis

In order to visualize and characterize non-apical progenitor populations in the developing embryonic spinal cord I imaged a 5-somite length of the spinal cord, approximately between somite 9 and 14, and analysed dorsal views and transverse reconstructions of z-stacks of the tissue. While the majority of mitoses are located on the apical surface, a small number of mitoses are found at the basal surface of the neural tube 24, 36, 48 and 72 hpf (arrowheads in **Figure 3-2**A-H).

Quantification of the total number of PH3-positive cells in each 5-somite length of spinal cord shows that proliferation in the spinal cord peaks at 36 hpf (mean ± SEM = 35.11 ± 1.69 PH3+ cells; n = 9 embryos; **Figure 3-2**I). The number of mitotic cells then decreases towards zero at 72 hpf (mean ± SEM = 3.43 ± 1.41 PH3+ cells; n=7 embryos).

On average only one non-apical division was observed per 5-somite length of spinal cord from 24 to 48 hpf (mean ± SEM = 24 hpf: 1 ± 0.43, n = 7 embryos. 36 hpf: 1.11 ± 0.31; n = 9 embryos. 48 hpf: 0.67 ± 0.33; n = 7 embryos; **Figure 3-2**J). I have only observed 1 non-apical division at 72 hpf (n = 19 embryos, **Figure 3-2**D and H). Non-apical progenitors represent around 3% of all divisions in the spinal cord between 24 and 48 hpf (% ± SEM: 24 hpf = 3.4 ± 1.5; 36 hpf = 3.2 ± 0.9; 48 hpf = 3.3 ± 1.7). Reconstructions in the transverse plane show that non-apical divisions are located within a particular ventral region of the spinal cord throughout early development (**Figure 3-2**E-H). Furthermore, non-apical mitoses coexpress HuC/D (**Figure 3-2**K-N; 86%, n = 4 embryos), which is often assumed to be a neuronal protein.

In summary, these data show that the spinal cord contains a small yet stable population of non-apical progenitors in the first three days of embryonic development, which are restricted to a ventrolateral region of the developing spinal cord.

Figure 3-2: Non-apical progenitors in the spinal cord are found in a specific dorsoventral location. Single z-slices of dorsal views (**A**-**D**) and transverse reconstructions (**E**-**H**, dorsal is up) of the spinal cord at 24 hpf (**A** and **E**), 36 hpf (**B** and **F**), 48 hpf (**C** and **G**) and 72 hpf (**D** and **H**) embryos showing immunoreactivity for PH3 (mitotic cells, magenta) and counterstained with Sytox (nuclei, blue). Mitoses can be seen at the apical and basal surfaces. Arrowheads show non-apical divisions. Dashed line shows the basal surface. Gap in Sytox staining at the midline shows the apical surface, highlighted by the dotted line in C, D, G and H. Scale bars show 20 μm. **I**) Graph showing the average number (± SEM) of PH3-positive cells per 5-somite length of spinal cord. Asterisks refer to P values from Tukey's multiple comparisons test of one-way ANOVA ($F = 47.29$; $P < 0.0001$; d.f. = 3, 25). **J**) Graph showing the mean number ± SEM of non-apically located PH3-positive cells in a 5-somite length of the spinal cord. The number of non-apical mitoses does not vary significantly through embryonic development (Kruskal-Wallis; $H = 7.343$; d.f. = 4,29; $P = 0.0617$). **K**-**N**) Single z-slice of a dorsal view of the spinal cord of a 36 hpf embryo counterstained for nuclei (Sytox, blue, K) and showing immunoreactivity for HuC/D (green, L) and PH3 (magenta, M). A non-apical mitotic cell is circled; showing immunoreactivity for HuC/D. Apical surface is shown by dotted line. Scale bars show 20 μm.

Figure 3-2

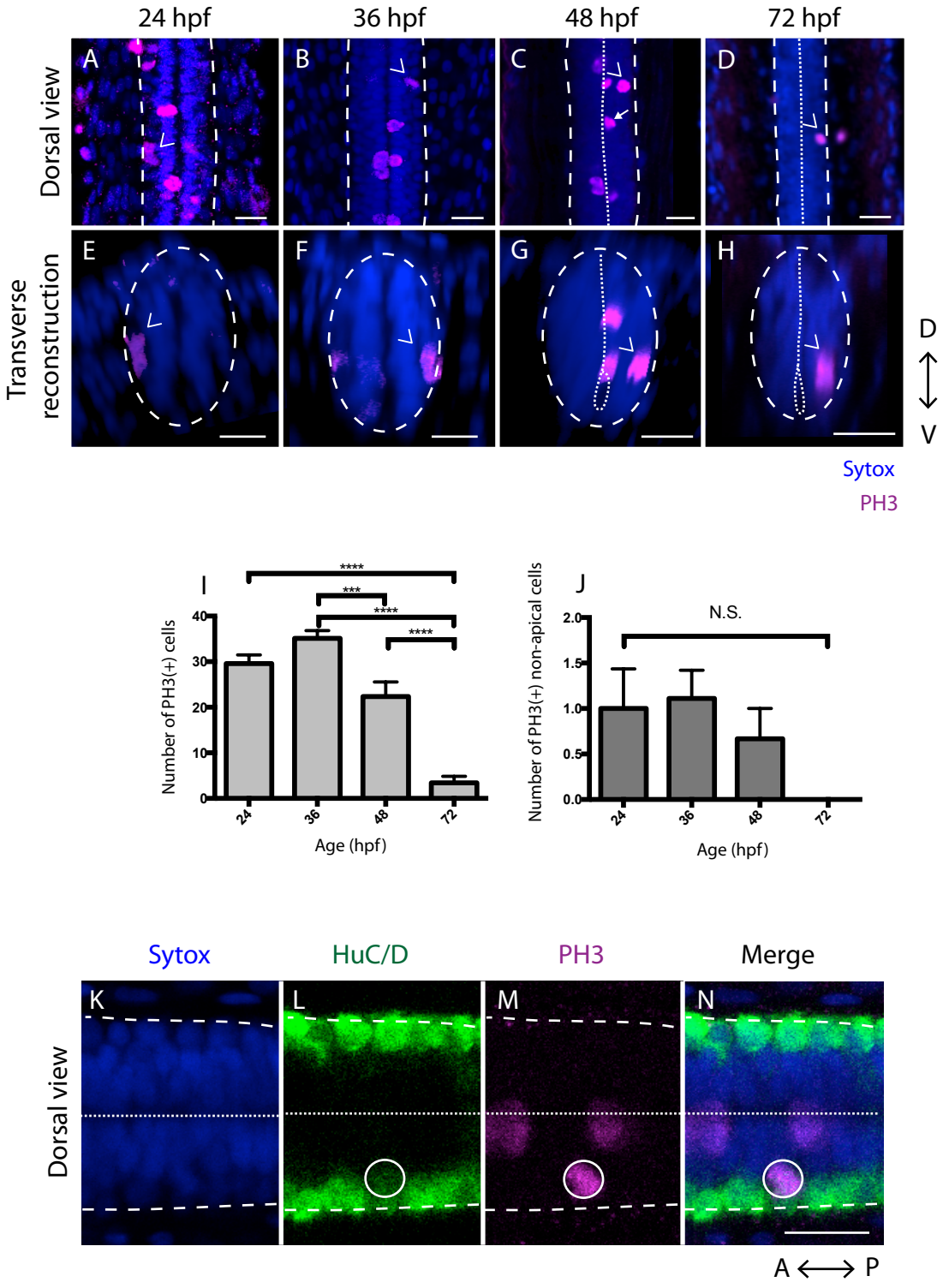
24 hpf
36 hpf
48 hpf
72 hpf
Dorsal view
Transverse reconstruction
A
B
C
D
E
F
G
H
D
V
Sytox
PH3
I
Number of PH3(+) cells
Age (hpf)
****
***
****
****
J
Number of PH3(+) non-apical cells
N.S.
Age (hpf)
Sytox
HuC/D
PH3
Merge
K
L
M
N
Dorsal view
A ⟷ P

3.3.1.2 Non-apical progenitors in the spinal cord express *vsx1*:GFP

Currently the only published non-apical neuronal progenitor population in zebrafish expresses *vsx1*:GFP (Kimura et al. 2008). To determine what proportion of the observed population of non-apical progenitors express *vsx1*:GFP I examined PH3 immunolabelled cells in *vsx1*:GFP embryos. I only looked at 24 – 48 hpf embryos as I found that the non-apical progenitors are extremely scarce at 72 hpf. At 24 hpf, *vsx1*:GFP expression can be seen in a few cells in the developing spinal cord in dorsal 3D reconstructions (mean ± SEM = 55.8 ± 5.69 *vsx1*:GFP+ cells per 5-somite length; n = 5 embryos; **Figure 3-3**A and J). These cells are located at the basal edge of the neural tube (**Figure 3-3**A and D) and limited growth of axons is observed at this stage (arrow in **Figure 3-3**D). In dorsal views at 36 and 48 hpf the *vsx1*:GFP axon tracts running along the anteroposterior axis are more visible and a greater number of GFP-expressing cells can be seen (mean ± SEM = 36 hpf: 100.25 ± 9.93 vsx1+ cells per 5-somites; n = 4 embryos; **Figure 3-3**B and J. 48 hpf: 178 ± 13.6 vsx1+ cells per 5-somites; n = 4 embryos; **Figure 3-3**C and J). Reconstructions in a transverse plane show that *vsx1*:GFP-expressing cells are restricted to a ventral domain of the spinal cord (**Figure 3-3**D-I).

I next looked at PH3 immunoreactivity in Tg(*vsx1*:GFP) embryos. At 24 hpf almost all non-apical mitoses expressed *vsx1*:GFP (9/10 PH3-positive cells express *vsx1*:GFP; n = 5 embryos; **Figure 3-4**A, B and G). At 36 hpf and 48 hpf approximately 80% of non-apical divisions expressed *vsx1*:GFP (36 hpf: 4/6 PH3-positive cells express *vsx1*:GFP; n = 4 embryos; **Figure 3-4**C, D and G. 48 hpf; 7/9 PH3-positive cells express *vsx1*:GFP; n = 5 embryos; **Figure 3-4**E, F and G). These data show that the majority of non-apical divisions in the spinal cord express *vsx1*.

To confirm this I analysed mitoses in time-lapse movies taken of the spinal cord of Tg(*vsx1*:GFP) embryos. The zebrafish spinal cord is well suited to live imaging experiments, mostly due to the transparency of the embryos. In this model system, cell divisions in the whole spinal cord from 18 – 30 hpf can be monitored by the injection of mRNA encoding nuclear-RFP at the 1 cell stage and following changes in the morphology of the nucleus. I carried out this experiment in Tg(*vsx1*:GFP) embryos in order to see if all non-apical mitoses do in fact express *vsx1*:GFP. In these movies, all observed nuclear-RFP labelled nuclei that underwent non-apical division also expressed *vsx1*:GFP (**Figure 3-5**A and **Supplementary Movie 3-1**; n = 6 embryos). This supports the data obtained from fixed embryos, that suggests almost all non-apical divisions express *vsx1* at 24 hpf (**Figure 3-4**). In these movies, *vsx1*:GFP cells appear in a spaced or periodic pattern along the anteroposterior axis of the spinal cord at 20 hpf, and the next *vsx1*:GFP neurons appear in the intervening space (**Figure 3-5**B; **Supplementary Movie 3-2**; and discussed in detail in Chapter 4)

Taken together these data show that *vsx1* is expressed by all non-apical progenitors from 18 to 28 hpf but as development and neurogenesis progresses, the proportion that express this marker decreases to around 80%. As *vsx1*:GFP-expressing cells have previously been shown to generate pairs of V2a/V2b interneurons, the majority of non-apical progenitors in the zebrafish spinal cord directly contribute to the production of these spinal cord interneurons.

Figure 3-3: *Vsx1* expression in the embryonic spinal cord is restricted to a single dorsoventral domain throughout embryonic development. Single z-slices of dorsal view (**A**-**C**) and transverse reconstructions (**D**-**F**) of the spinal cord of Tg(*vsx1*:GFP) embryos (green) counterstained with Sytox (nuclei, blue). A dashed line shows the basal surface, apical surfaces are shown by gap in nuclei at the midline of the tissue. *Vsx1*:GFP signal is initially seen in a small number of individual cells at the basal surface (A) and restricted to a ventral region of the spinal cord at 24 hpf (D). The number of *vsx1*:GFP-expressing cells increases at 36 and 48 hpf (B and C, respectively and J). Axons can be seen extending ventrally, shown by arrow in D and F. **G**-**I**) Schematic representations of the location of *vsx1*:GFP expression on the dorsoventral axis. Green boxes represent region of GFP expression, blue line shows the basal surface and the orange line shows the apical surface. **J**) Graph showing the average number of *vsx1*:GFP-expressing cells at different stages of development.

Figure 3-3

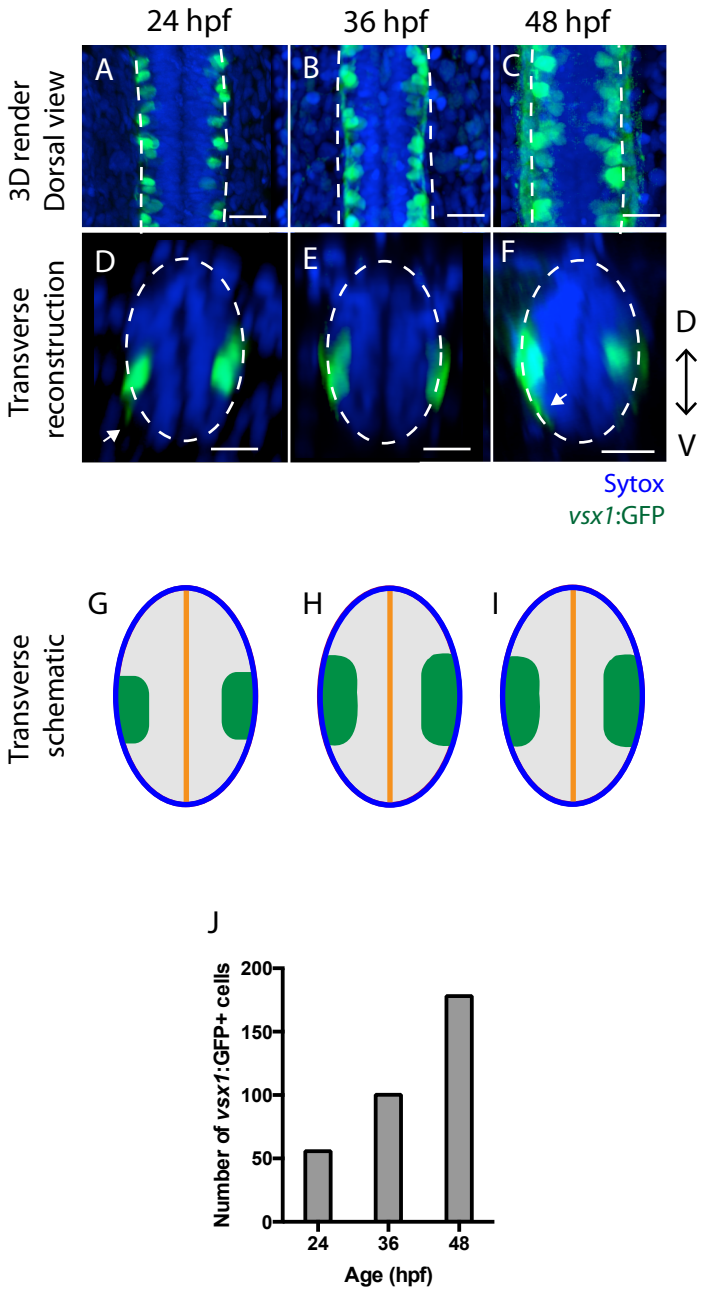
24 hpf
36 hpf
48 hpf
3D render
Dorsal view
A
B
C
Transverse
reconstruction
D
E
F
D
V
Sytox
vsx1:GFP
Transverse
schematic
G
H
I
J
Number of vsx1:GFP+ cells
200
150
100
50
0
24
36
48
Age (hpf)

Figure 3-4: Non-apical progenitors in the spinal cord express *vsx1:*GFP. Single z-slices of dorsal views (A, C and E) and transverse reconstructions (B, D and F) of the spinal cord of *vsx1*:GFP (green) expressing embryos showing immunoreactivity for PH3 (mitotic cells, magenta) and counterstained with Sytox (nuclei, blue). These images show non-apical mitoses expressing *vsx1*:GFP at 24 (A and B), 36 (C and D) and 48 hpf (E and F). A dashed line shows the basal surface, apical surface is shown by gap in nuclei at the midline of the tissue or dotted lines. Arrowheads show non-apical divisions. Scale bars = 20 μm. **G**) Graph showing the percentage of non-apical divisions observed expressing *vsx1*:GFP. Between 24 and 48 hpf a high proportion of non-apical progenitors express *vsx1*:GFP.

Figure 3-4

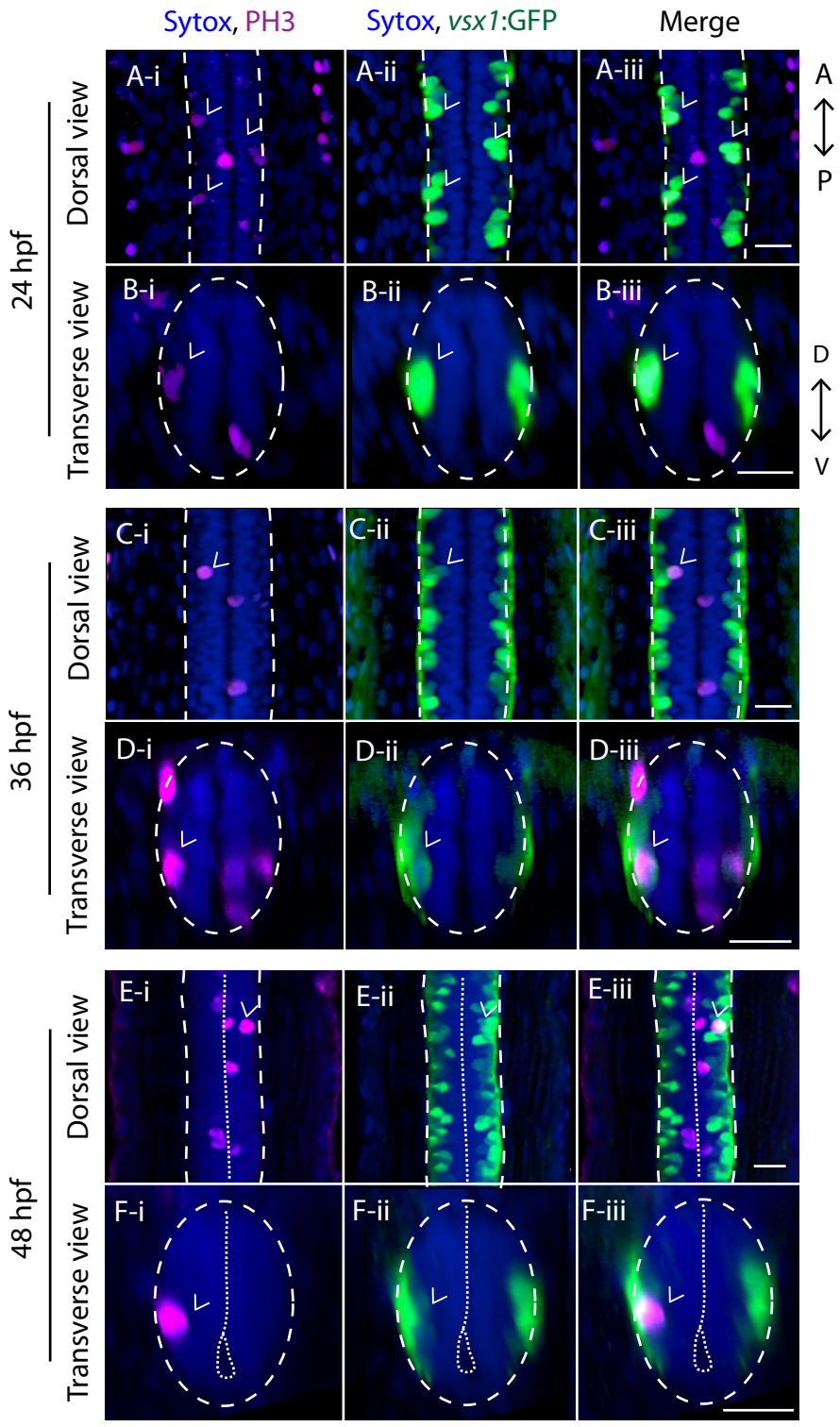
Sytox, PH3
Sytox, vsx1:GFP
Merge
24 hpf
36 hpf
48 hpf
Dorsal view
Transverse view
A-i
A-ii
A-iii
B-i
B-ii
B-iii
C-i
C-ii
C-iii
D-i
D-ii
D-iii
E-i
E-ii
E-iii
F-i
F-ii
F-iii
A
P
D
V

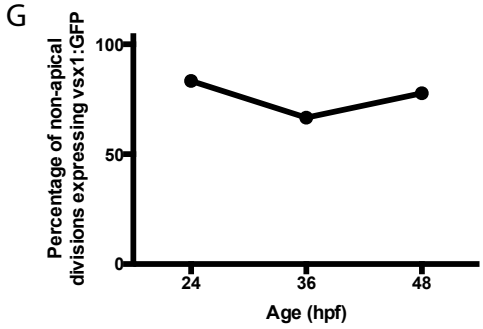
G
Percentage of non-apical divisions expressing vsx1:GFP
100
50
0
24
36
48
Age (hpf)

Figure 3-5: Live imaging in the early embryonic spinal cord shows the whole population of non-apical divisions at 24 hpf expresses *vsx1*:GFP. **A)** 3D reconstruction of a non-apical mitosis in Tg(*vsx1*:GFP) embryos injected with nuclear-RFP and imaged from 18 – 30 hpf. Divisions can be observed by change in the morphology of the nucleus. In (**i**) the nucleus is rounded and the separated chromosomes can be observed in (**ii**). The nuclei of the daughter cells can be seen to condense again from 10 mins after division (**iii**). All of the mitoses observed in a non-apical location expressed *vsx1*:GFP. **B**) Early in development *vsx1*:GFP cells show a long distance spacing pattern along the anteroposterior axis (**i**). Later on, new *vsx1*:GFP cells appear in the intervening space (**ii**). The first dividing cells are shown by blue dots and later dividing cells are shown by purple dots. Dotted line shows the apical surface and dashed line shows the basal surface. Scale bar = 25 μm.

Figure 3-5

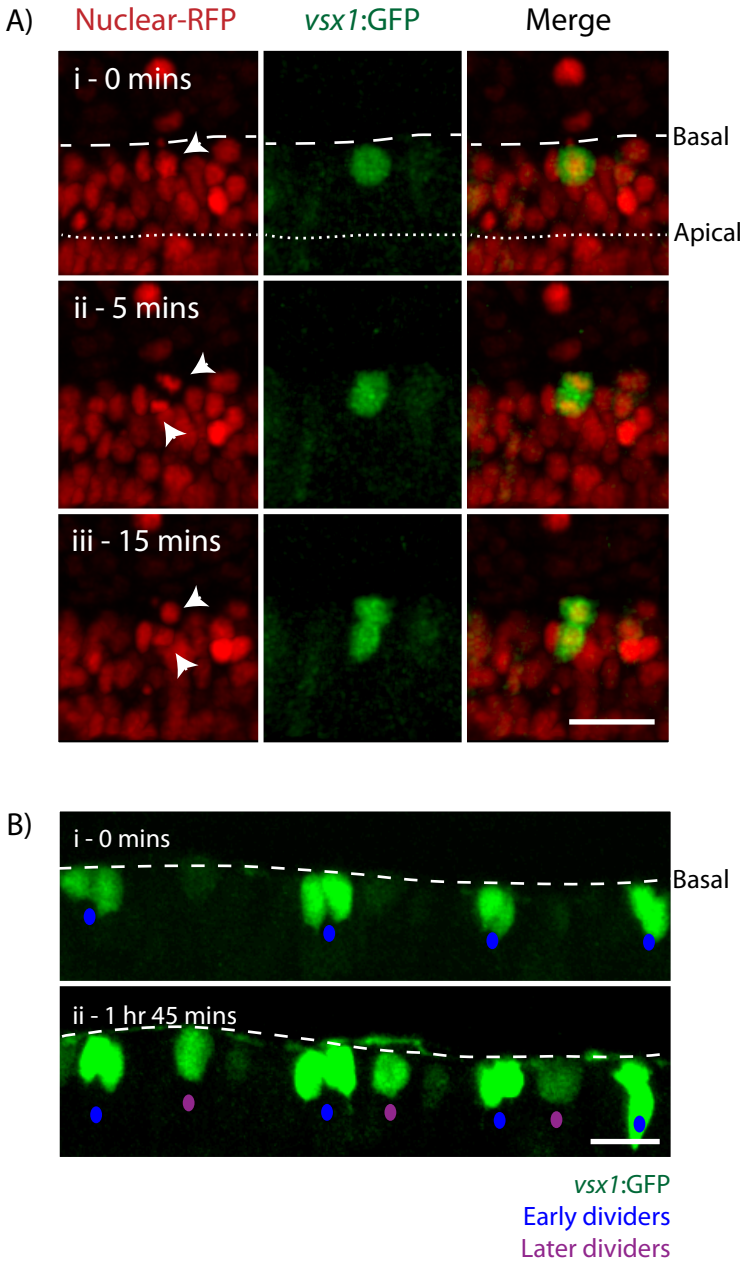
A)
Nuclear-RFP
vsx1:GFP
Merge
i - 0 mins
ii - 5 mins
iii - 15 mins
Basal
Apical
B)
i - 0 mins
ii - 1 hr 45 mins
Basal
vsx1:GFP
Early dividers
Later dividers

3.3.1.3 A small proportion of spinal cord non-apical progenitors express *olig2*

Our data characterizing non-apical progenitors in the embryonic spinal cord has identified that a small proportion of non-apical progenitors do not express *vsx1*. These non-apical mitoses are still restricted to a ventrolateral region of the tissue and are most common at time points that correspond to later stages of neurogenesis and the onset of gliogenesis (36 hpf and later). IT has previously been shown that oligodendrocyte precursor cells (OPCs) undergo non-apical divisions during spinal cord gliogenesis (Roberts & Appel 2009). OPCs are derived from the *olig2*-expressing pMN progenitor domain located directly ventral to the *vsx1*-expressing V2 domain (**Figure 3-1**A). Therefore, the molecularly unidentified proportion of non-apical progenitors in the spinal cord might be derived from the pMN domain, which expresses *olig2*:GFP. From 24–48 hpf GFP expression in the Tg(*olig2*:GFP) reporter line is found in cells in the ventral spinal cord (**Figure 3-6**). At 24 hpf I observed non-apical mitoses just dorsal to the *olig2*:GFP expression domain, but none expressing this transgene (**Figure 3-7**B and I). At 36 and 48 hpf, a small population of non-apical progenitors coexpress *olig2*:GFP (36 hpf: 3/9 PH3-positive cells; n = 5 embryos; arrowheads in **Figure 3-7**D; example of an *olig2*-negative PH3 cells shown by an arrowhead in **Figure 3-7**E. 48 hpf: 2/7 PH3-positive cells; n = 6 embryos; arrowheads in **Figure 3-7**F-G; example of an *olig2*-negative PH3 cells shown by arrowhead in **Figure 3-7**H. **Figure 3-7**I shows the quantification).

From this data we can say that the pMN progenitor domain marker *olig2*:GFP is expressed in a small proportion of spinal cord non-apical progenitors during embryonic development. This suggests that non-apical progenitors contribute to the generation of the progeny of this progenitor domain; although whether or not these progenitors contribute a specific cell type (motor neurons, interneurons or oligodendrocytes) is currently unknown.

3.3.1.4 Non-apical progenitors in the spinal cord – summary and conclusion

I have identified a small population of non-apical mitoses in the developing zebrafish spinal cord that are present from 24 to 48 hpf. The size of this population stays constant over this developmental period, despite an increase in the total number of proliferating cells. The non-apical progenitors in the spinal cord appear to be restricted to a ventral region of the spinal cord. Further analysis revealed that the spinal cord contains two molecularly distinct populations of non-apical progenitors during early zebrafish development. At 24 hpf nearly all non-apical progenitors express *vsx1* and at 36 and 48 hpf a large proportion of the non-apical progenitor population express this marker (approximately 80%). A smaller population express *olig2* at 36 and 48 hpf (20-30%). It is likely that *vsx1* and *olig2* together mark the entire population of non-

apical progenitors. These data indicate that non-apically dividing progenitor cells contribute to the generation of *vsx1* interneurons as well as progeny of the *olig2*+ progenitor domain.

Figure 3-6: *olig2*:GFP is expressed ventrally in the spinal cord. Dorsal views (**A**, **B** and **C**) and transverse reconstructions (**D**, **E** and **F**, dorsal is up) of the spinal cord of *olig2*:GFP-expressing embryos (green) counterstained for nuclei (Sytox, blue). At 24 (**A** and **D**), 36 (**B** and **E**) and 48 (**C** and **F**) hpf ventral cells in the spinal cord express *olig2*:GFP. A dashed line shows the basal surface. The gap in the nuclei at the midline of the tissue shows the apical surface. Scale bars show 20 μm. **G-I**) Schematic representations of the location of *olig2*:GFP expression. Dorsal is up. Green regions represent GFP expression, blue line shows the basal surface and the orange line shows the apical surface.

Figure 3-6

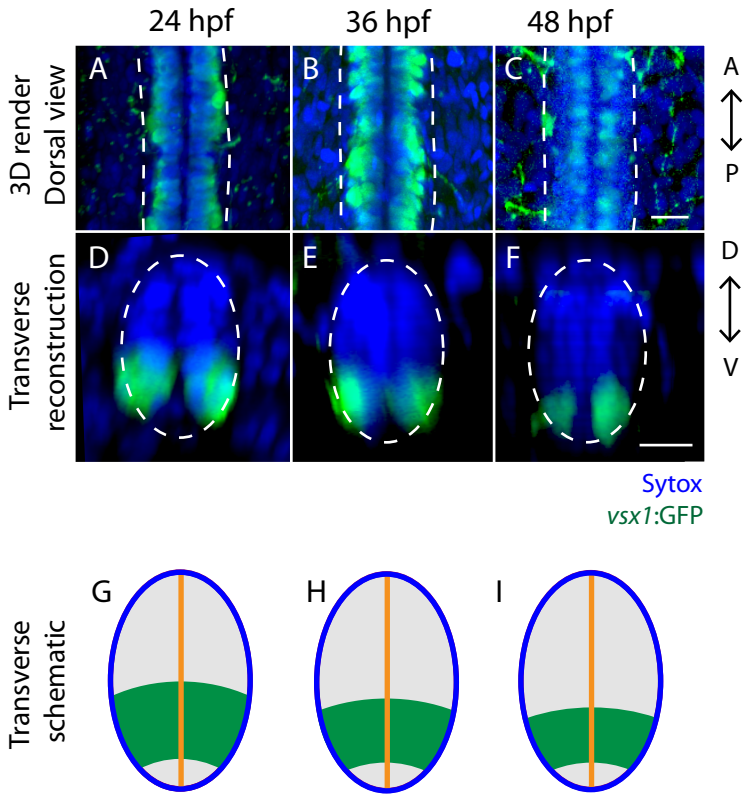
24 hpf
36 hpf
48 hpf
3D render
Dorsal view
A
B
C
A
P
Transverse
reconstruction
D
E
F
D
V
Sytox
vsx1:GFP
Transverse
schematic
G
H
I

Figure 3-7: A small proportion of non-apical progenitors express *olig2*:GFP during embryonic development. Dorsal views (**A**, **C** and **F**) and transverse reconstructions (**B**, **D, E, G** and **H,** dorsal is up) of the spinal cord of *olig2*:GFP-expressing embryos (green) showing immunoreactivity for PH3 (mitotic cells, magenta) and counterstained with Sytox (nuclei, blue). **A** and **B**) At 24 hpf, non-apical mitoses are found adjacent to *olig2*:GFP-expressing cells, but are rarely seen expressing GFP. At 36 (**D**) and 48 hpf (**G**) a number of non-apical mitoses express *olig2*:GFP, shown by empty arrowheads. At these time points, PH3 cells are also found adjacent to, but not coexpressing *olig2*:GFP (**E** and **H**, respectively). A dashed line shows the basal surface, apical surfaces are shown by gap in nuclei at the midline of the tissue or by a dotted line. Scale bars show 20 μm. **G**) Graph showing the percentage of non-apical divisions observed expressing *olig2*:GFP.

Figure 3-7; Page 1

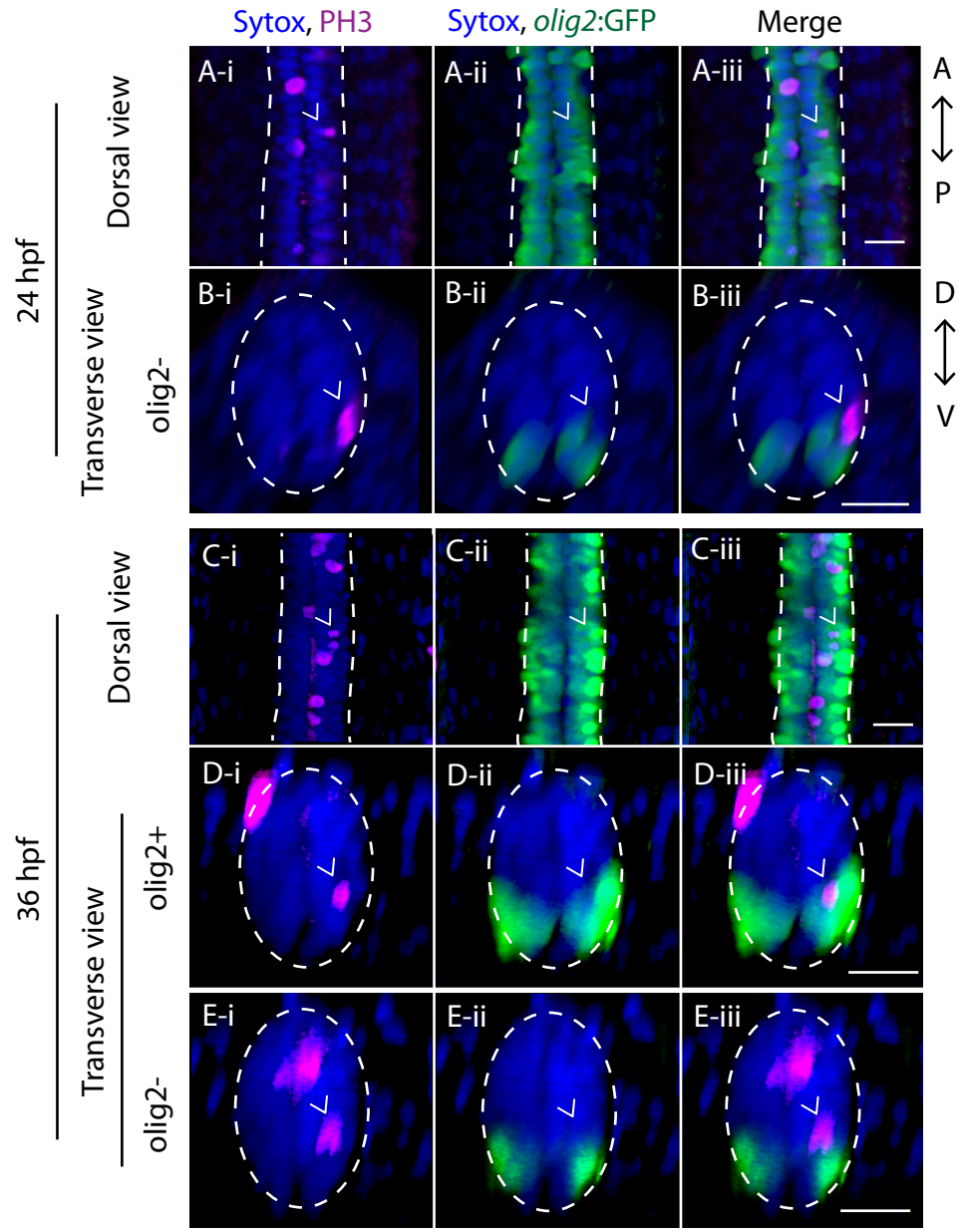

Figure 3-7; Page 2

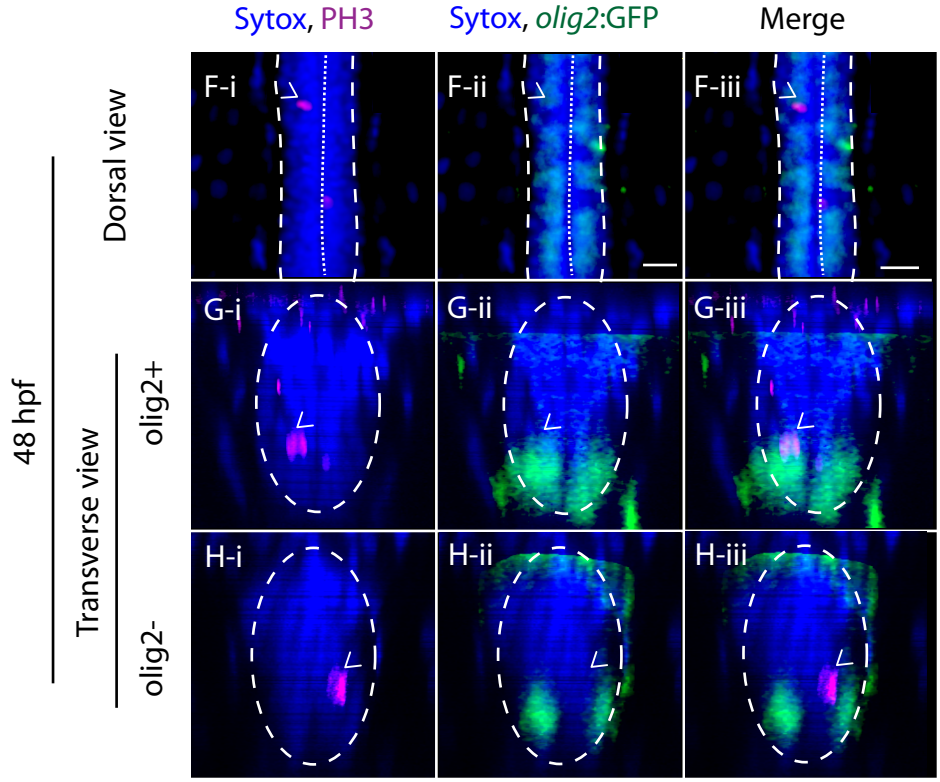

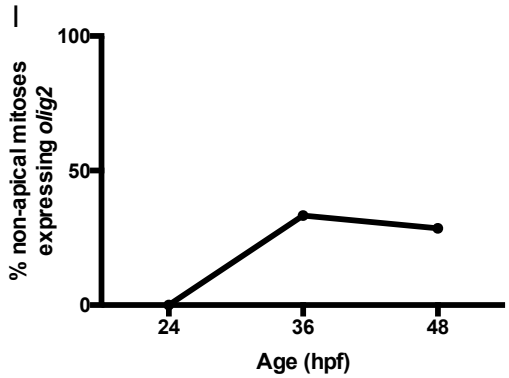

3.3.2 Hindbrain

The zebrafish hindbrain undergoes large-scale morphological change and growth between 17 and 24 hpf. Shortly after the apical surface is formed at the midline of the neural tube (around 17 hpf), the two lateral sides of the tube separate to create a lumen that then inflates to form the fourth ventricle. During this process the dorsal most aspect of the tube expands, the roof plate thins and stretches as the rhombic lips move apart. This results in a Y-shaped apical surface of the neural tissue facing the ventricle from 24 hpf (**Figure 3-8**). The neuroepithelial cells maintain contact with the apical and basal surfaces through this morphological change, resulting in each cell taking on a curved morphology (shown schematically in **Figure 3-8**K-M). Neuroepithelial cells continue to divide at the apical surface and the neurons migrate basally into the mantle zone, which gradually increases in size through embryonic development (Lyons et al. 2003). The marginal layer, which contains the axons and dendrites (neuropil) of the neurons, is located on the ventrolateral aspect of the neural tube at 24 hpf and then on the ventral aspect of the hindbrain at 36 and 48 hpf (light grey area, **Figure 3-8**K-M).

In order to analyse the location of divisions in the developing hindbrain in comparable regions across multiple embryos, I analysed the tissue from the caudal border of rhombomere 2 to 150 μm posterior to the otic vesicles.

3.3.2.1 Non-apical progenitors are present in three spatial locations in the hindbrain

Most mitoses are found at the apical surface in the hindbrain, visible as a gap in the nuclear counterstain (**Figure 3-8**A-J). The number of mitotic cells peaks at 36 and 48 hpf (mean ± SEM = 36 hpf: 163.38 ± 20.3; n = 8 embryos. 48 hpf: 161.13 ± 31.1; n = 8 embryos; **Figure 3-8**N). The number of proliferative cells decreases dramatically to 19.6 (± 3.4) mitotic cells per hindbrain at 72 hpf (n = 5 embryos; **Figure 3-8**N). Non-apical PH3-expressing mitoses can be seen in dorsal views and transverse reconstructions of the tissue (arrowheads in **Figure 3-8**A-J). There is a significant increase in the number of non-apical divisions observed from 24 hpf to 48 hpf (**Figure 3-8**O). As well as increasing in number as development progresses, non-apical progenitors represent an increased proportion of all mitotic cells (% ± SEM 24 hpf = 3.3 ± 1; 36 hpf = 7.2 ±1.7; 48 hpf =17.9 ± 3.8). No non-apical progenitors were observed in the hindbrain at 72hpf (**Figure 3-8**O).

Transverse reconstructions of the hindbrain indicate that non-apical progenitors are spatially restricted at 24 hpf, appearing in a ventral region reminiscent of where I observed non-apical mitosis in the spinal cord (**Figure 3-8**D). At this stage all non-apical divisions appear to take place on the basal edge of the mantle zone (**Figure 3-8**D). However, at 36 and 48 hpf non-apical

divisions occur in different spatial compartments: (1) at the basal extremity of the mantle zone in the ventromedial quadrant of the tissue (ventromedial basal; VMB; **Figure 3-8**E and F); (2) a cell diameter or more away from both the apical and basal surface (subapical; SA; **Figure 3-8**G and H); and (3) on the basal surface of the hindbrain in the dorsolateral quadrant (dorsolateral basal; DLB; **Figure 3-8**I and J). The spatial distribution of non-apical mitoses does not differ significantly between 36 and 48 hpf, **Figure 3-8**O). These non-apical mitotic cells are found on the edge of HuC/D-labelled marginal zone in the hindbrain and the majority show immunoreactivity for HuC/D (percentage coexpressing ± SEM: 59.4 ± 14.9; n = 3 embryos; **Figure 3-8**Q-S).

The observation that non-apical mitoses are found in three spatial locations the hindbrain suggests that different subpopulations of non-apical neural progenitors may exist in the hindbrain.

3.3.2.2 A subpopulation of hindbrain non-apical progenitors express *vsx1*:GFP

In the spinal cord the majority of non-apical progenitors express *vsx1*:GFP. I wanted to determine if the non-apical progenitors in the hindbrain also express *vsx1*. Three dimensional renders of dorsal views of the hindbrain at 24 hpf show a small number of cells expressing *vsx1*:GFP at 24 hpf and that the number increases through 36 and 48 hpf (**Figure 3-9**A-C). Transverse reconstructions of the tissue (**Figure 3-9**i and ii, taken at dotted lines in **Figure 3-9**A-C) show that these cells are restricted to a dorsal region of the tissue at 24 and 36 hpf (**Figure 3-9**Ai, D, Bi, Bii and E) and that at 48 hpf in some regions there is a dorsolateral zone of *vsx1*:GFP expression (arrow in **Figure 3-9**Ci and F).

Next, I looked at PH3 immunoreactivity in Tg(*vsx1*:GFP) embryos. At 24hpf, all observed non-apical mitoses expressed *vsx1*:GFP (6/6 PH3-positive cells; n = 4 embryos; **Figure 3-10**A, B and K), but at 36 and 48 hpf the number of non-apical divisions expressing *vsx1:*GFP drops to around half (36 hpf: 35/51 PH3-positive cells; n = 5 embryos; **Figure 3-10**C-F and K. 48 hpf: 36/89 PH3-positive cells; n = 5 embryos **Figure 3-10**G-K). Within the different spatial populations in the hindbrain, at 36 hpf almost all VMB and SA divisions coexpressed *vsx1*:GFP (18/22 VMB PH3+ cells; 17/18 SA PH3+ cells; n = 5 embryos; **Figure 3-10**), while no coexpressing DLB cells were observed (0/11 DLB PH3+ cells, n=5 embryos). At 48 hpf, the proportion of VMB and SA divisions expressing *vsx1*:GFP decreased (2/5 VMB PH3+ cell; 28/70 SA PH3+ cells; n = 5 embryos, **Figure 3-10**L) and an increased number of DLB divisions expressed *vsx1*:GFP (6/14 DLB PH3+ cells, n = 5 embryos, **Figure 3-10**L). In summary, *vsx1* expression in spatial subgroups of non-apical progenitors in the hindbrain shifts during the first three days of development.

Figure 3-8: Non-apical divisions are found in multiple spatial locations in the developing embryonic hindbrain. **A-J**) Wild type embryos showing immunoreactivity for PH3 (mitotic cells, magenta) and counterstained for nuclei with Sytox (blue). Single z-slices of dorsal views of the hindbrain at 24 hpf (**A**), 36 hpf (**B**), 48 hpf (**C**) show PH3-positive cells at non-apical locations (arrowheads). Insets show higher magnifications of the boxed regions. **D-J**) Transverse reconstructions allow the visualisation of the location of non-apical divisions on the dorsoventral and mediolateral axis in the hindbrain. At 24 hpf basal divisions are located on the basal extremity of the mantlezone (**D**), while at 36 hpf and 48 hpf divisions can be seen at ventromedial basal (**E** and **F**), subapical (**G** and **H**) and dorsolateral basal locations (**I** and **J**). Dashed line shows basal surface. OV = otic vesicle. Scale bars show 20 μm. **K-M**) Schematic diagrams illustrating the structure of the hindbrain from a transverse view, at the level of the otic vesicle at 24 hpf (**K**), 36 hpf (**L**) and 48 hpf (**M**). The dark grey shows the mantlezone, which contains the cell bodies and can be visualized using a nuclear counterstain and the light grey shows the marginal zone containing the axons. The orange line shows the apical surface, the solid blue line shows the basolateral surface and the dashed blue line shows the basal extremity of the mantlezone. The shape of neuroepithelial cells is shown by black lines and circles, which represent nuclei. Purple regions represent the three spatial locations non-apical progenitors are found in. **N**) Graph showing the average number (± SEM) of divisions in the hindbrain through early development. Asterisks refer to P values from Tukey's multiple comparisons test of one-way ANOVA ($F = 11.64$; $P < 0.0001$; d.f. = 3, 24). **O**) Graph showing the average number (± SEM) of non-apical divisions in the hindbrain at each stage. Asterisks refer to P values from Tukey's multiple comparisons test of (Kruskal-Wallis; $U = 22.86$; d.f. = 4,28; $P < 0.0001$). **P**) Graph showing the proportion of non-apical divisions occurring in each spatial compartment. The number of non-apical mitoses in each location is significantly different (Two-way ANOVA, $F(1,36) = 0.8752$; $MSE = 174.1$; $P = 0.4255$) but the number of non-apical mitoses in each location does not change significantly between 36 and 48 hpf (Two-way ANOVA, $F(2,36) = 9.14 \times 10^{-15}$; $MSE = 1.819 \times 10^{-15}$; $P > 0.99$). **Q-R**) 36 hpf wild type embryo showing immunoreactivity for HuC/D (green) and PH3 (magenta) and counterstained for nuclei (Sytox, blue). Non-apical mitotic cells are found on the medial edge of HuC/D expression and express HuC/D. Dotted line shows the apical surface. Scale bars show 20 μm. DLB = dorsolateral basal, SA = subapical, VMB = ventromedial basal.

Figure 3-8

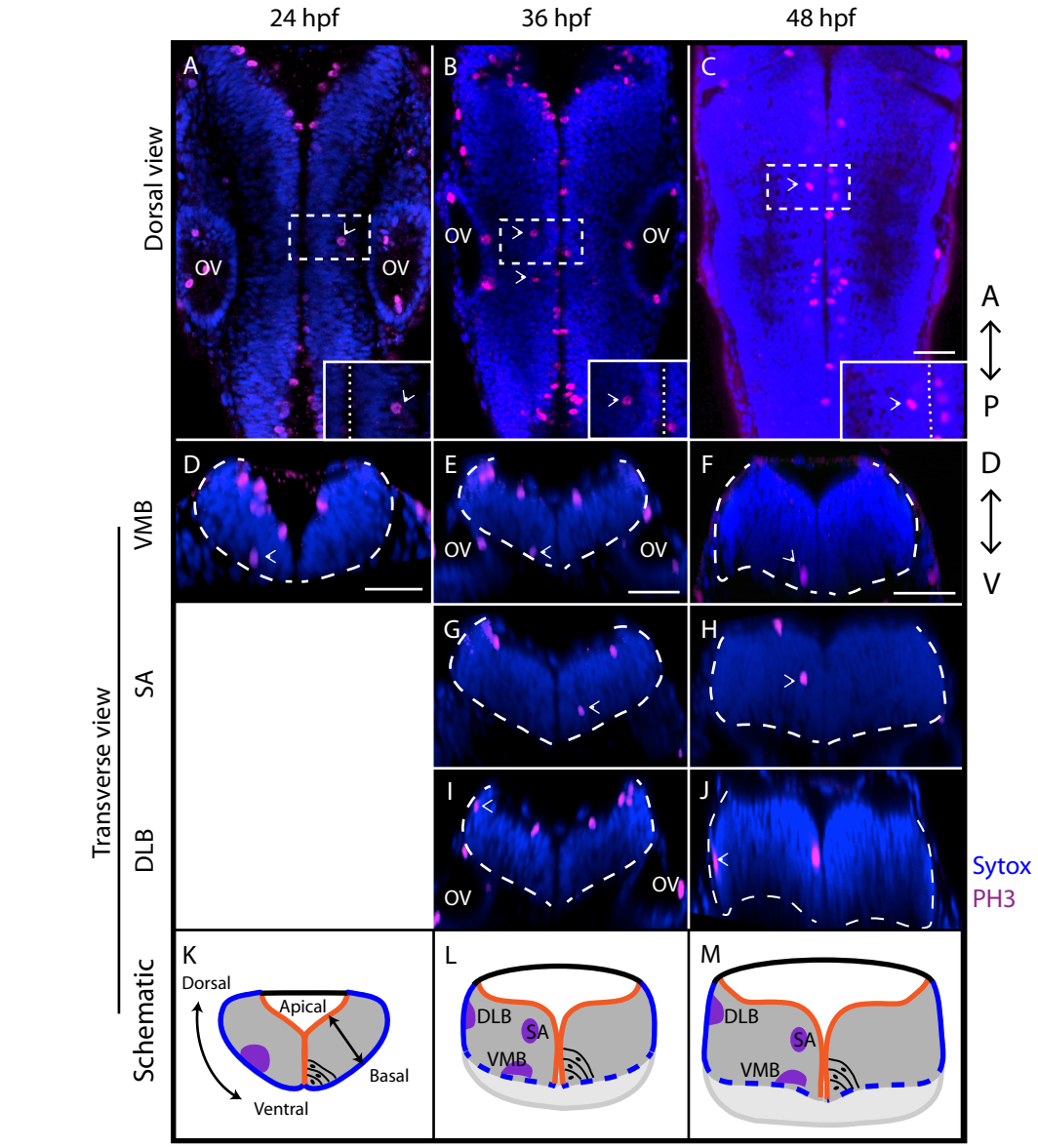
24 hpf
36 hpf
48 hpf
Dorsal view
Transverse view
VMB
SA
DLB
Schematic
A
P
D
V
Sytox
PH3
OV
Dorsal
Apical
Basal
Ventral
DLB
SA
VMB

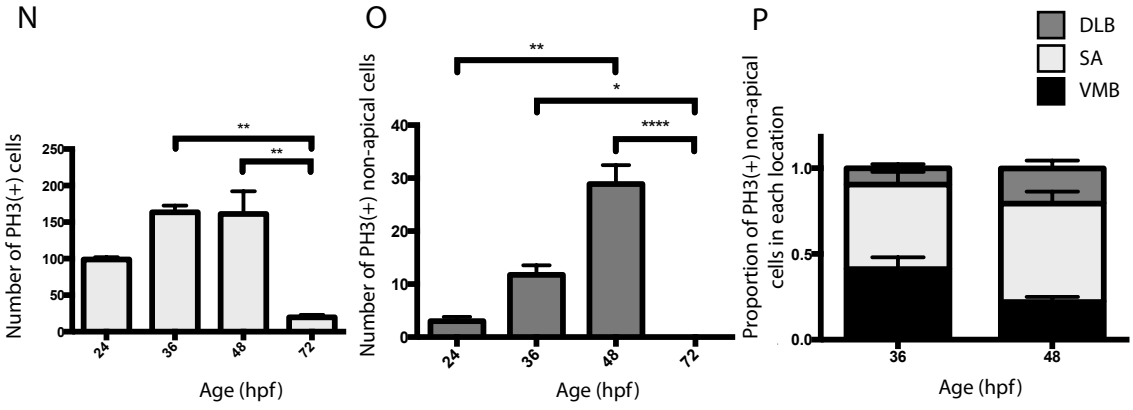
N
Number of PH3(+) cells
Age (hpf)
O
Number of PH3(+) non-apical cells
Age (hpf)
P
Proportion of PH3(+) non-apical cells in each location
DLB
SA
VMB
Age (hpf)

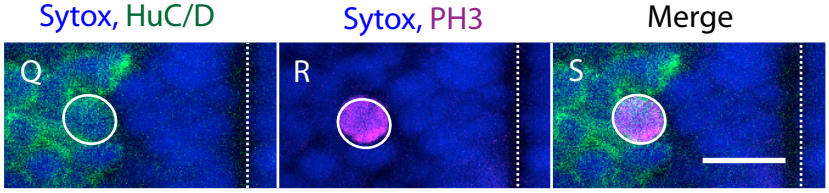
Sytox, HuC/D
Sytox, PH3
Merge
Q
R
S

Figure 3-9: Expression of *vsx1*:GFP in the hindbrain. **A-C**) Dorsal views of 3D renders of the hindbrain of Tg(*vsx1*:GFP) embryos (anterior is up), counterstained for nuclei (Sytox, blue) at 24 (**A**), 36 (**B**) and 48 hpf (**C**) show increasing numbers of *vsx1*:GFP cells through development. Transverse reconstructions (labelled **i** or **ii,** taken at dotted lines in A-C; dorsal is up) of the tissue show that *vsx1*:GFP expression is limited to a ventral region of the neural tube. At 48 hpf there is also some *vsx1*:GFP expression in the dorsolateral quadrant (Ci, shown by an arrow). Dashed line shows the basal surface. **D-F**) Schematic representations of the location of *vsx1*:GFP expression in transverse views. Green area shows *vsx1*:GFP expression. The orange line shows the apical surface, solid blue line shows the basolateral surface and dashed blue line shows the basal extremity of the mantlezone. Scale bars = 25 μm.

Figure 3-9

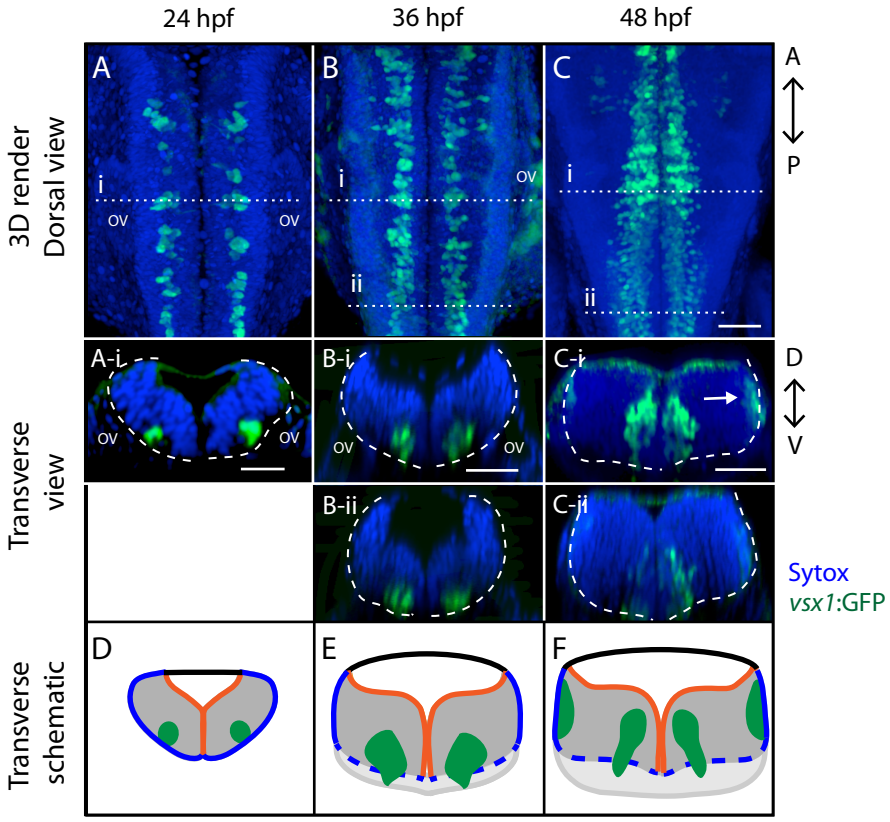
24 hpf
36 hpf
48 hpf
3D render
Dorsal view
Transverse
view
Transverse
schematic
A
B
C
i
ii
ov
A
P
D
V
A-i
B-i
C-i
B-ii
C-ii
D
E
F
Sytox
vsx1:GFP

Figure 3-10: A large proportion of non-apical progenitors in the hindbrain express *vsx1*. Single z-slices of dorsal views (anterior is up) or transverse reconstructions (dorsal is up) of the hindbrain of Tg(*vsx1*:GFP) (green) embryos at 24 (**A** – **B**) , 36 (**C** – **F**) and 48 (**G** – **J**) hpf showing immunoreactivity for PH3 (magenta) and counterstained with Sytox (nuclei, blue). Insets show a higher magnification of the boxed region in the dorsal views. At 24 hpf, non-apical progenitors (arrowheads) can be seen expressing *vsx1*:GFP in dorsal views (**A**) and transverse reconstructions (**B**). At 36 hpf, the *vsx1:*GFP signal colocalises with ventromedial basal and subapical PH3-positive cells (arrowheads in **D** and **E**, respectively), but not with cells dividing in dorsolateral basal locations (**F**). At 48hpf, non-apical mitoses can be seen in dorsal views (**G**) and transverse reconstructions (**H-J**). Examples of non-apical PH3-positive cells coexpressing *vsx1*:GFP in ventromedial basal (**H**), subapical (**I**) and dorsolateral basal (**L**) locations (See arrowheads). OV = otic vesicle. Dashed line shows basal surface. Scale bars = 25 μm. **K**) Graph showing the percentage of non-apical divisions that coexpress *vsx1*:GFP. The asterisks refer to P values from Dunn's multiple comparisons test of Kruskal-Wallis U test (H = 8.427; P = 0.0046; d.f. = 3, 13). **L**) Percentage of non-apical divisions in each location that coexpress *vsx1*:GFP. Asterisks refer to P values from Tukey's multiple comparisons test of two-way ANOVA (F (2,329) = 12.7, P = 0.0001). DLB = dorsolateral basal, SA = subapical, VMB = ventromedial basal.

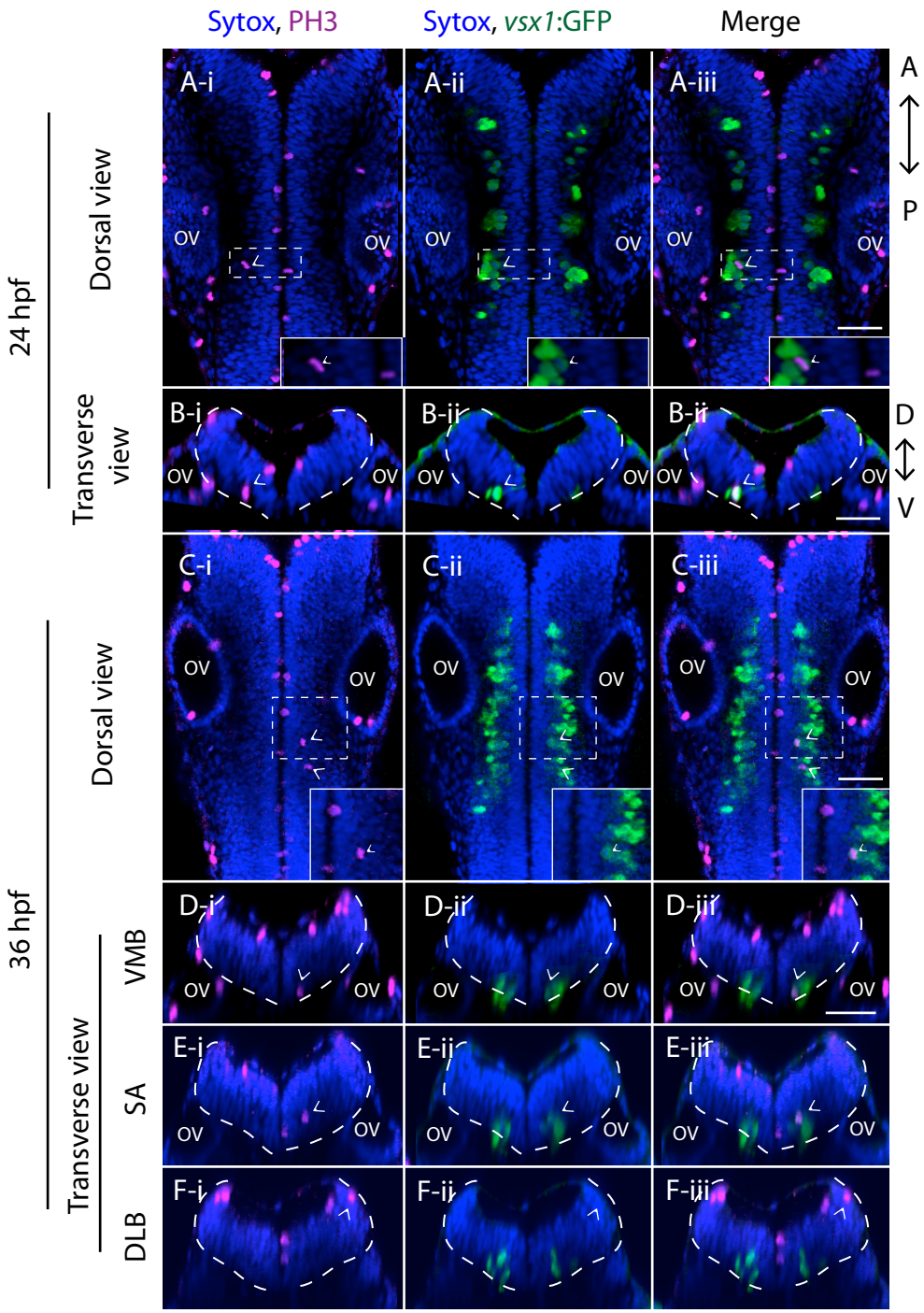
Sytox, PH3
Sytox, vsx1:GFP
Merge
24 hpf
Dorsal view
Transverse view
36 hpf
Dorsal view
Transverse view
VMB
SA
DLB
A-i
A-ii
A-iii
B-i
B-ii
B-iii
C-i
C-ii
C-iii
D-i
D-ii
D-iii
E-i
E-ii
E-iii
F-i
F-ii
F-iii
ov
A
P
D
V

Figure 3-10; Page 2

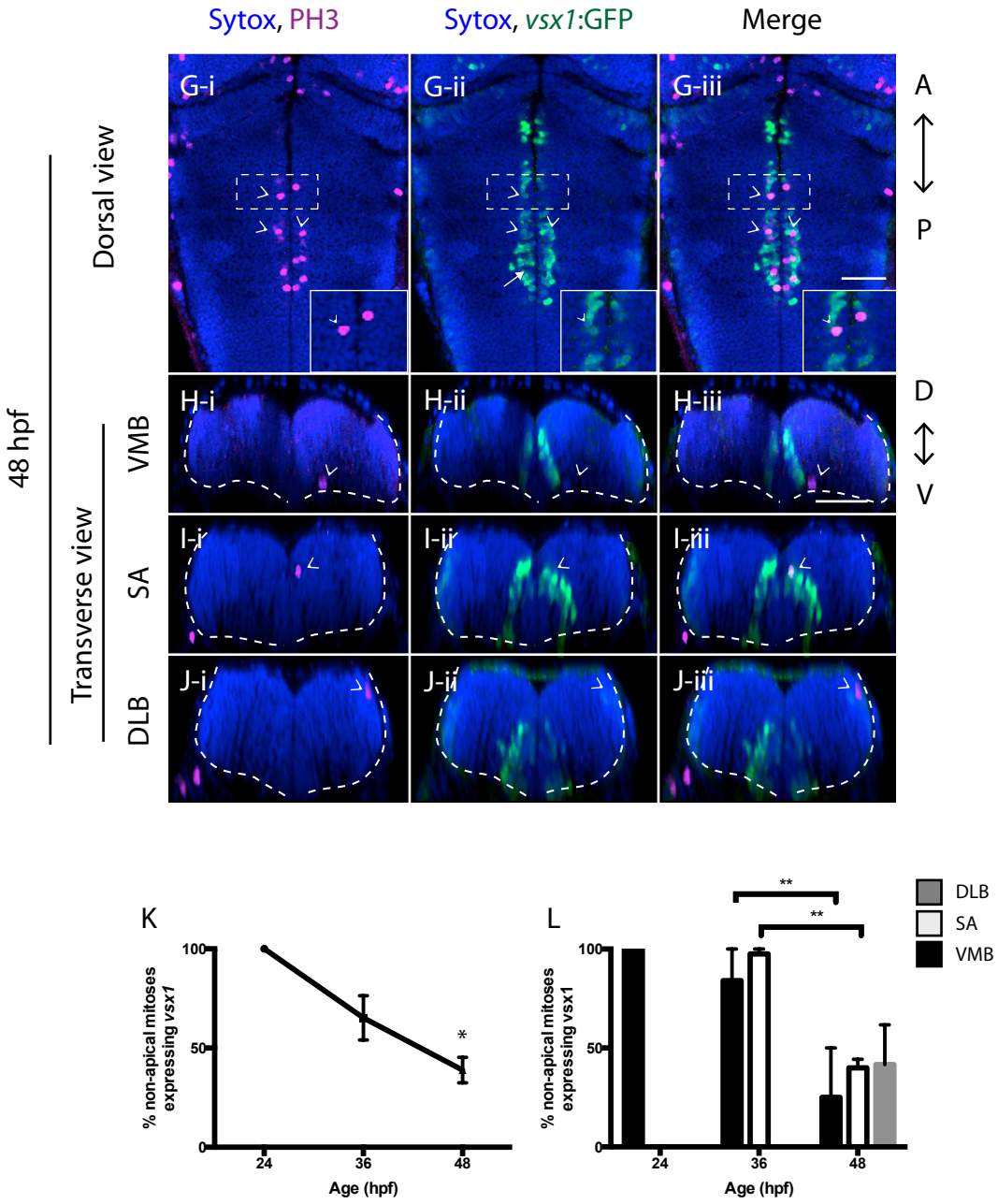

3.3.2.3 *Olig2*-expressing non-apical mitoses are rare in the zebrafish hindbrain

During the first two days of development expression of *olig2*:GFP is limited to a small number of cells in the hindbrain (**Figure 3-11**A-C). At 24 hpf, two spatial groups of *olig2*:GFP-expressing cells are seen: (1) rostral to the otic vesicles, small numbers of *olig2*:GFP cells are visible in a dorsolateral location rostral to the otic vesicles (**Figure 3-11**A and A-i); and (2) a cluster of *olig2*:GFP-expressing cells are present in the ventromedial region of the hindbrain at the level of the otic vesicles (**Figure 3-11**A and A-ii). A similar expression pattern is found at 36 hpf (**Figure 3-11**B-i and B-ii), however at this stage two ventromedial clusters of *olig2*:GFP-expressing cells are seen (**Figure 3-11**B). By 48 hpf the *olig2*:GFP-expressing cells have become more spread throughout the tissue and individual GFP-positive cells can be identified (**Figure 3-11**C). In transverse reconstructions more rostral regions contain dorsolateral *olig2*:GFP-expressing cells (**Figure 3-11**C-i) while adjacent to the otic vesicles there is a ventromedial population of *olig2*:GFP-expressing cells (**Figure 3-11**C-ii). These expression patterns are summarised in the schematic in **Figure 3-11**D-F).

When I analysed PH3-labelled divisions in Tg(*olig2*:GFP) embryos (**Figure 3-12**) I found that, for the most part, in *olig2*:GFP embryos GFP expression appeared in different regions of the hindbrain to where non-apical divisions were seen (**Figure 3-12**). However, I did observe a very small number non-apically dividing cells expressing the pMN progenitor domain marker *olig2*:GFP at 36 hpf (3/76 PH3-positive cells; n = 5 embryos; **Figure 3-12**E and I).

3.3.2.4 Hindbrain summary and conclusions

These data show that the hindbrain contains spatially distinct populations of non-apical progenitors in early embryonic neurogenesis. At 24 hpf the non-apical progenitors are restricted to a ventrolateral region of the tissue, as is seen in the spinal cord. As the tissue grows, at 36 and 48 hpf populations of non-apical progenitors are found in ventromedial basal, subapical and dorsolateral basal locations. The majority of non-apical mitoses in the hindbrain express *vsx1* while a scarce population expresses *olig2,* and at 36 and 48 hpf there is an expanding population of non-apical divisions that do not express either marker. At 36 hpf the non-apical divisions in dorsolateral regions lack *vsx1* expression and by 48 hpf *vsx1* expression in ventromedial basal and subapical progenitors has decreased but increased in the dorsolateral basally dividing cells. We do not know the identity of the *vsx1*:GFP and *olig2*:GFP-negative non-apical progenitors.

Figure 3-11: Expression of *olig2*:GFP in the hindbrain. Dorsal views of a 3D render (A-C, anterior is up) and transverse reconstructions (i and ii, taken at dashed lines in A-C; dorsal is up) of the hindbrain of *olig2*:GFP (green) embryos with nuclear counterstain (Sytox, blue) at 24 (A), 36 (B) and 48 hpf (C). A) At 24 hpf there is a limited amount of *olig2:*GFP expression which includes a small number of cells at the level of the otic vesicle which span the apicobasal axis of the tube in ventromedial regions (A-ii) and a second small region caudal to the otic vesicles which contains GFP signal in a lateral ventral region (A-i). In 36 and 48 hpf embryos the ventromedial population of *olig2:*GFP cells expands along the anteroposterior axis (B and C) and the lateral expression region extends along the dorsoventral axis (B-i and C-i). Dashed lines show the basal surface. OV = otic vesicle. D-F) Schematic representations of the location of *olig2*:GFP expression in transverse views. Green area shows *olig2*:GFP expression. The orange line shows the apical surface, solid blue line shows the basolateral surface and dashed blue line shows the basal extremity of the mantlezone. Scale bars show 25 μm.

Figure 3-11

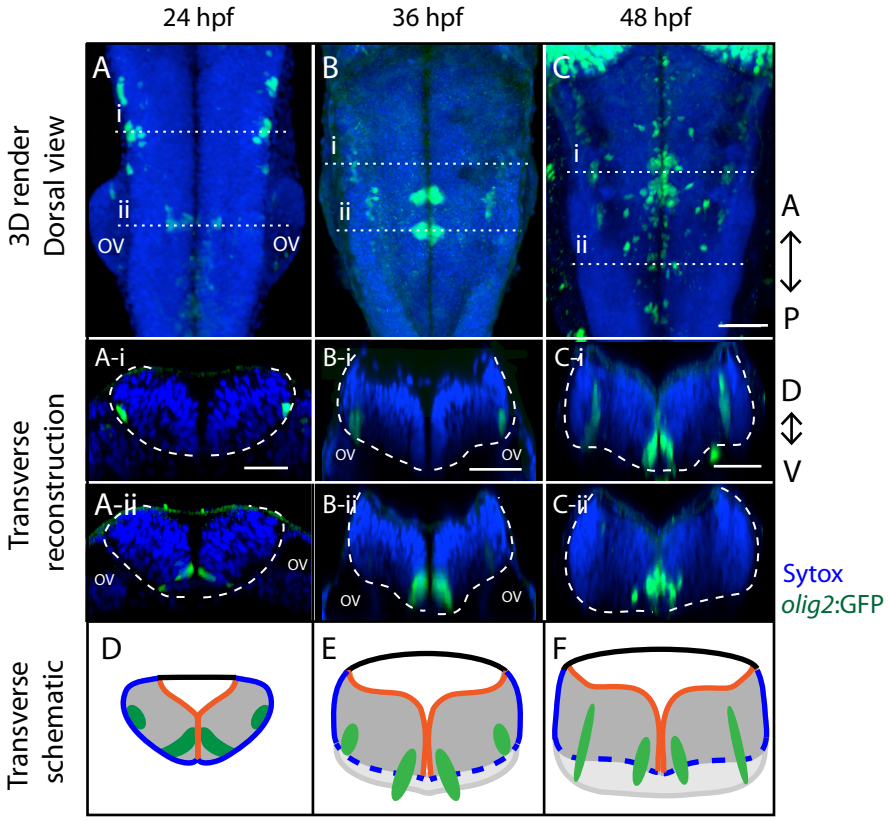
24 hpf
36 hpf
48 hpf
3D render
Dorsal view
Transverse
reconstruction
Transverse
schematic
A
B
C
i
ii
ov
A-i
B-i
C-i
A-ii
B-ii
C-ii
D
E
F
A
P
D
V
Sytox
olig2:GFP

Figure 3-12: Non-apical progenitors in the hindbrain rarely coexpress *olig2*:GFP. Non-apical mitotic cells are shown by arrowheads in single z-slices of dorsal views and transverse reconstructions at 24 (**A** and **B**, respectively), 36 (**C** and **D-E**, respectively) and 48 hpf (**F** and **G**, respectively) of the hindbrain of Tg(*olig2:*GFP) embryos showing immunoreactivity for PH3 (magenta) and counterstained with Sytox (blue). At 36 hpf (D) shows an example of a non-apical mitosis that does not express *olig2*:GFP, while (E) shows an example of a non-apical mitosis that is *olig2*:GFP-positive. OV = otic vesicle. Basal surface by dashed line. Insets show a higher magnification of boxed area in **A**, **C** and **G**. Scale bars show 25 μm. **J)** Percentage of non-apical divisions in each location that coexpress *olig2*:GFP. DLB = dorsolateral basal, SA = subapical, VMB = ventromedial basal.

Figure 3-12

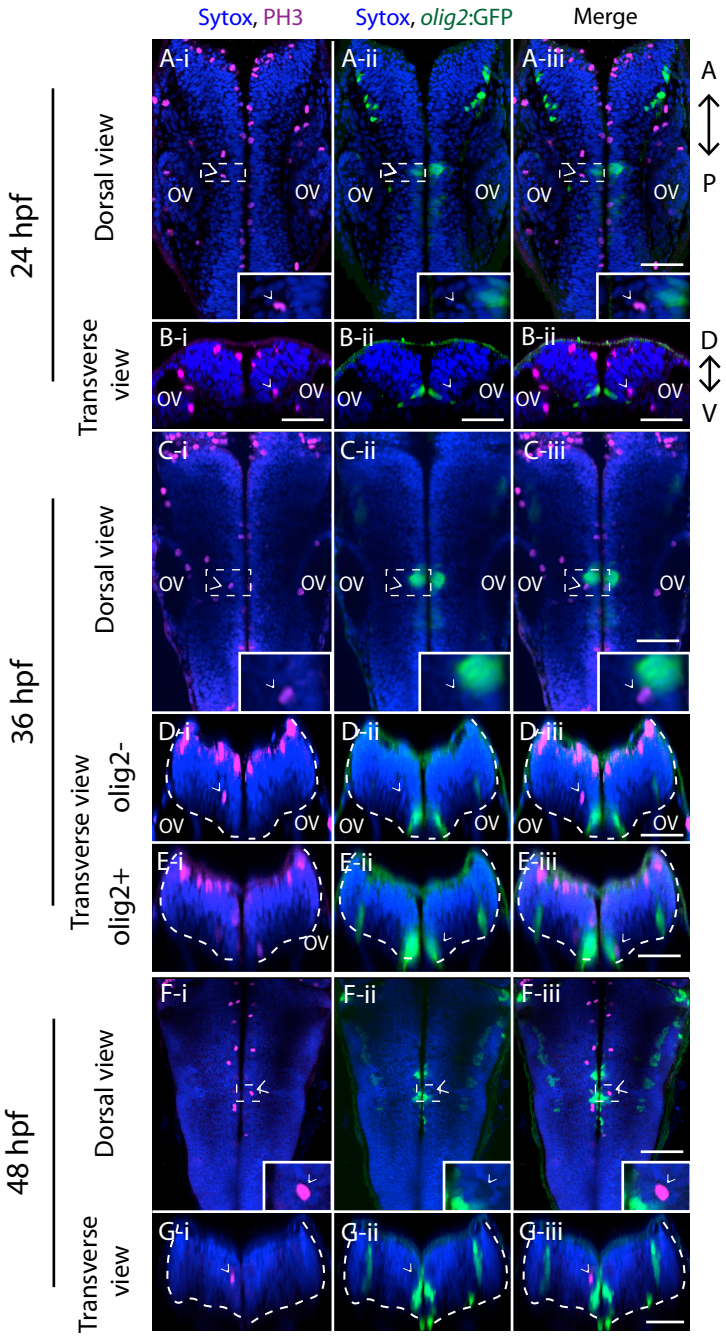
Sytox, PH3
Sytox, olig2:GFP
Merge
24 hpf
36 hpf
48 hpf
Dorsal view
Transverse view
olig2-
olig2+
A-i
A-ii
A-iii
B-i
B-ii
B-ii
C-i
C-ii
C-iii
D-i
D-ii
D-iii
E-i
E-ii
E-iii
F-i
F-ii
F-iii
G-i
G-ii
G-iii
ov
A
P
D
V

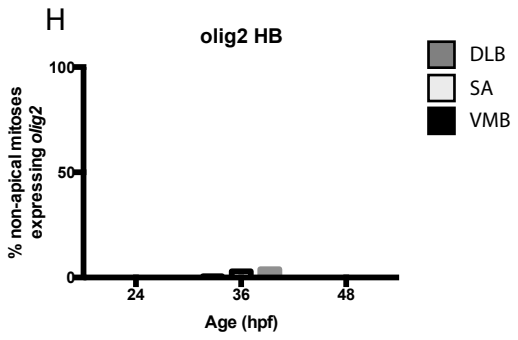
H
olig2 HB
DLB
SA
VMB
% non-apical mitoses expressing olig2
100
50
0
24
36
48
Age (hpf)

3.3.3 Telencephalon

The majority of the current understanding of mammalian non-apical (basal) neuronal progenitors has come from studies of the mammalian neocortex, which develops from the dorsal telencephalon (pallium). Therefore, we were interested to find out whether this region of the zebrafish neural tube also contains non-apical neuronal progenitors. Like all ray-finned fishes, the adult teleost telencephalon has an everted structure, composed of two telencephalic lobes separated by a T-shaped ventricle and covered by a thin tela choroidea, formed by stretching the roof plate over the lobes (see schematics in **Figure 3-13**). This structure is distinct from the hollow telencephalic lobes containing inflated lateral ventricles (evaginated telencephalon) seen in the majority of other vertebrate species.

The developing zebrafish telencephalon has a complex 3D shape and structure that undergoes large scale changes in the first days of development (Folgueira et al. 2012). Like the hindbrain and spinal cord, the zebrafish telencephalon develops from a tube-like tissue. Between 19 and 27 hpf the posterior cells of the two lobes of the pallium are displaced laterally to form the posterior telencephalic wall that faces the anterior intraencephalic sulcus (AIS). Following this, from 2 to 5 dpf the pallium expands along the anteroposterior axis and the posterior telencephalic wall also expands, moving dorsally and posteriorly. The embryonic telencephalon can be considered to have three ventricular surfaces: (1) the medial ventricular surface separates the two telencephalic lobes (MS; **Figure 3-13**); (2) the dorsal surface of the telencephalic lobes (DS; **Figure 3-13**); and (3) the posterior telencephalic wall (PTW; **Figure 3-13**). There is little differentiation in the telencephalon before 36 hpf (Folgueira et al. 2012) so, to most closely match the developmental age range that I examined in the hindbrain and spinal cord, I chose to analyse non-apical divisions in the telencephalon from 36 hpf to 3 dpf.

In order to standardise the region of the telencephalon analysed between specimen and ages, I carried out this characterisation in the *gata2*:GFP enhancer trap lane (Et(*gata2*:GFP)^{bi105}) (Folgueira et al. 2012). This line expresses GPF in neurons in the dorsal pallium and is a good marker of this region of the tissue from 30 hpf (Folgueira et al. 2012). Therefore, I imaged the telencephalon frontally from the most superficial surface to the caudal limit of *gata2*:GFP-expression around the posterior wall of the telencephalon. I split the volume imaged into quarters, where quarter 1 (Q1) is the most frontal and Q4 is the most rostral. Q1 does not contain any *gata2*:GFP-expressing cells as this quadrant contains predominantly the olfactory bulb. Small numbers of *gata2*:GFP-expressing cells are seen in Q2 and the majority of *gata2*:GFP expression is found in Q3 and Q4 from 36 – 72 hpf (**Figure 3-14**).

The number of PH3-positive nuclei in fixed tissue was used to estimate the proliferation in the telencephalon from 36 to 72 hpf. The number of apical divisions starts high at 36 hpf (mean per embryo ± SEM = 72.33 ± 4.78; n = 6 embryos; **Figure 3-15**M) and decreases through embryonic development (48 hpf: mean per embryo ± SEM = 50.40 ± 5.89; n = 5 embryos; 72 hpf: mean ± SEM = 41.80 ± 2.08; n = 5 embryos; **Figure 3-15**M). The number of proliferative cells at 72 hpf is much higher in the telencephalon than the hindbrain or spinal cord. However, only a very small number of non-apically located PH3+ nuclei were observed in the telencephalon at all stages from 36 to 72 hpf (shown by arrowheads in **Figure 3-15**). These cells are not found at the basal extremity of the telencephalon but instead reside in subapical locations. The number of non-apical mitoses does not change significantly between 36 and 72 hpf (mean per embryo ± SEM = 36 hpf: 0.83 ± 4.78; 1.2% of total divisions; n = 6 embryos; **Figure 3-15**N. 48 hpf: 2.40 ± 0.60; 4.8% of total divisions; n = 5 embryos; **Figure 3-15**N. 72 hpf: 1.00 ± 0.55; 2.4 % of total divisions; n = 5 embryos; **Figure 3-15**N).

Next, to investigate the molecular identity of non-apical progenitors in the dorsal telencephalon I looked specifically at *vsx1* and *olig2*, as in the hindbrain and spinal cord, as well as *tbr2*.

3.3.3.1 *Olig2* is not expressed in the zebrafish pallium

In the spinal cord, *olig2*:GFP labels a population of non-apical progenitors that increases over the first 3 days of development. In order to see if the non-apical progenitors in the telencephalon also express *olig2*:GFP I analysed Tg(*olig2*:GFP) transgenic embryos. However, I found that *olig2*:GFP is only expressed in the ventral telencephalon (subpallium) from 24 hpf to 72 hpf (n: 36 hpf = 6 embryos; 48 hpf = 6 embryos; 72 hpf = 7 embryos; data not shown). Therefore, as GFP expression is not seen in the same region of the telencephalon that contains non-apical mitoses, *olig2* is not a marker of non-apical progenitors in the telencephalon.

3.3.3.2 *Tbr2* is expressed in post-mitotic neurons in the telencephalon

In the mammalian cortex, *Tbr2* is expressed in basal intermediate progenitors (bIPs; Englund et al. 2005). However, in the zebrafish neural tube, *tbr2* (eomesa) has only been reported to be expressed in a subset of differentiated neurons in the pallium (Mueller et al. 2008). To address whether *tbr2* might also label non-apical progenitor cells in the zebrafish telencephalon, I carried out immunohistochemistry on 36, 48 and 72 hpf in Tg(*tbr2a*:dsRed) embryos to visualise PH3-expressing cells and nuclei. However, I did not observe any dividing *tbr2*:dsRed-expressing cells (data not shown; n: 36 hpf = 6 embryos; 48 hpf = 5 embryos; 72 hpf = 6 embryos). These data suggests *tbr2* is a marker of post-mitotic neurons in the zebrafish telencephalon, not basal (non-apical) progenitors as is known in the mammalian cortex.

3.3.3.3 *Vsx1* is expressed in the telencephalon and may label non-apical progenitors

Vsx1 expression has been reported in the zebrafish retina, hindbrain and spinal cord by *in situ* hybridisation and GFP expression in the Tg(*vsx1*:GFP) transgenic line (Passini et al. 1998; Kimura et al. 2008). However, I noticed that a small number of cells expressed *vsx1*:GFP in the telencephalon of Tg(*vsx1*:GFP) embryos. To see if this GFP expression is evidence of endogenous *vsx1* expression I carried out *in situ* hybridisation for this gene in 2 dpf Tg(*vsx1*:GFP) embryos. *Vsx1* mRNA-expressing cells are located in medial regions of the pallium, just lateral to the VZ (**Figure 3-16**B and D), while *vsx1*:GFP cells are located more laterally (**Figure 3-16**C and D). There are a small number of cells that express both *vsx1* mRNA and *vsx1*:GFP (arrow head in **Figure 3-16**A-D). As there is little overlap between *vsx1* mRNA and *vsx1*:GFP-expressing cells, it is likely that *vsx1* is only expressed in cells for a short period of time, after leaving the ventricular surface. In this case, as GFP protein is relatively stable its expression acts as a lineage marker, allowing us to follow the fate of cells that once expressed *vsx1* mRNA.

I next looked at PH3-labelled mitoses in 36, 48 and 72 hpf Tg(*vsx1*:GFP) fixed embryos. I did not observe any non-apical mitoses that coexpressed *vsx1*:GFP at these stages (data not shown; n: 36 hpf = 7 embryos; 48 hpf = 6 embryos; 72 hpf = 6 embryos). However, as *vsx1*:GFP expression is visible from earlier in development, I also looked at 24 hpf embryos. In these samples I observed a single *vsx1*:GFP-expressing cell undergoing mitosis in a subapical location (**Figure 3-16**E; n= 8 embryos). This observation suggests that *vsx1* is expressed in a scarce population of non-apical progenitors in the telencephalon at 24 hpf.

3.3.3.4 Telencephalon summary

These data show that between 36 and 72 hpf the zebrafish telencephalon contains a population of non-apical progenitors. These mitotic cells are located in a subapical location, do not express either *olig2* or *tbr2* but a small faction of this population of progenitors might express *vsx1* at 24 hpf. The identity of non-apical progenitors in the telencephalon therefore is currently unknown.

Figure 3-13: Morphology of the telencephalon. Schematics of the 3D structure of the telencephalon (shown in grey). **A**) Dorsal view of the forebrain. Anterior to the left. Dotted lines show the location of B and C. **B**) Schematic parasagittal section, dorsal is up. **C**) Schematic frontal section, dorsal is up. Orange line shows the ventricular surface. Grey line shows tela choroidea. AC: Anterior Commissure; Di: diencephalon; DS: Dorsal surface; Ha: Habenula; MS: Medial surface; PTW: posterior telencephalic wall; OB: Olfactory Bulb; R: rostral; C: caudal; D: dorsal; V: ventral.

Figure 3-13

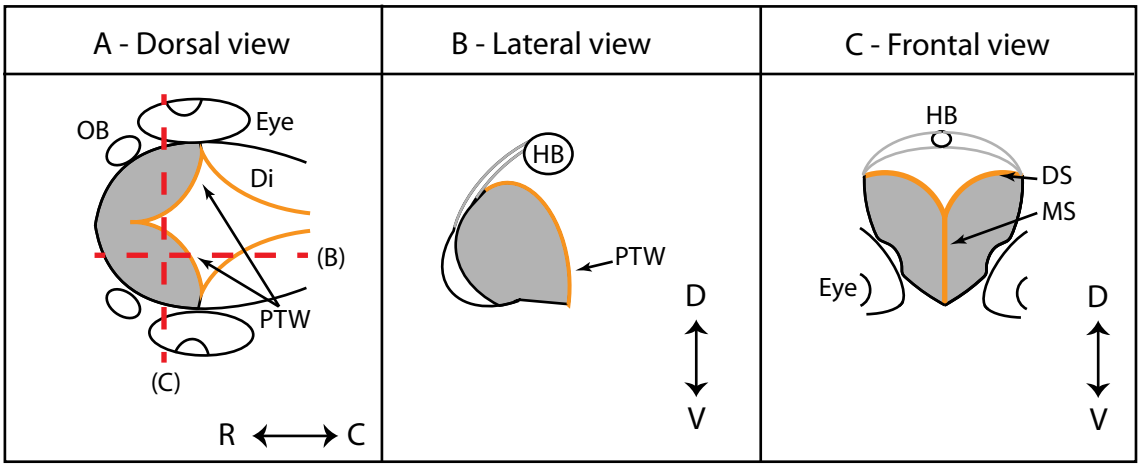
A - Dorsal view
B - Lateral view
C - Frontal view
OB
Eye
Di
(B)
PTW
(C)
R
C
HB
PTW
D
V
HB
DS
MS
Eye
D
V

Figure 3-14: *Gata2* is expressed in neurons in the dorsal telencephalon. **A – L**) Outline of different quartiles of the telencephalon at 36, 48 and 72 hpf showing the approximate location of *gata2*:GFP-expression (green). Orange line shows apical surface and grey line shows the tela choroidea. Q1-Q4: Quartile 1 (Q1) is the most frontal – Q4 is the deepest region. **A' - L'**) Single confocal z-slices of frontal views of the telencephalon of *gata2*:GFP embryos 36, 48 and 72 hpf embryos counterstained for nuclei (Sytox, blue) showing example *gata2*:GFP expression patterns. Dorsal is up. AC: Anterior Commissure; Ha: Habenula; OE: Olfactory Epithelium. Scale bar = 25 μm.

Figure 3-14

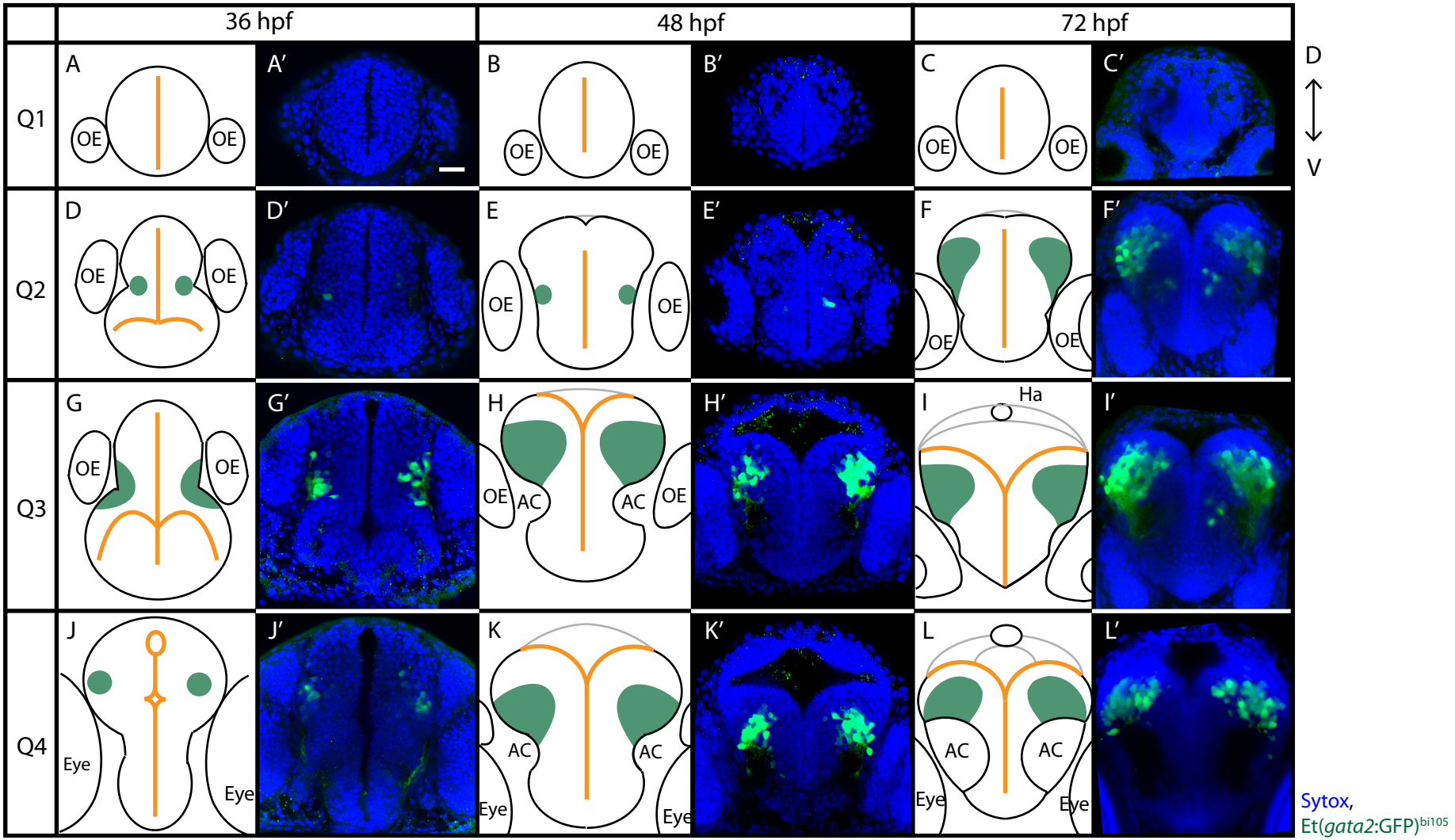
36 hpf
48 hpf
72 hpf
Q1
Q2
Q3
Q4
A
A′
B
B′
C
C′
D
D′
E
E′
F
F′
G
G′
H
H′
I
I′
J
J′
K
K′
L
L′
OE
AC
Eye
Ha
D
V
Sytox,
Et(gata2:GFP)bi105

Figure 3-15: Non-apical divisions in the telencephalon are found in subapical locations. **A – L**) Outline of different quarters of the telencephalon at 36, 48 and 72 hpf show the position of each non-apical mitosis (magenta spots) observed in that quarter. Orange line shows apical surface and grey line shows the tela choroidea. Green regions show the likely location of *gata2*:GFP expression (from **Figure 3-14**). **A' - L'**) Single confocal z-slices of frontal views of the telencephalon of 36, 48 and 72 hpf embryos counterstained for nuclei (Sytox, blue) and immunostained for PH3 (magenta) showing example non-apical divisions (arrowheads). Q1-Q4: Quarters 1 (Q1) is the most frontal – Q4 is the deepest region. Dorsal is up. AC: Anterior Commissure; Ha: Habenula; OE: Olfactory Epithelium. Scale bar = 25 μm. **M**) Graphs showing the mean (± SEM) number of apical mitoses in the telencephalon per embryo. A significant decrease is seen from 36 to 72 hpf. Asterisks refer to the p value from Dunn's multiple comparisons test of Kruskal-Wallis U test ($H = 9.125$; $P = 0.0041$; d.f. = 3, 16). **N**) Graph showing the mean (± SEM) number of non-apical mitoses in the telencephalon per embryo. The number of non-apical divisions does not vary significantly from 36 to 72 hpf (One-way ANOVA $F(2, 150) = 2.781$, $p < 0.0987$).

Figure 3-15; Page 1

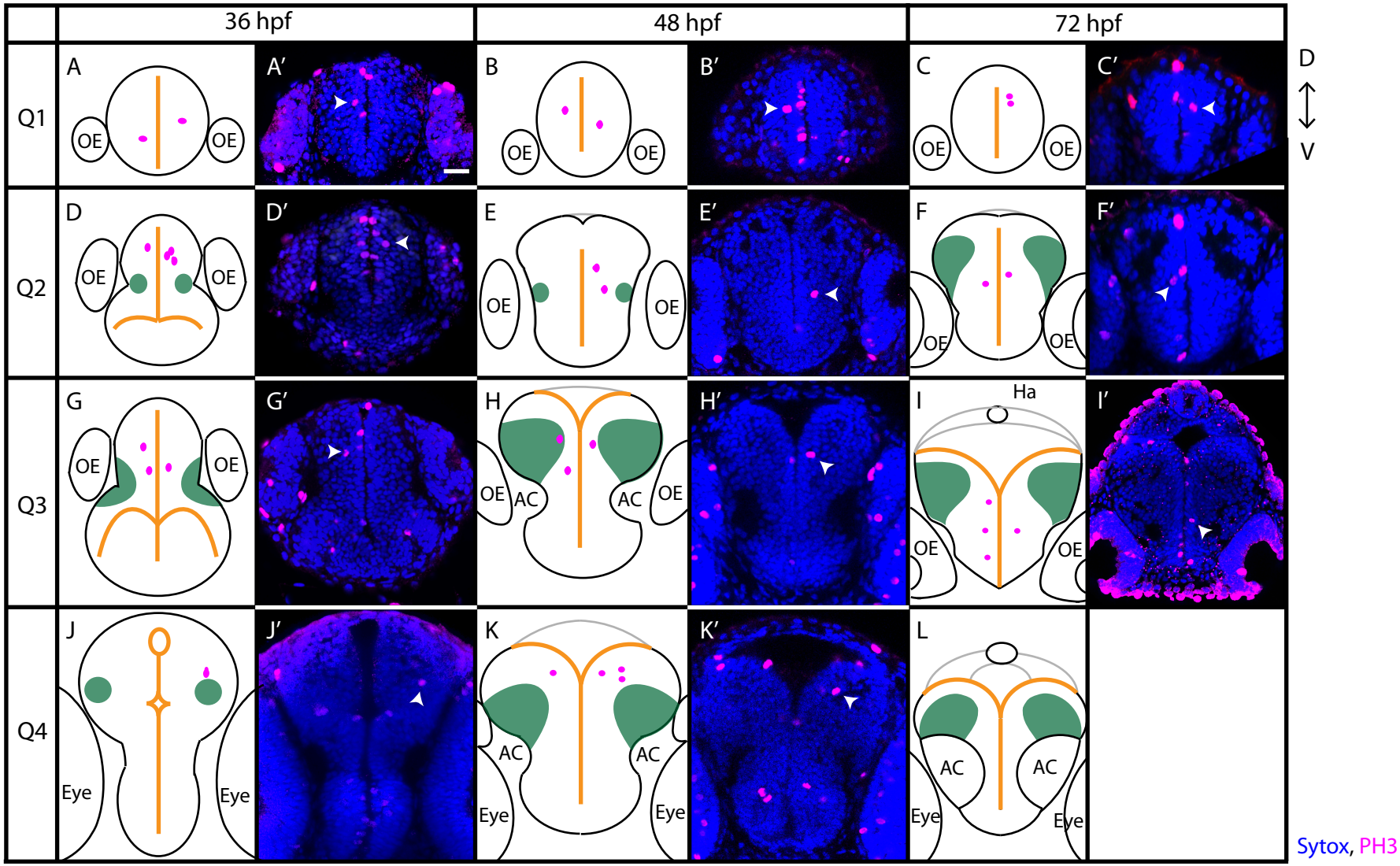

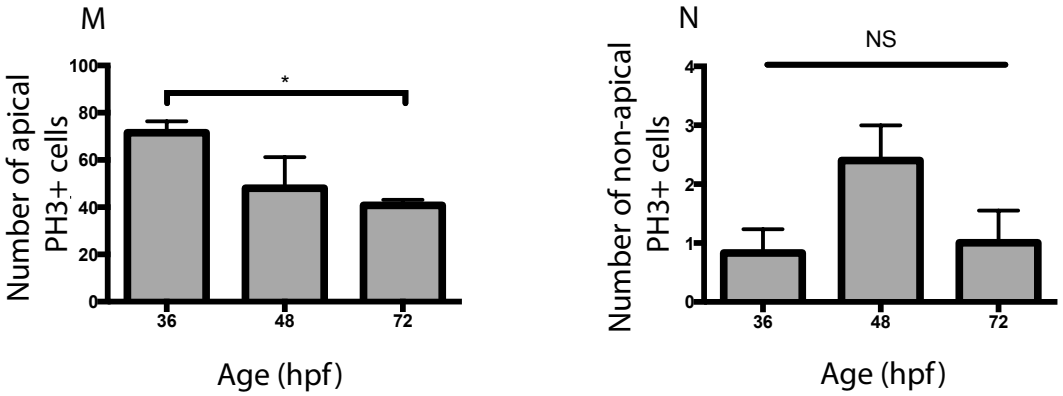
M
Number of apical PH3+ cells
100
80
60
40
20
0
*
36
48
72
Age (hpf)
N
Number of non-apical PH3+ cells
4
3
2
1
0
NS
36
48
72
Age (hpf)

Figure 3-16: *Vsx1* is expressed in the telencephalon and may label non-apical mitotic cells. **A-D**) Single z-slices of a dorsal view of 2 dpf Tg(*vsx1*:GFP) embryos (green) after *in situ* hybridisation for *vsx1* mRNA (red), counterstained for nuclei (Sytox, blue). Cells expressing *vsx1* mRNA are located in more medial regions than *vsx1*:GFP-expressing cells. Cells positive for both *vsx1* mRNA and *vsx1*:GFP are visible (arrow head). Apical surface shown by dotted line. Scale bar = 25 μm. OE = olfactory epithelium. **E**) A frontal view of the telencephalon of a 24 hpf Tg(*vsx1*:GFP) (green) embryo showing immunoreactivity for PH3 (magenta) and counterstained for nuclei (Sytox, blue). **Ei-iii**) Higher magnification of the boxed region in E. Arrow shows a non-apical mitotic cell that expresses *vsx1*:GFP. Scale bar = 25 μm. OE = olfactory epithelium.

Figure 3-16

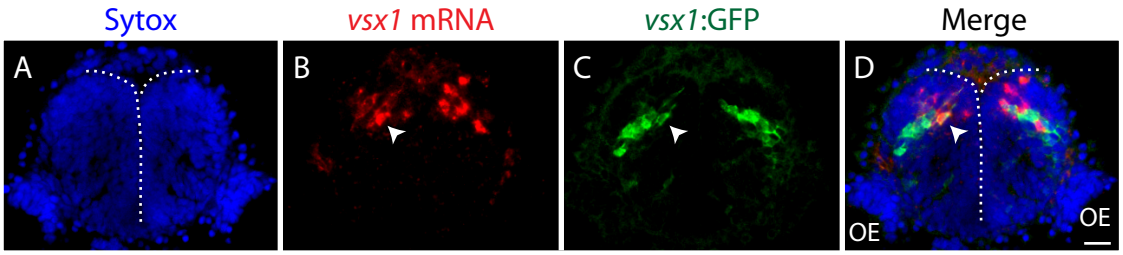

2 dpf

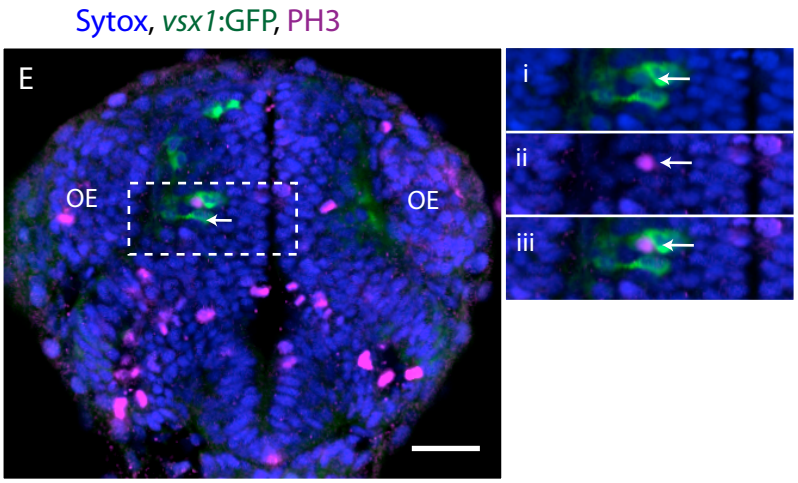

24 hpf

3.4 Discussion

Previous studies of non-apical (basal) progenitors have been largely limited to the developing mammalian cortex. The data presented in this chapter identifies a small population of non-apical progenitors in the zebrafish embryonic spinal cord, hindbrain and telencephalon during neurogenesis. The spatial and molecular characteristics of these non-apical progenitors vary between regions of the neural tube and through development (summarised in **Table 3-1**). This is the first thorough characterisation of non-apical divisions in the zebrafish neural tube. To our knowledge, this is also the first thorough characterisation of non-apical progenitors in the spinal cord of any species.

Non-apical progenitors in the mammalian cortex have been postulated to generate the increased neuron numbers that underlie evolutionary mammalian cortical expansion (see section 1.2 for a full discussion), however non-apical progenitors are present in small and compact brains (this thesis and Martínez-Cerdeño et al. 2006; Kimura et al. 2008). Studying these progenitors in the relatively small and compact zebrafish neural tube could provide us with insights into this hypothesis as well as any non-expansive functions of these progenitors.

To better understand the role of non-apical progenitor population in zebrafish neurogenesis I specifically analysed their number, location and the markers they express in fixed specimen between 24 and 72 hpf. A major limitation to characterising mitotic cells in fixed tissues is that each specimen only provides a snapshot of the mitoses that are occurring in a very short space of time. I tried to overcome this by carrying out live imaging in embryos injected with nuclear-RFP at the 1 cell stage. However, it is technically challenging to carry out these experiments in embryos older than 30 hpf as nuclear-RFP signal has decreased due to the metabolism of the injected mRNA. I found that loss of nuclear-RFP signal was most notable in the marginal zone, specifically interfering with the observation of non-apical divisions. Furthermore, in the hindbrain and telencephalon I found it hard to follow single nuclei in time-lapse movies as the tissue shows a high density of mobile nuclei in the marginal zone. It might be possible to overcome all of these issues by carrying out these experiments in a transgenic line that marks different stages of the cell cycle (e.g. FUCCI) however the lines that are currently available label G2/S/M stages together and do not show specificity for M-phase.

Table 3-1: Summary of non-apical progenitors in the zebrafish neural tube. Number of non-apical progenitors shown as percentage of total PH3-labelled mitoses ± SEM. Expression of *vsx1*:GFP, *olig2*:GFP or *tbr2*:dsRed by non-apical progenitors (if observed) is listed. Unknown refers to the existence of non-apical progenitors that do not express any of these genes. VMB; ventromedial basal; SA: Subapical; DLB; dorsolateral basal.

	Age	Percentage	Location	Marker
Spinal cord	**24 hpf**	3.4 ± 1.5	Ventral, basal	Vsx1
	36 hpf	3.2 ± 0.9	Ventral, basal	Vsx1 and olig2
	48 hpf	3.3 ± 1.7	Ventral, basal	Vsx1 and olig2
	72 hpf	None observed		
Hindbrain	**24 hpf**	3.3 ± 1	Ventral, basal	Vsx1
	36 hpf	7.2 ± 1.7	VMB	Vsx1
			SA	Vsx1
			DLB	Unknown
	48 hpf	17.9± 3.8	VMB	*Vsx1* and unknown
			SA	*Vsx1* and unknown
			DLB	*Vsx1* and unknown
	72 hpf	None observed		
Telencephalon	**24 hpf**	?	Subapical	Unknown
	36 hpf	1.2 ±0.5	Subapical	Unknown
	48 hpf	4.8 ± 0.6	Subapical	Unknown
	72 hpf	2.4 ± 0.6	Subapical	Unknown

3.4.1 The links between non-apical mitoses and tissue growth in the embryonic zebrafish neural tube

In the mammalian cortex larger numbers and more varied populations of non-apically dividing progenitors are correlated with increased tissue size and complexity (Betizeau et al. 2013; Johnson et al. 2015; Florio et al. 2015). Similarly, the zebrafish hindbrain undergoes large-scale expansion over the period of time examined here (Lyons et al. 2003) and the non-apical progenitor population increases significantly, both in number and location. In comparison, despite extensive differentiation occurring in the spinal cord, this tissue remains relatively compact in the period of development up until 72 hpf. In this region, the number of non-apical

mitoses does not change through embryonic development. Therefore, it is possible that increasing the proportion of non-apical progenitors could aid in generating the numbers of neurons that are required for tissue growth and expansion in the hindbrain of zebrafish embryos, as is thought for mammalian species.

Whether or not non-apical progenitors play a role in tissue growth is not clear in the zebrafish telencephalon. This brain region is known to undergo growth in the period analysed (Folgueira et al. 2012), however I found that the size of the non-apical progenitor population remains very small between 36 and 72 hpf. This might suggest that non-apical progenitors do not play a substantial role in the extensive growth that occurs in this tissue. Alternatively, it is known that the period of growth in the telencephalon continues until 5 dpf (Folgueira et al. 2012). Therefore, it will be useful to extend this characterisation in the telencephalon to 5 dpf in order to fully explore the role of non-apical progenitors in the development of this region.

The observation that individual brain regions contain non-apical progenitors with different characteristics strongly suggests that the role of non-apical progenitors in tissue growth, expansion and neurogenesis may be region specific.

3.4.2 Non-apical progenitors are seen region specific spatial locations

In each of the regions of the neural tube analysed in this chapter, non-apical mitoses were located in different spatial compartments. Non-apical progenitors in the spinal cord are confined to a specific ventrolateral location throughout embryonic development. At 24 hpf non-apical progenitors the hindbrain are found in a similar location to those in the spinal cord but at 36 and 48 hpf I identified three, non-overlapping spatial populations of non-apical progenitors: ventromedial basal (VMB), subapical (SA) and dorsolateral basal (DLB). Finally, the non-apical divisions in the telencephalon were found in subapical locations, often only a single cell diameter from the VZ. This is qualitatively different to the non-apical divisions in the hindbrain and spinal cord, which are frequently located on the basal surface of the ventral neural tube.

It is possible that subapical divisions in the hindbrain, which occur at a distance from both the apical and basal surfaces, are restricted from reaching the basal extremity of the neural tube by the expansion of the marginal zone, containing differentiating and mature neurons. This is supported by the observation that subapical progenitors in the hindbrain are located on the edge of HuC/D expression. The idea that the formation of tissue compartments impairs a cell's ability to divide in a specific location resembles one put forward to explain the production of basal progenitors in the zebrafish retina (Weber et al. 2014). This idea might also explain the subapical location of non-apical divisions in the telencephalon, adjacent to the VZ. In this case,

proliferation of neuroepithelial cells might mean that the VZ becomes crowded and a cell is unable to return to the VZ prior to division and therefore divides in a subapical location.

In summary, the non-apical progenitors in the zebrafish neural tube are found in different spatial locations in each brain region analysed. This is further evidence that each brain region has different requirements for non-apical progenitors during development.

3.4.3 Molecular subtypes of non-apical progenitors vary by brain region

From the literature I identified three genes that could potentially be expressed in non-apical progenitors in the zebrafish: (1) *vsx1* had been identified as a basally dividing interneuron progenitor in a previous study (Kimura et al. 2008); (2) *olig2* is expressed in oligodendrocyte precursors which migrate dorsally from the ventral spinal cord and divide basally to generate neurons (Park et al. 2002); and (3) the mammalian intermediate neuronal progenitor marker Tbr2 (Englund et al. 2005).

In the hindbrain and spinal cord non-apical divisions are found in a specific ventral region through embryonic development. At 24 hpf this region corresponds to a single progenitor domain, p2 from which *vsx1* cells are derived. Data from live imaging and fixed tissue shows that all non-apical divisions at this stage express the Tg(*vsx1*:GFP) transgene. Therefore, at 24 hpf non-apical progenitors generate solely V2a and V2b interneurons. As development continues, non-apical divisions continue to be found in the same ventrolateral region in the spinal cord but an increasing number of non-apical divisions do not express *vsx1*:GFP and instead have been found to express the pMN marker *olig2*:GFP. The pMN progenitor domain produces motor neurons and interneurons as well as oligodendrocyte precursors (OPCs). The identity of the daughter cells of *olig2*:GFP-expressing non-apical progenitors is currently unknown. However, it is unlikely that the daughters of *olig2*:GFP-positive non-apical progenitors will be oligodendrocytes because OPCs are thought to divide much later in development and migrate to dorsal locations prior to division (Lee et al. 2010). Theoretically, it is possible to answer this question regarding the lineage of the daughter cells of *olig2*:GFP non-apical divisions using live imaging. However, the small number of these progenitors is, again, the main obstacle to such an experiment. From the data presented here it appears that *vsx1* and *olig2* can be used to mark the entire population of non-apical progenitors in the spinal cord. To confirm this we could look PH3-expression in embryos expressing both GFP reporter genes.

In the hindbrain at 36 and 48 hpf, the proportion of non-apical progenitors that coexpress *vsx1*:GFP decreases, similar to what was seen in the spinal cord. Unlike the spinal cord, these *vsx1*:GFP negative cells were not found to express *olig2*:GFP. In fact, there is a large population

of non-apical divisions at 36 and 48 hpf, which do not express either of the markers I investigated. The identity and daughter cell fates of these cells are currently unknown. It is possible that I have underestimated the proportion of *vsx1*-experssing non-apical progenitors in the hindbrain as it can be challenging to visualise *vsx1*:GFP in younger cells expressing low levels of GFP when they are situated adjacent to older, highly expressing cells. It is also possible that these cells represent a currently unknown molecular subtype of non-apical progenitors.

Whether *tbr2* is expressed in the zebrafish spinal cord and hindbrain is a matter of debate. Tbr2 immunoreactivity has been reported in the zebrafish spinal cord (Ohata et al. 2011), however the antibody used in these experiments was not zebrafish specific and its specificity in these embryos has not been verified. Furthermore, in our hands we were unable to observe Tbr2 expression in the hindbrain or spinal cord by *in situ* hybridisation, immunohistochemistry or in the Tg(*tbr2a*:dsRed) reporter line (data not shown).

Our current data provides a very limited view of the identity of non-apical progenitors in the telencephalon as I only observed a single non-apical mitosis expressing *vsx1* and did not observe any expressing either *olig2* or *tbr2*. Analysis of *vsx1* mRNA and *vsx1*:GFP expression in the telencephalon indicates that *vsx1* mRNA is transiently expressed by cells migrating away from the apical surface and expression of GFP is not seen until later in this migration. Therefore, if expression of the fluorophores is not seen until after the cell has undergone mitosis then *vsx1*:GFP, or *tbr2*:dsRed, cells might be daughters of non-apical divisions.

In summary, two molecularly distinct populations of non-apical progenitors were observed in the spinal cord and hindbrain, contributing different types of neurons during early neurogenesis. The larger population expresses *vsx1*:GFP in both the spinal cord and hindbrain. In the spinal cord the second population expresses *olig2*:GFP. Our data suggests that these two markers cover the entire non-apical progenitor population in the spinal cord. However, *olig2*-expressing non-apical progenitors are scarce in the hindbrain and there is a large population of unidentified non-apical progenitors in this region. Similarly, we currently do not have any direct data regarding the identity of non-apical progenitors in the telencephalon.

3.4.4 The morphology of non-apical progenitors in the hindbrain and telencephalon is unknown

The different populations of mammalian basal progenitors are primarily characterised based on their morphology at mitosis (see **Table 1-1** and **Table 3-2**). Currently we have limited information on the morphology of non-apical progenitors in the zebrafish neural tube. Knowing

whether these non-apical progenitors have apical or basal processes and attachments to the apical or basal surfaces would be particularly usefully when drawing comparisons between non-apical progenitors in zebrafish and mammals.

Previous work in the Clarke lab suggests that non-apical progenitors in the spinal cord and hindbrain between 18 and 30 hpf retract their apical attachment shortly before division (P. Alexandre, and J. Clarke, unpublished). The cell bodies of these non-apical progenitors are more or less at the basal surface but we do not know if they are in contact with the basal laminae.

The morphology of the different spatial populations of non-apical progenitors in the hindbrain at division is currently unknown. Ideally, I would carry out live imaging experiments of mosaically labelled cells to characterise the morphology of non-apical progenitors in the different locations in the hindbrain. However, this experiment is currently challenging, as the number of non-apical divisions is very small at any one time, meaning it is unlikely that we will specifically label these cells using mosaic labelling techniques. It might be possible to overcome this issue if we are able to promote neurogenesis, as has been achieved in the chick neural tube by the electroporation of the proneural gene *Neurog2* (Das and Storey, 2014). Ideally, I would use a method by which we could promote differentiation of specifically the *vsx1* progenitors (see Chapter 6). This might be possible using the Gal4/UAS system and the transcription factor code that is known to specify the p2 domain but generating the transgenic lines required for this experiment would be extremely time consuming.

3.4.5 The proliferative capacity of non-apical progenitors in the zebrafish neural tube is unknown

A key feature of a subset of non-apical progenitors commonly found in the developing neocortex of mammalian species with large, gyrified cortex, specifically bRG, is the ability to self renew (see **Table 1-1** and **Table 3-2**). Previous experiments in the Clarke lab have shown that non-apical progenitors only undergo self-consuming divisions in the spinal cord (P. Alexandre, unpublished). Supporting this, my data at early stages (24 hpf) shows that all non-apical progenitors start to express *vsx1*:GFP shortly before terminal divisions. This data suggest that at 24 hpf non-apical progenitors in the spinal cord undergo a single, terminal division, contributing mainly to neurogenesis. We have not been able to observe non-apical divisions in live embryos after 30 hpf, so we do not know if non-apical divisions continue to divide terminally after this point. However, given the small size of the spinal cord tissue through embryonic development we might assume that non-apical divisions after 30 hpf are terminal. In contrast, taking into account (1) the fact that the hindbrain and telencephalon do undergo a certain amount of growth

and (2) our understanding of mammalian non-apical progenitors, it could be predicted that non-apical progenitors in the hindbrain and telencephalon might show some self-amplification. In the hindbrain, approximately 40% of non-apical mitoses do not express HuC/D, which might indicate that these cells are not undergoing neurogenic divisions. This would be an interesting route of investigation to follow.

3.4.6 Do precursors of V2 cells in other systems divide non-apically?

The data I have presented in this thesis identified *vsx1*-expressing progenitors as the major population of non-apical progenitors in the zebrafish neural tube. In this system *vsx1* progenitors undergo a single terminating division to generate V2a/V2b interneuron pairs (Kimura et al. 2008). Similarly, in the mouse and chicken spinal cord, approximately equal numbers of V2a/V2b are derived from a common progenitor pool composed of genetically identical cells (Li et al. 2005; Del Barrio et al. 2007; Peng et al. 2007; Lundfald et al. 2007; Al-Mosawie et al. 2007; Kang et al. 2013). Furthermore, in all three model systems Notch signalling has been shown to play a role in the V2a/V2b fate choice (Batista et al. 2008; Kimura et al. 2008; Kang et al. 2013).

However, it is currently unknown if non-apical progenitors contribute to the development of V2 interneurons in the mouse or chicken spinal cord. In mice, the population of V2 neurons before they have taken on a V2a or V2b fate are referred to as 'early neurons' (Batista et al. 2008) and it is currently thought that the interaction between specified, post-mitotic cells leads to them taking on different fates. Due to other characteristics murine and avian V2 cells share with those in the zebrafish, it is possible that the V2a/V2b diversity in amniote embryos diversity is generated by a pair-producing intermediate progenitor, as in zebrafish (Kimura et al. 2008). Currently there is no published data on the presence of non-apical divisions in the spinal cord of either mice or chicken embryos, but it is an exciting prospect that non-apical progenitors might be present in the spinal cord of other species.

3.4.7 Summary of non-apical progenitors in the zebrafish neural tube

The data presented in this chapter shows that the zebrafish neural tube contains a small population of non-apical progenitors during embryonic neurogenesis and that the spatial and molecular characteristics of non-apical progenitors vary between brain regions. This is the first thorough characterisation of non-apical divisions embryonic development of a teleost species, and the first to fully characterise non-apical progenitors in the developing spinal cord of any vertebrate.

Table 3-2: Comparison of the progenitors in the zebrafish neural tube and mammalian neocortex. Adapted from **Table 1-1** and Florio & Huttner 2014 and modified to include data gathered in this chapter. Question marks show aspects of the cell biology that we do not have data on. VMB = ventromedial basal. SA = subapical. DLB = dorsolateral basal. NE: neuroepithelial cell; aRG: apical radial glial cell; aIP: apical intermediate progenitor; bIP: basal intermediate progenitor (N: neurogenic; P: proliferative); bRG: basal radial glia; P: directed process (see Betizeau et al. 2013).

	Apical progenitors				**Basal progenitors**					**Non-apical progenitors**				
	Mammals			**Zebrafish**	**Mammals**					**Zebrafish**				
	NEC	**aRG**	**aIP**	**NEC**	**bIP**	**Basal radial glial cell**				**Spinal cord**	**Hindbrain**			**Telen-cephalon**
						Basal-P	**Apical-P**	**Both-P**			**VMB**	**SA**	**DLB**	
Location of mitosis	Apical surface			Apical surface	SVZ/ iSVZ	oSVZ				Basal surface	Basal surface	Subapical	Basal surface	Subapical
Apical domain at mitosis	Yes			Yes	No	No				No	?	?	?	?
Basal lamina contact at mitosis	Yes		No	Yes	No	Yes/No	No	Yes/No		?	?	?	?	?
Process retention at mitosis	Basal		No	Basal	No	Basal	Apically directed	Basal + apically directed		No	?	?	?	?
Tbr2 expression	No			No	Yes	Some Tbr2				No	No	No	No	No
Proliferative potential	Yes		No	Yes	N bIP No	P bIP Yes	Yes			No	?	?	?	?
HuC/D expression				Rare	Yes					Yes	Some	Some	Some	

CHAPTER 4
SPATIOTEMPORAL DEVELOPMENT OF *VSX1* PROGENITORS

4 Spatiotemporal development of *vsx1* progenitors

4.1 Introduction

The majority of the understanding of vertebrate neurogenesis comes from studies of fixed tissues or slice cultures. As live imaging in large, opaque tissues is technically challenging, the dynamics of neuronal differentiation in the neural tube have not yet been extensively studied. This is particularly true for questions regarding spatiotemporal patterning along the anteroposterior axis of the vertebrate spinal cord. Zebrafish embryos are an ideal model to address this question due to the ease of live imaging and the ability to label subpopulations of neurons.

In Chapter 3 I showed that non-apical progenitors predominantly express *vsx1* in early stages of neurogenesis in the zebrafish neural tube. Time-lapse imaging of the spinal cord of Tg(*vsx1*:GFP) embryos shows progenitors beginning to express *vsx1*:GFP from 18 hpf and that they divide in a spaced or periodic pattern along the anteroposterior axis (**Figure 3-5**). Following the formation of this initial pattern, subsequent *vsx1*:GFP-expressing progenitors appear to fill in the space between existing *vsx1* cells (**Figure 3-5** and **Supplementary Movie 3-2**). Similar patterns of initial periodicity and subsequent space filling is seen in the expression of multiple neuronal subtype markers in zebrafish (including, *vsx1, eng1b*, *islet2,* **Figure 4-1**A; Thisse & Thisse 2004; Thisse et al. 2001; Hutchinson & Eisen 2006) as well as GABAergic neurons in the *Xenopus* hindbrain and spinal cord (**Figure 4-1**B; Roberts et al. 1988; Roberts et al. 1987; Dale et al. 1987). This data suggests that this spatiotemporal pattern of differentiation might be a common feature of vertebrate spinal neurogenesis. However, the spatiotemporal dynamics of the differentiation of *vsx1*, or any other neuronal subtype, have not yet been studied.

In this chapter I am to characterise the spatiotemporal pattern of *vsx1*:GFP differentiation and to begin to probe the mechanisms underlying this patterning event.

4.1.1 Mechanisms of patterning neurogenesis

A large number of mechanisms are known to contribute to the control of neurogenesis in time and space, including intrinsic and extrinsic cues (see section 1.3). A variety of mechanisms to pattern neurogenesis through a tissue have been described in the neural tube and neuronal patterning along the anteroposterior axis is often related to overt patterning of the tissue. A good example of this is the zebrafish hindbrain, where the tissue is divided into repeated segments (rhombomeres) that are separated by specialised boundary cells. In this tissue multiple

interactions between boundary and non-boundary cells patterns neurogenesis within each rhombomere (Cheng et al. 2004; Amoyel et al. 2005; Gonzalez-Quevedo et al. 2010; Terriente et al. 2012; described in detail in section 1.3.2).

In contrast, the spinal cord is not overtly segmented into repeated structural or molecular subsections and does not contain any cells that are analogous to the boundary cells seen in the hindbrain. Furthermore the pattern of neurons in *Xenopus* and zebrafish spinal cords are more fine grained than that seen in the hindbrain (Dale et al. 1987; Roberts et al. 1987; Roberts et al. 1988; Eisen & Pike 1991; Lewis & Eisen 2004; England et al. 2011). These patterns appear to be composed of single neuronal cells separated by distances of more than one cell diameter. This suggests that alternative mechanisms act to pattern neurons and neurogenesis in the spinal cord. Two potential mechanisms that might generate this pattern are mesoderm-derived signals and long distance lateral inhibition.

4.1.2 Mesoderm-derived signals pattern primary motor neurons

The embryonic zebrafish spinal cord does not show molecular or structural segmentation, however the adjacent mesoderm is segmented into repeated structures known as somites. One group of neurons that are periodically spaced along the anteroposterior axis of the neural tube are primary motor neurons and the location of these cells correlates with the neighbouring somite (Lewis & Eisen 2004; Eisen & Pike 1991). A number of studies have demonstrated that mesoderm-derived signals act to pattern primary motor neurons in the spinal cord. Defects in paraxial mesoderm formation have been shown to result in irregular spacing and clustering of primary motor neurons (Lewis & Eisen 2004; Eisen & Pike 1991). Furthermore, shortening of somites along the anteroposterior, as occurs in convergent extension mutant zebrafish, causes a concurrent change to the spacing of primary motor neurons (Lewis & Eisen 2004). Specifically for CaP motor neurons, correct positioning of these cells in the middle of the overlying somite is depending on Sema3ab expression by the posterior half of each somite. Sema3ab acts to chemorepel CaP neurons through the Neurophilin1a receptor and thereby refine the position of this class of primary motor neurons prior to axon outgrowth (Bernhardt et al. 1998; Sato-Maeda et al. 2006; Sato-Maeda et al. 2008). Interference with Sema3ab/Neuropilin1a signalling pathway results in irregular spacing of CaP neurons (Sato-Maeda et al. 2008).

Therefore, some subtypes of neurons are patterned by the segmented paraxial mesoderm (i.e. somites; Eisen & Pike 1991; Lewis & Eisen 2004; Sato-Maeda et al. 2008) however, it is currently unknown whether this mechanism affects patterning and periodicity in other neuronal subtypes.

4.1.3 Long-range Delta Notch lateral inhibition

Delta Notch lateral inhibition, whereby a Delta-expressing cell activates the Notch signalling pathway in its neighbours and inhibits them from differentiating (discussed in detail in section 1.3.1), is an obvious signalling mechanism that might generate a fine grain pattern of differentiation, like that seen in *vsx1* progenitors. However, in conventional lateral inhibition Delta Notch signalling requires cell-to-cell contact and therefore only occurs between immediately adjacent cells, generating a pattern whereby neurons are only separated by a small number (usually one) of non-neural cells. However, in *vsx1* progenitor cells (this thesis and Kimura et al. 2008), and other neuronal populations in zebrafish (Thisse & Thisse 2004; Thisse et al. 2001; Hutchinson & Eisen 2006; England et al. 2011; **Figure 4-1**A) and *Xenopus* (Roberts et al. 1988; Roberts et al. 1987; Dale et al. 1987; **Figure 4-1**B), cells are seen spaced by much greater distance (between 5-10 cells). Therefore this pattern cannot be explained by conventional Delta Notch signalling.

A long-range mechanism for Delta Notch signalling has been described in *Drosophila.* Sensory organ precursors (SOPs) in the epithelium of the pupal *Drosophila* thorax (notum) are also known to develop separated by 3-5 cell diameters (**Figure 4-1**Ci; Renaud & Simpson 2001; De Joussineau et al. 2003; Cohen et al. 2010). The notum is initially a tissue composed of cells that are equally competent to differentiate as SOPs. The number of cells that upregulate proneural genes early in the development of the pattern is greater than the number of SOP cells that eventually make up the pattern (**Figure 4-1**Cii; Cohen et al. 2010). Nascent SOP cells have been shown to extend 'webs' of filopodia into the surrounding tissue to deliver Delta ligand over long distances (**Figure 4-1**Cii'; Renaud & Simpson 2001; De Joussineau et al. 2003; Cohen et al. 2010). This long distance activation of Notch signalling inhibits cells within a 5 cell diameter range from also differentiating as SOPs (De Joussineau et al. 2003; Cohen et al. 2010). It has been shown that interfering with the formation or elongation of filopodia or Notch signalling from SOPs results in the loss of the normal spacing and patterning of SOPs within the notum ectoderm (**Figure 4-1**Ciii and iv; De Joussineau et al. 2003; Cohen et al. 2010). Therefore, in the *Drosophila* notum, differentiating cells use basal filopodia to refine a self-organised pattern of neuronal cells via the Delta Notch signalling pathway (De Joussineau et al. 2003; Cohen et al. 2010). In summary, this long distance Delta Notch lateral inhibition driven by dynamic cellular extensions provides a mechanism by which sparse induction of differentiation can be generated. It is currently unknown whether a similar mechanism exists in vertebrate neurogenesis.

4.1.3.1 Differentiating neurons and non-apical progenitors in the zebrafish hindbrain and spinal cord undergo a stereotyped, dynamic morphological transition

In order to visualise the behaviour and morphology of single cells in the zebrafish neural tube the Clarke and Alexandre labs inject membrane (CAAX-fluorophore) into a single cell of a 64-128 cell embryo, which mosaically labels individual cells in an otherwise unlabelled embryo (Alexandre et al. 2010). Using this technique, we have observed that differentiating neurons undergo a characteristic morphological transition (n = 25/25 neurons; P. Alexandre and J. Clarke, unpublished). The cell first translocates its soma to the basal surface while maintaining contact with the apical surface via an apically directed process. The cell then extends two long membrane extensions, containing microtubules, along the basal surface, one anteriorly and the other posteriorly (**Figure 4-2**A). I will refer to these structures as basal arms so as not to confuse them with the basal processes, which is a radial projection that contacts the basal lamina of the neural tube. The basal arms are not randomly directed. Instead, they appear to be largely restricted to elongating along the same dorsoventral domain as the neuron cell body. At this stage, the newborn neurons have a characteristic shape that we refer to as a T-shaped morphology. The T-shaped cell then retracts its basal arms and apical process before axonogenesis begins. The morphological changes that occur from neuroepithelial cell to neuron, including the transition through a T-shaped morphology, are dynamic and I will refer to them as the T-shaped morphological transition. During early stages of neural tube development, this transient T-shape morphology is a reliable predictor of neuronal differentiation in the hindbrain and spinal cord of the zebrafish, however this behaviour is absent from differentiating neurons in the telencephalon (P. Alexandre and J. Clarke, unpublished).

We have also observed that non-apical progenitors undergo the T-shaped morphological transition prior to division (n = 7/7 non-apical progenitors). In these cells the T-shape morphological transition is almost identical: the cells soma is moved to the basal surface, while an apical attachment is maintained, and the cell then extends two basal arms. Non-apical progenitors then retract their apical process and basal arms and the cell undergoes mitosis following which both daughter cells begin axonogenesis and take on an interneuron fate (**Figure 4-2**B). As *vsx1* is expressed in all non-apical progenitors in the spinal cord early in neurogenesis, we know that *vsx1*:GFP non-apical progenitors also go through this process. However, expression of GFP is not seen until shortly before cell division, after the cell has fully retracted its processes and, therefore, unfortunately the Tg(*vsx1*:GFP) line cannot be used to visualise the T-shaped morphological transition.

The function of the transient basal arms is currently unknown. However, in some respects they resemble the filopodia-based extensions seen in nascent SOP cells in the *Drosophila* notum (see section 4.1.3). SOP cells are patterned or spread throughout the *Drosophila* notum, and during the formation of this pattern, the cells extend transient membrane extensions into the surrounding tissue. Therefore, we hypothesise the basal arms may a deliver long-distance inhibitory signal to organise the spacing of neuronal differentiation in the zebrafish neural tube, similar to patterning in the *Drosophila* notum. To further support this hypothesis we have observed T-shaped cells expressing a *deltaD*:GFP reporter as well as showing immunoreactivity for a deltaD antibody (**Figure 4-2**Ci and Cii, respectively, P. Alexandre, unpublished), which suggests that Delta Notch signalling, as in *Drosophila*, might mediate the long distance inhibitory signal. If this were indeed their function, we would expect pattern formation to occur in the following way: newly specified neurons translocate their nucleus to the basal side of the neuroepithelium and begin to extend basal arms (**Figure 4-3**A). These T-shaped cells are found repeated down the anteroposterior axis of the tissue. The basal arms of T-shaped cells provide an inhibitory signal to surrounding cells predominantly at the same dorsoventral level as the neurons cell body, preventing them from differentiating in the same time and place as the differentiating T-shaped cells (**Figure 4-3**B). As the T-shaped cells retract their basal arms, cells in the intervening space are released from inhibition allowing new cells to differentiate (**Figure 4-3**C). The new cells then begin to extend basal arms, re-establishing the inhibitory signal, stopping all but a single cell from differentiating in between each initial pair (**Figure 4-3**C). This process can occur iteratively throughout neurogenesis. Further experiments are required to test whether such a mechanism acts during the patterning of *vsx1*:GFP progenitors.

4.2 Aim of chapter

The regulation of neuronal differentiation in space and time is only partially understood. Preliminary observations suggest that *vsx1*:GFP progenitors are specified in a sparse pattern along the anteroposterior axis. In this chapter I am to quantitatively characterise the spatiotemporal dynamics of *vsx1*:GFP progenitor differentiation in time and space to better understand the development of this pattern.

Mesoderm-derived signals are known to pattern motor neurons in the zebrafish spinal cord and, in *Drosophila*, membrane extensions that deliver Delta-mediated inhibition have been shown to play a key role in spacing neuronal cells throughout the tissue. I aim to test whether similar mechanisms are involved in the spatiotemporal patterning of non-motor neuron subtypes in the zebrafish spinal cord.

Figure 4-1: Patterning of neurons in *Drosophila* and vertebrates. **A**) Neurons are periodically spaced along the anteroposterior axis of the zebrafish spinal cord. Lateral views of the spinal cord of zebrafish embryos showing expression (by *in situ* hybridisation) of **i**) *vsx1* (taken from Kimura et al. 2008), **ii**) islet2 (taken from Hutchinson & Eisen 2006) and **iii**) en1 (taken from Gribble et al. 2007). Neurons expressing the different markers appear separated by a number of cell bodies. **B**) Lateral view of the *Xenopus* hindbrain and spinal cord showing the distribution of somata with GABA-like immunoreactivity (black, filled in cells; taken from Roberts et al. 1987). At stage (St) 28, individual neurons appear separated by large distances and by ST 29/30 these spaces have been filled by newborn neurons. **C**) Adapted from the specified figures in Cohen et al. 2010. Neuronal cells express Neu-GFP (Neuralized-GAL4, UAS Moesin-GFP; grey scale, the darker the colour the higher the expression level) and the outlines of the cells in the tissue are labelled with E-Cadherin-GFP. **i**) The final pattern of SOP cells is ordered and shows regular spacing between individual precursor cells (adapted from Figure 1 in Cohen et al. 2010). **ii**) In early stages of pattern formation an excess number of cells expressing Neu-GFP appear in the notum, generating an overcrowded and poorly organised arrangement of precursor cells (Figure 4 in Cohen et al. 2010). **ii'**) The nascent SOP cells in this tissue extend membrane protrusions into the surrounding tissue (Figure 7 in Cohen et al. 2010). **iii**) Expression of dominant negative Rac or a mutant form of *scar* (regulators of filopodia formation in the notum) in Neu-expressing cells results in a disordered final pattern of SOP cells (Figure 7 in Cohen et al. 2010). **iv**) Inhibiting Notch signalling while the pattern is being refined results in rows of Neu-GFP-expressing SOPs (adapted from Figure 2 in Cohen et al. 2010).

Figure 4-1

A) Pattern of neuronal markers in zebrafish spinal cord

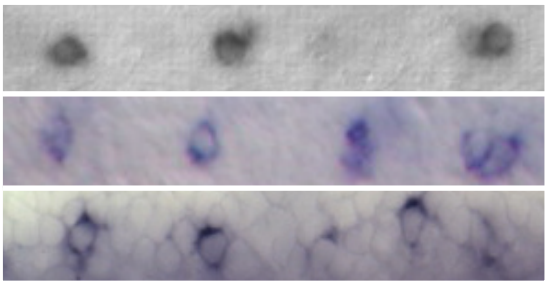

B) Pattern GABAergic neurons in the Xenopus hindbrain and spinal cord

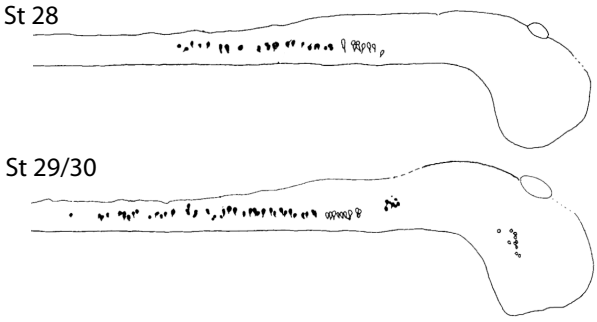

C) Patterning of sensory organ precursor cells (SOPs) in *Drosophila*.

i) Final pattern of SOPs

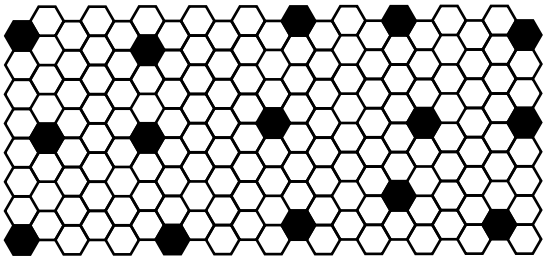

ii) Early stages of pattern formation

ii') Nascent SOP

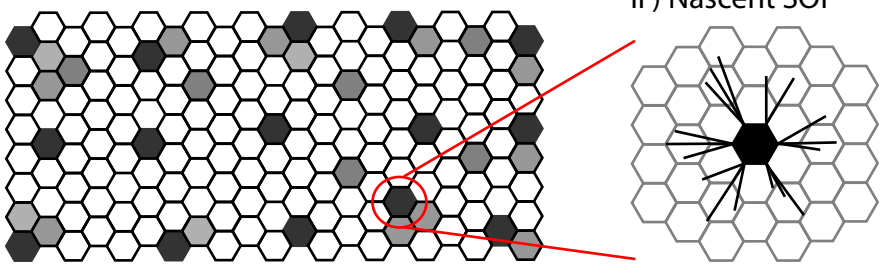

iii) Pattern formed after interference with filopodia extension

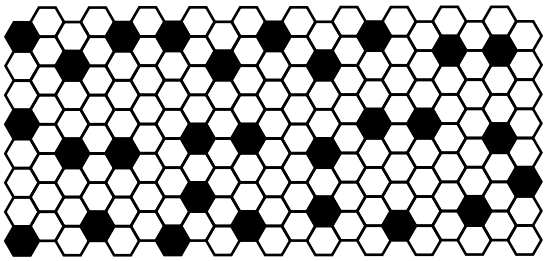

iv) Pattern formed if Delta Notch signalling is abrogated

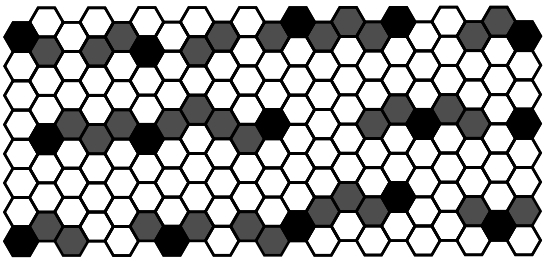

Figure 4-2: Differentiating neurons and non-apical progenitors in the embryonic zebrafish spinal cord undergo a characteristic T-shape morphological transition prior to axonogenesis or division, respectively. The differentiation of neurons (**A**) and non-apical progenitors (**B**) starts with the cell soma translocating to the basal surface. Initially these cells maintain an apical attachment (arrow head) and extend basal arms (arrow) along the basal surface (dotted line), giving these cells a T-shaped morphology. After the basal arms and apical process are retracted, the cell rounds up. Neurons then begin axonogenesis (double headed arrow) and non-apical progenitors undergo division (asterisks) and both of its daughter cells can be seen extending axons (double headed arrows). **C)** T-shaped cells labelled by membrane RFP (**i**) or GFP (**ii**) express deltaD, shown by Tg(*deltaD*:GFP) (**i**) expression and staining of endogenous deltaD by immunohistochemistry (**ii**). P. Alexandre collected the data shown in this figure (unpublished).

Figure 4-2

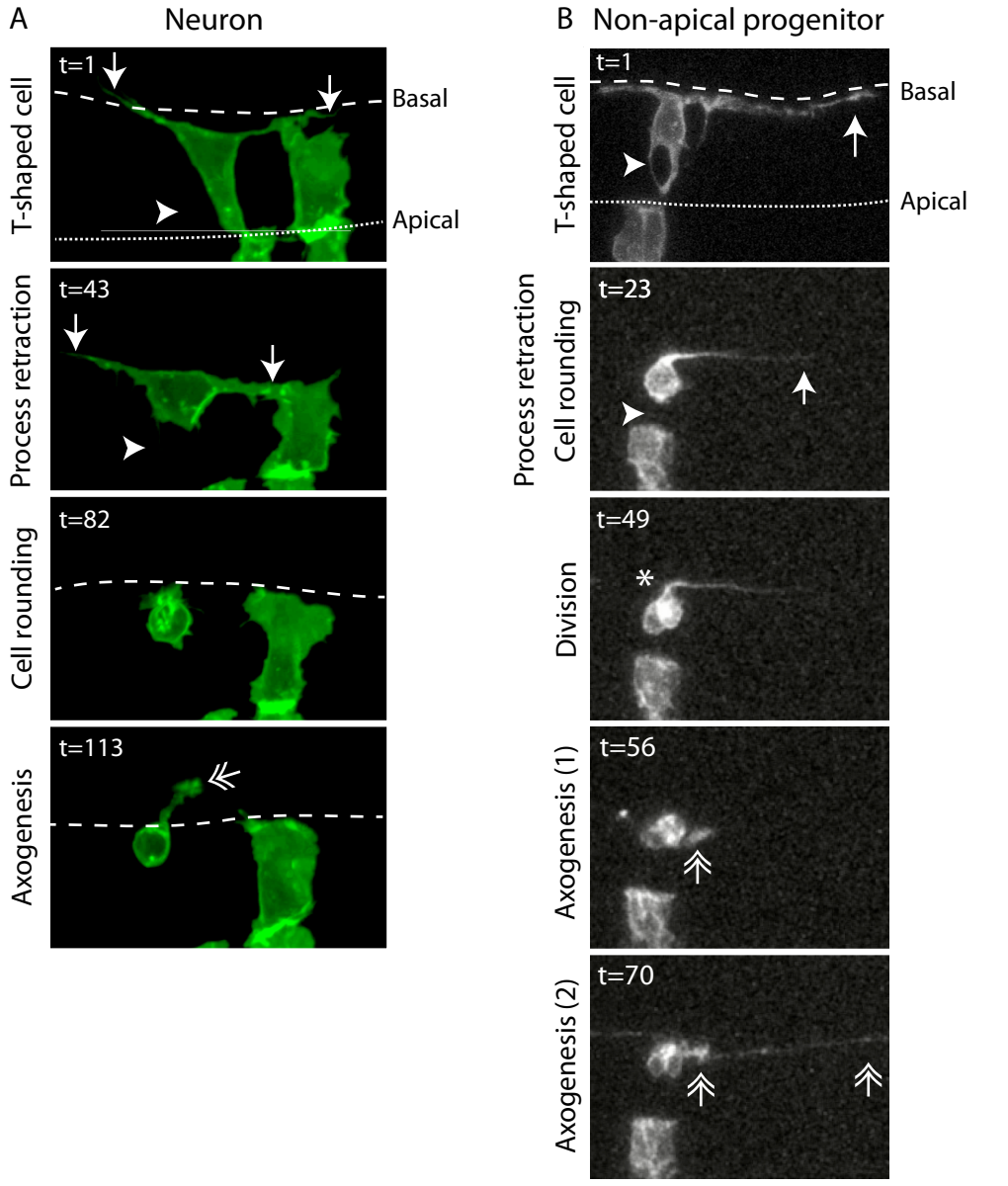
A
Neuron
T-shaped cell
Process retraction
Cell rounding
Axogenesis
t=1
t=43
t=82
t=113
Basal
Apical
B
Non-apical progenitor
T-shaped cell
Process retraction
Cell rounding
Division
Axogenesis (1)
Axogenesis (2)
t=1
t=23
t=49
t=56
t=70
Basal
Apical

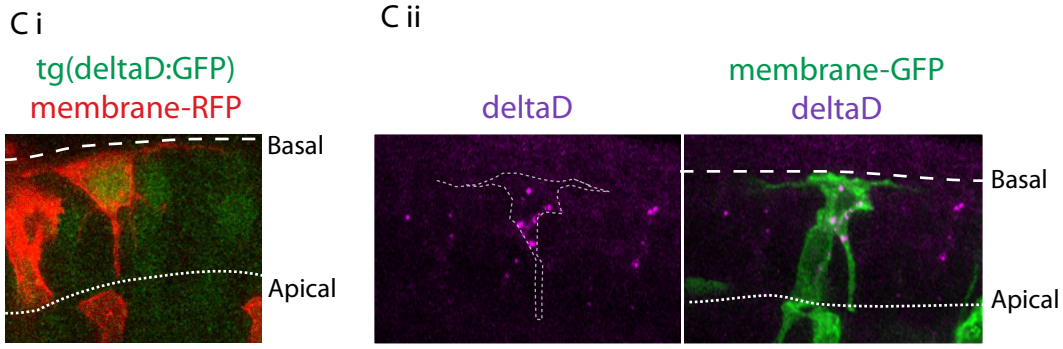
C i
tg(deltaD:GFP)
membrane-RFP
Basal
Apical
C ii
deltaD
membrane-GFP
deltaD
Basal
Apical

Figure 4-3: Model of T-shaped cell provided Delta Notch-mediated lateral inhibition. **A**) Differentiating neurons (brown cells) extend basal arms along the basal surface of the neural tube, while maintaining contact with the apical surface, taking on a T-shaped morphology. **B**) These membrane extensions allow cells to deliver inhibitory signals to cells at a distance from the differentiating cell's soma inhibiting neighbouring cells from differentiating. **C**) As the T-shaped cell retracts its basal arms and detaches from the apical surface, cells in the intervening space are released from inhibition and new cells (yellow) are permitted to begin to differentiate, starting by extending basal arms. **D**) The older progenitor then rounds up and (**E**) divides while the new T-shaped cell continues the basal arms behaviour, itself now inhibiting other cells in the neural tube (**E**). A solid line shows the basal surface and the apical surface is shown by dashed line. Green arrows show the direction of arm growth. The blue arrows denote the direction of the inhibitory signal (i.e. from the basal arms to the neighbouring cells).

Figure 4-3

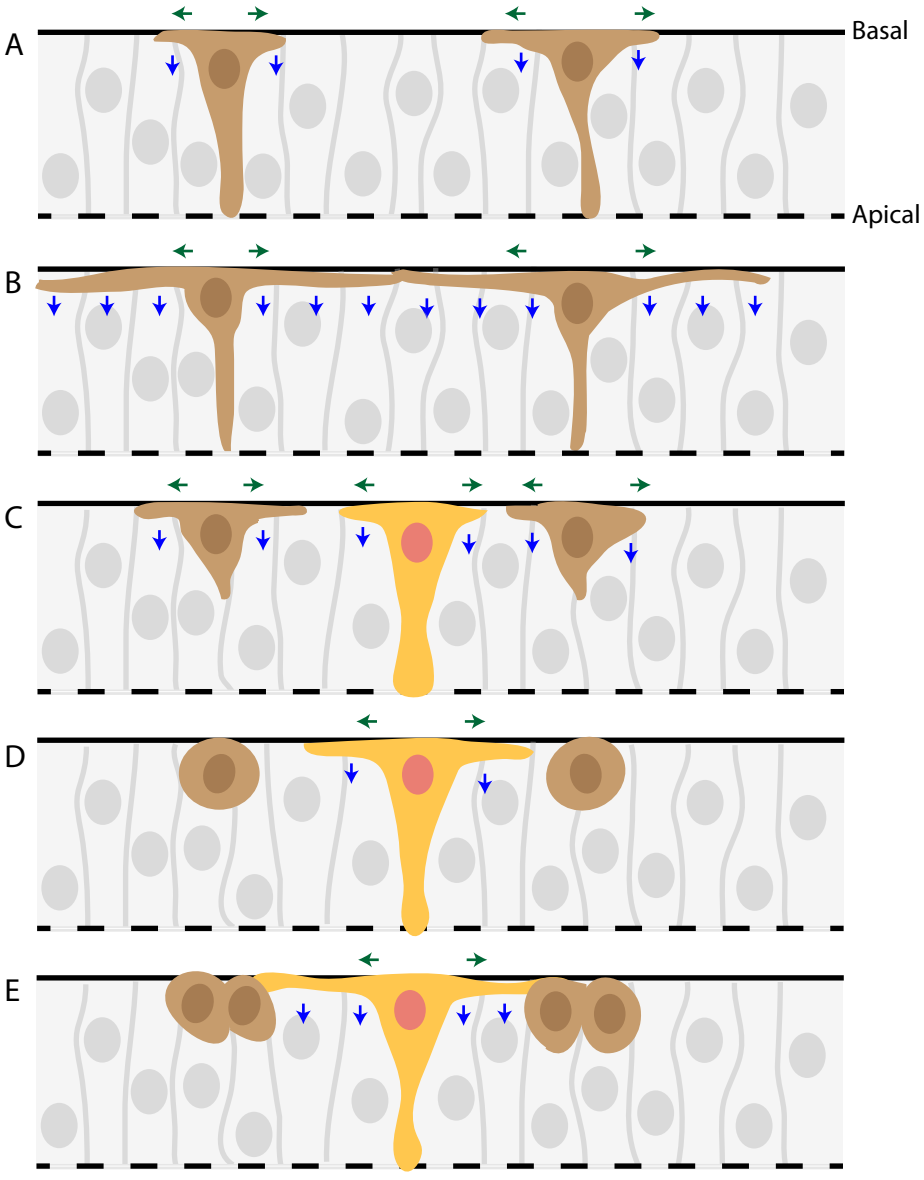

4.3 Materials Methods

4.3.1 Transgenic and mutant zebrafish lines

The transgenic and mutant zebrafish lines used in this chapter are listed in General Materials and Methods.

4.3.2 Morpholinos

Table 4-1: Anti-sense oligo morpholinos. The following morpholino were injected at the one cell stage.

Gene Target	Referred to as	Sequence	Source	Amount injected	Reference
Prickle	Pk1 morpholino	5′GCCCACCGTGATT CTCCAGCTCCAT 3′	Gene Tools	0.4 pM	(Carreira-Barbosa et al. 2003)
Standard control	Control morpholino	5'CCTCTTACCTCAG TTACAATTTATA 3'	Gene Tools	Equivalent concentrations	Control morpholino

4.3.3 *In situ* probes

Vsx1, gift from Chen Lou Lab, Zheijiang University, People's Republic of China (He et al. 2014).

4.3.4 Live imaging

The spinal cord was imaged dorsally, at approximately 9-14 somites, from approximately 18 hpf. Imaging was optimised so that a z-stack was taken at a 5 min interval and that z-step sizes were no larger than 2 μm.

4.3.5 Quantification of spacing in fixed embryos

The length of the somites along the anteroposterior axis was measured in single Z-planes, where the somites meet the neural tube. The distance between *vsx1* expressing neurons was also measured in single planes, from the centre of the neurons.

4.3.6 Quantification of time-lapse movies

Each movie was processed for drift correction in IMARIS®. V2a and V2b interneurons have descending axons (Batista et al. 2008), so the AP orientation of an embryo in a time-lapse movie can be identified by the direction of axon growth.

4.3.7 Analysis of spacing pattern development

To pick a defined point in the cellular history of non-apical progenitors we choose the time of its mitosis, as this is a clearly defined and short lasting cell state. We chose to use this behaviour

as the point to measure, as the length of time GFP expression was visible prior to division was variable. The distance between progenitor daughter pairs was measured from the centre of each pair using IMARIS® software.

4.3.7.1 Construction of pattern diagrams

We plotted the time and location of each observed differentiative division in pattern diagrams, where pairs of green circles represent a division. After division the neurons' cell bodies did not move on the anteroposterior axis, therefore straight lines were drawn through time to show their location in space through time.

4.3.7.1.1 Initial cells

Initial cells are defined as the first *vsx1* expressing progenitors to undergo division in the spinal cord and their daughter cells (in pairs). In the region analysed here this usually occurred before 20 hpf.

4.3.7.1.2 First iteration cells

The first *vsx1* division that occurred after the initial cells are referred to as first iteration progenitor divisions. However, if two first iteration progenitors divided within 1.5 hours of each other in between two initial cells, then these were counted as pairs of first iteration divisions.

The position of first iteration progenitors divisions relative to the closest two initial cells was measured and normalised so that the location of anterior initial cell = 0 and the location of the posterior initial cell = 1 and the midway point between the initial cell = 0.5.

4.4 Results

Vsx1:GFP cells are the only population of non-apical progenitors present in the zebrafish spinal cord during early neurogenesis (up to 36 hpf, see Chapter 3). Preliminary observations suggest that these progenitors differentiate in a periodic pattern in time and space. In this chapter I quantify the spatiotemporal dynamics of this population of non-apical neuronal progenitors.

4.4.1 Quantitative characterisation of the spatiotemporal pattern of *vsx1*:GFP differentiation

Vsx1 expression between somites 9 and 14 in the spinal cord can be observed from 17 hpf (Kimura et al. 2008). At this stage cells expressing *vsx1* mRNA (**Figure 4-4**A) or *vsx1*:GFP (**Figure 4-4**B) can be observed as isolated pairs of cells located on the basal surface of the neural tube. Time-lapse imaging of the spinal cord of Tg(*vsx1*:GFP) embryos shows that GFP expression is first observed in the non-apical progenitors just before they divide to produce pairs of GFP expressing neurons (**Figure 4-4**C and Kimura et al. 2008). These cells are approximately equally spaced along the anteroposterior axis and often, but not always, appear to be symmetrical across the midline (**Figure 4-4**A and B).

To understand the dynamics of *vsx1* progenitor appearance and division patterns I quantified *vsx1*:GFP progenitor differentiation events in time and space using time-lapse microscopy. It would be inaccurate to use the onset of GFP expression to define the time of *vsx1* progenitor differentiation, as it is difficult to objectively state the time point in which GFP expression is first observed. Furthermore, the time lag between GFP expression and division is variable making it a difficult metric to accurately compare between different *vsx1* expressing progenitors. However, the divisions of *vsx1*:GFP progenitors are easy to visualize and accurately record a precise time. Therefore, we chose to record the moment of division of *vsx1*:GFP progenitors as the read out of a differentiation event.

By recording the time of every division observed in 12 embryos and measuring the distance between these cells I was able to assemble pattern diagrams representing *vsx1*:GFP progenitor divisions in time and space (**Figure 4-5**). In the pattern diagrams each progenitor division is represented by a pair of green circles, the location of the dividing progenitor along the anteroposterior axis is shown on the x-axis (anterior to the left) and the y-axis represents the time of division. From the time-lapse movies of these embryos it is clear that newborn pairs of *vsx1*:GFP daughter cells undergo minimal movement after division so the lines on the diagram represent the position held by these cells through time. In these pattern diagrams you can see that differentiative divisions are spread out in space and time, as instances of two progenitors dividing close together in space and time are rare (**Figure 4-5**).

Early born *vsx1* cells establish a regularly spaced pattern of 'initial' *vsx1*:GFP cells by approximately 20 hpf (distance between initial cells, mean ± SEM, 46.28 µm ± 1.52, **Figure 4-4**A and B). The pattern diagrams suggest that initial progenitors mostly divide in a rostrocaudal gradient, with a cell dividing on average 12 mins (± 5.45 min SEM) after the cell most rostral to it. As development continues, the next set of progenitors can be observed dividing in the intervening spaces (**Figure 4-4**D). There is a time delay between the division of the initial and that of subsequent progenitors, which gives the impression of repeated 'waves' or rounds of *vsx1*:GFP progenitor divisions (**Figure 4-4**D and **Figure 4-5**). From the pattern diagrams it is fairly intuitive to identify initial cells and the first space filling divisions, however it is much harder to identify progenitors that would belong to the next 'waves' (**Figure 4-5**). To more accurately describe this repeating pattern I will refer to it as iterative. Therefore, the cells that divide after the initial cells are the first iteration and subsequent rounds of differentiation are referred to as second iteration, third iteration etc. Using this classification we can calculate the average time difference between iterations of progenitor divisions (mean ± SEM, initial to first iteration: 2 hr 39 mins ± 1 hr and first to second iteration: 3 hr 17 mins ± 1 hr 24 mins). The observed lengthening of time between iterations is statistically significant (two-tailed t test: $t = 2.351$, d.f. = 99, $P = 0.027$).

Figure 4-4: *vsx1* is expressed in non-apically dividing progenitors that divide spread out in space and time. **A** and **B)** Dorsal 3D renders of the spinal cord show that cells expressing *vsx1* mRNA (**A**) and *vsx1*:GFP (**B**) are located on the basal surface of the neural tube. Structure of the tissue is shown by nuclear counterstain (Sytox, blue, **A**) or brightfield image (**B**). **C**) Maximum projection of a lateral view of a Tg(*vsx1*:GFP) embryo. *Vsx1*:GFP expression is first seen in single cells (full arrowhead), which round up before undergoing division (asterisks). Following division, axonogenesis can be followed in both daughter cells (double headed arrows). **D**) *Vsx1*:GFP progenitors divide spread through space and over time. The left panel shows *vsx1*:GFP cells initiating expression of GFP and dividing. The sequential addition of *vsx1*:GFP expressing cells occurs over time. In the right hand panel, cells have been colour coded to highlight when they divide. New progenitors appear to fill in the gaps of existing cells. Blue dots denote the initial cells, purple dots show first iteration cells and orange show second iteration cells. Dashed line shows basal surface shown. Scale bar = 25 μm.

Figure 4-4

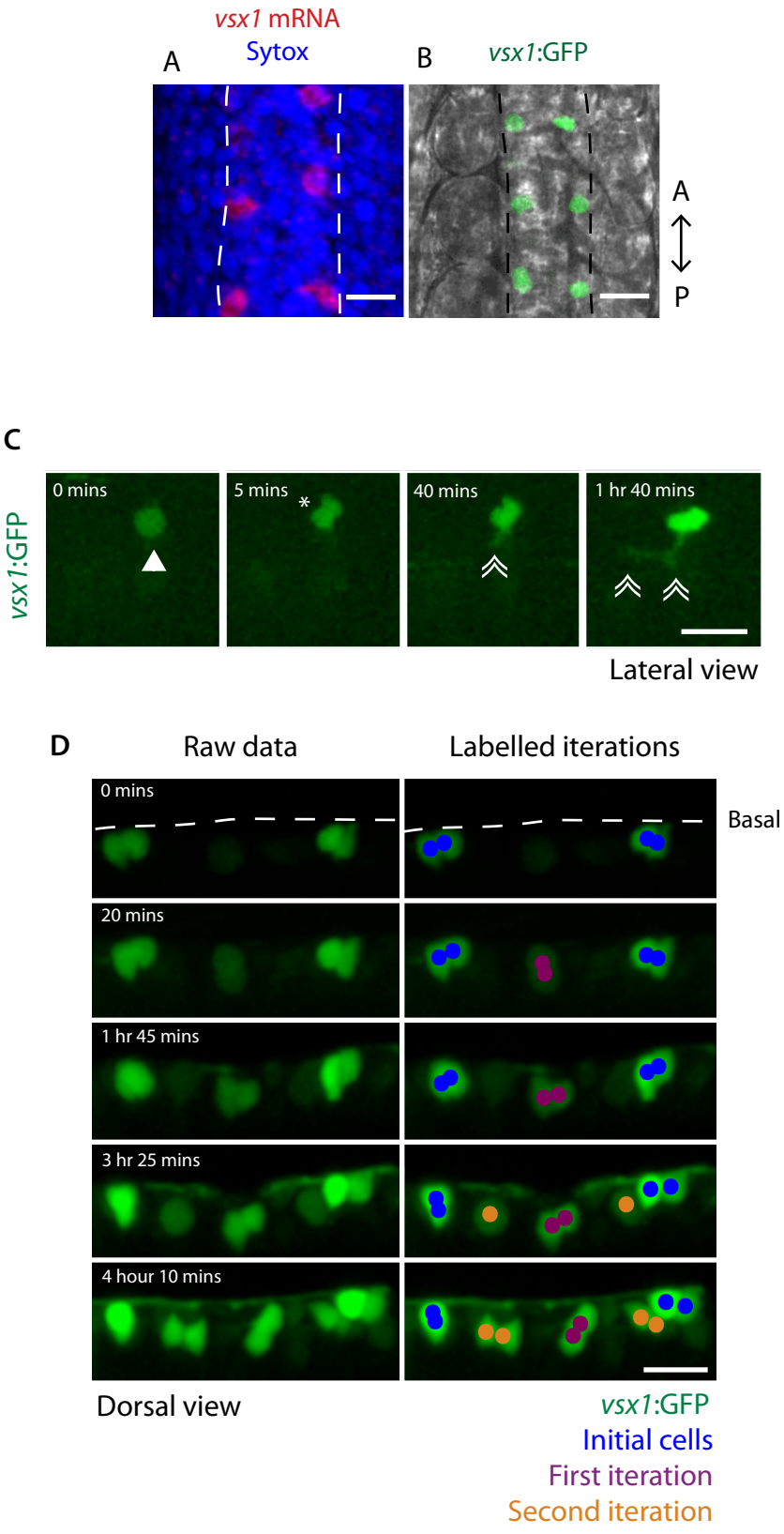
A
vsx1 mRNA
Sytox
B
vsx1:GFP
A
P
C
vsx1:GFP
0 mins
5 mins
40 mins
1 hr 40 mins
Lateral view
D
Raw data
Labelled iterations
0 mins
Basal
20 mins
1 hr 45 mins
3 hr 25 mins
4 hour 10 mins
Dorsal view
vsx1:GFP
Initial cells
First iteration
Second iteration

Figure 4-5: Pattern diagrams of *vsx1*:GFP progenitor differentiation in space. The location of *vsx1*:GFP progenitor divisions in time (y-axis) and space (x-axis) is represented in these pattern diagrams by pairs of green circles. The lines from the division, going through time, represent the position held by the daughter cells after division. Each pair of diagrams show data from a single embryo, with each diagram showing all of the divisions observed in one half of the neural tube. Divisions shown on the line representing the x (distance) axis occurred before the recording/time-lapse began. Anterior to the left. The pattern of differentiation observed on each side of the neural tube is shown for all embryos analysed.

Figure 4-5; Page 1

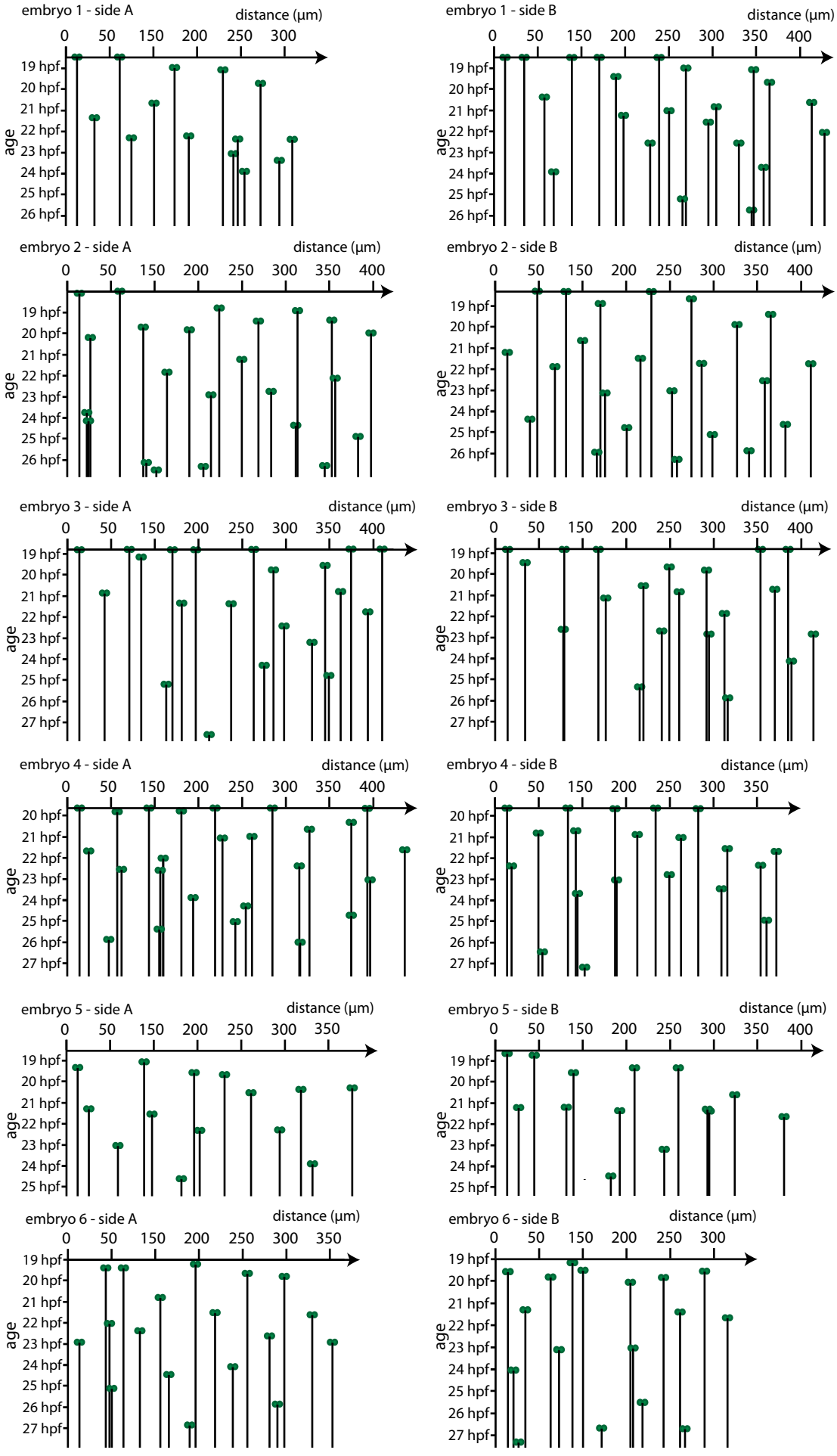

Figure 4-5; Page 2

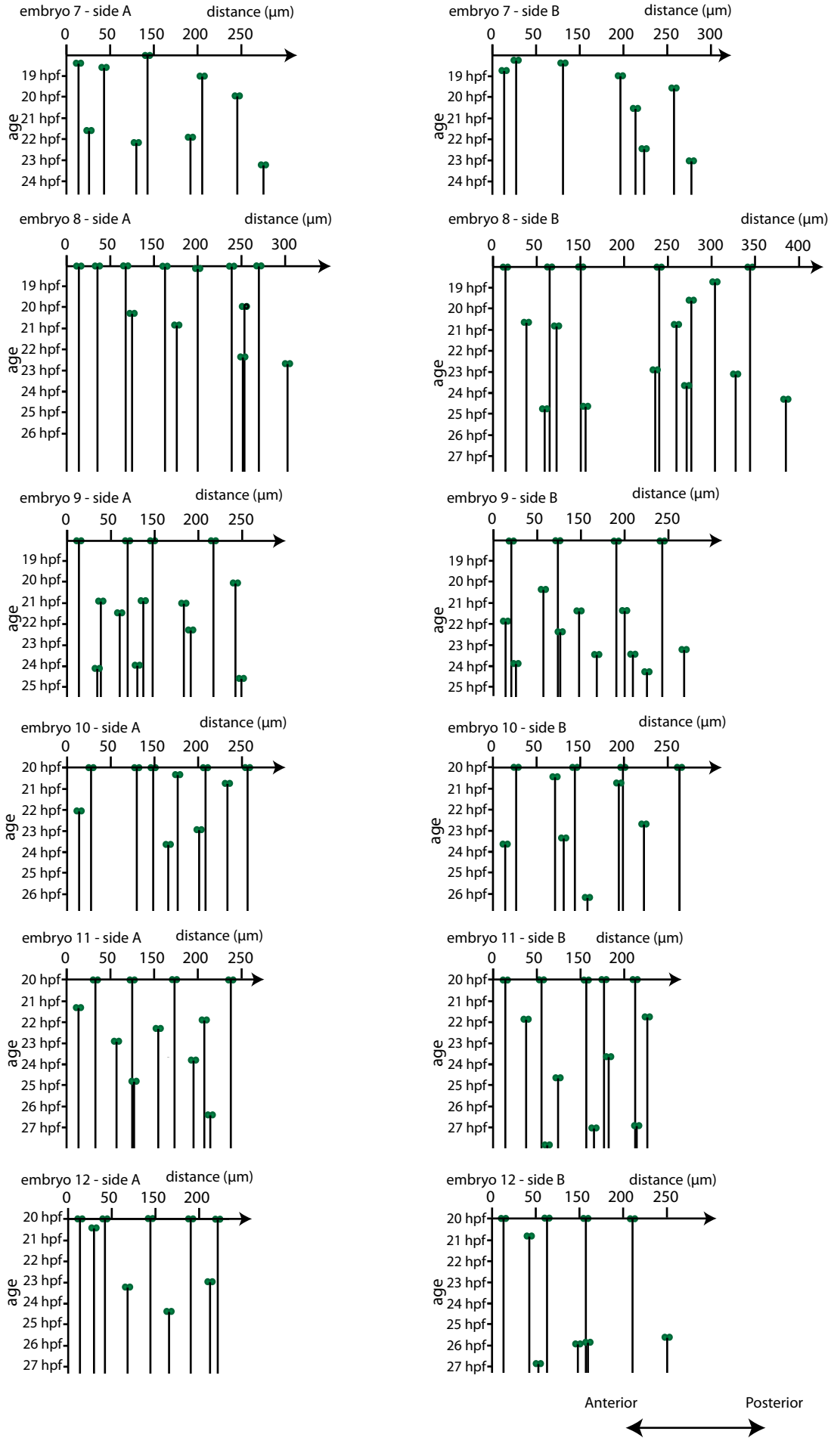

4.4.2 *vsx1*:GFP differentiation occurs with a long distance pattern in through time and space

As *vsx1*:GFP cell are the only non-apical progenitors in the spinal cord at this stage we know that these cells have gone through the T-shaped morphological transition prior to division. If the basal arms of T-shaped cells are delivering long-range inhibitory signals to the intervening cells, as described in our hypothesis (section 4.1.3.1 and **Figure 4-3**), we would expect to see the following in the pattern of differentiation:

- New *vsx1* progenitors are generated in the middle of the space between existing cells.
- Two *vsx1* progenitors are unlikely to divide close together in time and space.

We can use the dataset generated from the quantitative characterisation of *vsx1*:GFP described above to test these predictions.

4.4.2.1 *Vsx1* progenitors tend to divide in the middle of the space between existing *vsx1*:GFP pairs

Our hypothesis that T-shaped cells might deliver transient long-range inhibitory signals to the intervening cells predicts that new *vsx1* progenitors are likely to divide and differentiate in the middle of the space between existing *vsx1* cells. From time-lapse movies it is clear that the exact location of first iteration divisions relative to existing cells is variable. We observed first iteration *vsx1*:GFP-expressing progenitors dividing exactly in the middle of the space between initial *vsx1*:GFP cells (Figure **4-6**A), some very near one of the existing pairs of *vsx1* cells (Figure **4-6**B) and some off centre (Figure **4-6**C). To quantify this I measured the distance between an anterior initial cells and the first iteration progenitor and normalized this to the distance between the anterior and posterior initial cells (**Figure 4-6**D). This analysis shows that divisions occur with a normal distribution along the space between existing *vsx1*:GFP cells and that most new *vsx1* progenitors tends to divide in the middle of the space between existing *vsx1* cells (**Figure 4-6**D; D'Agostino & Pearson, H_0 – values are samples from a normal distribution: K2 = 4.010, P = 0.1347).

These data suggest that a mechanism exists to bias the first iteration *vsx1*:GFP progenitors to divide and differentiate as far away as possible from initial *vsx1* progenitors. This adds precision to our observation of the space filling behaviour of new progenitors and supports our hypothesis that long-range signalling is driving this pattern formation.

Figure 4-6: New *vsx1*:GFP progenitors tend to differentiate in the middle of existing *vsx1*:GFP cells. **A-C**) Examples of the location of first iteration cells (red dot) relative to existing *vsx1:*GFP cells (blue dot). New progenitors that appear in the middle of existing cells (**A**), close to one of the initial cells (**B**) or off centre between initial cells (**C**) Scale bar = 20 μm. Dashed line shows the basal surface. **D**) Histogram showing the percentage of first iteration *vsx1*:GFP divisions that occur at different points along the axis between initial cells. The highest frequencies are found in the region in the middle of existing cells. 0 = anterior initial cell, 1 = posterior initial cell.

Figure 4-6

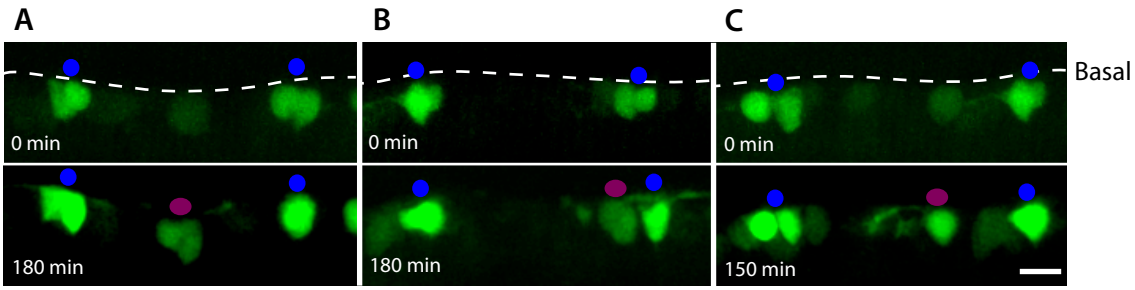
A
B
C
Basal
0 min
0 min
0 min
180 min
180 min
150 min
Dorsal view
vsx1:GFP
Intial cells
First iteration

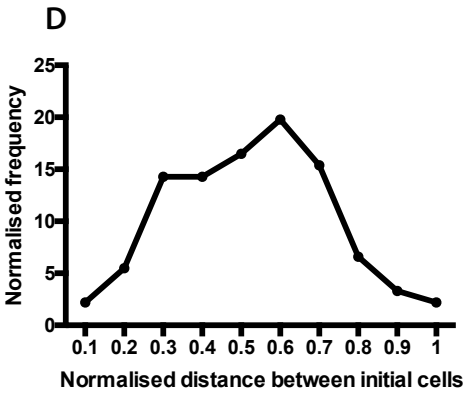
D
Normalised frequency
25
20
15
10
5
0
0.1 0.2 0.3 0.4 0.5 0.6 0.7 0.8 0.9 1
Normalised distance between initial cells

4.4.2.2 *Vsx1* progenitors are unlikely to divide close together in time and space

In order to understand the spatial and temporal aspects of *vsx1*:GFP differentiation I calculated the pair-wise difference in time (ΔT) and the distance (ΔD) between each observed *vsx1* progenitor division. Cells that underwent division before the start of imaging were excluded from this analysis.

Taking all the pairwise date together, progenitors most frequently divide 60 – 80 µm apart (seen as a peak in the distribution, asterisks in Error! Reference source not found.**A**) and the average pairwise distance between progenitors at division is 110 µm (± 78.01 S.E.; n = 1967 pairs)**.** To see if the time between division events affects the spacing of progeneitors I separated those progenitors that divide close together in time (ΔT < 1 hr 30 mins; **Figure 4-7B**) from those with a long time lag between their divisions (ΔT > 1 hr 30 mins; **Figure 4-7C**). For pairs of progenitors with a small ΔT, the divisions with a ΔD of 40 – 60 µm become more frequent, with a loss of divisions with a ΔD of < 40 µm (red and blue asterisks, respectively, in **Figure 4-7**Error! Reference source not found.**B**). The mean pairwise distance for cells with a ΔT < 1 hr 30 mins is 121.26 µm (± 75.4 S.E.; n = 638 pairs), which is significantly different to the mean pairwise distance for all pairs (compare **Figure 4-7A** and **Figure 4-7B**; T-test, $p < 0.005$). On the other hand, when considering only progenitor pairs with a large ΔT (> 1 hr 30 mins), there is an increase in the frequency of divisions occurring between 0 and 40 µm of each other and a decreased frequency of progenitors with a ΔD of 40 – 60 µm (red and blue asterisks, respectively, in **Figure 4-7C**). This is seen as a significant decrease in the mean pairwise distance for cells with a large ΔT (mean ± S.E. = 104.72 µm ± 79.2; ; T-test, $p < 0.025$**;** Error! Reference source not found.**C**).

In summary, this analysis shows that *vsx1* progenitors that divide close together in time (< 1 hr 30 mins) are unlikely to be close in space (> 40 µm), but if there is a large difference in the time of the division of these progenitors, then they are more likely to be close together in space.

4.4.2.3 Summary

The quantitative analysis of *vsx1*:GFP progenitor differentiation described above suggests that a long distance mechanism exists to ensure that two division events occur spread out in time and space. We hypothesise that this mechanism involves the extension of basal arms we have observed on nascent neurons and non-apical progenitors. Further experiments are required to directly test this hypothesis.

Figure 4-7: *vsx1*:GFP progenitors are unlikely to divide close together in time and space. (**A – C**) Histograms showing the frequency of pairwise *vsx1*:GFP progenitor division events binned by the distance between them at division (ΔD). **A**) Graph showing the frequency of all progenitor divisions in each ΔD bin. The asterisk shows the peak frequency of ΔD. **B**) Graph showing the frequency of all progenitor divisions in each ΔD bin when only considering progenitors where ΔT < 1.5 hrs. The frequency of divisions close together (ΔD > 50 μm) decreases (blue asterisk) and the frequency of of divisions with a ΔD of 40 – 60 μm increases (red asterisk. **C**) When only considering progenitors where ΔT > 1.5 hrs, the frequency of divisions close together (ΔD > 50 μm) increases (blue asterisk) and the frequency of of divisions with a ΔD of 40 – 60 μm decreases (red asterisk). N = 12 embryos.

Figure 4-7

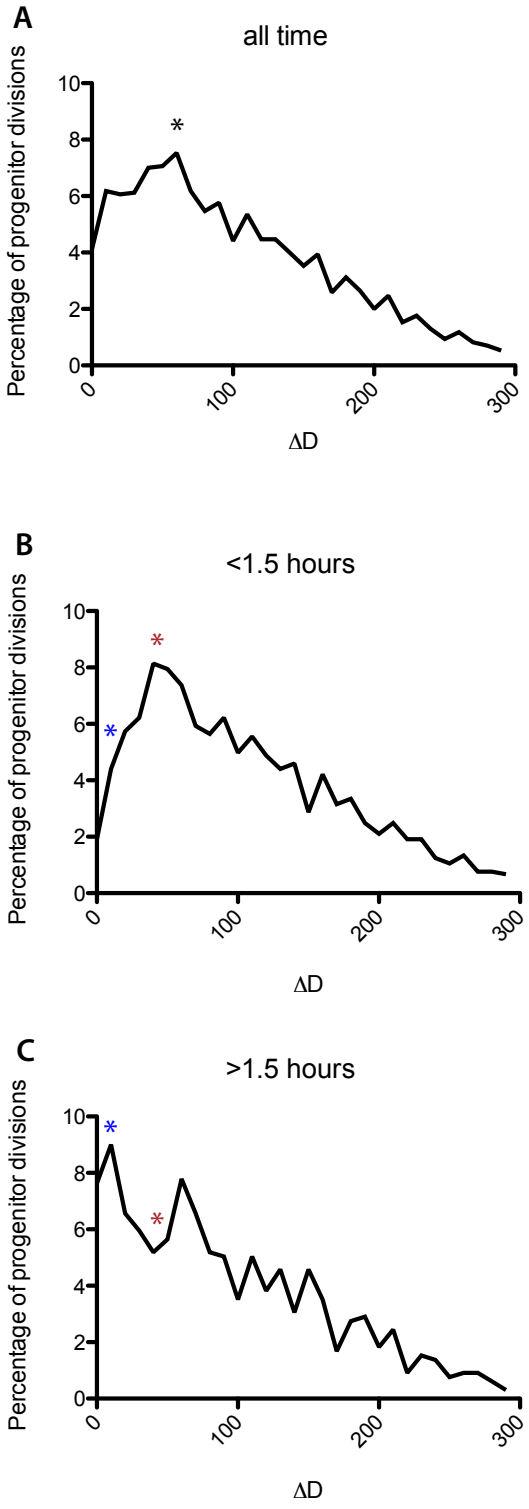
A
all time
Percentage of progenitor divisions
10
8
6
4
2
0
0
100
200
300
ΔD
B
<1.5 hours
Percentage of progenitor divisions
10
8
6
4
2
0
0
100
200
300
ΔD
C
>1.5 hours
Percentage of progenitor divisions
10
8
6
4
2
0
0
100
200
300
ΔD

4.4.3 Initial *vsx1*:GFP progenitor spacing is independent of mesoderm signals

The sparse pattern of initial cells I have observed in *vsx1*:GFP cells resembles the periodic pattern of primary motor neurons in the spinal cord (Hutchinson & Eisen 2006; Gribble et al. 2007; Kimura et al. 2008). Mesoderm-derived signals have previously been shown to play an important role in the patterning of primary motor neurons along the anteroposterior axis (Eisen & Pike 1991; Lewis & Eisen 2004; Sato-Maeda et al. 2008). To investigate whether or not mesoderm-derived signals are involved in patterning *vsx1* cells I looked at the spacing of *vsx1*:GFP progenitors in embryos with altered somite patterning, specifically *prickle* (*Pk1*) morpholino-injected embryos and *fused somite* mutant (*fss*-/-) embryos. If a patterning signal from the paraxial mesoderm is responsible for patterning *vsx1* progenitors we would expect that: (1) *vsx1* neurons would align with the somite, (2) there would be a correlation between the size of the somites and the spacing of *vsx1* progenitors and (3) alterations to the somites would results in a corresponding change to the spacing of *vsx1*:GFP progenitors. All of these are seen in the pattern of primary motor neurons (Lewis & Eisen 2004).

To test for a relationship between somite development and *vsx1* patterning, Tg(*vsx1*:GFP) embryos were injected at the 1 cell stage with a morpholino targeted against aPKC and *vsx1*:GFP differentiation was imaged live in Pk1-depleted embryos. Reducing the level of Pk1 protein by anti-sense oligo-morpholino injection generates embryos with a shortened body axis and significantly compacted somites (Carreira-Barbosa et al. 2003, and **Figure 4-8**E). Instead of forming square somites, embryos injected with the *Pk1* morpholino have long, thin somites, shortened along the anteroposterior axis and elongated on the mediolateral axis (compare bright field images in **Figure 4-8**A and B). *Pk1* morpholino-injected embryos contained the same number of initial *vsx1*:GFP cells as seen in control embryos (**Figure 4-8**C; two tailed t test, P = 0.02195, d.f. = 35), showing that neurogenesis is unaffected by loss of Pk1.

I then looked at the location of initial *vsx1*:GFP progenitors in relation to the nearest somite. I found that *vsx1*:GFP were distributed randomly along the anteroposterior axis of the adjacent somite (**Figure 4-8**D; χ^2 (9, n = 49) = 2.45, p > 0.1). Furthermore, the spacing between *vsx1* cells and the length of the somites in *Pk1* morpholino-injected embryos was significantly different, suggesting there is no correlation between neuronal spacing and mesoderm segmentation (**Figure 4-8**E). I also found the distance between initial *vsx1*:GFP cells was not significantly different in *Pk1* morpholino-injected embryos compared to controls (**Figure 4-8**E). To support this, I calculated the ratio between the observed distance between initial *vsx1* progenitor cells and the average somite length in wild type embryos. In this analysis, the individual ratios of initial distance to somite length are variable and the average ratio was 0.82

(± 0.33 SD; **Figure 4-8**F). This indicates that neuronal spacing in the spinal cord does not directly correlate with somite size. These data suggest that establishing the spacing of *vsx1*:GFP progenitors is independent of Prickle signalling and mesodermal patterning.

To further test a potential link between mesoderm and neuronal patterning I looked at the spacing of *vsx1*:GFP progenitors in *fused somites* mutant fish (*fss*^{te314a}, referred to as *fss*-/-; van Eeden et al. 1996). Embryos homozygous for this mutant fail to form boundaries between all of their somites, resulting in a continuous paraxial mesoderm (van Eeden et al. 1996), while their siblings appear wild type (compare **Figure 4-9**A and C). The organisation of the tissue within the spinal cord appear normal in both *fss*-/- and sibling embryos, with a clear delineation between the notochord and neural tube (arrows **Figure 4-9**B and D). I carried in an *in situ* hybridisation against *vsx1* in these embryos to look at the spacing of *vsx1*:GFP progenitors (**Figure 4-9**E and F) and found that there was no difference in the average distance between *vsx1*:GFP progenitors in *fss*-/- and sibling embryos (**Figure 4-9**G).

Taking together these data strongly suggest that mesoderm-derived signals are not involved in patterning *vsx1*:GFP progenitors.

Figure 4-8: Prickle morpholino-injected embryos show shorted somite length but unaffected *vsx1*:GFP progenitor spacing.**A** and **B)** Dorsal 3D renders of the spinal cord of control (C) (**A**) and prickle (Pk1) (**B**) morpholino (mo)-injected Tg(*vsx1*:GFP) embryos at 20 hpf. GFP-expression shows the pattern of initial *vsx1*:GFP cells and somites are visible in the bright field image. The somites of *Pk1*mo-injected embryos appear shorter on the anteroposterior axis (flat-ended lines) and lengthened on the mediolateral axis, compared to Cmo embryos. Scale bar = 25 μm. **C**) The number of *vsx1*:GFP divisions that occur before 20 and 22 hpf in Cmo (black bar) and *Pk1*mo (grey bar)-injected embryos. No difference was found in the number of divisions in Cmo or *Pk1*mo-injected embryos at either time point (ANOVA $F(1, 70) = 0.0055$; $p < 0.94$). **D**) Location of *vsx1*:GFP cells in relation to the anteroposterior axis of the adjacent somite. 0 = anterior border, 100 = posterior border. *Vsx1* cells are evenly spread in relation to the somite (χ^2 (9, n = 49) = 2.45, $p > 0.1$). **E**) The measured somite size and distance between initial progenitor cells for control (black bars) and *Pk1* (grey bars) morpholino-injected embryos. Somites were measured in a single plane, where they met the neural tube (flat ended line in A and B) and the distance between pairs of *vsx1*:GFP progenitors was measured from the centre of each daughter cell pair (arrow headed lines in A and B). Compared to Cmo, *Pk1*mo embryos have significantly smaller somites (Mann-Whitney $U = 40$; $n_1 = 25$, $n_2 = 38$; $P < 0.001$), but the initial distance between *vsx1*:GFP progenitors is not significantly different between the treatment groups (unpaired two tailed t-test, $t = 3.568$, $P = 0.0006$, d.f. = 99). The somite size and initial cell distance is not significantly different in control embryos but are different in *Pk1*mo embryos (Unpaired Two tailed T-test, $t = 4.371$, $p < 0.0001$, d.f. = 92). **F**) The ratio of somite size to initial spacing in Cmo and Pk1mo embryos. This ratio is significantly increased by injection of *Pk1* morpholino (Mann-Whitney $U = 451$; $n_1 = 45$, $n_2 = 49$; $P < 0.0001$). N = 13 Cmo embryos and 8 *Pk1*mo embryos.

Figure 4-8

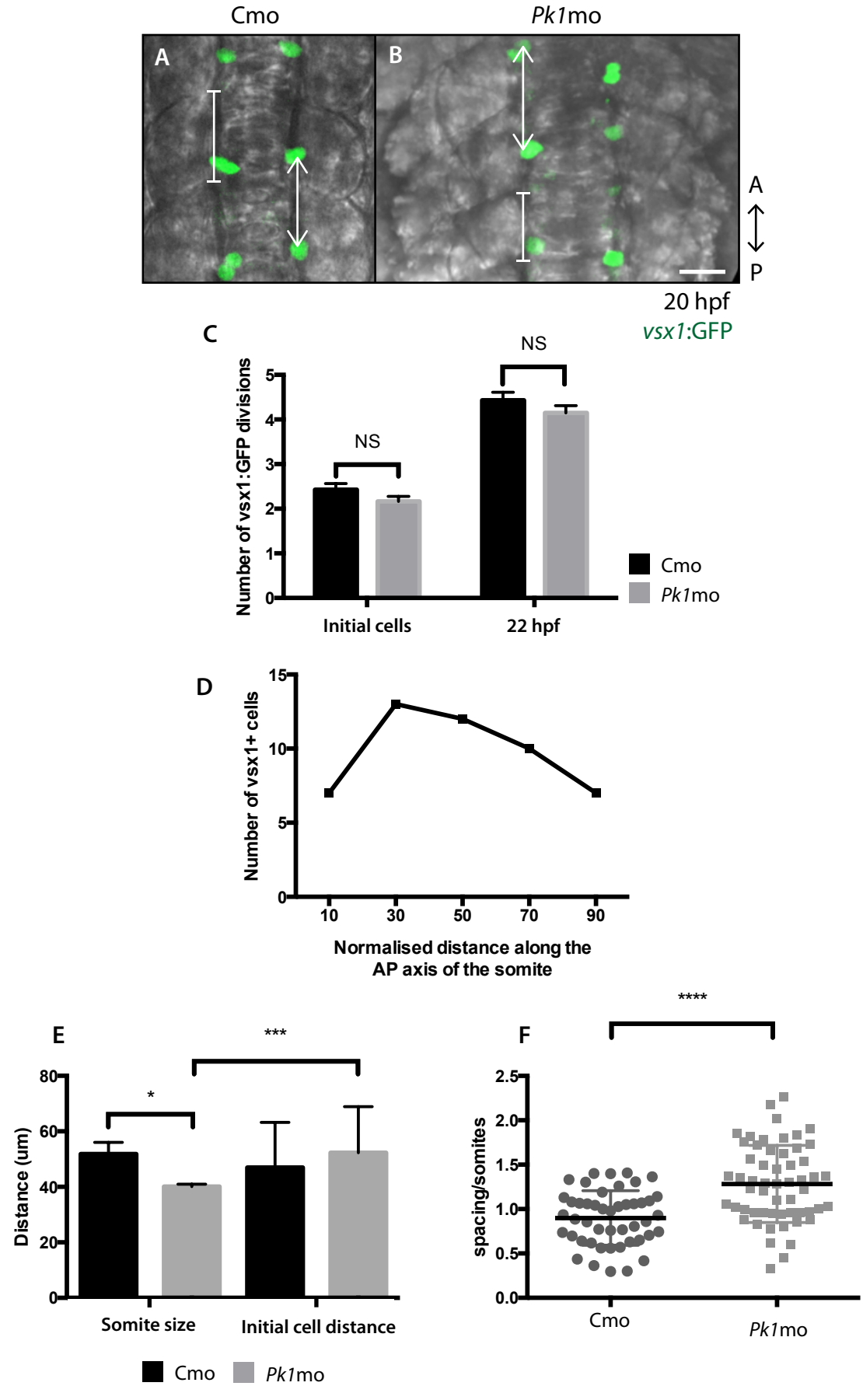
Cmo
Pk1mo
A
B
A
P
20 hpf
vsx1:GFP
C
NS
NS
Number of vsx1:GFP divisions
0
1
2
3
4
5
Initial cells
22 hpf
Cmo
Pk1mo
D
Number of vsx1+ cells
0
5
10
15
10
30
50
70
90
Normalised distance along the AP axis of the somite
E
***
*
Distance (um)
0
20
40
60
80
Somite size
Initial cell distance
Cmo
Pk1mo
F
****
spacing/somites
0.0
0.5
1.0
1.5
2.0
2.5
Cmo
Pk1mo

Figure 4-9: Fused somite mutant embryos show unsegmented mesoderm but unaffected *vsx1*-expressing progenitor spacing. **A-D**) DIC images of the lateral view of *fss*-/- and sibling embryos at 26 hpf. **A** and **C**) Focusing in the myotome allows the visualisation of the chevron shape of segmented somites in sibling embryos. In *fss*-/- embryos, this clear segmentation is lost. **B** and **D**) Focusing on the neural tube, the gross structure looks normal in *fss*-/- compared to sibling embryos. Arrows show the border between the neural tube and notochord. Anterior is to the left. NT = neural tube. NC = Notochord. **E** and **F**) Maximum projection of a dorsal view of the spinal cord of sibling and fss-/- embryos after *in situ* hybridisation for *vsx1* (white) and counterstain for nuclei (Sytox, blue). Arrowheads show *vsx1*-expressing neurons in the neural tube. Asterisks are place in the centre of each somite. Dotted lines show the apical surface and dashed lines show the basal surface. Scale bar = 25 μm. **G**) Graph showing the mean (± SEM) distance between *vsx1*-expressing neurons in sibling and *fss*-/- embryos. No difference in *vsx1* spacing was observed between sibling and *fss*-/- embryos (unpaired t-test, P = 0.1539, t = 1.439, d.f. = 94).

Figure 4-9

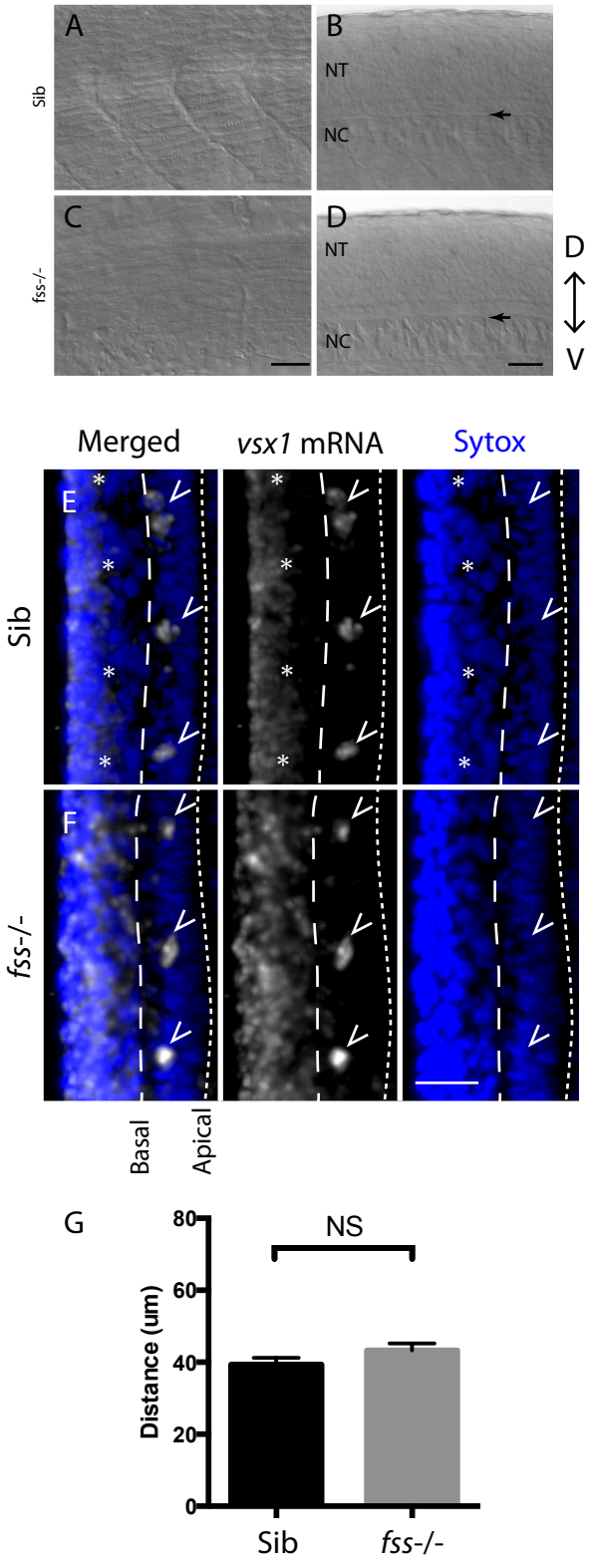
A
B
NT
NC
Sib
C
D
NT
NC
fss-/-
D
V
Merged
vsx1 mRNA
Sytox
E
F
Sib
fss-/-
Basal
Apical
G
NS
Distance (um)
80
60
40
20
0
Sib
fss-/-

4.4.4 DeltaD-GFP BAC transgenic zebrafish labels T-shaped cells

The Clarke and Alexandre labs have previously characterised differentiating neurons and non-apical progenitors extending membrane protrusions (basal arms) into the surrounding tissue (unpublished, described in section 4.1.3.1). As *vsx1*:GFP cells are the only population of non-apical progenitors in the tissue at this stage, we know that these cells undergo the T-shaped morphological transition prior to division. The function of basal arms in zebrafish neuronal differentiation is currently unknown, however there are a number of similarities between basal arms and the membrane extensions known to pattern the development SOPs in *Drosophila* (described in detail in section 4.1.3). This suggests that neurogenesis in the zebrafish spinal cord might employ a similar long-range mechanism to space and pattern neurons as has been characterised in the *Drosophila* notum.

Patterning of SOPs is known to require Delta Notch signalling (De Joussineau et al. 2003; Cohen et al. 2010). Therefore, to address the hypothesis that neurogenesis in zebrafish is patterned in time and space by the activation of Notch signalling by Delta ligand delivered by basal arms, similar to what is known for *Drosophila*, I have analysed the expression of a deltaD-GFP fusion protein in transgenic zebrafish embryos (embryos provided by Dr Oates, UCL, unpublished). This fusion protein has been shown to rescue the phenotype of the deltaD mutant line, demonstrating that the fusion protein is functional (B-K. Liao and A. Oates, unpublished). While puncta of deltaD-GFP are present throughout the neuroepithelium, the cells that express the highest levels of deltaD-GFP are in the T-shaped transition (**Figure 4-10**). In fact, T-shaped cells are the only cells whose morphology is clearly labelled in this line. Importantly, deltaD-GFP expression is seen along the basal arms of these cells (shown by the arrows in **Figure 4-10**). This data suggests that the basal arms are able to deliver Delta-mediated lateral inhibition.

This is strong circumstantial evidence that Delta Notch signalling might mediate the inhibitory signal provided by basal arms.

Figure 4-10: DeltaD BAC is expressed in T-shaped cells. Maximum projection of a dorsal view of the spinal cord of a Tg(*deltaD*-GFP) embryo. GFP expression is shown in grey scale. **A**) DeltaD-GFP puncta are highly expressed in the basal arms (arrows), apical process (empty arrowhead) and basal soma of a T-shaped cell (asterisks). These puncta are mobile (most obvious in the cell soma in **A**-**C**). Apical surface is shown by a dotted line and basal surface by a dashed line. Scale bar represents 25 μm.

Figure 4-10

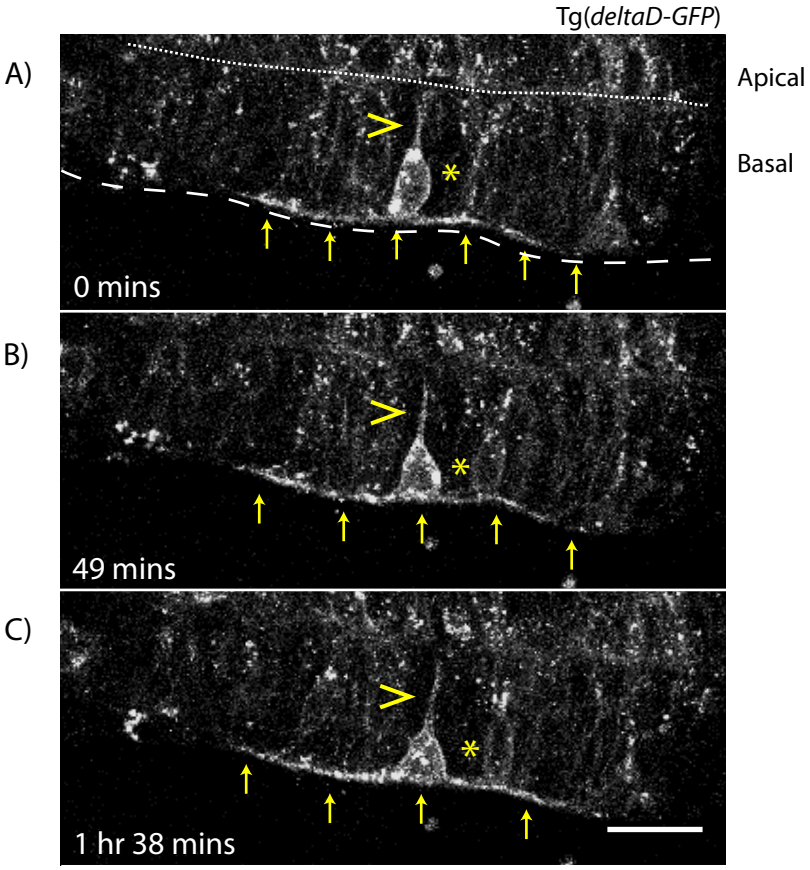

4.5 Discussion

Studies of vertebrate neurogenesis have historically been limited to fixed tissues or transverse slice cultures due to technical difficulties associated with live imaging opaque and large tissues. Therefore, the dynamics of a population of neurons differentiating in space and time in a whole tissue have not yet been studied, particularly in the vertebrate spinal cord. However, there are data from zebrafish and *Xenopus* embryos, which indicate that early long distance patterning of neuronal subtypes followed by younger cells filling in the gaps is a common feature of vertebrate neurogenesis (Roberts et al. 1988; Roberts et al. 1987; Dale et al. 1987; Kimura et al. 2008; England et al. 2011), and one that is currently unexplained. Zebrafish embryos are an ideal model to address this question due to the ease of live imaging and the ability to label subpopulations of neurons. Here, I generated a quantitative characterisation of the spatiotemporal dynamics of the differentiative divisions of *vsx1*-expressing progenitors in the zebrafish spinal cord. *Vsx1* non-apical neuronal progenitors are an ideal neuron subtype to use for this study as they do not change position after division, unlike other neuronal subtypes that are known to migrate into their correct position after differentiation (Sato-Maeda et al. 2006).

Quantitative analysis of the spatiotemporal pattern of differentiation shows that *vsx1*:GFP cells have an initial long distance spacing pattern along the anteroposterior axis of the neural tube and this pattern is formed independent of mesoderm-derived signals. The progenitors that divide next will most likely do so in the space between existing cells. Further analysis reveals that *vsx1* progenitors are unlikely to divide close together in time and space. This suggests that dividing *vsx1* progenitors are employing a mechanism to inhibit neighbouring cells within 40-60 μm from also differentiating in a 1 hr 30 min window. I also show that cells undergoing the T-shaped transition express Delta-GFP, suggesting that the inhibitory signal is delivered by Delta Notch signalling.

Taken together the data presented in this chapter suggests that a long distance inhibitory mechanism exists to stop progenitors undergoing division at the same time and in the same place. These data support our hypothesis that the basal arms we have observed on differentiating neurons might play a role in inhibiting adjacent cells from differentiating too. However, more direct and precise experimental evidence will be necessary to fully test this hypothesis.

4.5.1 Comparing patterning mechanisms in the *Drosophila* notum and zebrafish spinal cord

The hypothesis that I have been discussing in this chapter, that a long-range signal generates a spatiotemporal pattern of neuronal differentiation, is based on observations of SOP development

in *Drosophila* and previous data from the Clarke lab on the cell morphological changes that occur during neuronal differentiation.

A self-organising patterning mechanism has been well characterised during the development of a specific neuronal cell type, sensory organ precursor cells (SOPs), in the *Drosophila* notum (Cohen et al. 2010; De Joussineau et al. 2003). In the single-layered epithelial sheet that forms the notum, differentiation of SOPs is limited to a small number of cells, spread throughout the tissue, by long-range Delta Notch-mediated lateral inhibition, delivered by filopodia-based membrane extensions present on differentiating cells (Cohen et al. 2010; De Joussineau et al. 2003). We hypothesise that differentiating neurons and non-apical progenitors in the zebrafish spinal cord space themselves out using a similar mechanism. During differentiation these cells undergo the T-shaped morphological transition and extend basal arms along the basal surfaee. These cellular processes provide lateral inhibition signals to inhibit the differentiation of cells within their reach.

As well as the similarities I have discussed, a number of important differences exist between the two systems.

First, neuronal differentiation in the notum lacks a temporal dimension, meaning that all cells differentiate within a short time period. In this system the patterning cue acts, the specified cells differentiate as SOPs and the induced spacing pattern is maintained. In contrast, during neurogenesis in the zebrafish spinal cord differentiation occurs spread through time and over a long neurogenic phase. Therefore, the patterning system is not inhibiting neurogenesis in the region adjacent to the T-shaped cell but delaying neuronal differentiation to spread it out through time. This requires the patterning cue to be flexible, allowing it to be dismantled and re-established through time. (Incidentally, this adds support to our finding that mesoderm-derived cues are not required for this pattern, as any cue coming from the somites is most likely to be set through time and should result in accumulation of neurons in a location, not the space filling that we see.)

Second, in *Drosophila* the notum is a 2D epithelial sheet, while the zebrafish spinal cord is a 3D tube structure with domains of neuroepithelial cells that produce different neural cell types stacked along the dorsoventral axis. Our current model is based on spatial selectivity of T-shaped cells, whereby the basal arms are limited to a single dorsoventral plane and therefore only come into contact with one type of differentiating cell (in this case *vsx1* progenitors). However, we have observed filopodia extending radially from the soma and basal arms of T-shaped cells, suggesting they are able to signal to multiple cells across different dorsoventral

levels and therefore might contact and interact with multiple subtypes of progenitors and differentiating neurons. In spite of this, we have preliminary data that suggests the spacing of different neuronal subtypes is established independently of each other (P. Alexandre, unpublished). This might indicate that T-shaped cells are only able to interact with and specifically inhibit progenitors of the same type, mediated through an unknown molecular selectivity for differentiating cells of the same subtype.

These differences, and others (summarised in **Table 4-2**), that exist between SOPs and *vsx1* progenitors during pattern development will mean that differentiation in the zebrafish neural tube may be significantly more complex and nuanced than in the Drosophila notum.

Table 4-2: Comparison of the role of cellular protrusions in patterning sensory organ precursor cell (SOPs) in *Drosophila* and *vsx1* progenitors in zebrafish.

	***Drosophila* SOPs**	**Zebrafish *vsx1* progenitors**
Number of protrusions	High number: forms a web.	Two per cell, one anterior, one posterior. Radial filopodia on the soma and basal arms.
Length of protrusions	6.5 – 12 µm.	45.89 ± 15.88 µm.
Location of protrusions	Highest concentration at basal surface.	Extend along the basal surface of the neural tube
Spacing between cells	3-5 cell diameters.	Up to 5 nuclei at basal surface, up to 10 at the apical surface.
Mechanisms driving arm growth	Delta overexpression increases the size of the filopodia web.	Unknown.
Composition	Actin-based filopodia.	Microtubules.
Contact between protrusions on neighbouring cells?	Yes. 'Sustained physical interaction'	Yes.
Patterning outcome	Binary cell fate choice.	Delay of neurogenesis over embryonic neurogenesis.
Sources	Cohen et al. 2010; De Joussineau et al. 2003	This chapter. P. Alexandre (unpublished).

4.5.2 Limitations of this live imaging and quantification method.

The purpose quantifying the spatiotemporal patterning of differentiation was to establish an unbiased method of investigating a large scale patterning event. However, it is hard to achieve this mainly due to two technical limitations of our live imaging set up. First, the field of view of the objective means we can only image a certain length of the spinal cord at any one time

(maximum of 400 μm). We could overcome this and capture differentiation in the whole spinal cord through tiling, however gathering and analysing data from multiple embryos would become extremely time-consuming. Second, although we are able to maintain samples and image them for very long periods of time, after approximately three iterations of differentiation, the high number of *vsx1*:GFP expressing cells makes it difficult to observe new divisions. This has limited my analysis to around 6 hours after the first *vsx1*:GFP progenitors are seen. We might be able to extend this in time if we were able to photoconvert the 'old' neurons at a given time point, perhaps using the photoconvertible protein Kaede, allowing clearer visualisation of newborn cells. Together these limitations mean there is a decreased likelihood of observing divisions occurring far about in time and space. These limitations, however, do not affect observations of 'close' dividing cells (>40 μm and >1 hr 30 mins), allowing accurate analysis of the distribution of divisions that occur within this range, which is ideal for studying local pattern formation as we have addressed here.

Another, perhaps more important, limitation concerns the Tg(*vsx1*:GFP) transgenic line. This transgenic line allows clear visualisation of cell divisions but GFP expression is only visible from when the cell has rounded up. Therefore, we are unable to visualize the T-shaped morphological transition that occurs prior to this stage. This is a major limitation as we are unable to observe the behaviour of T-shaped cells and the positioning of the next iteration of divisions at the same time. We tried performing this analysis with other available transgenes (*ngn*:GFP, *pax2*:GFP and *En*:GFP) but we found that GFP was either expressed in proliferative progenitors or too late in the differentiation process, which made the data analysis complex (P. Alexandre; unpublished).

Despite these technical limitations, here we were able to generate a quantitative description of *vsx1* differentiation through time and space. This data could be used to model this pattern formation in order to test and refine our hypothesis (see Chapter 5, below).

4.5.3 Are differentiating neurons spaced by long distance signals delivered by protrusions in mammals?

Long protrusions, similar to those described here, have been reported in the rodent cortex. bIP cells in the rat and mouse SVZ were described as having a large number of multidirectional membrane extensions (Noctor et al. 2004; Nelson et al. 2013). The authors of the first study that observed this phenomena stated that the presence of these transient processes suggest that the cell is "sensing local factors" prior to division (Noctor et al. 2004). Since then these processes have been shown to be involved in mediating Delta Notch signalling between bIP and aRG cells, which maintains the proliferative progenitor population (Nelson et al. 2013).

Comparing these studies to our data suggests that differentiating neurons in the zebrafish and rodent cortex share morphological similarities. It would be interesting to investigate both whether bIP cells in the rodent cortex are spread in time and space, like I have shown in the zebrafish and whether basal arms in the zebrafish are involved in maintaining proliferative progenitor populations, as is seen in rodents.

4.5.4 Summary

In this chapter I quantitatively analysed the spatiotemporal pattern of differentiation of *vsx1* non-apical neuronal progenitors in the zebrafish spinal cord. These data show that initial cells arise with a long distance spacing pattern and first iteration cells divide in the space between initial cells. Formation of this pattern is independent of mesoderm-derived signals. We hypothesise that basal arms deliver a long distance inhibitory signal to the surrounding cells to spread neuronal differentiation in time and space. This would explain the observation that the division of any two *vsx1* progenitors is unlikely to occur within 40 μm and 1.5 hours of each other. Finally, I observed the expression of deltaD protein on the basal arms, suggesting that the long distance inhibitory signal is mediated by Delta Notch signalling.

Currently we do not have a method to visualise the entire process of pattern formation. However, we should be able to model it using this dataset as well as that quantitative description of the T-shaped morphological transition. This approach would allow us to test and refine the hypothesis we have generated. I discuss this work in the next chapter.

CHAPTER 5
SIMPLE MODELLING OF THE FORMATION OF THE PATTERN OF *VSX1* PROGENITOR DIFFERENTIATION IN SPACE AND TIME

5 Simple modelling of the formation of the pattern of *vsx1* progenitor differentiation in space and time

5.1 Introduction

Brain development is a dynamic process that needs to be regulated concurrently in time and space. The spatiotemporal dynamics of neurogenesis in the vertebrate central nervous system, and how they are regulated, are not well understood. To address this gap in our knowledge, in Chapter 4 I generated a detailed description and quantification of the spatiotemporal dynamics of *vsx1* intermediate progenitor differentiation in the zebrafish spinal cord. These analyses showed that differentiative divisions of *vsx1* progenitors occur regularly spaced along the anteroposterior axis and through developmental time. Our data suggest that this spatial pattern is established independent of mesoderm-derived signals.

As *vsx1*:GFP-expressing progenitors are the only population of non-apical progenitors in the zebrafish spinal cord at early stages (see Chapter 3), we know they undergo the T-shaped morphological transition prior to division. During this stereotyped behaviour, differentiating cells extend two long protrusions (referred to as basal arms), along the basal surface of the neural tube, one anteriorly and one posteriorly (unpublished, but described in detail in sections 4.1.3.1 and 5.1.1, **Figure 4-2**). The function of basal arms in neuronal differentiation is currently unknown. However, the similarities between these basal arms and the membrane extensions on SOPs in *Drosophila* suggest that neurogenesis in the zebrafish spinal cord might employ a long-range mechanism to space and pattern neurons as has been characterised in the *Drosophila* notum (discussed in detail in 4.1.3). Therefore, we hypothesise that basal arms of T-shaped cells deliver signals over long distances to inhibit cells that they contact from differentiating. As the T-shaped cells retract their basal arms, cells will be released from inhibition and some are then able to differentiate. The new cells will then begin the process of differentiation, extending basal arms themselves and thereby affecting the next iteration of divisions (**Figure 4-3**). In this way, differentiating cells provide a long distance inhibitory signal to space the differentiation of other cells through time and space (**Figure 4-3**). In *Drosophila,* the inhibitory signal is mediated by the activation of Notch signalling by Delta on long filopodia (Cohen et al. 2010). It is possible that Delta Notch signalling also provides the inhibitory signal during long distance pattern formation in the zebrafish spinal cord as we have observed that these T-shaped cells, and importantly, their basal arms express deltaD (P. Alexandre, unpublished and **Figure 4-10**).

Since *vsx1*:GFP expression is not visible until after the T-shaped transition is complete we are unable to directly visualise the precise interplay between basal arms and the spatiotemporal

pattern of *vsx1*:GFP differentiative divisions simultaneously. However, we do have detailed quantitative data on the T-shape transition from randomly labelled neurons and non-apical progenitors (data obtained by Paula Alexandre; discussed below and section in 4.4.1) as well as the data I obtained from *vsx1*:GFP time-lapse analyses on the spatiotemporal pattern of differentiation (Chapter 4; summarised in section 5.1.2). In this chapter, I use both of these data sets to generate a simple conceptual model to test and refine our long-distance patterning hypothesis.

5.1.1 The quantified dynamics of the T-shaped morphological transition

Previous work has quantitatively characterised the behaviour of T-shaped cells (n = 25 neurons and 7 non-apical progenitors; P. Alexandre, unpublished), allowing us to calculate values for the mean maximum basal arm length as well as speed of growth and speed of retraction of the basal arms (summarised in **Table 5-1**). In the majority of cases, time-lapse movies do not capture the beginning of this behaviour but we have observed the full behaviour in 14 cells (12 neurons and 2 non-apical progenitors). Basal arms were measured from the edge of the cell soma to the tip of the basal arms. To track their behaviour over time, this measurement was taken every hour. Differentiating neurons have been seen to extend basal arms with an average maximum length of 42.58 μm (SD = 20.23 μm) from cell body to the tip of the basal arm. The speed of growth was calculated as the speed of basal arm extension to the maximum observed length. The rate of retraction is the speed at which the basal arms withdrew from their maximum length to complete retraction into the cell body.

From these data we found that the basal arms persist for between 3 and 10 hrs from initial growth to full retraction. In the majority of cases axonogenesis occurs after the basal arms have fully retracted (23/27 differentiating cells; average = 1 hr 6 mins after full retraction). We noticed that the behaviour of the basal arms is variable between individual, even neighbouring, cells. We frequently found that the basal arms on a single T-shaped cell behave differently from each other in every aspect measured, showing that the behaviour of basal arms on a single T-shaped cell is not symmetric. Although the basal arms appear to be restricted to a single dorsoventral level, they also emanate radial filopodia, and therefore there is potentially interaction between cells at different dorsoventral levels (data not shown). Moreover, we have observed the basal arms from adjacent T-shaped cells overlapping, and therefore potentially interacting, over periods of several hours.

5.1.2 The quantified spatiotemporal pattern of *vsx1*:GFP differentiation

Previously, I quantified the spatiotemporal dynamics of neuronal differentiation in the Tg(*vsx1*:GFP) transgenic line as GFP expression is only seen in a single subtype of cells. From

this characterisation I found that *vsx1*:GFP expression in the spinal cord is present in individual progenitors and their daughter cells on the basal surface of the neural tube by 20 hpf. These 'initial' cells are found periodically spaced along the anteroposterior axis, separated by an average of 45.9 µm (± 15.9 SD). After the establishment of the initial pattern, further differentiation events occur in repeated 'iterations' of divisions, where the cells that differentiate after the initial pattern are referred to as first iteration cells and the subsequent iteration is the second iteration. It is possible to estimate the time lag between different iterations. (These data are summarised in **Table 5-1**.) This quantification of pattern formation showed that first iteration progenitors are most likely to divide in the middle of the space between two initial cells and two progenitors are unlikely to divide close together in time and space.

5.2 Aim of chapter

Currently we are unable to directly visualise and test our hypothesis of long distance patterning of neurons in the zebrafish spinal cord. In this chapter I aim to generate a simple conceptual model that simulates the basic tenets of our hypothesis using the features that we have currently observed and quantified. This simple model will allow us to conceptualise the interaction between cells. A simple model also offers the opportunity to test and refine our current hypothesis by carrying out thought experiments and analysing the effect on pattern formation.

Table 5-1: Summary of the data derived from quantification of the T-shaped morphological transition (of neurons and non-apical progenitors) and the development of *vsx1* non-apical progenitors in time and space.

	T-shaped morphological transition			***Vsx1*:GFP progenitor patterning**		
	Speed (µm/hr)		**Max basal arm length (µm)**	**Initial spacing (µm)**	**Iteration lag time**	
	Growth	**Retraction**			**Initial to 1st**	**1st to 2nd**
Mean	10.48	16.44	42.58	45.89	2 hr 39 mins	3 hr 17 mins
SD	7.83	7.59	20.23	15.88	1 hr 3 mins	1 hr 24 mins
N	23 cells	21 cells	21 cells	12 embryos	12 embryos	12 embryos
Source	P. Alexandre (unpublished)			Chapter 4 of this thesis		

5.3 Results

5.3.1 The average T-shaped morphological transition covers a kymographic diamond shape in time and space

To visualise the behaviour of a real T-shaped cell over time from first basal arm extension to full retraction, I generated a kymograph from a movie of basal arms dynamics (**Figure 5-1**; P. Alexandre, unpublished). This image allows the visualisation of basal arm dynamics through time and shows that the process of basal arm growth and retraction *in vivo* is not smooth. In order to generate an average representation of T-shaped cell behaviour I used the data gathered characterising the T-shaped morphological transition of neurons and non-apical progenitors (n = 34 cells; P. Alexandre, unpublished; summarised in **Table 5-1**). I represented the growth of the basal arms from the cell body (approximately 5 μm wide) at the average speed of growth (solid lines; average speed + SEM = dotted line; and average speed – SEM = dashed line) to the average maximum length of the basal arms (purple diamond in **Figure 5-2**A). I represented the retraction of the basal arms in the same way: from the average maximum basal arm length to full retraction (i.e. cell body only; average speed = solid lines; average speed + SEM = dotted line; and average speed – SEM = dashed line). This average basal arm behaviour generates a kymographic diamond shape in space and time.

The observed variation in the maximum basal arm length will have an impact on the spatiotemporal spread of the T-shaped cells. To visualise this I repeated the above process to generate a representation of a T-shaped cell with 'short' basal arms (average maximum basal arm length minus 1 standard deviation; red diamond in **Figure 5-2**A) and another with 'long' basal arms (average maximum basal arm length plus 1 standard deviation; blue diamond in **Figure 5-2**A). These kymographic diamonds highlight how variable the T-shaped morphological transition is between cells, in terms of both the length of time to complete the behaviour as well as the length of neural tube the basal arms can cover. These representations of basal arm behaviour show that the T-shaped morphological transition, from start to finish, can vary from 3 hrs 4 mins to 11 hr 20 mins. This matches the actual range of time we know cells can spend in the T-shaped transition from time-lapse movies (3 hrs 40 mins – 10 hrs 40 mins; P. Alexandre).

In the representations of T-shaped behaviour in **Figure 5-2**A the inner most lines represent the minimum likely speed of growth and retraction of the basal arms and the outer most lines represent the maximum likely speed of growth and retraction of the basal arms. Therefore, the region between outer most lines and the inner most lines in the kymographic diamonds represent where, in time and space, the end of the basal arms are most likely to be (shaded area in **Figure 5-2**B).

To visualise real individual T-shaped cell behaviours, I plotted the length of the basal arms over time for all the non-apical progenitors that we have observed (**Figure 5-3**). In the majority of the time-lapse imaging data, we do not capture the whole T-shaped morphological transition. It is clear from the graphs that the behaviour of the basal arms on any given cell are often asymmetric, with each basal arm growing and retracting at different speeds and reaching different maximum lengths (**Figure 5-3**A, cells 3 and 7, for example). The red line represents when the progenitors divide, showing that one or both of the basal arms can persist after division (**Figure 5-3**A, cell 1, 3, 5 and 7), however on average both arms are fully retracted within 17 mins of division (± 48.04 SEM). From these representations, it is clear that the T-shaped behaviour is variable between individual cells (**Figure 5-3**B).

To compare real individual cell behaviours (from **Figure 5-3**A) with my averaged representations of the T-shaped transition (from **Figure 5-2**B), I superimposed graphs of real data with kymographic diamonds that most closely matched the maximum basal arm length on that cell (**Figure 5-3**C). I used the point where both arms are fully retracted as the common point for superimposition. Comparing the kymographic diamonds to real data, I found that the observed basal arm behaviour is closely matched by the kymographic diamonds for some cells (**Figure 5-3**C, cell 5, for example), while the kymographic representations only match one basal arm in others (**Figure 5-3**C, cell 3, for example). This shows that the average kymographic diamond shapes do not fully match the behaviour of all cells. This highlights that the real arm behaviour is quite variable from cell to cell; the rates of individual arm extension and retraction are often not smooth and the arms are rarely symmetric on both sides of the cell. Nonetheless, the kymographic diamonds are currently our best approximation of basal arm dynamics and are reasonable representations of average arm behaviour in space and time. Therefore, I will use these kymographic diamond shapes to approximate basal arm dynamics in the following models and thought experiments.

Figure 5-1: Kymograph of basal arms. **A**) 3D reconstruction of a mosaically labelled T-shaped cell, expressing membrane-cherry. A white dashed line shows the basal surface and a dotted line shows the apical surface. Arrows indicate the basal arms and the arrowhead indicates the apical process. **B**) Kymograph of the region in the yellow box in A. The white dotted line traces the maximum length of the basal arms through time. **C**) The image in B is cropped to show only the behaviour of the basal arms of this cell. Scale bar = 25 μm. The images in this figure are from a time-lapse movie generated by P. Alexandre (unpublished).

Figure 5-1

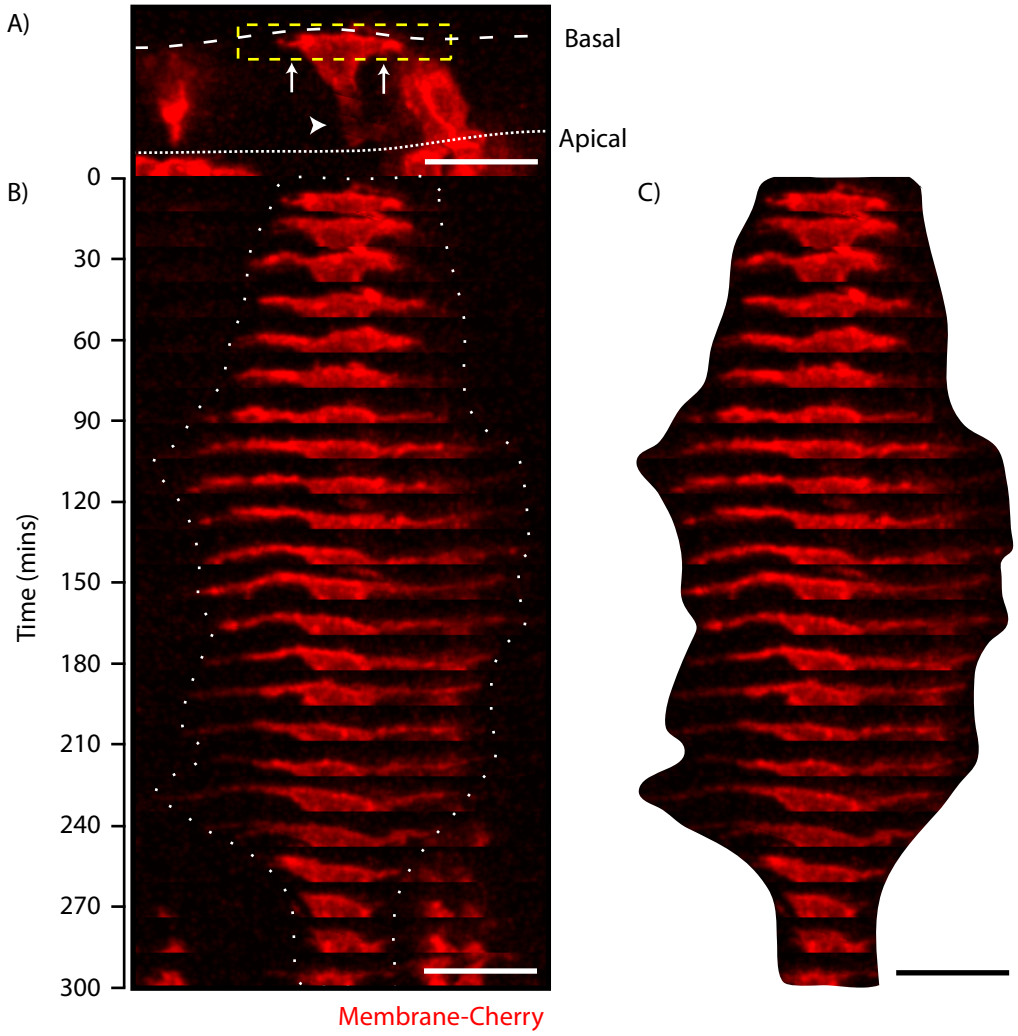
A)
Basal
Apical
B)
0
30
60
90
120
150
180
210
240
270
300
Time (mins)
Membrane-Cherry
C)

Figure 5-2: Modelling the dynamics of T-shaped cells in time and space. **A**) Kymographic representations of the growth of basal arms from the cell body to full extension and then from full extension to full retraction cover a diamond shape in space. Three different maximum arm lengths are modelled. The average speed of growth or retraction shown is by solid line. Dotted line shows average speed + SEM. Dashed line shows average speed – SEM. **B**) From the diamonds in **A**, the inner most lines represent the minimum growth/retraction (shown by the dotted line in **B**) while the outer most lines represents the maximum growth/retraction of the basal arms (shown by a dashed line in **B**). The shaded area represents the predicted location of the end of the basal arms through time and space. Orange = average maximum arm length – SD (short arms). Purple = average maximum arm length (average arms). Blue = average maximum arm length + SD (long arms).

Figure 5-2

Rules:
1. Basal arms grow and retract at the average observed speed (± SD)
2. Basal arms reach the maximum observed length (± SEM)

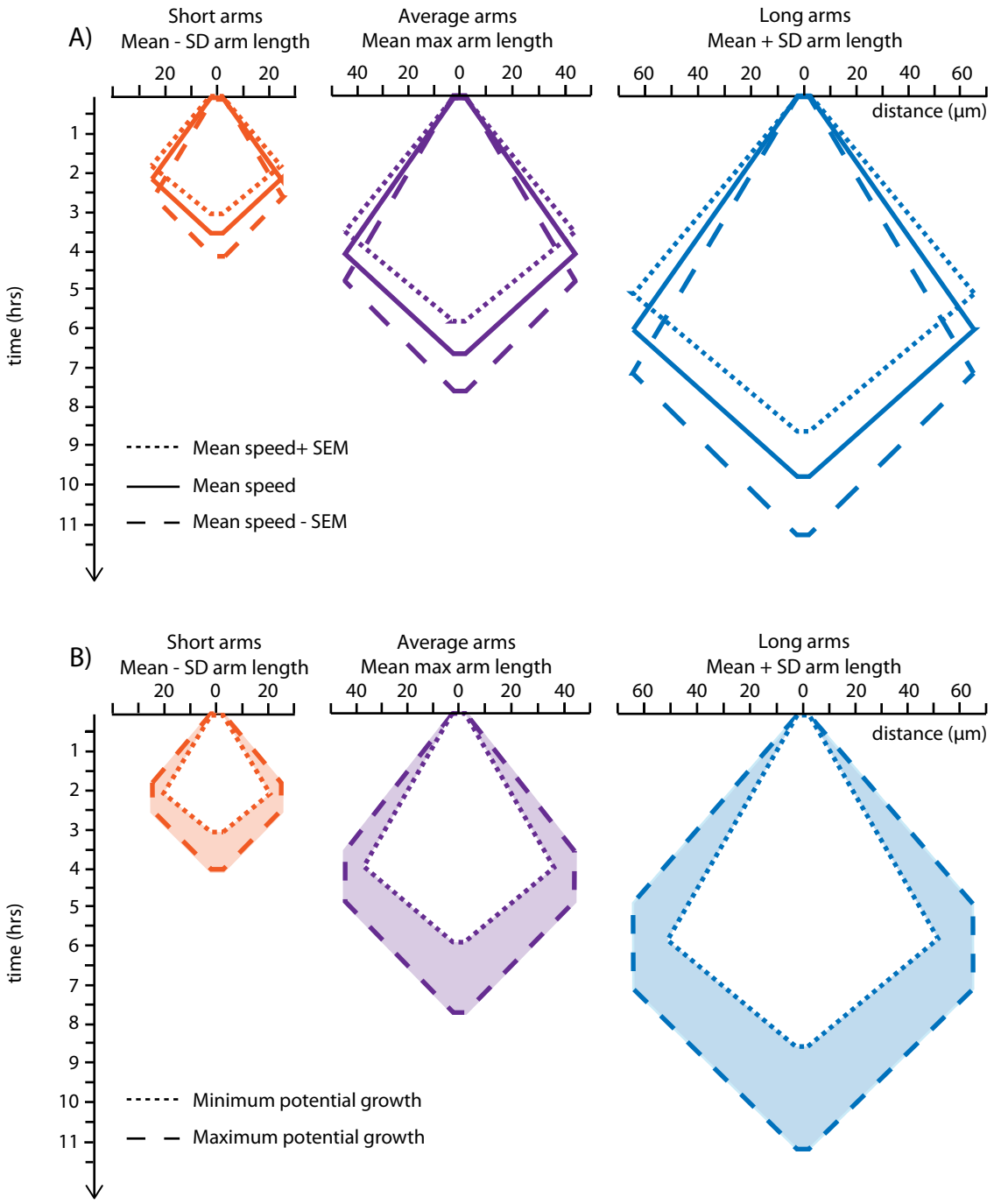

Outcome:
The growth and retraction of basal arms (T-shaped morphological transition) can be represented as a kymographic diamond in time and space.

Figure 5-3: The observed T-shaped dynamics of non-apical progenitors show high variability between individual cells. **A**) Graphs showing the change in the length of the basal arms over time observed on 7 individual non-apical progenitors. The black lines represent the maximum length of the arms over time, ending at the time point when axonogenesis occurs. **B**) All 7 cells plotted on the same axis, each colour refers to an individual progenitor. **C**) The graphs of individual non-apical progenitor's T-shaped behaviour are overlaid with kymographic diamonds showing where the end of the basal arms is likely to be in time and space (from **Figure 5-2**B). Orange = average maximum arm length – SD (short arms). Purple = average maximum arm length (average arms). Blue = average maximum arm length + SD (long arms). The grey line shows the location of cell body. The red line indicates when the non-apical progenitors divide.

Figure 5-3; Page 1

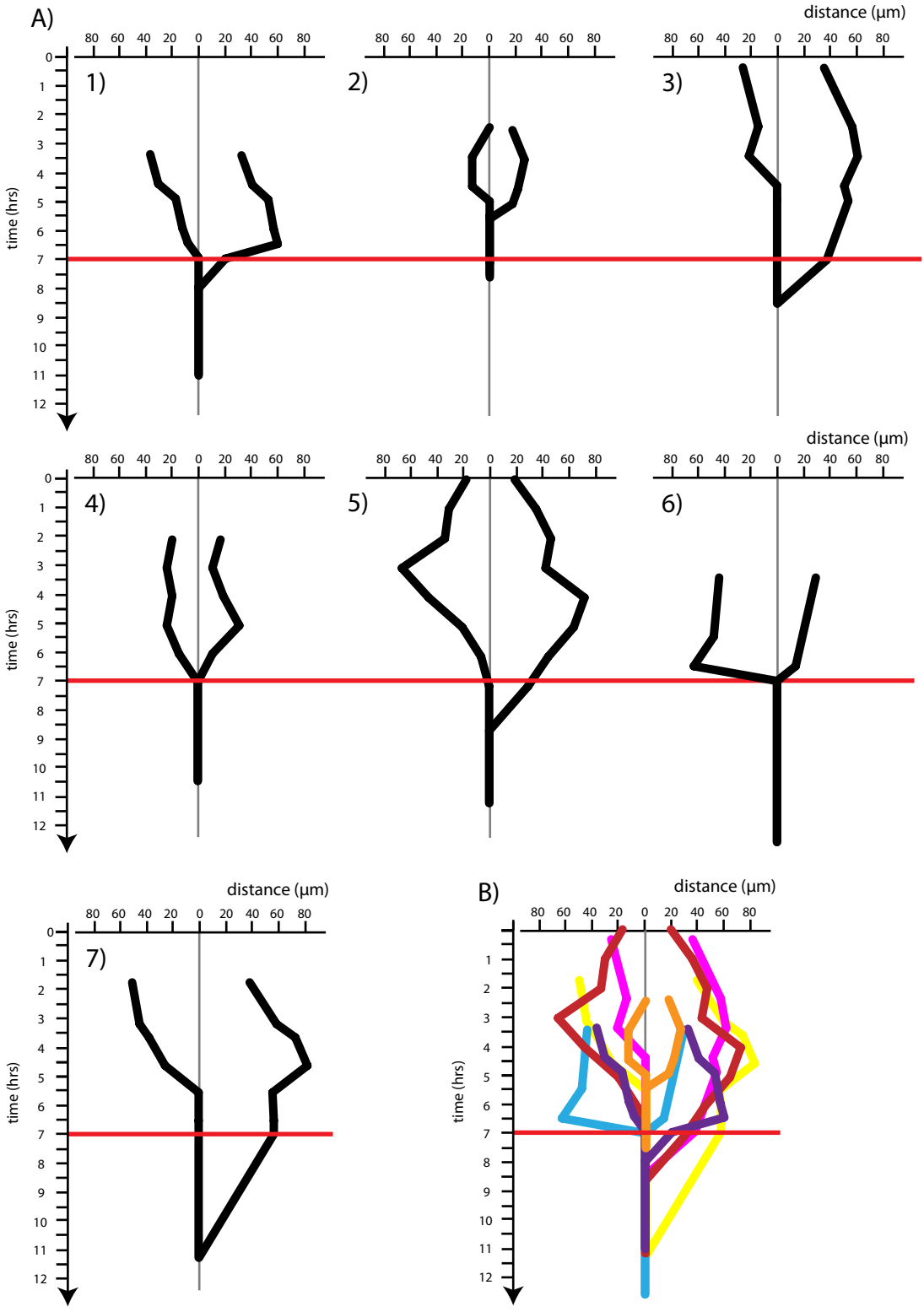

Figure 5-3; Page 2

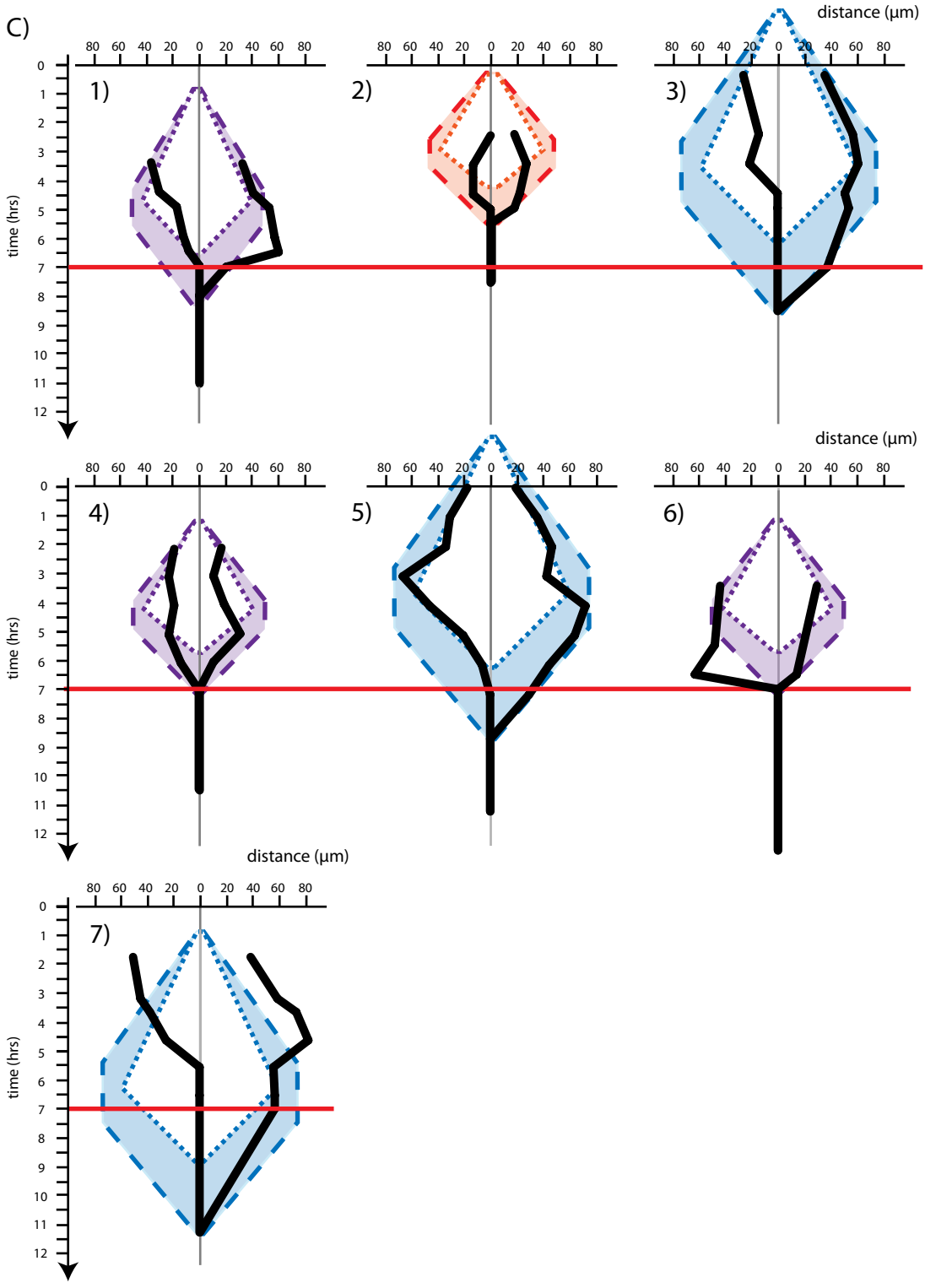

5.3.2 Cells in between a pair of *vsx1* initial progenitors are likely to be contacted by the basal arms of both initial cells

To generate a simple model of cell behaviour during pattern formation according to our current hypothesis, I arranged average kymographic diamond representations of T-shaped cells in a line, separated by the average initial spacing observed in *vsx1*:GFP movies (average ± SD = 45.89 μm ± 15.88; initial cells in **Figure 5-4**A). I assumed that all initial cells begin this behaviour at the same time. It is striking that the average distance between initial cells is approximately equal to the average length of a basal arm (**Figure 5-4**A and **Table 5-1**). This implies that the basal arm of one *vsx1* cell can contact the cell body of the next differentiating *vsx1* cell and that the basal arms from adjacent differentiating *vsx1* cells are likely to be in close proximity for a long period of time. This matches observations from time-lapse data where mosaically labelled cells are relatively close to one another (P. Alexandre, unpublished data). Furthermore, the cells that lie in between two initial *vsx1* progenitors are likely to be contacted by the basal arms from both of the nearest T-shaped cells.

5.3.3 Modelling the role of basal arms in patterning the first iteration of progenitors differentiation

Next, I suggested some rules for how basal arm behaviour could regulate the differentiation of intervening cells and then modelled the spatiotemporal pattern of *vsx1* differentiation that would result, using average kymographic diamonds.

I tested each of the following rules:

A) **Proposed rule 1**. 'New' *vsx1* progenitors will only begin the T-shaped differentiation programme when basal arms of earlier *vsx1* cells retract, releasing the inhibitory signals. This is the assumption we make in our hypothesis (**Figure 4-3**).

B) **Proposed rule 2**. 'New' *vsx1* progenitors will begin their differentiation programme when the basal arms of earlier cells meet in the middle of the intervening space. This tests the assumption that the basal arms deliver a signal that induces differentiation, which is the opposite of our current hypothesis (**Figure 4-3**).

C) **Proposed rule 3**. First iteration cells will divide 2 hrs 39 mins after the division of initial cells. Two hrs 39 mins was the average time interval observed between the initial and first iterations of *vsx1* progenitor division events (mean ± SD = 2 hrs 39 mins ± 1 hr 3 mins). This should reveal the real interaction between the T-shaped cell behaviour of initial and first iteration *vsx1* progenitors.

In the resulting modelling, Proposed rule 1 generates a time interval of 5 hr 15 minutes between division of the initial and the first iteration of *vsx1* progenitors (**Figure 5-4**A) and Proposed rule

2 generates an equivalent time interval of 1 hr 30 minutes (**Figure 5-4**B). Neither of these matches the real observed time interval of 2 hrs 39 mins. For Proposed rule 3, I imposed the observed time interval of 2 hrs 39 mins and the resulting model suggests that first iteration cells must start their T-shaped transition 45 mins - 1 hr after the basal arms of initial cells have met in the middle of the intervening space (shown by the asterisks in **Figure 5-4**C).

5.3.3.1 Implications of testing Proposed rules 1, 2 and 3

Most importantly, the simple hypothesis that intervening cells begin the differentiation process after retraction of basal arms removes the inhibitory signal is wrong. Instead, these models show that new progenitors are most likely to start the T-shaped behaviour approximately 1 hr after the basal arms of older differentiating cells meet. This output of the model could be interpreted two ways. First, if two basal arms contact a cell then it is induced to differentiate and will begin the T-shaped behaviour. Alternatively, if the basal arms do in fact provide an inhibitory signal, these models suggest that the cells in between initial *vsx1* progenitors become competent to differentiate while the initial cells are extending their basal arms. In this case, the longer a cell is free from basal arm-derived inhibition the more likely it is that the cell will begin differentiation. Therefore, the next cell to differentiate is most likely to be approximately where the basal arms meet, as these cells have been inhibition-free for the longest period.

Whatever the mechanism that causes this pattern, from these models it is reasonable to set a rule that later differentiating cells begin the T-shaped morphological transition 1 hr after the basal arms of earlier differentiating cells meet. This time lag between basal arms meeting and the start of the T-shaped behaviour in the new cells could indicate that the neuronal differentiation programme does not start with the extension of basal arms. Alternatively, this observation might be due to an unknown feature of this patterning event that the model does not account for.

Additionally, modelling Proposed rule 3 (observed time between iterations) also shows that basal arms of initial cells can be in contact with cell bodies of first iteration cells that have also started the T-shaped transition for up approximately 4 hrs. The basal arms from the initial and first iteration cells are likely to superimpose for similar lengths of time. This suggests that once a cell has begun to extend basal arms, contact with the basal arms of nearby T-shaped cells can no longer inhibit it. This observation also highlights the potential for interaction between early and later differentiating cells despite being several cell body diameters apart. This hints at the possibility that earlier and later differentiating cells could influence the rate that each other pass through the T-shaped morphological transition.

5.3.3.2 Testing Proposed rules 1, 2 and 3 using different arm lengths

I next looked at the effect of different basal arm lengths on pattern formation in time and space. I generated **Figure 5-4** again using kymographic diamonds representing average speeds of basal arm growth and retraction for T-shaped cells with 'long' basal arms (average + 1 standard deviation; **Figure 5-5**) and 'short' basal arms (average – 1 standard deviation; **Figure 5-6**). In these diagrams the initial spacing is still the average observed distance.

In these simple models, applying Proposed rule 1 to pattern the first iteration of cells results in a time difference between initial cell divisions and first iteration divisions of 8 hr 50 mins for the long arms and 2 hr 30 mins for the short arms (**Figure 5-5**A and **Figure 5-6**A). The time lag between iterations generated by the long arms is nearly 3 times longer than observed (**Figure 5-5**A). In the case of the short arms, the time difference between iterations matches the observed data (**Figure 5-6**A). Applying Proposed rule 2 to representations of long and short arm behaviour can result in a time difference between iterations of 1 hr 30 mins, as in the models using average basal arm lengths (**Figure 5-5**B and **Figure 5-6**B; compared to **Figure 5-4**B). Interestingly, in both cases imposing the observed time difference (Proposed rule 3) suggests that first iteration progenitors begin to extend basal arms approximately 1 hr after the basal arms of initial cells meet (see asterisks in **Figure 5-5**C and **Figure 5-6**C). In these models, the long arms show high levels of overlap, with each basal arm contacting up to 5 other T-shaped cells (**Figure 5-5**C). In contrast, the diagrams modelling small arm behaviour show incompletely tiling of the tissue by T-shaped cells, in other words, there are gaps in between the regions that are under inhibition (**Figure 5-6**C).

5.3.3.3 Modelling the pattern of differentiation over multiple iterations

These first models only account for the generation of two iterations of differentiation (initial and first), but we know that during development this continues through multiple iterations. From my characterisation of *vsx1*:GFP progenitor divisions in time and space, I have calculated the average time lag between the differentiative divisions of the first and second iteration of *vsx1*:GFP progenitors as 3 hr 17 mins (± 1 hr 24 SD; **Table 5-1**). Therefore, I added second iteration cells to the model so that they finished the T-shaped behaviour 3 hr 17 mins after the first iteration progenitors (**Figure 5-7**A). This diagram shows how T-shaped cells might tile in space and time, potentially to provide signals to pattern the whole tissue. In order for second iteration cells to divide at the right time after the first iteration, these cells need to begin the T-shaped morphological transition 1 hr to 1 hr 15 mins after the basal arms of the first iteration meet (shown by the asterisks in **Figure 5-7**A), resembling the modelled initiation of the first iteration.

This simple model generates a regular pattern, with all the *vsx1*-expressing progenitors in an iteration undergoing division at the same time (orange lines in **Figure 5-7**A) and the divisions evenly spaced so that the cells in iteration 'n + 2' are at the same place as iteration 'n'. However, this clustering of divisions from separate iterations in the same space is rare in my movies of the differentiation of *vsx1*:GFP progenitors. Furthermore, the observed spacing of *vsx1*:GFP progenitors does not appear as regular as these models in pattern diagrams of *vsx1*:GFP differentiation (**Figure 4-5**). Therefore, the simple modelling shown here does not generate the variability seen in the real biology. Both the T-shaped morphological transition and the patterning of *vsx1*:GFP progenitors contain a large amount of variation that we have not yet incorporated into this model. Such variation might account for the inconsistencies between the modelled and observed patterns.

5.3.3.4 Implication of modelling pattern formation through time

Taken together, these simple models all suggest that the basal arms of newer T-shaped cells begin to extend 1 hr after the basal arms from the previous iteration have met in the space between them. To visualise this phenomenon in future models I have generated an altered kymographic diamond shape, where the extended rectangular shape at the top of the diamond represents the 1 hr period of time where the cell has been committed to start the T-shaped behaviour but has not yet begun to extend its basal arms (highlighted by a asterisks in **Figure 5-7**B).

We could interpret these data in one of two ways to explain how basal arms might pattern *vsx1* progenitor divisions: 1) contact from two basal arms provide an *activating signal* that induce a cell to differentiate and begin the T-shape morphological transition and 2) basal arms provide an *inhibitory signal* to stop cells they are in contact with from differentiating. If the signal is inhibitory then first iteration cells are specified in the space between initial progenitors before they receive inhibition from basal arms.

Figure 5-4: Modelling the patterning of first iteration progenitors using average arms (average maximum basal arm length). Using the following assumptions derived from previous observations: 1) the T-shaped morphological transition can be represented by kymographic diamond shapes over time and space (where the maximum arm length is the average observed in time-lapse movies; purple cells; from **Figure 5-2**; black circles represent the division event); 2) initial cells are spaced by the observed average initial spacing (**Table 5-1**); and 3) all initial cells begin the T-shaped behaviour at the same time. **A**) If first iteration cells can only begin the T-shaped transition after initial cells have retracted their basal arms then the time difference between iterations will be 5 hr 15 mins. **B**) If the point at which the basal arms of initial cells meet induces first iteration cells begin to extend arms, the time difference between iterations can be as small as 1 hr 30 mins. **C**) In our data we observed the mean time difference between initial and first iteration cell division as 2 hrs 39 mins. In order for the first iteration to divide 2 hrs 39 mins after the initial cells then the first iteration cells will need to begin the T-shaped morphological transition approximately 1 hr after the basal arms of initial cells meet (shown by the asterisks).

Figure 5-4; Page 1

Assumptions based on observations:
1. The T-shaped behaviour is represented by average kymographic diamonds (purple).
2. Initial cells are separated by average observed spacing (from *vsx1*:GFP movies).

Proposed rules to test:
1) 'New' *vsx1* progenitors will only begin the T-shaped behaviour when the basal arms of earlier *vsx1* cells have been retracted.
OR
2) 'New' *vsx1* progenitors will begin the T-shaped behaviour when the basal arms of earlier cells meet in the middle of the intervening space.
OR
3) The time lag between divisions of initial and first iteration cells is set at 2 hr 39 mins, as was observed in *vsx1*:GFP movies.

A) Proposed rule 1

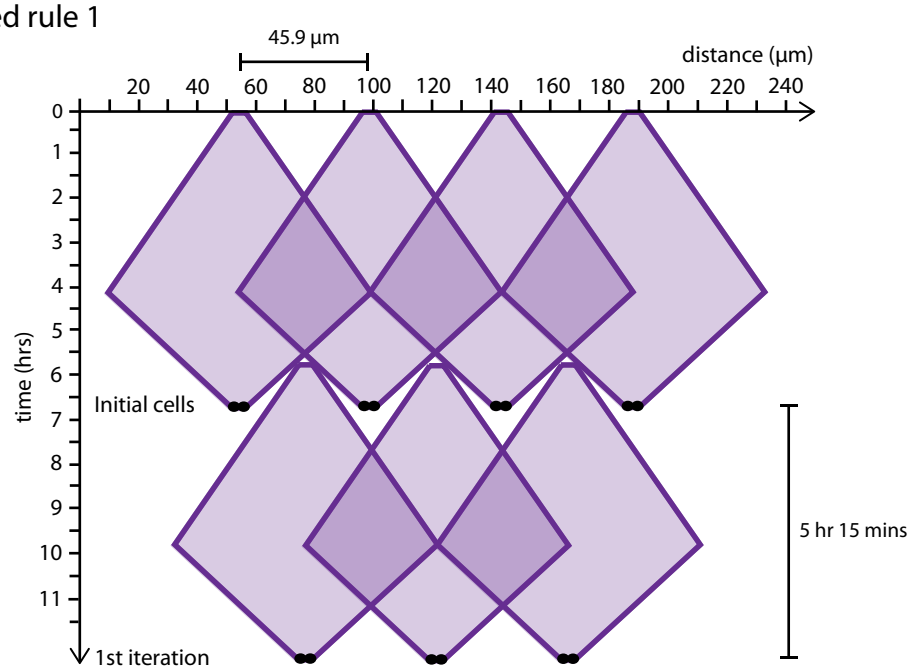

B) Proposed rule 2

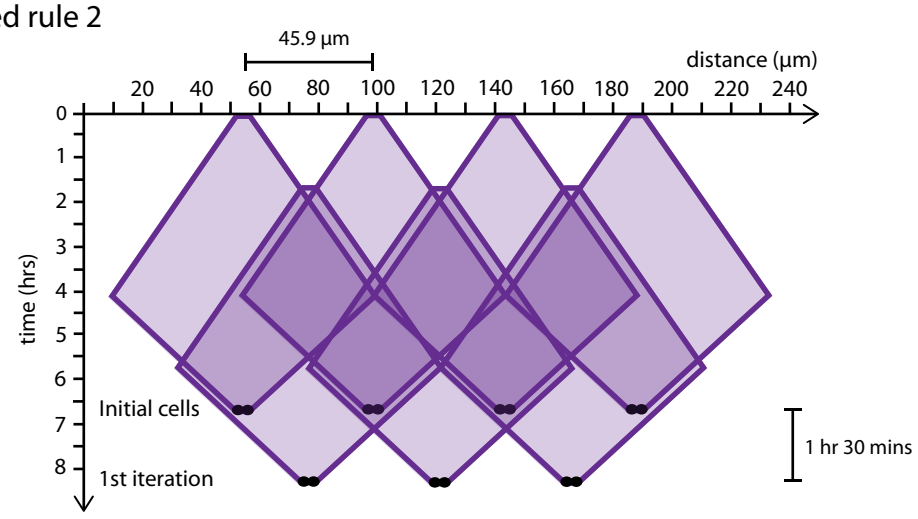

Figure 5-4; Page 2

C) Proposed rule 3

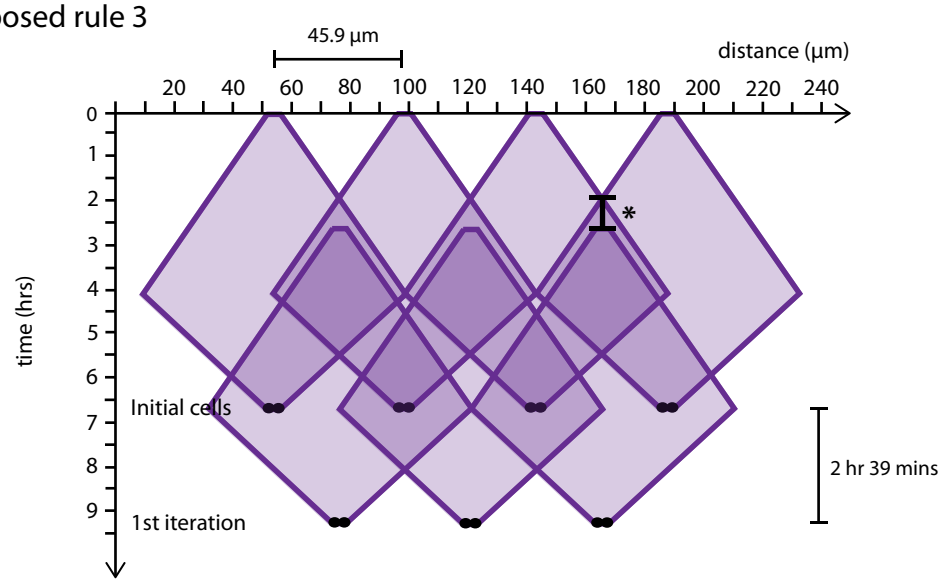

Outcomes:
- Proposed rules 1 and 2 result in a time lag between the initial and first iteration that is different to what was observed in *vsx1*:GFP movies.
- Imposition of the observed time lag of 2 hr 39 mins shows that the T-shaped transition should start around 1 hr after the basal arms of the initial cells meet.

Figure 5-5: Modelling the patterning of first iteration progenitors using long arms (average maximum basal arm length + SD). Using the following assumptions derived from previous observations: 1) the T-shaped morphological transition can be represented by kymographic diamond shapes over time and space (where the maximum arm length is the mean + 1 SD observed in time-lapse movies; from **Figure 5-2**; blue cells, black circles represent the division event); 2) initial cells are spaced by the observed average initial spacing (**Table 5-1**); and 3) all initial cells begin the T-shaped behaviour at the same time. **A**) If first iteration cells begin the T-shaped cells only after initial cells have retracted their basal arms then the time difference between iterations will be approximately 8 hr 50 mins. **B**) If new progenitors begin the T-shaped morphological transition when and where the basal arms of previous progenitors first meet, the time difference between iterations could be as short as 1 hr 30 mins. **C**) If the time difference between initial and first iteration cell division is as observed in *vsx1*:GFP progenitor pattern, then there is a time lag of approximately 1 hr between the arms of initial cells meeting and the first iteration cell beginning to extend arms (shown by the asterisks).

Figure 5-5; Page 1

Assumptions based on observations:
1. The T-shaped behaviour is represented by kymographic diamonds for cells with long basal arms (blue).
2. Initial cells are separated by average observed spacing (from *vsx1*:GFP movies).

Proposed rules to test:
1) 'New' *vsx1* progenitors will only begin the T-shaped behaviour when the basal arms of earlier *vsx1* cells have been retracted.
OR
2) 'New' *vsx1* progenitors will begin the T-shaped behaviour when the basal arms of earlier cells meet in the middle of the intervening space.
OR
3) The time lag between divisions of initial and first iteration cells is set at 2 hr 39 mins, as was observed in *vsx1*:GFP movies.

A) Proposed rule 1

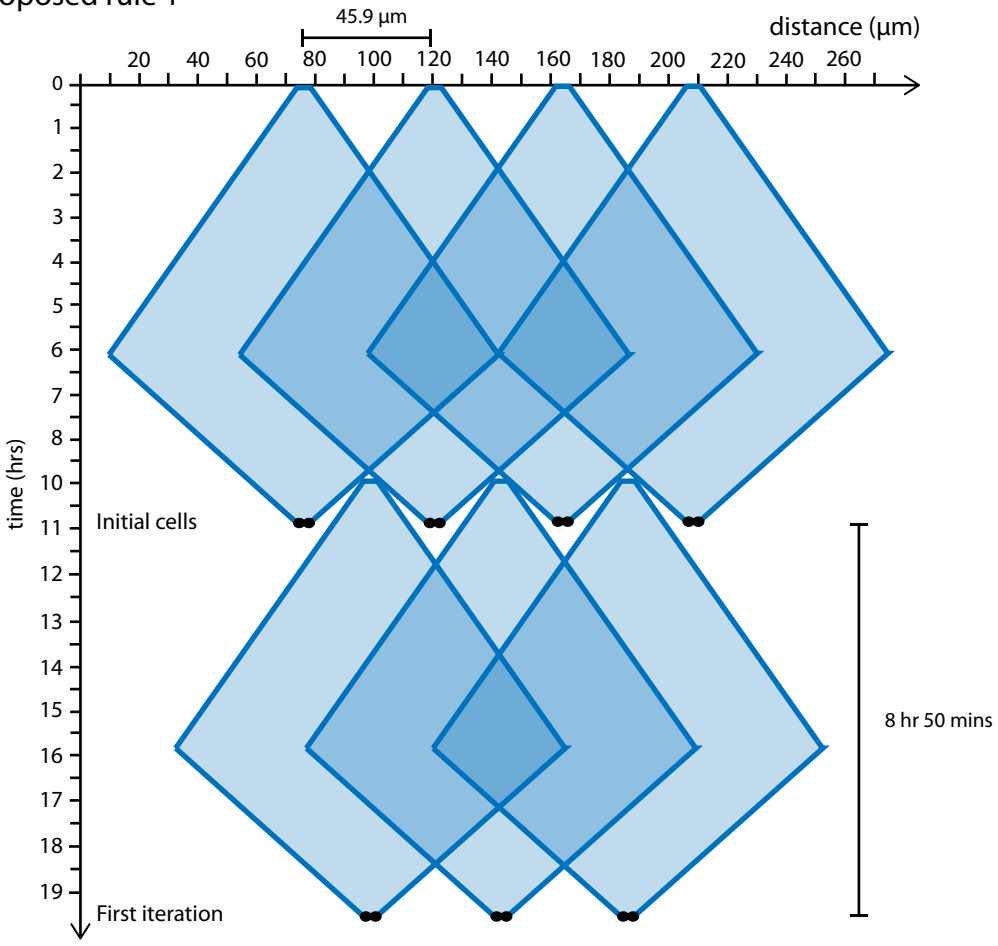

Figure 5-5; Page 2

B) Proposed rule 2

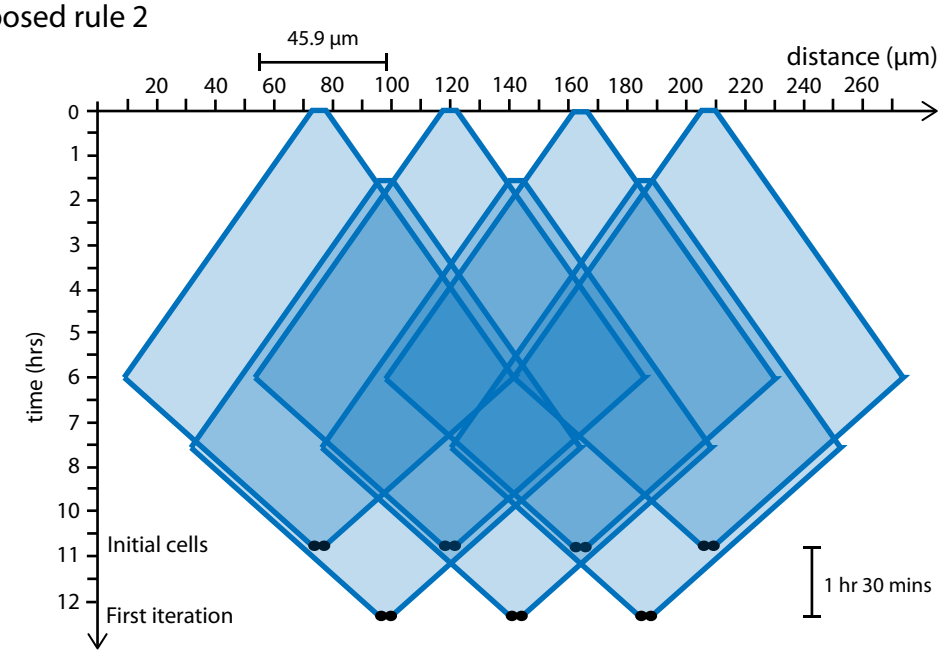

C) Proposed rule 3

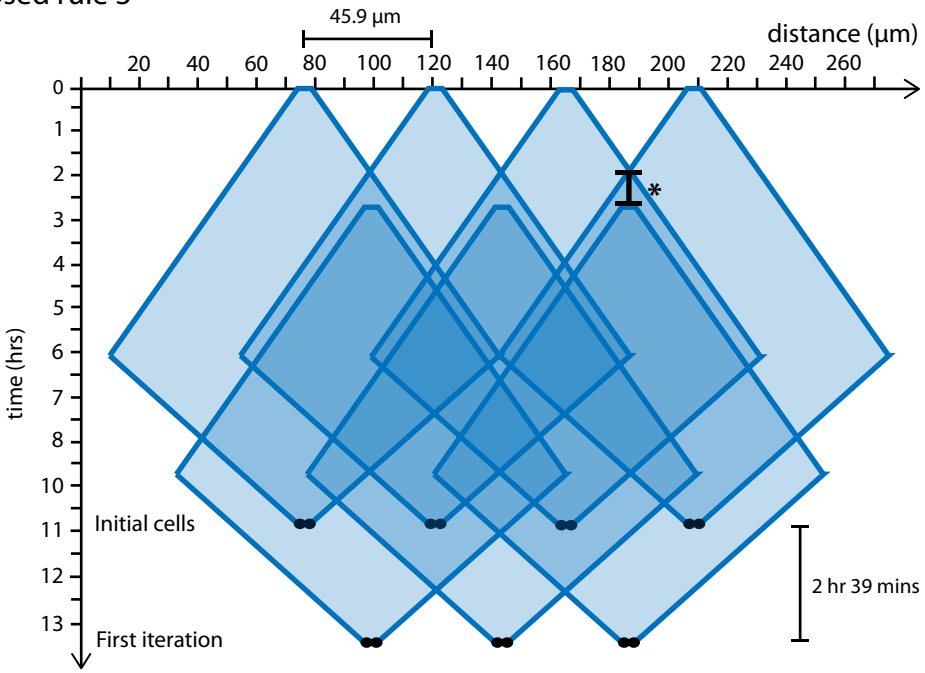

Outcomes:
- Neither Proposed rule 1 or 2 result in a time lag between initial and first iteration cells that is similar to what was observed in *vsx1*:GFP movies.
- Imposition of the observed time lag of 2 hr 39 mins predicts that the T-shape transition of first iteration cells will start around 1 hr after the basal arms of the initial cells meet.

Figure 5-6: Modelling the patterning of first iteration progenitors using short arms (average - SD maximum basal arm length). Using the following assumptions derived from previous observations: 1) the T-shaped morphological transition can be represented by kymographic diamond shapes over time and space (where the maximum arm length is the mean - 1 SD observed in time-lapse movies; from **Figure 5-2**; orange cells, black circles represent the division event); 2) initial cells are spaced by the observed average initial spacing (**Table 5-1**); and 3) all initial cells begin the T-shaped behaviour at the same time. **A**) If first iteration cells can only begin the T-shaped behaviour after initial cells have retracted their basal arms then the time difference between iterations will be 2 hr 30 mins. **B**) If new progenitors begin the T-shaped morphological transition when and where the basal arms of previous progenitors first meet, the time difference between iterations could be as small as 1 hr 30 mins. **C**) If the time difference between initial and first iteration cell division is as observed in the *vsx1*:GFP progenitor pattern, then there is a time lag of approximately 1 hr between the arms of initial cells meeting and the first iteration cell beginning to extend arms (shown by the asterisks), generating a similar pattern as Proposed rule 1 (A).

Figure 5-6

Assumptions based on observations:
1. The T-shaped behaviour is represented by kymographic diamonds for cells with short basal arms (red).
2. Initial cells are separated by average observed spacing (from *vsx1*:GFP movies).

Proposed rules to test:
1) 'New' *vsx1* progenitors will only begin the T-shaped behaviour when the basal arms of earlier *vsx1* cells have been retracted.
OR
2) 'New' *vsx1* progenitors will begin the T-shaped behaviour when the basal arms of earlier cells meet in the middle of the intervening space.
OR
3) The time lag between divisions of initial and first iteration cells is set at 2 hr 39 mins, as was observed in *vsx1*:GFP movies.

A) Proposed rule 1

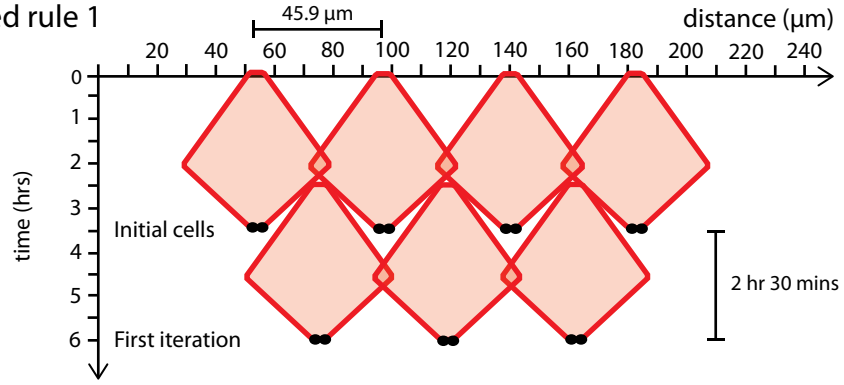

B) Proposed rule 2

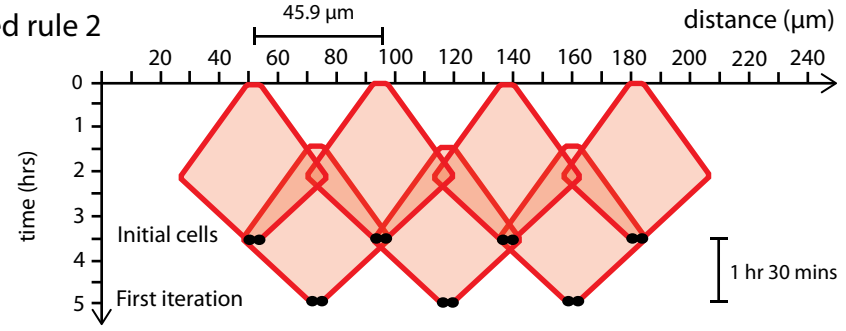

C) Proposed rule 3

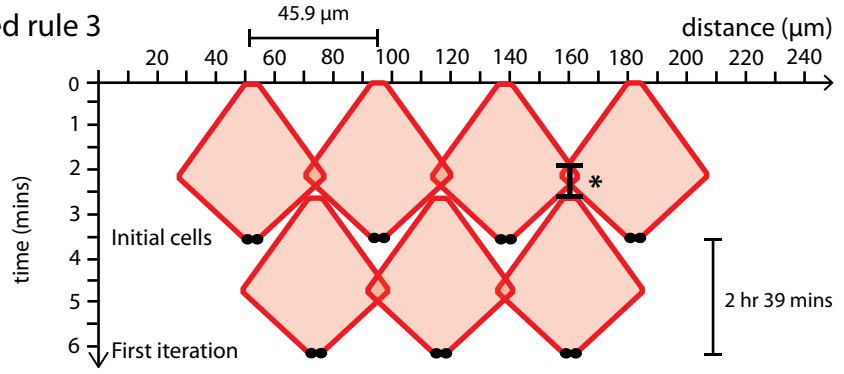

Outcomes:
- Proposed rule 1 shows a time lag between initial and first iteration cells similar to that observed in *vsx1*:GFP movies. This rule and the imposition of the observed time lag (proposed rule 3) predict that the T-shape transition should start around 1 hr after the basal arms of the initial cells meet
- Proposed rule 2 results in a time lag shorter than is observed in *vsx1*:GFP movies.

Figure 5-7: Modelling the differentiation pattern of multiple iterations. Assuming that the T-shaped morphological transition can be represented as average kymographic diamond shapes over time and space (where the maximum arm length is the average observed in time-lapse movies), that all initial cells begin the T-shaped behaviour at the same time and that initial cells are spaced by the observed average initial spacing. **A**) Applying the established patterning rules to a second iteration of differentiation, which we know divide around 3 hrs 17 mins after first iteration cells, shows how multiple rounds of iteration might interact over time. This model shows a time lag of 1 hr – 1 hr 15 between the basal arms of initial cells meeting and first iteration cells extending basal arms (shown by the asterisks). An orange line joins divisions from the same iteration and the black line holds the location of division through time. The number of progenitors generated in each iteration is shown. **B**) Modified average kymographic diamond shape, altered to show that the cell has been committed to start the T-shaped morphological transition at least 1 hr before it begins to extend basal arms. This is shown by the rectangular extension at the top of the diamond (see asterisks).

Figure 5-7

Assumptions based on observations:
1. The T-shaped behaviour is represented by average kymographic diamonds (purple).
2. Initial cells are spaced by average observed spacing.
3. The time lag between each iteration is as observed in *vsx1*:GFP movies.
4. The behaviour of T-shaped cells does not change over time/iterations.

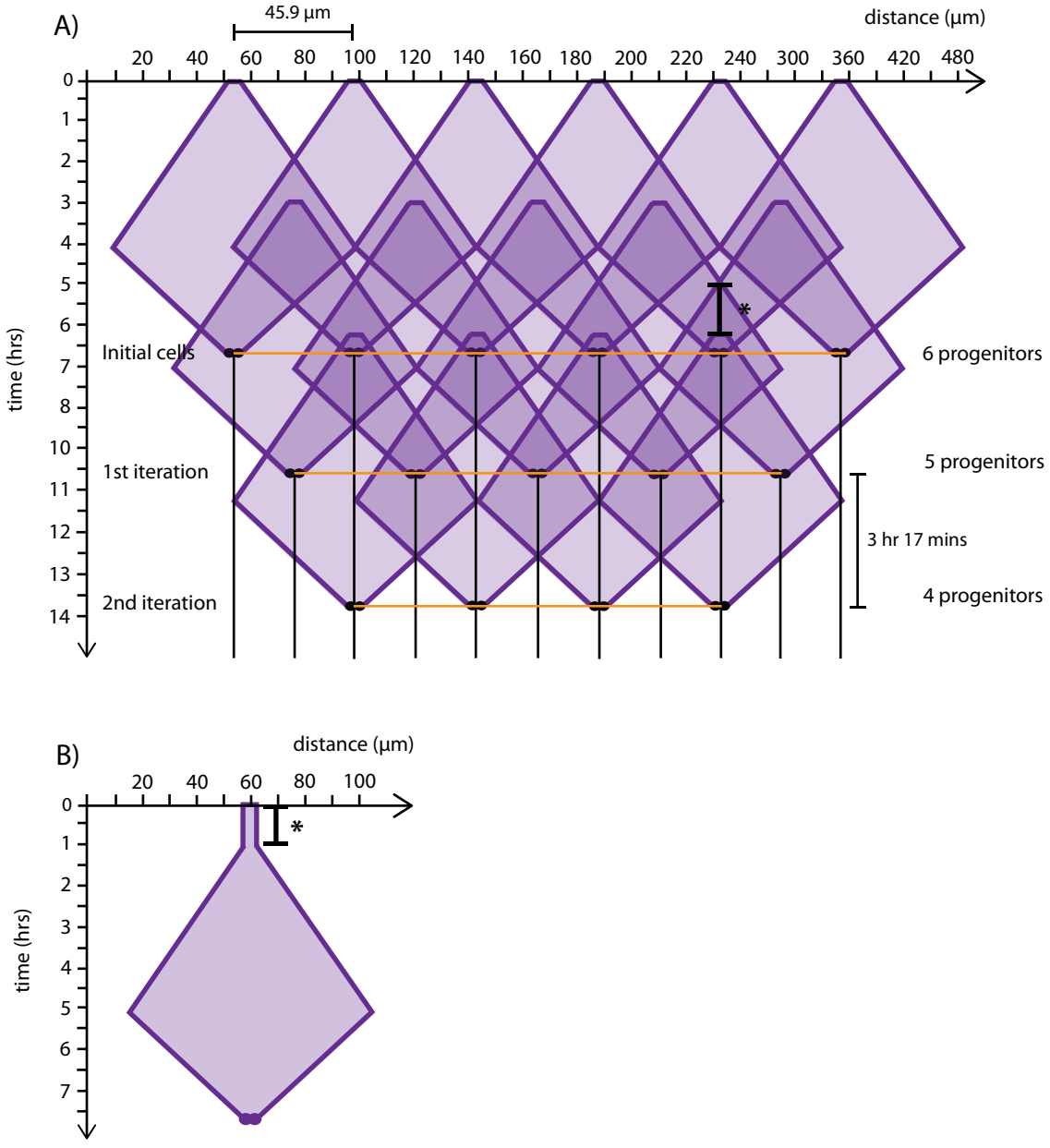

Outcomes:
- Cells from all iterations begin the T-shaped behaviour transition approximately 1 hr after the basal arms of cells from the previous iterations meet.

5.3.4 Adding elements of variability to models of *vsx1* progenitor dynamics

In the previous simple models I have assumed that the field of *vsx1* cells is uniform; the T-shaped behaviour of all the cells is the same, the initial cells are evenly spaced and they divide at the same time. However, in real embryos all of these elements are variable. These simple models offer the opportunity to look at the effect a single form of variation can have on the pattern development over time.

Here, I look at the effect of variation in the spacing of initial *vsx1* progenitors on the patterning of the next iterations of progenitor divisions. In order to do this, I generated simple models of a uniform field of cells and then altered the spacing between a single pair of initial cells. To generate a uniform field of cells I assumed that average kymographic diamonds can represent the T-shaped behaviour of all of the cells in the uniform field and that initial cells are separated by the mean initial spacing observed in *vsx1*:GFP progenitors (purple kymographic diamonds in **Figure 5-8**). I then altered the distance between one pair of initial cells to the average initial distance minus one standard deviation (**Figure 5-8**A) or plus one standard deviation (**Figure 5-8**B). Red diamonds, pairs of circles and lines show initial cells with altered spacing. I also used the best timing rule established by my previous models to predict the time and location of first iteration cells in the uniform section of the field – i.e. new iterations begin the T-shaped morphological transition 1 hr after the basal arms of the previous iteration meet (represented by modified kymographic diamonds; from **Figure 5-7**B). To make the visualisation of iterations and spacing easier, I have drawn an orange line connecting all cells from the same iteration, as well as a black line from each division holding its position in space through time.

The obvious effect of altering the spacing of a pair of initial cells is that the time taken for the basal arms of the altered cells to meet changes. The basal arms of initial cells that are the average distance apart meet after approximately 2 hrs, but decreasing the distance between two initial cells mean their basal arms meet after 1.5 hrs (**Figure 5-8**A) and after increasing the distance between two initial cells this time lag is around 3 hrs (**Figure 5-8**B).

I previously showed that first iteration cells are mostly likely to begin the T-shaped transition around 1 hr after the basal arms of initial cells meet. Theoretically, it is possible this phenomenon is generated by either 1) an activating signal provided by contact from two basal arms or 2) an inhibitory signal that acts over the field of cells in contact with the basal arms (see section 5.3.3.4). Altering the time at which basal arms meet will have different impacts on pattern formation depending on whether the signal provided by the basal arms is activates the start of the T-shaped behaviour or inhibits it.

5.3.4.1 The effect of assuming an activating signal on pattern formation

In the following thought experiment, I assume that the basal arms of T-shaped cells are providing an activating signal, and that contact from two basal arms induces a cell to begin the T-shaped transition. To visualise this, I used the timing rule established earlier and placed first iteration progenitor kymographic diamonds so that they start the behaviour 1 hr after the basal arms of initial cells meet (black modified kymographic diamonds in **Figure 5-9**).

I first looked at the effect of reducing the distance between a single pair of initial cells. In this case, the basal arms of the differentiating cells meet sooner than the basal arms of other cells in the field. This results in the first iteration of progenitors dividing sooner than other cells in the same iteration (***Figure 5-9**A). Cells in the second iteration are also affected by the change to initial cell spacing, dividing sooner than other second iteration cells. Interestingly, second iteration cells also show an altered spacing pattern, appearing just outside of the altered first iteration cells, rather than in the same location, as seen in the uniform pattern (** in **Figure 5-9**A, compare to **Figure 5-7**).

In the opposite manipulation, increasing the distance between a pair of initial cells to the average initial distance plus 1 standard deviation, the meeting of the basal arms of altered initial cells is delayed. The predicted first and second iteration cells show a concurrent delay in division time, relative to the rest of the field (* and **, respectively, in **Figure 5-9**B). Again, in the second iteration the affected cells show changes in location as well as time of division, appearing in the space between the initial cell and first iteration cells, in a way that is not seen in uniform patterns (** in **Figure 5-9**A, compare to **Figure 5-7**).

In these thought experiments, small changes to the distance between initial cells can have knock-on effects on the location and timing of subsequent divisions. This indicates that time and space are interdependent in this patterning process.

5.3.4.2 The effect of assuming an inhibitory signal on pattern formation

In the following thought experiments I consider how variation in initial progenitor spacing might affect pattern formation if I assume that basal arms are providing an inhibitory signal to all cells they are in contact with. In this case, the length of time any cell is free from inhibition (i.e. contact with basal arms) increases the chance that it will begin the T-shaped transition. Here I also assume that once a cell has begun to differentiate, contact with basal arms cannot inhibit it anymore, which is suggested by earlier models (see section 5.3.3.1). In model of pattern formation within a uniform field of cells (**Figure 5-7**), the first iteration cells are free from contact with basal arms for at least 2 hrs. So here I will assume that the cells in between

the initial progenitors require 2 hrs free from inhibition before they can begin to differentiate as first iteration progenitors.

In the models showing decreased spacing between one pair of initial cells, the basal arms of the initial cells are in contact with all of the intervening cells before the 2 hrs required to induce differentiation has lapsed (**Figure 5-10**A). Therefore, no first iteration cells will differentiate between the altered initial cells (**Figure 5-10**A). Instead, the cell that fills the gap between the near-spaced initial cells divides after the second iteration progenitors in the rest of the field (asterisks in **Figure 5-10**A).

In the case of increasing the distance between two initial progenitors, a wider space is still free from inhibition 2 hrs after the initial cells started to extend their basal arms (**Figure 5-10**B). It is possible that more than one first iteration progenitor could be generated in this larger space. It is mostly likely that a pair of first iteration cells will begin the T-shaped transition at approximately the same time and with a small distance between them (* in **Figure 5-10**B). A small shift is also seen in the spacing of second iteration cells but no effect is seen in the timing of these divisions (** in **Figure 5-10**B).

These thought experiments suggest there are situations in which either 1) no first iteration cell or 2) two first iteration cells could be generated between two initial progenitors. Examples of such patterns were observed in real *vsx1* progenitor pattern diagrams (**Figure 5-11**A and B, respectively), demonstrating that these phenomena occur in real patterns of *vsx1* differentiation.

5.3.4.3 Implications of adding variability to the models of pattern formation

If I assume that all cells, and their behaviour, are equal during pattern formation, then the resulting pattern of differentiation is uniform and regular (**Figure 5-7**). The addition of one element of variability generates models that show noisier patterns of *vsx1* divisions that more closely resemble patterns seen in real data (**Figure 5-9** and **Figure 5-10**). These simple models of spacing pattern development show how one small change can have knock-on effects that reach over multiple iterations. Interestingly, adding variation to the spacing of initial progenitors can result in alterations to the location *and* timing of subsequent iterations. This suggests that time and space are interdependent in the formation of this pattern.

In the context of variable initial spacing, assuming that the basal arms provide a signal that activates the T-shaped transition or inhibits it generated qualitatively different patterns of divisions in time and space. The patterns generated in these models suggest that 'new' progenitors can be specified without the need for two basal arms to meet (**Figure 5-10**B). There

are also examples where no 'new' progenitor is specified despite the meeting of basal arms from 'older' T-shaped cells (**Figure 5-10**A). Real patterns of differentiation show examples of these events (**Figure 5-11**), which strongly suggests that contact from two different T-shaped cells is not necessary and is insufficient to induce the next cell to start the T-shaped behaviour, and therefore, the basal arms are unlikely to be delivering a signal that activates neuronal differentiation. Instead, these data support the idea that basal arms provide an inhibitory signal. Furthermore, this data suggests that there is a minimum time that an undifferentiated cell in the neuroepithelium must be free from basal arm-derived inhibition before it is able to start the T-shaped behaviour itself.

Currently these models assume that the cells in the intervening space between T-shaped cells are equivalent (equally competent to differentiate). However, we know that neuronal fate choice is heavily biased during asymmetric division of apical progenitors in zebrafish (Alexandre et al. 2010; Kressmann et al. 2015). Therefore, basal arms are unlikely to be regulating neurogenesis directly, but delaying when the new neuron integrates into the developing circuitry. This would add in another form of variation, as cells competent to differentiate will be generated independent of basal arm growth. In this case, we do not know when the nascent neurons are competent to respond to basal arms after asymmetric division.

Figure 5-8: Generating a model of controlled variation in the initial spacing. A uniform field of initial cells (shown in purple) was generated assuming that average kymographic diamonds showed the behaviour of cells in space and time and all initial cells are spaced by average initial spacing (observed in *vsx1*:GFP movies). The space between two initial cells was then altered to average initial spacing – one standard deviation (**A**) or average initial spacing + one standard deviation (**B**). Red diamonds and lines show progenitors with altered initial spacing. An orange line connects progenitor divisions belonging to the same iteration. The location of division is held in time by a black line.

Figure 5-8

Assumptions based on observations (for the uniform field of cells; shown in purple):
1) The T-shaped behaviour of initial cells is represented by average kymographic diamonds.
2) The T-shaped behaviour of first iteration cells is represented by modified kymographic diamonds.
3) Initial cells are spaced by average observed initial spacing.

Variation (marked by red diamonds and lines):
A) Decreased spacing between two cells to average - 1 standard deviation.
B) Increased spacing between two cells to average + 1 standard deviation.

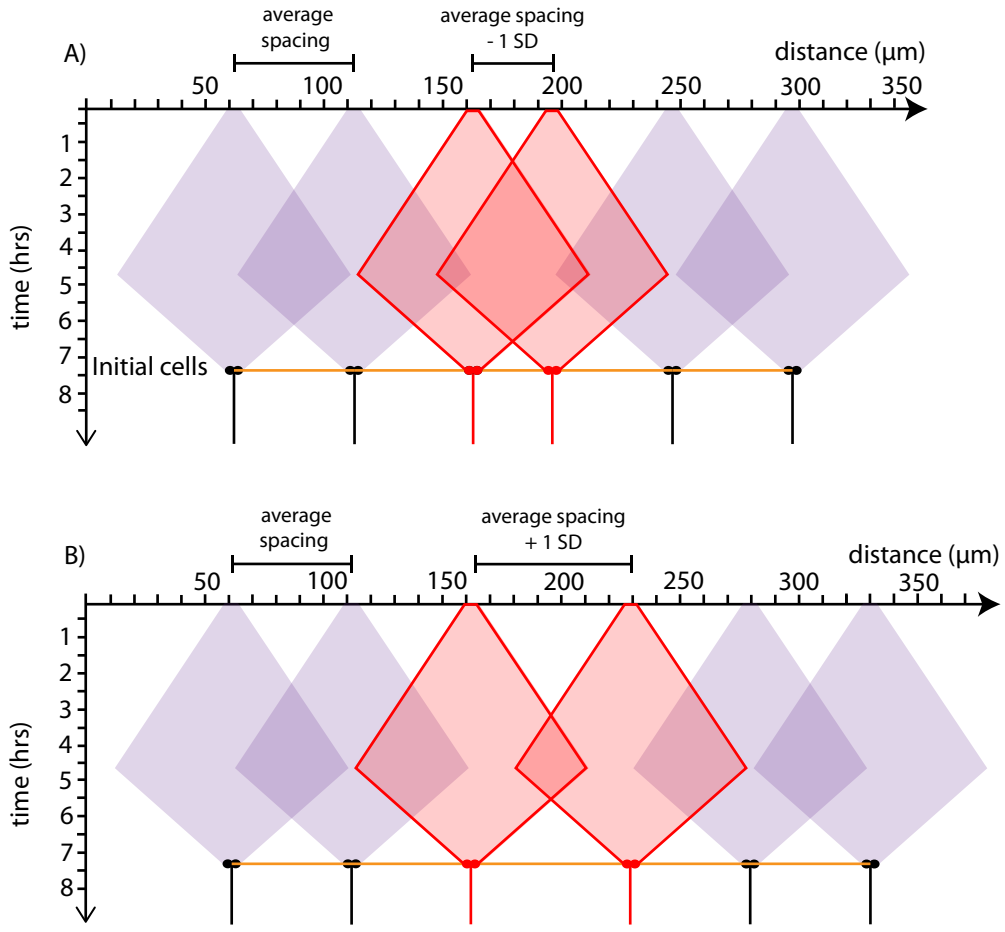

Figure 5-9: Variations in the initial spacing pattern can impact pattern formation over time, assuming basal arms provide an activating signal. Patterns of differentiation over time were generated using the models of controlled variation in initial spacing from **Figure 5-8**. First and second iteration cells are represented by modified kymographic diamonds to show the predicted 1 hr lag between the onset of differentiation and the extension of basal arms. The behaviour of first iteration cells affected by the altered patterning of initial cells was determined by the assumption that basal arms deliver a signal that activates the T-shaped transition. In both **A** and **B,** alterations to the spacing of initial progenitors results in changes to the location of first and second iteration cells in space and time. Affected cells in the first and second iteration are shown by * and **, respectively. Red diamonds and lines show progenitors with altered initial spacing and black diamonds show cells affected by this change. An orange line connects progenitor divisions belonging to the same iteration. The location of division is held in time by a black line.

Figure 5-9

Assumptions based on observations (for the uniform field of cells; shown in purple):
1) The T-shaped behaviour of initial cells is represented by average kymographic diamonds.
2) The T-shaped behaviour of first iteration cells is represented by modified kymographic diamonds.
3) Initial cells are spaced by average observed initial spacing.

Variation (marked by red diamonds and lines):
A) Decreased spacing between two cells to average - 1 standard deviation.
B) Increased spacing between two cells to average + 1 standard deviation.

Assumption to test: Basal arms deliver an activating signal.

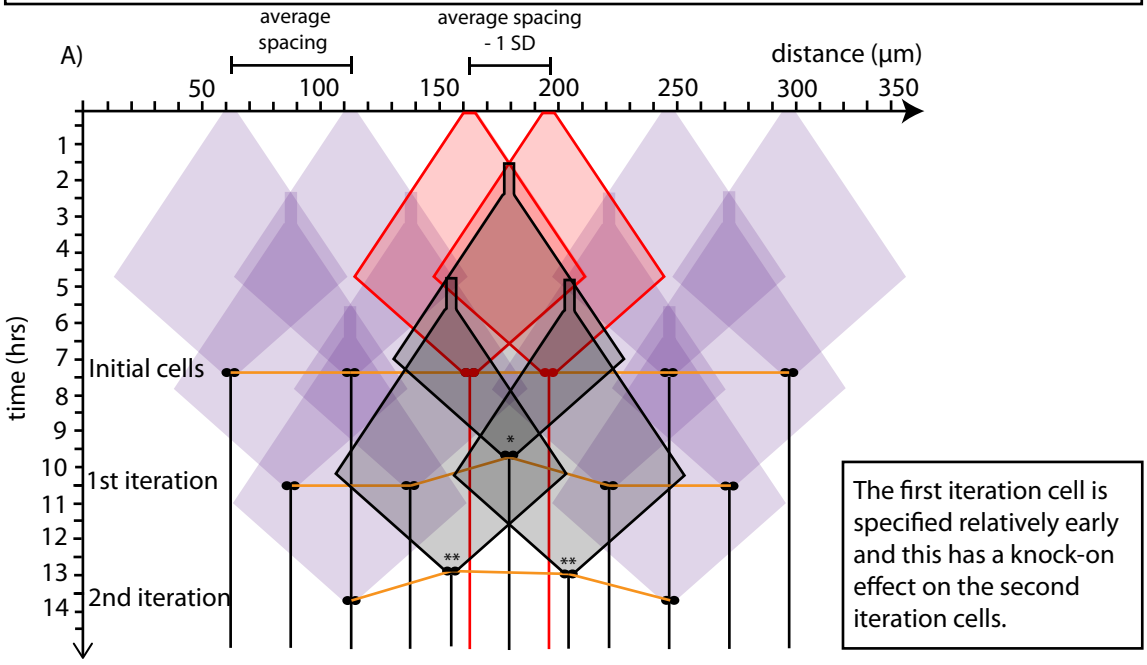

The first iteration cell is specified relatively early and this has a knock-on effect on the second iteration cells.

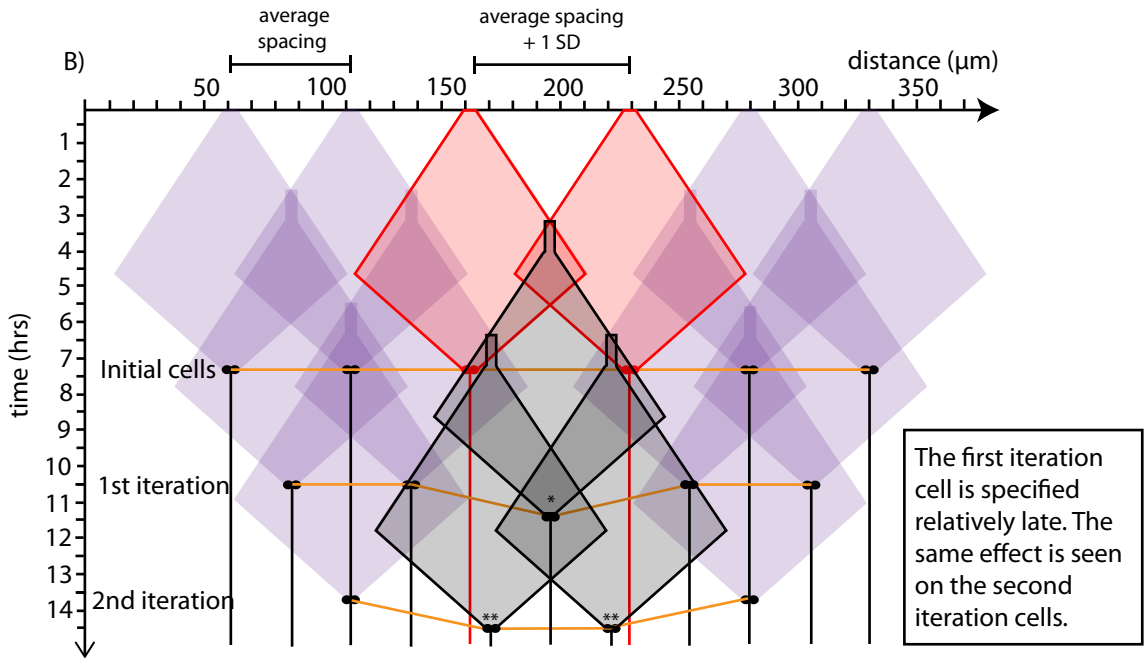

The first iteration cell is specified relatively late. The same effect is seen on the second iteration cells.

Outcomes:
- Altering the distance between initial cells affects the location and timing of divisions in subsequent iterations

Figure 5-10: Variations in the initial spacing patterns can impact pattern formation over time, assuming that basal arms provide an inhibitory signal. Patterns of differentiation over time were generated using the models of controlled variation in initial spacing from **Figure 5-8**. First and second iteration cells are represented by modified kymographic diamonds to show the predicted 1 hr lag between the onset of differentiation and the extension of basal arms. The behaviour of first iteration cells affected by the altered initial cells was determined by the assumption that basal arms deliver a signal that inhibits cells from entering the T-shaped transition. **A**) Narrowing the space between two initial cells can result in the loss of a progenitor from the pattern and **B**) expanding the spacing between initial cells might add progenitors to the pattern. Affected cells in the first and second iteration are shown by * and **, respectively. Red diamonds and lines show progenitors with altered initial spacing and black diamonds show cells affected by this change. An orange line connects progenitor divisions belonging to the same iteration. The location of division is held in time by a black line.

Figure 5-10

Assumptions based on observations (for the uniform field of cells; shown in purple):
1) The T-shaped behaviour of initial cells is represented by average kymographic diamonds.
2) The T-shaped behaviour of first iteration cells is represented by modified kymographic diamonds.
3) Initial cells are spaced by average observed initial spacing.

Variation (marked by red diamonds and lines):
A) Decreased spacing between two cells to average - 1 standard deviation.
B) Increased spacing between two cells to average + 1 standard deviation.

Assumption to test: Basal arms deliver an **inhibitory** signal.

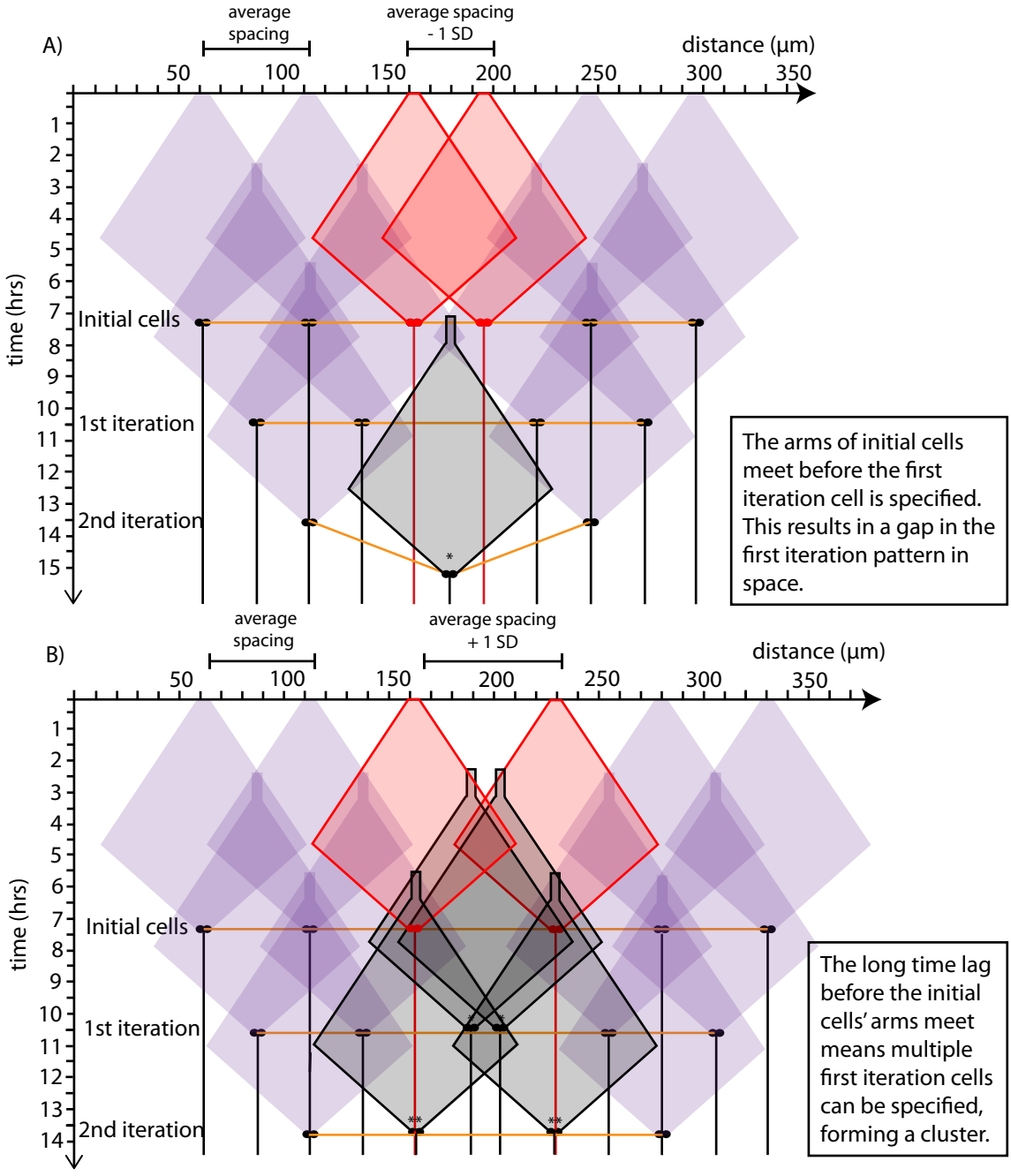

The arms of initial cells meet before the first iteration cell is specified. This results in a gap in the first iteration pattern in space.

The long time lag before the initial cells' arms meet means multiple first iteration cells can be specified, forming a cluster.

Outcome:
- Altering the distance between initial cells can add or remove progenitors from the pattern.

Figure 5-11: Examples of real pattern diagrams showing loss or addition of progenitors. Example pattern diagrams of *vsx1*:GFP progenitor divisions from **Figure 4-5**. **A**) In the highlighted region there is a pair of closely spaced initial progenitors (shown by the red lines) with no first iteration progenitor between them, as predicted by **Figure 5-10**A. **B**) The highlighted region shows a pair of initial progenitors that are widely spaced (shown by the red lines) and two first iteration progenitors divide with a small time difference in the space between them (shown by the asterisks), as predicted by **Figure 5-10**B. In the pattern diagrams, the location of observed *vsx1*:GFP progenitor divisions in time (y-axis) and space (x-axis) is represented diagrams by pairs of green circles. The lines from the division, going through time, represent the position held by the daughter cells after division. Anterior to the left.

Figure 5-11

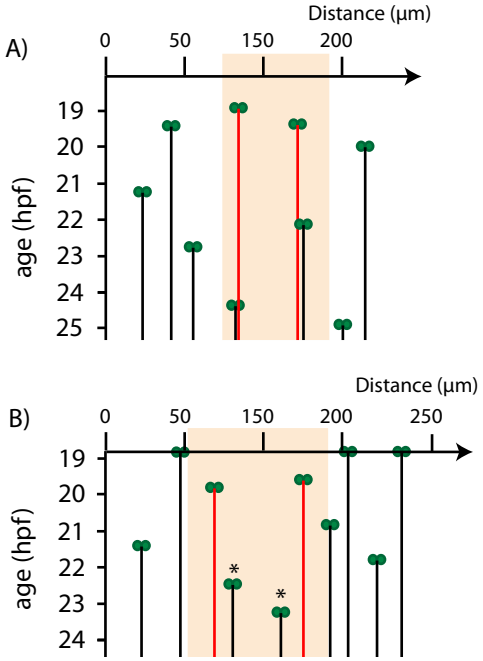
A)
Distance (µm)
0
50
150
200
19
20
21
22
23
24
25
age (hpf)
B)
Distance (µm)
0
50
150
200
250
19
20
21
22
23
24
age (hpf)
*
*

5.3.5 Modelling pattern formation using observed patterns of initial progenitor divisions in time and space

In the previous section I looked at the effect of altering the spacing between a single pair of initial cells, in an otherwise uniform field of cells, on pattern formation in time and space. However, data from time-lapse movies of *vsx1*:GFP progenitor divisions shows that there is variation in the spacing of initial cells and the time at which they divide throughout the field. It is extremely challenging to look meaningfully at the effects of variation on pattern formation in a whole field using the simple conceptual models I have generated. An alternative approach is to use actual patterns of initial *vsx1*:GFP progenitor divisions in time and space (generated in Chapter 4; see **Figure 4-5**) and the kymographic diamonds to model the behaviour of T-shaped cells prior to division to predict the pattern of first iteration divisions in time and space. I restricted this analysis to differentiation pattern diagrams in which I observed the division of all the first iteration cells (n = 3 embryos). For these simple models I looked at the effect of average basal arm diamonds (mean maximum basal arm length; purple diamonds), as well as representations of long (average + SD maximum basal arm length; blue diamonds) and short basal arm (average - SD maximum basal arm length; red diamonds).

It is possible to ask two questions using these simple models:

- When are initial cells likely to begin the T-shaped transition?
- Can we use the principles identified from simple conceptual modelling to predict the location and time of division of first iteration *vsx1*:GFP progenitors.

5.3.5.1 When do initial cells begin the T-shaped transition?

Working back from observed initial *vsx1*:GFP divisions in pattern diagrams, the kymographic diamonds can be used to estimate when the cell would have begun the T-shaped transition. The representations of average and shot basal arms indicate that initial cells begin the T-shaped transition around 15 or 12 hpf, respectively (**Figure 5-12**A-B). This would place the onset of differentiation of the initial *vsx1*-expressing progenitors in the neural keel stages of development, which is reasonable from the current understanding of the onset of neurogenesis in the neural tube (Kressmann et al. 2015). However, the representations of the long basal arms suggest the T-shaped behaviour of initial cells could start as early as 8 hpf (**Figure 5-12**C). Since this is prior to neural plate formation this seems extremely unlikely to be correct. A study of the birthdates of *vsx1* cells would be useful to determine whether these predictions match the biology.

5.3.5.2 Using principles identified through modelling to predict *vsx1* differentiation events as observed in *vsx1*:GFP movies

I next used real examples of *vsx1* differentiation patterns to test whether the principles established in previous models and thought experiments could be used predict the pattern of first iteration *vsx1* division events in time and space. First, I predicted the T-shaped transition of initial cells prior to division in pattern diagrams using different sized kymographic diamonds, as above (**Figure 5-12**). Next, I placed modified kymographic diamonds (from **Figure 5-7**B) representing first iteration cells onto the pattern diagrams so that the behaviour began when the basal arms of two initial cells meet (**Figure 5-13**), light diamonds with dotted outlines represent T-shaped behaviour of first iteration cells). The pattern diagrams that I used to provide the location of initial cell divisions contain the location and time of *vsx1*:GFP divisions that belong to the first iteration of divisions. Therefore, I was able to compare the location and time of observed *vsx1*:GFP divisions to those predicted by models using kymographic diamonds.

Based on the comparison of each predicted division with an observed division, I categorised each prediction as follows (**Table 5-2**):

- **Match:** Predicted division is within 1 hr and 20 μm of the observed division, i.e. at a similar time and place.
- **Wrong place:** Predicted division is more than 20 μm away from the observed division.
- **Early:** Predicted division occurs less than 1 hr before the observed division.
- **Late:** Predicted division occurs more than 1 hr after the observed division.
- **No match:** No observed division to compare to predicted division.
- **Not predicted:** First iteration cells not explained by a predicted division.
- **Not tested:** In a number of cases the short arm kymographic diamonds superimposed on observed initial divisions did not meet, which meant that I was unable to use our current rules to predict the location of the next division.

In the majority of cases, independent of the maximum length of the basal arms, the principles identified through modelling could accurately predict the location of first iteration divisions (96/99 predictions were within 20 μm of the observed division; **Table 5-2**). This data strongly suggests that the point at which the basal arms meet sets the location at which the next division will take place. However, our current modelling principles were not able to predict the time of these divisions accurately, instead this model tended to predict that a division would occur later than an observed division (21/99 predictions occurred 1 hr or more after the observed division; **Table 5-2**). There were also a number of observed divisions that were not explained by the predictions (20/99; **Table 5-2**).

This comparison supports the principles of our current hypothesis, as the 'rules' proposed by the models are able to reasonably accurately predict real data. However, some further refinement to

the hypothesis is required to account for aspects of observed data that we have not yet explained, mostly related to the time of division.

Figure 5-12: Predicting when initial progenitors begin the T-shaped transition using observed initial cell spacing and different size kymographic diamonds. Example patterns of initial *vsx1*:GFP differentiation events (from **Figure 4-5**) overlaid with the kymographic diamonds to represent the T-shaped cell behaviour of initial progenitors prior to division. Orange diamonds shows short basal arm behaviour (**A**), purple diamonds show average basal arm behaviour (**B**), and blue diamonds show long basal arm behaviour (**C**). *Vsx1:GFP* progenitor divisions in development time (hpf, y-axis) and space (x-axis) are represented in these pattern diagrams by pairs of green circles. Anterior is to the left. The black lines from the division, going through time, represent the position held by the daughter cells after division.

Figure 5-12

Assumptions based on observations:
1) Initial cell divisions are located in the positions in time and space observed in *vsx1*:GFP movies.
2) The T-shaped behaviour of initial cells can be predicted by different sized kymographic diamond shapes.

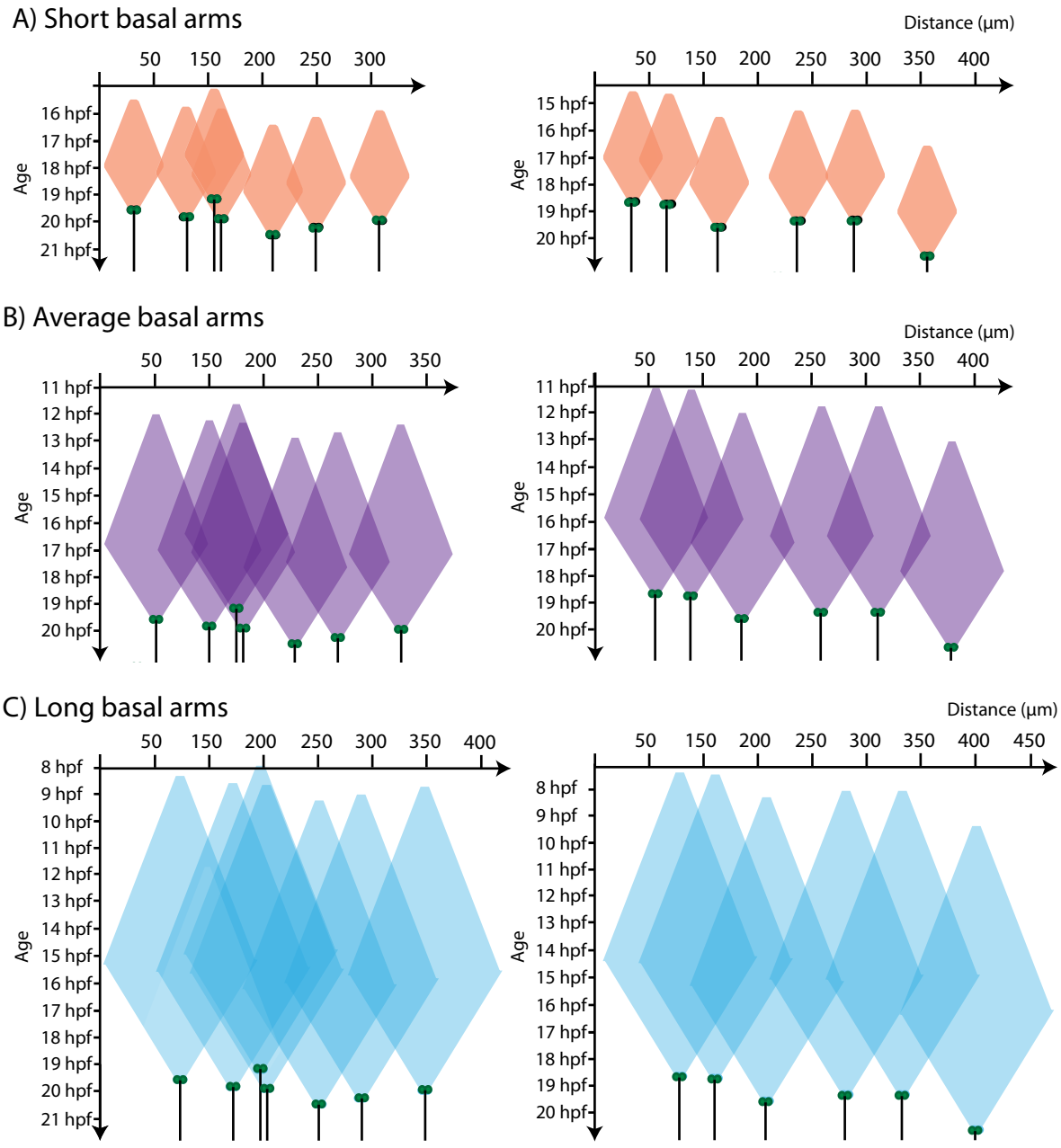

Outcomes:
- If initial T-shaped cells have short or average basal arms then they most likely begin the behaviour between 11 and 15 hpf.
- If the initial cells have long basal arms, they need to begin the behaviour around 8 hpf.

Figure 5-13: Predicting the location of first iteration divisions using observed patterns of initial progenitor divisions and different sized kymographic diamonds. Example pattern diagrams of *vsx1*:GFP differentiation, showing initial and first iteration divisions, overlaid with kymographic diamonds to estimate the T-shaped cell behaviour of initial progenitors prior to division (darker coloured diamonds; from **Figure 5-12**). *Vsx1:GFP* progenitor divisions in time (y-axis) and space (x-axis) are represented in these pattern diagrams by pairs of green circles. Anterior is to the left. The black lines from the division, going through time, represent the position held by the daughter cells after division. Lighter kymographic diamonds with dashed outlines, modified to show the 1 hr lag before the beginning of arm extension, were added to represent the behaviour of first iteration progenitors. Orange diamonds show short arm behaviour (**A**), purple diamonds show average arm behaviour (**B**) and blue diamonds show long arm behaviour (**C**).

Table 5-2: Comparing predicted divisions to observed divisions. Predicted divisions were categorised based on how accurately they predicted observed divisions. The numbers in brackets refer to the percentage of all cells analysed in each category. Match: Predicted division is within 1 hr and 20 μm of the observed division, i.e. at a similar time and place. Wrong place: Predicted division is more than 20 μm away from the observed division. Early: Predicted division occurs more than 1 hr before the observed division. Late: Predicted division occurs more than 1 hr after the observed division. No match: Predicted division that had no obvious observed division to compare to. Not predicted: Presumed first iteration cells that were not explained by a predicted division. Not tested: In a number of cases the short basal arm kymographic diamonds superimposed on observed initial distances did not meet, which meant that I was unable to use our current rules to predict the location of the next division.

	Match	Wrong place	Early	Late	No match	Not predicted	Not tested
Average arms	15 (38.46%)	1 (2.56%)	3 (7.70%)	10 (25.64%)	1 (2.56%)	9 (23.08%)	N/A
Long arms	15 (38.46%)	1 (2.56%)	3 (7.70%)	10 (25.64%)	1 (2.56%)	9 (23.08%)	N/A
Short arms	11 (28.20%)	1 (2.56%)	4 (10.26%)	1 (2.56%)	2 (5.13%)	2 (5.13%)	18 (46.15%)

Outcomes:

- Kymographic diamonds can be used to accurately predict the location of a first iteration division, from observed patterns of initial cell divisions, independent of the maximum basal arm length.
- This method is less accurate when predicting the time of the first iteration division.

Figure 5-13

Assumptions based on observations:
1) Initial cell divisions are located in the positions in time and space observed in vsx1:GFP movies.
2) The T-shaped behaviour of initial cells can be predicted by different sized kymographic diamond shapes
3) New cells start the T-shaped behaviour 1 hr after the arms of the previous iteration meet.

A) Short basal arms

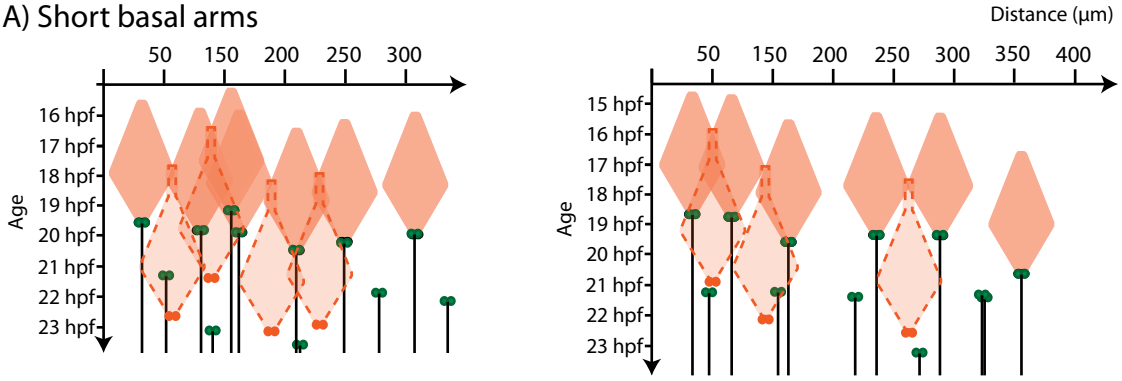

B) Average basal arms

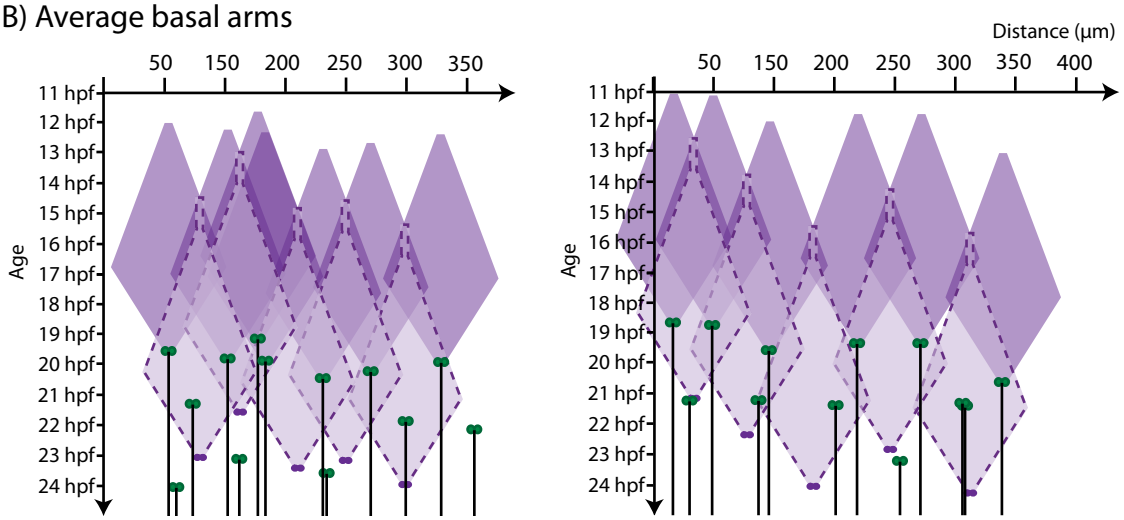

C) Long basal arms

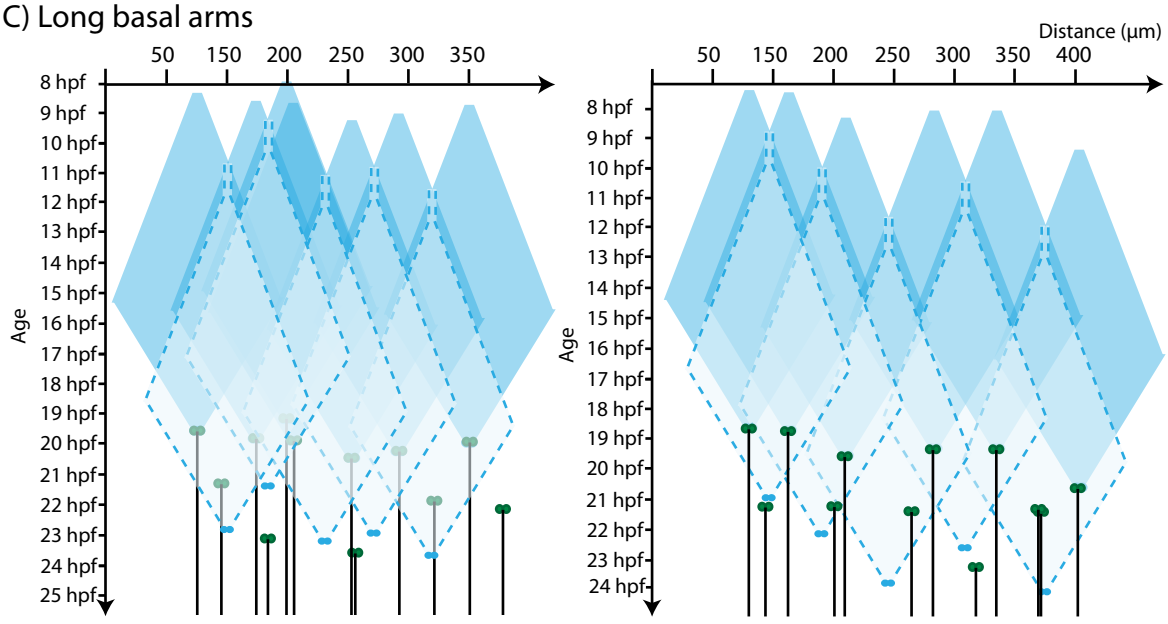

5.4 Discussion

The Clarke and Alexandre labs have developed a hypothesis of how the spaced pattern of *vsx1*:GFP progenitor differentiation might be generated. The hypothesis is based on published studies looking at sensory organ precursor (SOP) development in the *Drosophila* notum (Cohen et al. 2010; De Joussineau et al. 2003) as well as the observation of the T-shaped morphological transition in the zebrafish spinal cord (P. Alexandre and J. Clarke, unpublished; **Figure 4-2**). We propose that the basal arms of T-shaped cells provide Delta Notch-mediated long distance lateral inhibition to regulate the differentiation of neural cells (**Figure 4-3**). The work presented in this chapter aimed to test and refine our hypothesis regarding how the basal arms of differentiating cells might pattern differentiating neurons through time and space. I used previously obtained quantitative data on the T-shaped morphological transition (Paula Alexandre, unpublished) to model the spatiotemporal dynamics of this behaviour. The resulting kymographic diamond shapes are a reasonably accurate representation of the basal arm behaviour observed in non-apical progenitors. I then combined this with the data generated in Chapter 4 regarding the spatiotemporal dynamics of *vsx1*:GFP differentiation to model the potential interaction of multiple T-shaped cells in time and space to generate a pattern of differentiation. These models showed that new cells are likely to begin the T-shaped morphological transition around 1 hr after the basal arms of the previous iteration meet. By applying these modelling principles to real data we can accurately predict the location, but not the time, of observed divisions.

5.4.1 Activating versus inhibiting patterning signal

An outcome of the modelling shown in this chapter is that the point at which basal arms meet is correlated with the location of the next progenitor division. The simplest way to interpret this finding is that contact from two basal arms provides an activating signal to a cell, inducing it to begin the T-shaped morphological transition and differentiate. However, modelling the effect of variable initial progenitor spacing and comparing this to real data I have shown that the meeting of two basal arms is not necessary and is insufficient to induce the next cell to start the T-shaped behaviour. These observations strongly suggest that the basal arms do not induce or activate the T-shaped transition. Furthermore, if the contact from two basal arms did activate the T-shaped transition, from the degree of overlap between the basal arms of adjacent T-shaped cells observed in time-lapse movies and predicted by models we would expect more than one cell to differentiate in the space between initial cells, which we rarely see in the real patterns of *vsx1* differentiation. This might be explained by a conventional lateral inhibition signal, originating from the nascent neuron and acting on adjacent cells to limit the number of differentiation events. However, as the basal arms overlap across distances corresponding to multiple cell

diameters, if the basal arms were activating the T-shaped transition I would still expect to see *vsx1*:GFP progenitors differentiating closer together in time and space.

On the other hand, there is a wealth of theoretical and experimental data regarding how inhibitory signals can generate sparse patterns of differentiation. In 1952, Alan Turing proposed the reaction diffusion (RD) model to explain how pattern formation might occur through the interaction (reaction) of two substances: an activator and an inhibitor (Turing, 1952). In his mathematical model, Turing proposed that these two reacting substances could generate a variety of stable patterns from near uniform distributions of each component, if: 1) the reacting substances could control their own synthesis and that of their counterparts and 2) the substances are able to diffuse quickly through the space. As our understanding of molecular biology has deepened in the intervening decades, the definition of 'activator' and 'inhibitor' substances has been broadened to include single molecules, interacting molecular complexes or signalling pathways (Meinhardt & Gierer 2000). This idea has been refined in work by Gierer and Meinhardt, among others, who have demonstrated that this RD pattern formation requires one class of substances that are capable of short-range positive feedback and a second class of substances that are capable of long-range negative feedback (Meinhardt & Gierer 2000; **Figure 5-14**A). If the activating signal were to exist on its own it would cause an 'autocatalytic' explosion and differentiation throughout the tissue (Meinhardt & Gierer 2000). The inhibitory signals are important to stop this from occurring and instead they allow single, self-sustaining activation events to occur in a field of inhibition. Furthermore, experimental and modelling data has shown that diffusion is not necessary for the long distance inhibitory signal. In the differentiation of *Drosophila* SOPs Delta drives the growth of membrane extensions and these filopodia actively deliver the inhibitory signal over long distances (De Joussineau et al. 2003; Cohen et al. 2010). An RD model composed of short-range positive feedback and concurrent long-range negative feedback is now considered to be a common feature of differentiation and can be applied to multiple signal pathways (including Delta Notch **Figure 5-14**B) and a number of biological patterns (reviewed in Kondo & Miura 2010 and Meinhardt & Gierer 2000).

Therefore, I think that, if basal arms are patterning *vsx1*:GFP progenitor divisions in time and space they are most likely to be providing an inhibitory signal and I shall focus on this mechanism in the rest of the discussion.

5.4.2 Basal arms delay the T-shaped transition of differentiating neurons

The models and thought experiments in this chapter predict that there will be a time lag of at least 1 hr between the point at which the basal arms of the previous iteration meet and the beginning of the T-shaped morphological transition in the next iteration. The models also

suggest that once a cell has begun the T-shaped morphological transition, basal arms from surrounding cells can no longer inhibit this fate choice. Our current hypothesis cannot explain these phenomena (**Figure 4-3**). If the basal arms are providing an inhibitory signal to surrounding cells, then new cells must be selected to differentiate before the basal arms of previous cells meet, through a mechanism independent of the basal arms. From previous studies of neurogenesis in the zebrafish neural tube we know that cells are biased to differentiate during the asymmetric division of apical progenitors (Alexandre et al. 2010; Kressmann et al. 2015). With this in mind, it is likely that basal arms of T-shaped differentiating cells are not selecting cells from the neuroepithelium to differentiate, instead they are selecting a few cells, spread in time and space, to proceed through the neuronal differentiation pathway while delaying the rest of the competent tissue. From these findings, I have updated our hypothesis of how T-shaped cells might spread differentiation out in time and space (**Figure 5-15**).

Other studies of neurogenesis in the Clarke and Alexandre labs have shown that the extension of basal arms is not the first morphological change to occur after an asymmetric division generates a daughter committed neuronal differentiation (Alexandre, unpublished); the cell must first translocate its soma to the basal side of the tissue. We have observed that these cells exhibit variable lengths of time to complete the somal translocation and to begin the T-shaped behaviour (P. Alexandre, unpublished; **Figure 5-16**). The time taken to complete this behaviour might account for the 1 hr long time lag between the basal arms of one iteration meeting and the start of the T-shaped transition in the next iteration. Our data suggests there is a point in the differentiation process after which committed nascent neurons and non-apical progenitors are insensitive to basal arm-derived signals, resulting in the over lap of basal arms of T-shaped cells from subsequent iterations that we have observed in time-lapse movies (P. Alexandre, unpublished) and in these models. When modelling the effect of variable initial spacing on the final pattern I also found evidence for a minimum time that a neuroepithelial cell must be free of basal arm-derived inhibitory signals before it can begin the T-shaped morphological transition. Together this suggests that committed neurons and non-apical progenitors go through a transient phase during which their progression along the differentiation pathway can be delayed. We do not fully understand how the competency of the signal-receiving cell might change over time and development and how this affects the role of the basal arms. This is potentially a very interesting area of research to pursue.

In the absence of a method to visualise this whole process through time and space, a computation model is the best way to test the potential role of basal arms in generating the spatiotemporal pattern of *vsx1*:GFP differentiation. As we do not know the exact molecular basis of this patterning signal, generic equations describing a Turing-like RD could be used to

model our system. Building a computational model that includes all of our quantitative data could generate a data set that can be statistically compared to the quantified spatiotemporal dynamics of *vsx1* progenitors.

Figure 5-14: Overview of the reaction diffusion model of pattern formation. The formation of a number of biological patterns can be explained by the interaction of an activator and inhibitor, as first theorised by Turing in 1952. **A**) Schematic of the reaction diffusion model. The activator molecule/signal pathway (green square) must act over a short range, be capable of autocatalysis (blue arrow) and induce a long-range inhibitor molecule/pathway (red oval). The interaction between these two molecules/pathways can lead to a variety of stable patterns of cell differentiation states (adapted from Meinhardt & Gierer 2000). **B**) Core elements of the Delta Notch pathway and how they relate to the reaction diffusion model. Proneural basic helix-loop-helix (bHLH) genes are activators of neuronal differentiation. These molecules also activate the expression of Delta, which then activates Notch signalling in neighbouring cells to inhibit neural differentiation. Active and inactive elements of the pathway are shown in black and grey, respectively. Green shows components of the 'activator' pathway and components of the 'inhibitor' pathway are shown in red. The blue arrow signifies autocatalysis. Adapted from Chen et al. 2014.

Figure 5-14

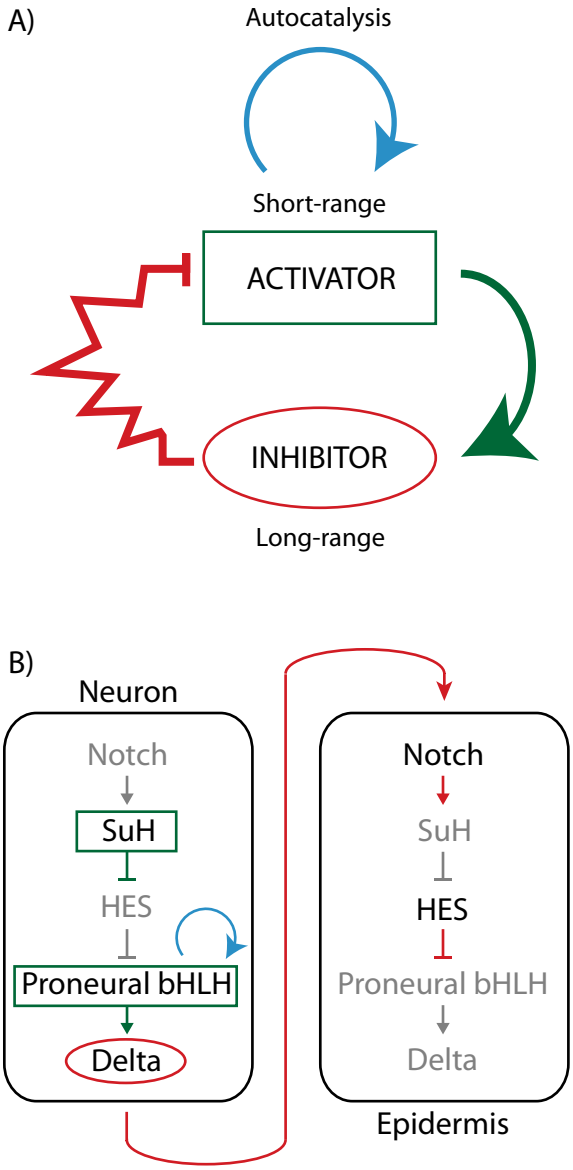
A)
Autocatalysis
Short-range
ACTIVATOR
INHIBITOR
Long-range
B)
Neuron
Notch
SuH
HES
Proneural bHLH
Delta
Notch
SuH
HES
Proneural bHLH
Delta
Epidermis

Figure 5-15: T-shaped nascent neuronal cells act to pattern differentiation of neurons along the anteroposterior axis. **A**) Differentiating neurons (brown cells) extend basal arms along the basal surface of the neural tube, while maintaining contact with the apical surface, taking on a T-shaped morphology (**B**). These membrane extensions allow cells to deliver inhibitory signals to cells at a distance from the differentiating cell's soma inhibiting neighbouring cells from differentiating. Blue arrows denote the direction of the inhibitory signal (i.e. from the basal arms to the neighbouring cells). The cells furthest away from other T-shaped cells as they extend their arms are free from inhibition for the longest period of time and can be selected to start the process themselves (yellow cell). **C**) While the new T-shaped cell extend their basal arms, the old cells begin to retract their basal arms and detach from the apical surface. **D**) The older progenitor then rounds up and (**E**) divides (**F**) while the new T-shaped cell continues T-shaped transition, itself now inhibiting other cells in the neural tube. The basal surface is shown by a solid line and apical surface by a dashed line. Green arrows show the direction of basal arm movement. Blue arrows show the direction of the signal.

Figure 5-15

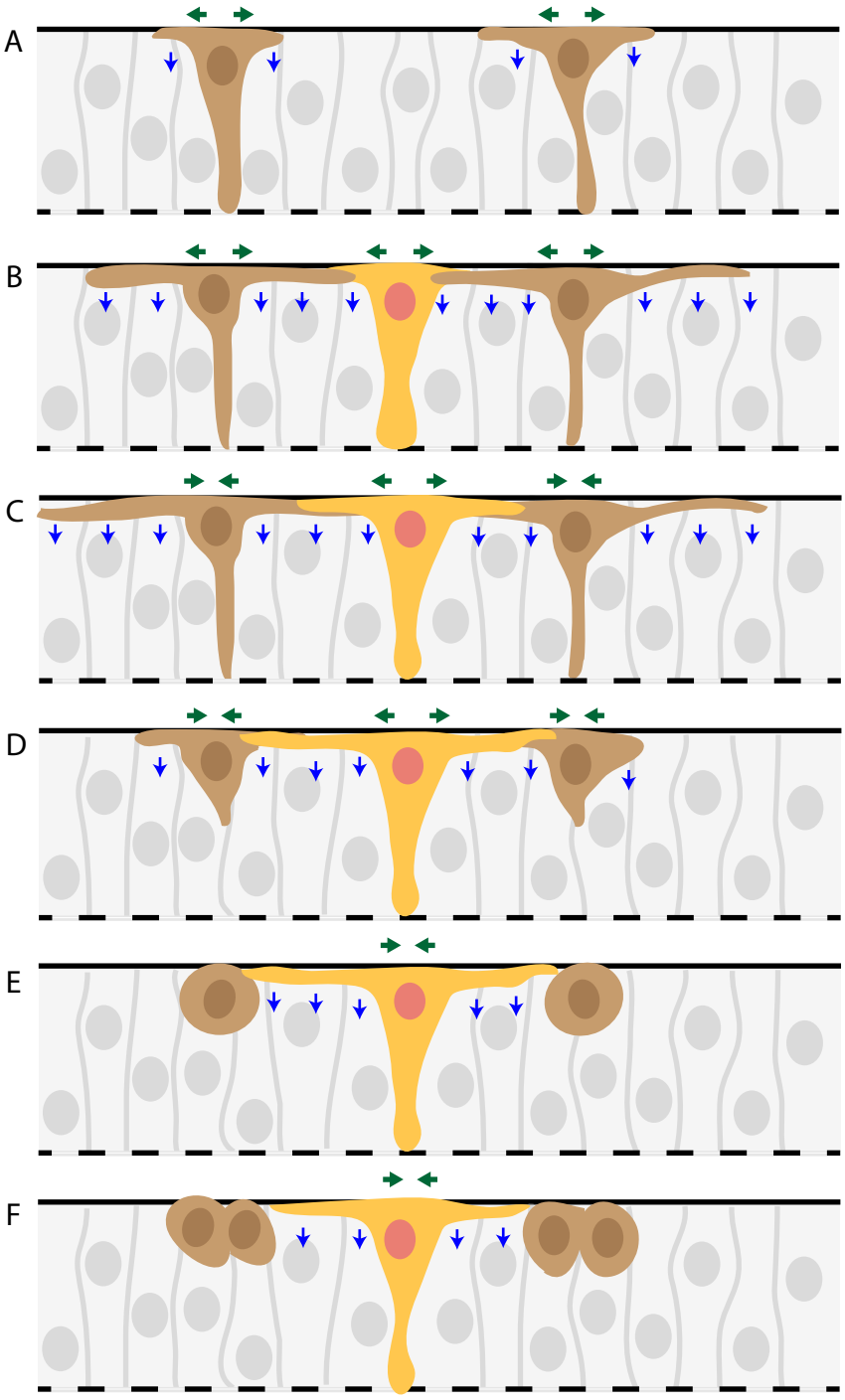

Figure 5-16: The morphological changes that occur during neurogenesis. (**1**) Neuroepithelial cells (**2**) undergo asymmetric divisions where the daughter that inherits the apical domain (red region) is committed to become a neuron. This cell maintains contact with the apical surface while its cell soma translocates to the basal aspect of the neural tube (**3**). Nascent neurons then undergo a stereotyped behaviour, first extending process along the basal surface (basal arms; **4**) to take on a T-shaped morphology (**5**). The cell then retracts its basal arms (**6**) and detaches from the apical surface (**7**) before rounding up and extending an axon (**8** and **9** in **A**) or undergoing a terminal differentiating division (**8** and **9** in **B**). P = daughter biased to remain a progenitor. N = daughter biased to differentiate as a neuron. ? = fate choice unknown.

Figure 5-16

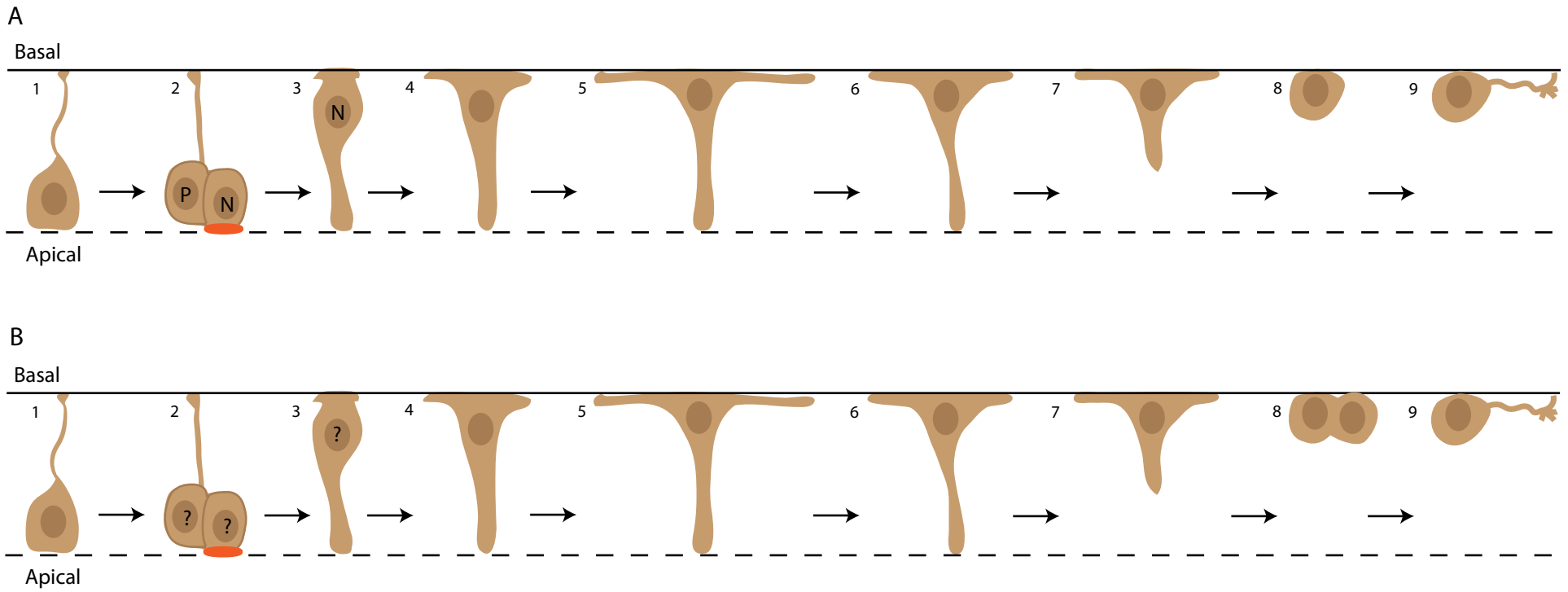

5.4.3 Variability in the T-shaped morphological transition generates noise in the pattern of *vsx1*:GFP progenitor differentiation

The patterns of differentiation generated in the models that assume invariant T-shaped behaviour and initial progenitor spacing were regular, depicting that all progenitors in a given iteration divide at the same time and with a consistent periodicity. In these models, a new iteration progenitor will divide exactly in the middle of the space between progenitors from the previous iteration. This resembles what I observed in real *vsx1*:GFP movies (see section 4.4.2.1). However, if the models reliably maintain the invariant conditions through the iterations they predict that divisions will occur in alternating, discreet locations resulting in clusters at these points (**Figure 5-4**). However, this is not seen in the *vsx1*:GFP population (**Figure 4-5**) where iterations of divisions occur in a manner that fills the entire space.

In contrast to the uniformity assumed by this version of the model, we have observed that both the T-shaped cell behaviour and the *vsx1*:GFP differentiation pattern are both variable. Adding variation to the initial spacing of progenitors to thought experiments had knock-on effects on the location and timing of predicted divisions throughout pattern development, adding noise to the predicted patterns. This suggests that space and time are interlinked in this patterning process. The pattern diagrams generated after introducing one form of variation also more closely resemble pattern diagrams of *vsx1*:GFP differentiation events. This suggests that variation in the T-shaped morphological transition during pattern development is important to limit clustering of *vsx1*:GFP progenitors over time. To support this idea, in the zebrafish telencephalon differentiating neurons do not go through the T-shaped morphological transition and in this region neurons do tend to cluster in the marginal zone (P. Alexandre, unpublished observations).

In summary, these findings suggest that variation in the patterning signal (i.e. T-shaped transition) are important to generate a self-organising, space-filling pattern, like that observed in patterning of *vsx1*:GFP differentiation.

5.4.3.1 Types of variation not addressed in the models

In the previous section I discussed the role and importance of variation in the development of this self-organising pattern. However, I have only modelled the effect of one form of variation on the resulting pattern. *In vivo* there are may more sources of variation, affecting more than two cells in the field, so its easy to imagine how this adds up to result in a noisy field of differentiating progenitors. Other sources of variation in the patterning signal that are important to keep in mind are discussed below.

First, observations of T-shaped cells suggest that the dynamics of basal arms might not be maintained through multiple iterations. P. Alexandre has reported that T-shaped cells which begin the behaviour later in neurogenesis display shorter arm lengths and shorter time to complete the behaviour. These observations need to be more thoroughly investigated.

Second, the current representation of the T-shaped morphological transition assumes both basal arms on a single T-shaped cell behave symmetrically, in terms of speed of growth and retraction as well as their maximum length. This is not what we see, but the asymmetry of basal arms on a single T-shaped cell is hard to add to this simple model.

Third, the T-shaped cells we have observed also do not grow or retract their basal arms at a constant speed or direction, often showing short periods of retraction doing the growth stage, or vice versa. These observations suggest that basal arm growth and retraction are not entirely cell autonomous processes and might indicate that the growth or retraction of basal arms might be influenced by signals within the tissue. The models generated in this chapter predict a high degree of overlap between the basal arms of adjacent T-shaped cells. This matches what P. Alexandre has observed in time-lapse movies of mosaically labelled cells in proximity to each other (unpublished observations). The models also predict that the basal arms of one T-shaped cell might reach the soma of the adjacent T-shaped cells. These observations, as well as the variability in the T-shaped morphological transition outlined above, hint at the potential that some sort of interaction occurs between the basal arms of early and later differentiating cells. If such an interaction were to occur, one could imagine that the wobbly path of basal arm growth and retraction seen in individual T-shaped cell behaviours and high levels of variation between different T-shaped cells might be a result of signalling between the basal arms of adjacent cells (**Figure 5-3**).

Therefore, the variation we observe in the pattern formation and the T-shaped morphological transition might indicate that the pattern of *vsx1*:GFP progenitor differentiation we have characterised might develop due to a responsive, malleable mechanism that allows cells to generate a self-organising pattern.

5.4.4 How is initial spacing established?

The data presented so far supports our hypothesis that T-shaped cells establish a long distance pattern of differentiation along the anteroposterior axis through time. In our current long distance patterning hypothesis we have assumed that initial cells are periodically selected from a field of neuroepithelial cells in a long distance pattern along the

anteroposterior axis at approximately the same time. In fact, we see a bias for more rostral progenitors to divide earlier than those located caudally. It is not immediately obvious how basal arms might establish the initial spaced pattern of *vsx1* neurons.

The reaction diffusion (RD) model of pattern formation states that patterns (termed Turing patterns) can be generated from uniform distributions of patterning molecules (reviewed in Meinhardt & Gierer 2000 and Kondo & Miura 2010), and has been shown for Delta Notch-mediated pattern formation (Cohen et al. 2013; Chen et al. 2014; see section 5.4.1 for full discussion of the RD model). Therefore, if long-range Delta Notch signalling, or a similar inhibitory signal, determines the *vsx1* differentiation pattern then it is possible that this system could spontaneously form a long-distance pattern of differentiation. This is best explored in a mathematical model.

It is possible that other signalling pathways distinct from the basal arms can either influence or determine the initial pattern of *vsx1* progenitors. As the initial progenitor pattern appears repeated or segmental, an overt segmentation signal would be an obvious mechanism to generate this pattern. However, the spinal cord itself lacks any overt segmentation, appearing uniform along the rostrocaudal axis (unlike the hindbrain, which is known to have both phenotypic bulges and segment-specific gene expression). We have shown the initial pattern of *vsx1* progenitors is independent of somite-derived signals, suggesting that the only overtly segmented structures in the tail, which lie adjacent to the spinal cord, are not involved in spacing *vsx1* neurons. An alternative explanation involves the elongating neural tube and the mechanism that generates the segmented somites. As the rostrocaudal axis of the embryo elongates, the neural tube forms as the somites are specified. Oscillation of Delta Notch target genes are known to pattern the presomitic mesoderm to form the somites (Soroldoni et al. 2014). As this tissue lies adjacent to the presumptive neural tube it is possible that the neural primordium is also affected by these oscillations but we do not know if this plays a role in initial *vsx1* patterning. However, as the oscillations are large-scale signals they are unlikely to generate fine grain patterns like initial *vsx1* progenitor patterning.

Another tissue that might segment or pattern the otherwise uniform spinal cord is the notochord. While this tissue does not show any obvious segmentation (like the overlying spinal cord neural tissue), there is growing evidence that signals from the notochord can influence patterning, segmentation and development of vertebrae along the rostrocaudal axis in teleosts (reviewed in Fleming et al. 2015). It is possible that the notochord will provide patterning signals to generate the initial spacing pattern observed in *vsx1*:GFP progenitors.

In summary, the pattern of initial *vsx1*:GFP progenitors might be established via a Turing patterning mechanism, where basal arms provide the long distance inhibitory signal. Furthermore, there are a number of other tissues and patterning signals that are known or suspected to be involved in patterning and segmenting the spinal cord. It is feasible that any of these patterning signals, or others not yet identified, might initiate the pattern of *vsx1* progenitor patterns.

5.4.5 Summary

The modelling presented in this chapter support the hypothesis that basal arms deliver long distance lateral inhibition to pattern differentiation in space and time. Taken together, the outcome of these models and thought experiments have generated a set of rules which reasonably accurately represent what occurs *in vivo*. Further refinement to the hypothesis or to our understanding of this process is required to account for the aspects of observed data that we have not yet explained. The majority of the remaining questions will be best answered using a computational model of this patterning process.

CHAPTER 6
INVESTIGATING THE REGULATION OF NON-APICAL PROGENITORS DURING ZEBRAFISH NEUROGENESIS.

6 Investigating the regulation of non-apical progenitors during zebrafish neurogenesis.

6.1 Introduction

Many studies have focused on the cellular and molecular mechanisms that are involved in regulating neurogenesis and progenitor maintenance in the developing brain (for example: Doe 2008; Miyata et al. 2010; Schmidt et al. 2013; and reviewed in Götz & Huttner 2005). Non-apical progenitors are often described as an intermediate between apical progenitor and differentiating neuron, as they have limited proliferative potential (Götz & Huttner 2005). However, the molecular and cellular processes involved in the production of non-apical progenitors are not well understood. Zebrafish embryos provide an excellent system in which to study the mechanisms controlling the production of non-apical progenitors as are amenable to live imaging at the single cell and subcellular level and genetic manipulation (Lyons et al. 2003; Alexandre et al. 2010; Kressmann et al. 2015).

My data, and previous work in the Clarke and Alexandre labs, have shown that non-apical progenitors share some characteristics with neurons in the embryonic zebrafish neural tube, including: the expression of the marker HuC/D (which is mostly commonly expressed in neurons (Kim et al. 1996); see Chapter 3); basal location of the soma; lack of contact to the apical surface at mitosis; and the T-shaped morphological transition prior to morphological differentiation (see section 4.1.3.1; unpublished observations, manuscript in preparation). As non-apical progenitors share some characteristics with neurons, here I investigate whether they also share common regulatory mechanisms. Specifically, I look at the effect of inhibiting expression of aPKCλ by injection of an anti-sense oligo morpholino, which reduced neurogenesis in zebrafish spinal cord (Alexandre et al. 2010), and overexpression of DN-Su(H), a Notch pathway inhibitor, which is known to promote neurogenesis (Wettstein et al. 1997; Chapouton et al. 2010).

6.1.1 Loss of apical domain proteins leads to the loss of neurogenic divisions

Neuroepithelial cells are a polarised cell type, with a specialised apical domain composed of adherens junctions. This domain contains Pard3, Pard6 and aPKC, which form part of an evolutionarily conserved complex of proteins (Wodarz, 2002). Unlike the majority of vertebrate systems, the zebrafish neural tube is not polarised at neural plate stages (Geldmacher-Voss et al. 2003; Buckley et al. 2013). However, neurons are produced before the apical domain has been established. As zebrafish neurulation continues, apicobasal polarity is established in late neural rod stages (Tawk et al. 2007; Buckley et al. 2013). Following the formation of the apical

domain and neural tube, during asymmetric divisions of apical progenitors the daughter cell that inherits this apical domain, and therefore apically localised proteins, is biased to differentiate as a neuron (Alexandre et al. 2010). Loss of aPKCλ or Pard3 by injection of an anti-sense oligo morpholino (morpholino) results in a loss of asymmetric neurogenic divisions, in favour of symmetric proliferative divisions, during the main stages of neurogenesis (20–40 hpf) (Alexandre et al. 2010). In contrast, the *heart and soul* (*has*) mutation of aPKCλ (also known as aPKCiota (i) or prkCi; Horne-Badovinac et al. 2001), which causes a loss of aPKCλ protein from 48 hpf, results in increased apical divisions, depletion of the progenitor pool and an increased production of oligodendrocyte precursor cells (OPCs; Roberts & Appel 2009). These data suggest that protein components of the apical domain have different functions depending of the developmental time: they are involved in promoting neurogenesis during neurogenic stages and maintaining precursor cells around the onset of gliogenesis. However, the role of aPKCλ in the regulation of non-apical progenitors during neurogenesis is unknown.

6.1.2 Overexpression of neurogenic genes increases neuronal differentiation

The negative regulation of neuronal differentiation by Notch signalling (lateral inhibition; see section 1.3.1 for a full discussion) requires cleaved Notch intracellular domain (NICD) to interact with DNA binding protein suppressor of hairless (Su(H); CBF1/RBPjκ in mammals) to activate the expression of the enhancer of split complex (E(Spl)-C) in *Drosophila* and the hairy and enhancer of split (HES) and HES-related (HER) family genes in vertebrates (**Figure 6-1**A). The E(SPL)-C and HESR/HER genes inhibit differentiation through repression of the transcription of basic helix-loop-helix (bHLH) proneural genes, including genes belonging to the achaete scute, neurogenin and atonal families (Campos-Ortega & Jan 1991; **Figure 6-1**A). Manipulating the pathways downstream of activated Notch signalling has been used to increase the incidence of differentiation in mosaically labelled cells the chick neural tube by the electroporation of the proneural gene *Neurog2* (Das & Storey 2014) or the overexpression of neurogenin in zebrafish (Kim et al. 1997). For the same purpose, the Clarke lab has been looking at the effect of overexpressing genes associated with promoting neurogenesis on the fate of mosaically injected neuroepithelial cells in zebrafish embryos. Previous work has shown that expression of a mutant form of suppressor of hairless with impaired DNA binding (dominant negative suppressor of hairless; DN-Su(H)) drives injected neuroepithelial cells to differentiate in the zebrafish (Wettstein et al. 1997; Chapouton et al. 2010; **Figure 6-1**B). The effect of overexpressing these genes on the genesis of non-apical progenitors is currently unknown.

6.1.3 Aim of chapter

In this chapter I look at the effect of manipulating the expression of genes that we know play a role in regulating the production of neurons on the population of non-apical progenitors in the zebrafish neural tube. Specifically, I analysed the effect of apical proteins (i.e. aPKCλ) and Notch signalling (i.e. DN-Su(H)) on the non-apical progenitor population, using *vsx1*:GFP as a marker of this population.

Figure 6-1: DN-Su(H) leads to insensitivity to Notch signalling. **A**) During lateral inhibition, interaction between Delta on one cell and Notch on another results in the cleavage of the notch intracellular domain (NICD) within the signal-receiving cell. NICD activates transcription of Hes/Her proteins by forming a complex with suppressor of hairless (Su(H)) and Mastermind (Mam) that binds to transcriptional enhancers of target genes. The result of activated Notch signalling is inhibited expression of proneural bHLH transcription factors, maintaining the cell in a progenitor state. **B**) The effect of a DNA-binding mutant of Su(H) on the Notch signalling pathway. DN-Su(H) binds to NICD, but is unable to activate Hes/Her protein transcription, making the cell insensitive to activated Notch signalling and driving it to differentiate.

Figure 6-1

A) Lateral inhibition

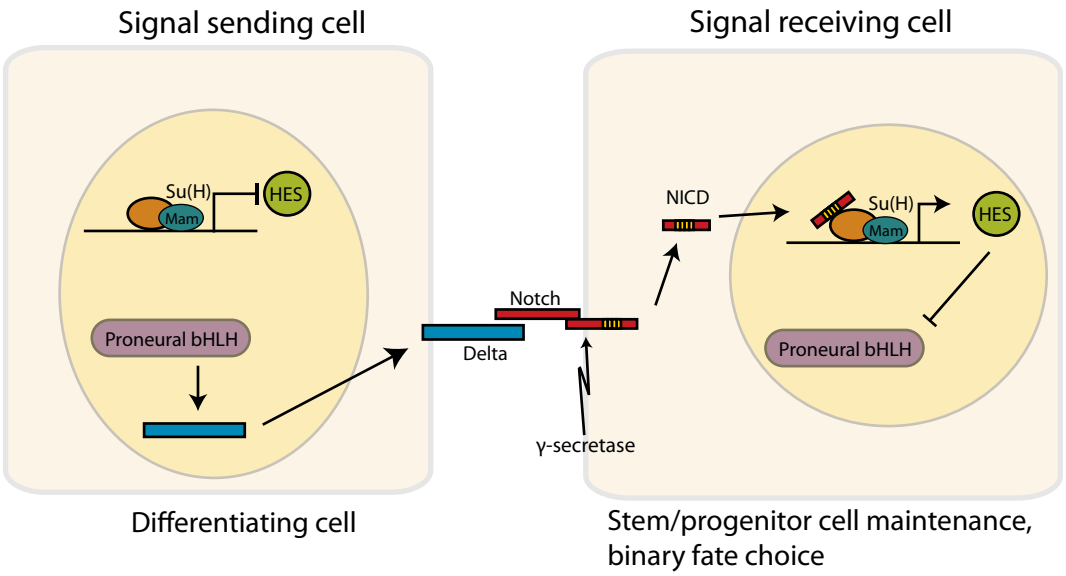

B) Effect of dominant negative supressor of hairless (DN-Su(H))

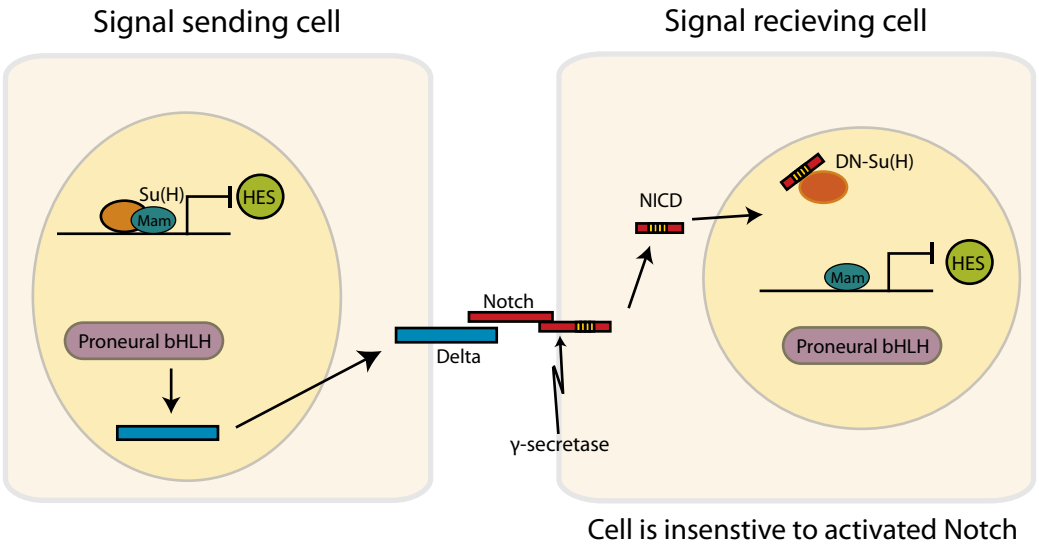

6.2 Materials and Methods

6.2.1 Morpholinos and mRNA constructs

The following anti-sense oligo morpholinos and mRNAs were injected, at the relevant stage, as described in the General Materials and Methods.

Table 6-1: Anti-sense oligo morpholinos.Injected at the one cell stage.

Gene Target	Referred to as:	Sequence	Source	Amount injected	Reference
aPKCλ	aPKCλ morpholino	5'TGTCCCGCA GCGTGGGCAT TATGGA 3'	Gene Tools	1 nl of 0.5 mM stock	Cui et al. 2007
Standard control	Control morpholino	5'CCTCTTACCT CAGTTACAATT TATA 3'	Gene Tools	Equivalent concentrations.	

Table 6-2: mRNA constructs.

Construct	Referred to as:	Stage used	Source	Amount injected	Reference
Dominant negative suppressor of hairless	DN-Su(H)	8-32 cell	Dr Bally Cuif, CNRS, France	1 nl of 0.1 µg/µl	(Wettstein et al. 1997; Chapouton et al. 2010)
***GFP-CAAX* (from human)**	Membrane - GFP	8-32 cell	(Alexandre et al. 2010)	0.25-0.5 nl of 0.1 µg/µl	(Alexandre et al. 2010)
***mCherry-CAAX* (from human)**	Membrane - RFP	8-32 cell	(Alexandre et al. 2010)	0.25-0.5 nl of 0.1 µg/µl	(Alexandre et al. 2010)
***Histone H_2B (H_2b)-RFP* (from human)**	Nuclear-RPF	8-32 cell	(Alexandre et al. 2010)	0.25-0.5 nl of 0.1 µg/µl	(Alexandre et al. 2010)

mRNA was synthesised as described in the General Materials and Methods

6.2.2 Immunohistochemistry

Primary antibodies, secondary antibodies and counterstains used in this chapter for wholemount immunohistochemistry are listed in General Materials and Methods.

6.2.3 Analysis

Analysis in the hindbrain was carried out on a 150 µm length of the tissue, starting from the posterior end of the otic vesicles (see **Figure 6-2**A). The number of *vsx1*:GFP-expressing cells and the number of mitotic cells (marked by PH3 expression) was counted and their location relative to the apical surface was recorded. When quantifying cell fate in the spinal cord, I looked at a 150 µm length of tissue and 35 µm dorsoventral sections, capturing the whole of the

vsx1:GFP expression domain. The number of injected cells as well as whether or not they expressed HuC/D and *vsx1*:GFP was quantified.

To measure the level of neurogenesis at 20 hpf the number of HuC/D expressing cells was counted. At 36 hpf the tissue size and neurogenesis was estimated by measuring the volume of Sytox or of HuC/D immunoreactivity, respectively, using the 'Surfaces' function in IMARIS®. This function uses the intensity of a specific fluorescent signal in a Z-stack to generate a surface around a specific object within the image (i.e. the tissue marked by Sytox nuclear counterstain or the mantle zone labelled with HuC/D). The threshold of intensity that was measured was manually selected to ensure that the entire volume of the signal was incorporated into surface.

6.3 Results

The molecular mechanisms that are involved in regulating non-apical progenitor production are currently unknown. Non-apical progenitors in the zebrafish neural tube, the majority of which express *vsx1* and are labelled in the Tg(*vsx1*:GFP) reporter line, appear to share a number of morphological and molecular characteristics with differentiating neurons. In this chapter I looked at the effects of manipulating genes that are known to impact neurogenesis (i.e. aPKCλ and DN-Su(H)) on the non-apical progenitor population.

6.3.1 aPKCλ knockdown results in ectopic non-apical divisions

The zebrafish *heart-and-soul (has)* mutation results in a loss of aPKCλ at the apical surface from 48 hpf and is known to disrupt apical polarity and adherens junctions in the spinal cord at 72 hpf (Roberts & Appel 2009). As neurogenesis largely takes place before 48 hpf (see Chapter 3), this mutant zebrafish line cannot be used to study the affect of the loss of aPKCλ on the production of neurons. In contrast, the aPKCλ morpholino can be injected at the one cell stage and therefore decrease levels of aPKCλ protein from earlier stages. I observed a marked decrease in aPKC immunoreactivity in aPKCλ morpholino-injected embryos at 20 hpf (compare **Figure 6-2**B and C), which is still present at 36 hpf (compare **Figure 6-2**D and E). This antibody recognises an epitope that is common to aPKCλ and aPKCζ (Horne-Badovinac et al. 2001; Cui et al. 2007), so the remaining aPKCλ immunoreactivity seen in aPKCλ morpholino-injected embryos is most likely to be aPKCζ. In these aPKCλ morpholino-injected embryos the effect on tight junction formation (marked by zona occludens-1; ZO-1) appears to be minimal at 36 hpf (compare **Figure 6-2**F and G). While the aPKCλ-depleted embryos appear to have a deflated hindbrain ventricle (compare **Figure 6-2**I to H), the size of the hindbrain tissue is not significantly different from control morpholino-injected embryos (**Figure 6-2**J). These data show that aPKCλ morpholino-injection generates a loss of aPKCλ protein with minimal disruption to tight junction formation and epithelial integrity. This provides an opportunity to investigate the role of aPKCλ on non-apical progenitors before and after the apical domain and neural tube has formed.

6.3.1.1 The effect of the loss of aPKCλ protein on pre-neural tube neurogenesis

The function of aPKCλ during neurogenesis is only known in the context of the polarised neural tube, after the apical domain has formed (from approximately 18 hpf), when it is required for neuronal differentiation (Alexandre et al. 2010). However, the first neurons are generated prior to apical domain formation in neural plate and neural rod stages. As there is a time lag between the division of an apical progenitor and the display of fate choice by the daughter cells (by HuC/D expression in the case of neurons and mitosis in the case of progenitor type daughter cells), any HuC/D expressing cells or non-apically dividing cells at 20 hpf should have been

generated prior to neural tube formation. Therefore, I asked what affect (if any) loss of aPKCλ protein has on non-apical progenitors during pre-neural tube neurogenesis in the caudal hindbrain by examining embryos at this stage shortly after the neural tube has been generated.

I injected Tg(*vsx1*:GFP) embryos with either a control or an aPKCλ morpholino at the one cell stage and then carried out immunohistochemistry for PH3 and HuC/D on fixed 20hpf embryos. In control morpholino injected embryos a small number of *vsx1*:GFP cells are present in the hindbrain at this stage and PH3-expressing cells are only visible on the apical surface (**Figure 6-3**A-D). In aPKCλ morpholino-injected embryos, again, a small number of *vsx1*:GFP can be see (**Figure 6-3**B) but unlike control embryos, in aPKCλ-depleted embryos I observed PH3-labelled cells at a distance from the apical surface (**Figure 6-3**E-H) When I quantified the effect of the morpholino injection on neurogenesis and cell division at 20 hpf, I found no significant difference in the number of apical divisions between control and aPKCλ morpholino-injected embryos (Cmo: mean ± SEM = 52 ± 5.04; n = 4 embryos; aPKCλmo: mean ± SEM = 64 ± 8.41; n = 5 embryos; **Figure 6-3**I) or the number of *vsx1*:GFP expressing cells (Cmo: mean ± SEM = 19.25 ± 2.25 ; n = 4 embryos; aPKCλmo: mean ± SEM = 16.6 ± 1.4; n = 5 embryos; **Figure 6-3**K). However, aPKCλ morpholino-injected embryos showed a small significant increase in the number of HuC/D expressing cells (Cmo: mean ± SEM = 52.5 ± 6.58; n = 4 embryos; aPKCλmo: mean ± SEM = 68.4 ± 2.48; n = 5 embryos; unpaired t-test, P = 0.0479, t = 2.394, d.f. = 7; **Figure 6-3**L-N). These data show that loss of aPKCλ increases the total number of HuC/D-expressing neurons but does not affect the number of *vsx1*:GFP interneurons.

I next examined the location of PH3-positive cells in control and aPKCλ morpholino-injected embryos. Non-apical mitoses were absent in control morpholino-injected embryos (**Figure 6-3**C, D and J), but the reduction of aPKCλ function resulted in a small number of non-apically dividing cells (mean ± SEM = 1.8 ± 0.58; n = 5 embryos; arrow heads in, **Figure 6-3**G, H and J). These non-apical divisions were mostly located dorsal to the *vsx1*:GFP-expressing domain and did not coexpress *vsx1*:GFP (n = 4 embryos). Therefore, depletion of aPKCλ generates excess non-apical divisions prior to neural tube formation in the hindbrain and these non-apical progenitors do not resemble endogenous non-apical progenitors at this stage, as they do not express *vsx1*.

6.3.1.2 The effect of the loss of aPKCλ protein on post-neural tube neurogenesis

To examine the effect of aPKCλ morpholino on neurogenesis after neural tube formation we examined control and aPKCλ morpholino-injected embryos at 36 hpf. Measuring the volume of HuC/D immunostaining in the caudal hindbrain showed that aPKCλ morpholino-injected embryos have a significant loss of differentiated neurons (compare Figure 6-4A and B; Figure

6-4C) confirming that the reduction of aPKCλ protein inhibits neurogenesis (Alexandre et al. 2010). Concurrently, I observed a significant decrease in the number of *vsx1*:GFP-expressing cells in aPKCλ morpholino-injected embryos compared to controls (compare Figure 6-4H and N; Figure 6-4Q). The depletion of aPKCλ did not significantly alter the number of non-apical divisions observed per embryo compared to control morpholino-injected embryos (Figure 6-4R). However, aPKCλ morpholino-injected embryos contained a larger proportion of non-apical divisions that do not express *vsx1*:GFP (Figure 6-4S). Most of these *vsx1*:GFP negative non-apical progenitors are located dorsal to the *vsx1*:GFP domain (arrow in Figure 6-4O). I have not observed non-apical mitotic cells in a similar dorsoventral location in wild type or control morpholino-injected embryos (see Chapter 3 and Figure 6-4I, respectively). A large proportion of the *vsx1*:GFP-negative non-apical progenitor cells in aPKCλ morpholino-injected embryos express HuC/D indicating that they are likely to be neurogenic divisions (**Figure 6-5**; mean ± SEM percentage of non-apical PH3+ cells that express HuC/D+ = 83.85% ± 6.3; n = 6 embryos).

The decreased numbers of neurons and *vsx1*:GFP cells observed in aPKCλ morpholino-injected embryos of could be explained by a general delay in the development. However, reduced levels of aPKCλ protein did not affect the number of apical PH3-labelled mitotic cells (Figure 6-4P), nor is the volume of the tissue altered (Figure 6-2C) in the caudal hindbrain at this stage. Together these data suggest that loss of aPKCλ does not induce a significant developmental delay, nor does it lead to an early depletion of the apical progenitor pool. This suggests that the effects reported above are due to loss of aPKCλ protein specifically.

6.3.1.3 Loss of aPKCλ protein generates ectopic non-apical divisions

In summary, depletion of aPKCλ results in decreased number of neurons both during and after neural tube formation, consistent with the idea that apical proteins promote neuronal differentiation in the zebrafish spinal cord (Alexandre et al. 2010). aPKCλ depletion also causes a decrease in *vsx1*:GFP-expressing non-apical progenitors at 36 hpf and generates an unidentified (*vsx1*:GFP-negative) population of non-apical mitotic cells at both stages examined. These divisions appear to express a HuC/D suggesting they might be neurogenic divisions.

Figure 6-2: Characterisation of the effect of aPKCλ morpholino on global growth and expression of apical domain markers. **A**) 3D reconstruction of a dorsal view of the hindbrain in a wild type embryo at 36 hpf, counterstained for nuclei (Sytox, blue). The caudal hindbrain, posterior to the OV was analysed (represented by dashed lines). **B-G**) Single z-planes from the hindbrains of control and aPKCλmo-injected embryos at 20 hpf (**B** and **C**, respectively) and 36 hpf (**D, F** and **E, G**, respectively). **B-E**) Embryos show immunoreactivity for aPKC (magenta) and counterstained with Sytox (blue). aPKCλ morpholino injection reduces aPKCλ immunoreactivity in the hindbrain. **F** and **G**) Embryos show immunoreactivity for ZO-1 (green) and counterstained with Sytox (blue). **H** and **I)** 3D reconstruction of a dorsal view of the hindbrain at 36 hpf of control (**H**) and aPKCλmo-injected embryos (**I**). aPKCλmo injection impairs the inflation of the hindbrain ventricle (compare **I** and **H**). Scale bar = 25 μm. **J**) The volume of tissue, measured by the volume of Sytox counterstaining is not significantly different between control and aPKCλ morpholino-injected embryos (Mann-Whitney $U = 0$, $n_1 = 5$, $n_2 = 6$, $p = 0.5281$). Cmo = control morpholino; aPKCλmo = aPKCλ morpholino; OV = otic vesicle.

Figure 6-2

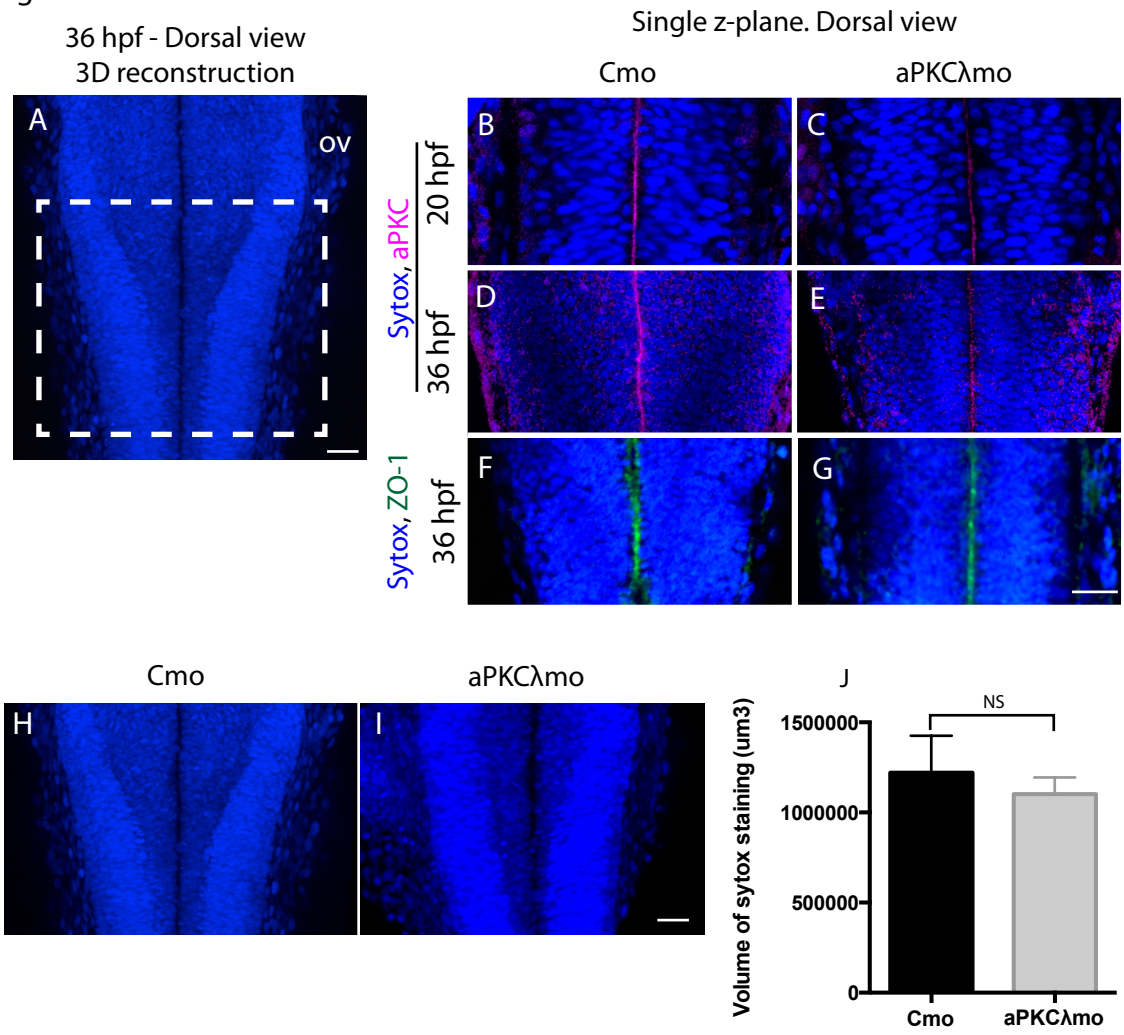
36 hpf - Dorsal view
3D reconstruction
Single z-plane. Dorsal view
Cmo
aPKCλmo
A
ov
B
C
D
E
F
G
Sytox, aPKC
20 hpf
36 hpf
Sytox, ZO-1
36 hpf
Cmo
aPKCλmo
H
I
J
NS
Volume of sytox staining (um3)
1500000
1000000
500000
0
Cmo
aPKCλmo

Figure 6-3: Loss of aPKCλ protein results in ectopic non-apical divisions at 20 hpf. **A-H**) Images of whole mount *vsx1*:GFP (green) embryos counterstained for nuclei (Sytox, blue) and cells in M-phase (anti-PH3, magenta). Single z-slice from a dorsal view or transverse reconstruction of the caudal hindbrain of control (**A**-**C** and **D**) and aPKCλ morpholino (**E**-**G** and **H**)-injected embryos. In aPKCλ-depleted embryos non-apical mitotic cells are only seen in regions dorsal to *vsx1*:GFP expression (arrow in **H**). **I**) Control and aPKCλ morpholino-injected embryos do not have significantly different numbers of apical PH3+ cells (unpaired t-test, P = 0.2916, t = 1.141, d.f. = 7). **J**) aPKCλ depleted embryos contain significantly more non-apical PH3+ cells than control morpholino-injected embryos (N (embryos): Cmo = 5; aPKCλmo = 6. Unpaired t-test, P = 0.0297, t = 2.722, d.f. = 7). **K**) There is no significant difference between the average number of *vsx1*:GFP cells in control and aPKCλ morpholino-injected embryos (unpaired t-test, P = 0.3306, t = 1.045, d.f. = 7). **L** and **M**) 3D renders showing nuclei (Sytox) and HuC/D immunoreactivity in the neural tube of Control (**L**) and aPKCλ morpholino-injected embryos (**M**). **N**) A small significant increase in the number of neurons (labelled with HuC/D) is seen in the neural tubes of aPKCλ morpholino-injected embryos compared to control (unpaired t-test, P = 0.0479, t = 2.394, d.f. = 7). Graphs show mean (± SEM). Cmo = control morpholino, aPKCλmo = aPKCλ morpholino. N (embryos): Cmo = 5, aPKCλmo = 5. Scale bar = 25 μm.

Figure 6-3

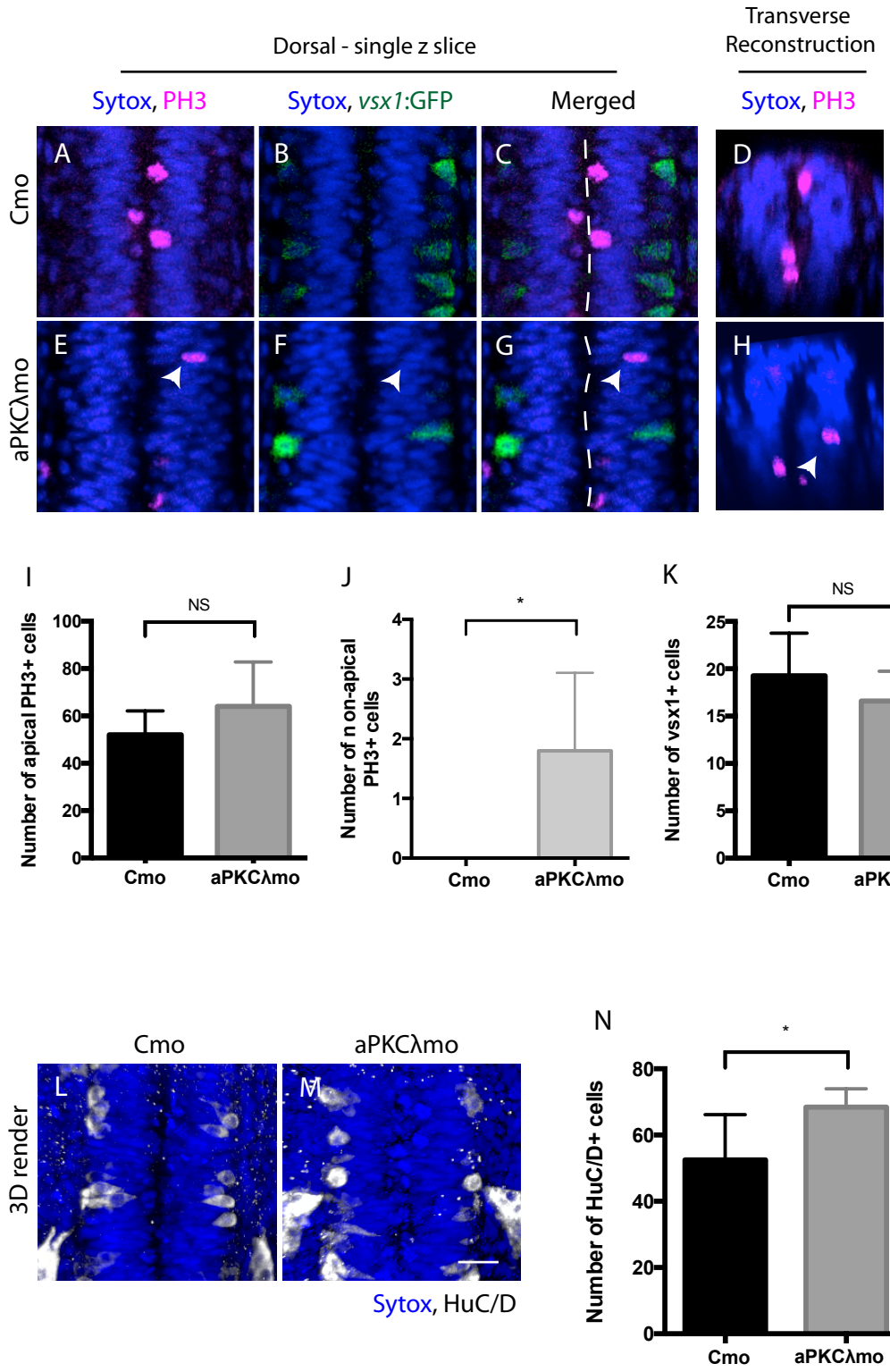
Dorsal - single z slice
Transverse Reconstruction
Sytox, PH3
Sytox, vsx1:GFP
Merged
Sytox, PH3
Cmo
aPKCλmo
A
B
C
D
E
F
G
H
I
Number of apical PH3+ cells
NS
Cmo
aPKCλmo
J
Number of n on-apical PH3+ cells
*
K
Number of vsx1+ cells
NS
Cmo
aPKCλmo
3D render
L
M
Sytox, HuC/D
N
Number of HuC/D+ cells
*

Figure 6-4: Loss of aPKCλ protein generates a population of *vsx1*:GFP-negative non-apical progenitors at 36 hpf. Dorsal reconstructions of the caudal hindbrains of control (**A**) and aPKCλ (**B**) morpholino-injected embryos showing immunoreactivity for HuC/D (white) and nuclear counterstain (Sytox, blue). **C**) The volume of HuC/D fluorescence is significantly decreased after aPKCλmo injection compared to control embryos (Mann-Whitney U = 11, $n_1 = 5$, $n_2 = 6$, P = 0.0095). **D-O**) Images of wholemount *vsx1*:GFP (green) embryos counterstained for nuclei (Sytox, blue) and showing immunoreactivity for PH3 (mitotic cells; magenta). Dorsal views (**D-F**) and transverse reconstructions (**G-I**) of control morpholino-injected embryos show non-apical mitoses coexpress *vsx1*:GFP (arrows in **F** and **I**). These non-apical mitoses are located in ventral regions of the tube (arrow heads in **G-I**). In dorsal views of aPKCλ-depleted hindbrains (**J-L**) non-apical mitoses appear adjacent to the *vsx1*:GFP domain, but do not express GFP. In transverse reconstructions (M-O) these mitotic cells appear to be located dorsal to the *vsx1*:GFP domain. **P-R**) All graphs show mean ± SEM. The number of M-phase cells at the apical surfaces is not altered by aPKCλ morpholino injection (**P**, Mann-Whitney U T= 11.50, $n_1 = 6$, $n_2 = 6$, P = 0.3312) nor is the number of non-apical mitotic cells (**R**, Mann-Whitney U = 12, $n_1 = 6$, $n_2 = 6$, P = 0.0.3723). However, the number of *vsx1*:GFP cells is significantly reduced in aPKCλ compared to control morpholino-injected embryos (**Q**, Mann-Whitney U = 0, $n_1 = 6$, $n_2 = 6$, $p = 0.0022$). **S**) The proportion (-SEM) of non-apical divisions that are *vsx1*:GFP positive (green bars) and *vsx1*:GFP negative (white bars) in aPKCλ and control morpholino-injected embryos. aPKCλ morpholino injection results in a significant increase in the proportion of *vsx1*:GFP negative cells (Fishers exact test $p < 0.0001$). Cmo = control morpholino, aPKCλmo = aPKCλ morpholino.

Figure 6-4

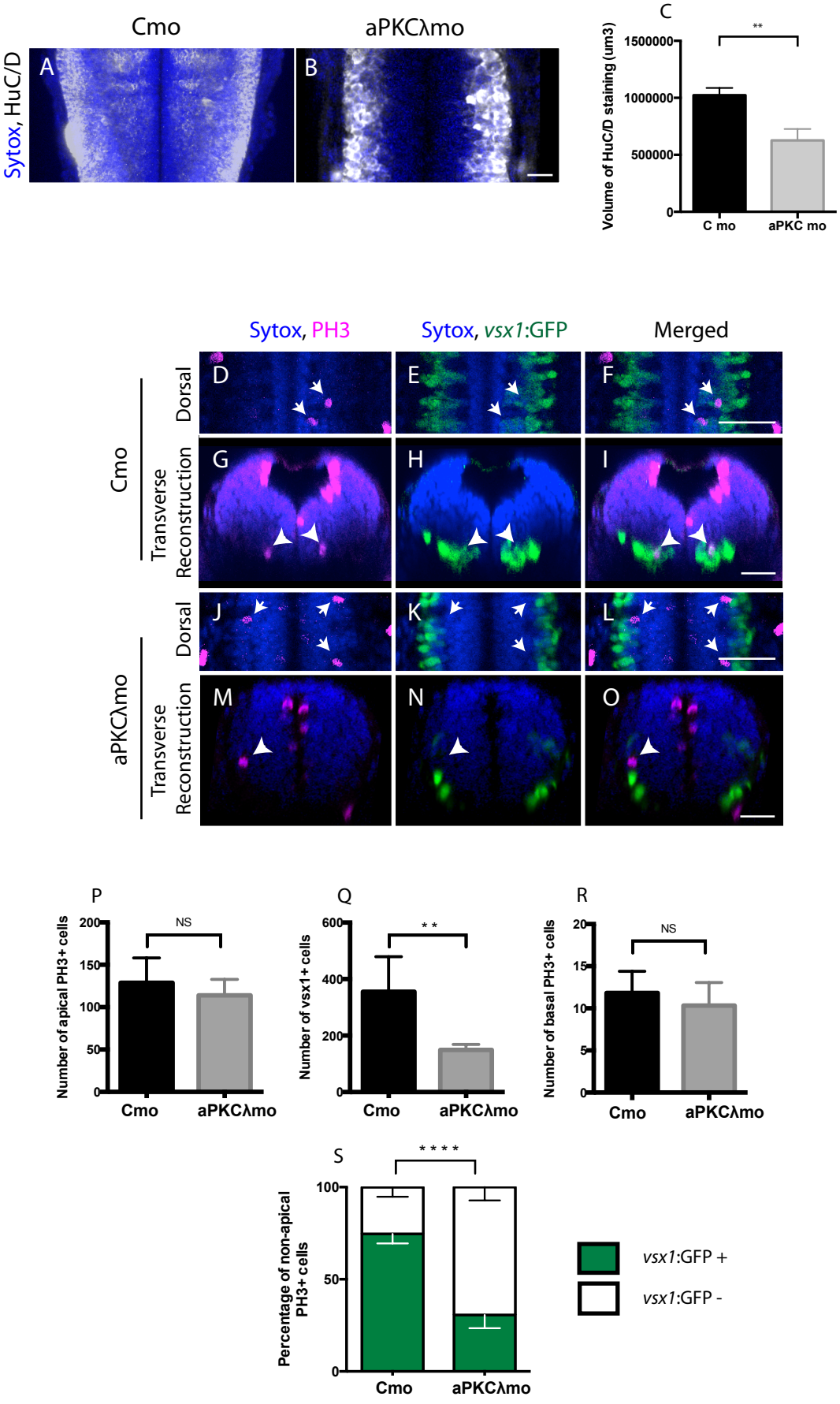
Cmo
aPKCλmo
Sytox, HuC/D
A
B
C
Volume of HuC/D staining (um3)
1500000
1000000
500000
0
**
C mo
aPKC mo
Sytox, PH3
Sytox, vsx1:GFP
Merged
Cmo
Dorsal
Transverse Reconstruction
aPKCλmo
D
E
F
G
H
I
J
K
L
M
N
O
P
Number of apical PH3+ cells
200
150
100
50
0
NS
Cmo
aPKCλmo
Q
Number of vsx1+ cells
600
400
200
0
* *
R
Number of basal PH3+ cells
20
15
10
5
S
Percentage of non-apical PH3+ cells
100
50
* * * *
vsx1:GFP +
vsx1:GFP -

Figure 6-5: Ectopic non-apical progenitors in aPKCλ morpholino-injected embryos express HuC/D. **A-C**) Single z-plane of the hindbrain of an aPKCλ morpholino-injected embryo, showing immunoreactivity for PH3 (magenta) and HuC/D (grey). Yellow dotted circle shows an example non-apical PH3-expressing cell is in the HuC/D+ marginal zone shows HuC/D immunoreactivity in its cytoplasm. Apical surface is shown by the white dotted line and the basal surface by the white dashed line. Scale bar = 25 μm.

Figure 6-5

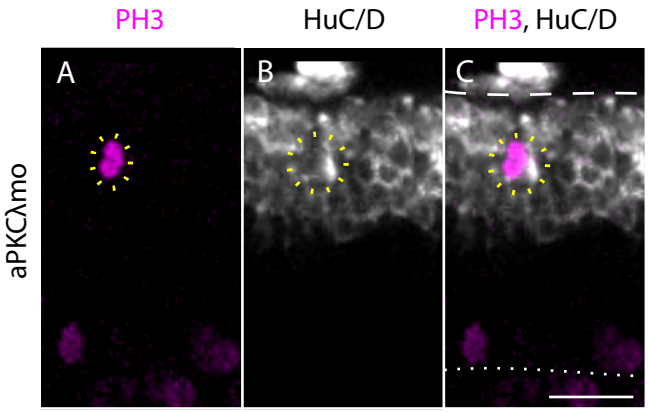

6.3.2 Mosaic overexpression of DN-Su(H) alters cell fate

Previous work has used the overexpression of genes inhibited by Notch signalling (Das et al. 2012; Kim et al. 1997) or genes involved in transducing activated Notch signals (Chapouton et al. 2010) to promote neurogenesis. The role of Notch signalling in the regulation of non-apical progenitors has not yet been addressed. Here I have examined the effect of the overexpression of dominant negative suppressor of hairless, DN-Su(H), which has been shown to induce neuronal differentiation of apical progenitors (Wettstein et al. 1997; Chapouton et al. 2010).

In order to look at the effect of overexpressing DN-Su(H) on (1) the overall level of neuronal differentiation and (2) the differentiation of the *vsx1*-expressing neuron population specifically, I injected *vsx1*:GFP embryos with DN-Su(H) mRNA at the 8-32 cell stage to generate a mosaic distribution of cells expressing the injected mRNA. DN-Su(H) mRNA was injected along with the mRNA encoding nuclear–RFP to mark the lineage of the injected cells. Embryos injected with nuclear-RFP only were used as controls. As I am interested in the impact of the overexpression of DN-Su(H) on non-apical progenitors, I focused my investigation on the *vsx1* domain by analysing a 35 μm wide dorsoventral region encompassing *vsx1*:GFP expression.

6.3.2.1 A small proportion of mosaically labelled cells differentiate as V2 interneurons

When Tg(*vsx1*:GFP) embryos were mosaically injected at the 8-32 cell stage with nuclear-RFP only, labelled nuclei in the spinal cord could be seen spread along the apicobasal axis at 28 hpf (**Figure 6-6**A). Within the region around *vsx1*:GFP expression less than a fifth of the injected cells differentiated as neurons (percentage of injected cells expressing HuC/D ± SEM = 15.26 % ± 1.95; n = 6 embryos; **Figure 6-6**C and I), while 1 in 40 injected cells expressed *vsx1*:GFP (3.39% ± 1.38; **Figure 6-6**I). It should be noted that all *vsx1*:GFP cells express HuC/D (**Figure 6-6**A-D; see Chapter 3). These data show that in wild type embryos mosaic labelling is likely include only 3% *vsx1* cells.

6.3.2.2 DN-Su(H) overexpression increases neuronal differentiation

When embryos are mosaically injected with DN-Su(H), the nuclei of the majority of injected cells are located on the basal surface of the tube at 28 hpf (illustrated by dashed line; **Figure 6-6**E and H). In these embryos the percentage of injected cells that express the neuronal marker HuC/D is increased compared to the injection of nuclear-RFP alone (mean ± SEM = 57.33 % ± 4.80; n = 6 embryos; **Figure 6-6**H and I), as expected. Overexpression of DN-Su(H) also increased the proportion of injected cells expressing the *vsx1*:GFP transgene (mean ± SEM = 16.84 % ± 3.30; n = 6 embryos; **Figure 6-6**H and I). In the *vsx1* domain, not all DN-Su(H)

injected cells that expressed HuC/D also expressed *vsx1*:GFP (asterisks in **Figure 6-6**H and I) but all *vsx1*:GFP cells expressed HuC/D. Taken together these data suggest that driving differentiation by the overexpression of DN-Su(H) can increase the chance of observing a *vsx1* progenitor division.

Next, I wanted to investigate whether DN-Su(H)-overexpressing cells that express *vsx1*:GFP behave as normal non-apical progenitors. In zebrafish embryos individual cells can be mosaically labelled using cell structure markers, allowing their cell behaviour to be monitored in an otherwise unlabelled embryo (Alexandre et al. 2010; Kressmann et al. 2015). In order to carry out this experiment, I co-injected membrane-GFP, nuclear-RFP and DN-Su(H) mRNA into 1 cell of Tg(*vsx1*:GFP) embryos at the 16-64 cell stage. This allowed me to clearly visualise the morphology of the injected cells, their behaviour as well as whether or not they express *vsx1*:GFP. Due to the low chance of labelling a *vsx1*-expressing cell by mosaic labelling (see section (6.3.2.1) I have only observed DN-Su(H)-expressing cells also expressing *vsx1*:GFP in one embryo. In this time-lapse movie I observed a cluster of three cells expressing DN-Su(H) (**Supplementary Movie 6-1**; labelled cell 1-3 in **Figure 6-7**). Cell number 2 is expressing cytoplasmic *vsx1*:GFP (seen as a yellow nucleus) from the start (**Figure 6-7**A) and undergoes division at the basal surface within 20 mins (asterisks in **Figure 6-7**B). Cell number 1 appears to have a T-shaped morphology, with basal arms extended along the basal surface (full arrowheads in **Figure 6-7**), a basal soma and apical attachment (empty arrowheads in **Figure 6-7**). The T-shaped cell 1 can then be seen retracting its basal arms and apical process (**Figure 6-7**D). This suggests that cells overexpressing DN-Su(H) go through the same morphological changes that have been characterised for differentiating neurons in wild type embryos (see Chapter 4). At the end of the movie, cells 1 and 3 are show intense expression of *vsx1*:GFP (**Figure 6-7**). As almost all *vsx1*:GFP cells divide to generate two interneuron daughters (98%; Kimura et al. 2008), it is likely that these cells will divide shortly too.

A cluster such as seen in this time-lapse movie is very rare in the normal spacing of *vsx1*:GFP cells (see Chapter 3) and suggests that inactivating Notch signalling by overexpression of DN-Su(H) also affects the normal spacing patterning. This further supports our hypothesis that spacing is established through the Delta Notch signalling.

Taking data from live imaging and fixed tissue together indicate that cell autonomously inhibiting Notch signalling by the mosaic overexpression of DN-Su(H) is able to increase the incidence of cells differentiating as *vsx1*:GFP non-apical progenitors.

Figure 6-6: Mosaic overexpression of DN-Su(H) changes the fate of injected cells in the hindbrain. The fate of spinal cord cells of embryos mosaically injected with Nuclear-RFP alone (**A-D**) or with DN-Su(H) mRNA (**E-H**) was investigated by looking at the expression of *vsx1*:GFP (green) and HuC/D (white) by nuclear-RFP labelled cells (magenta). **A-D**) When nuclear-RFP was injected on its own, labelled cells are found spread across the apicobasal axis of the tube (**A**) and a small number of injected cells coexpressed *vsx1*:GFP (**B**) or HuC/D (**C**). **E-H**) In embryos mosaically injected with nuclear-RFP and DN-Su(H), labelled nuclei are only located on the basal surface (**E**) and a small number of injected cells coexpressed *vsx1*:GFP (**F**), while most injected cells express HuC/D (**G**). Scale bar = 25 μm. **I**) Graph showing the proportion of injected cells HuC/D-negative (black) HuC/D-positive *vsx1*:GFP-negatiave (white) and HuC/D-positive *vsx1*:GFP-positive (grey). Stars refer to P values, compared to WT, of Tukey Multiple Comparisons Test, Two way ANOVA $F(2, 60) = 221.7$, $p < 0.05$.

Figure 6-6

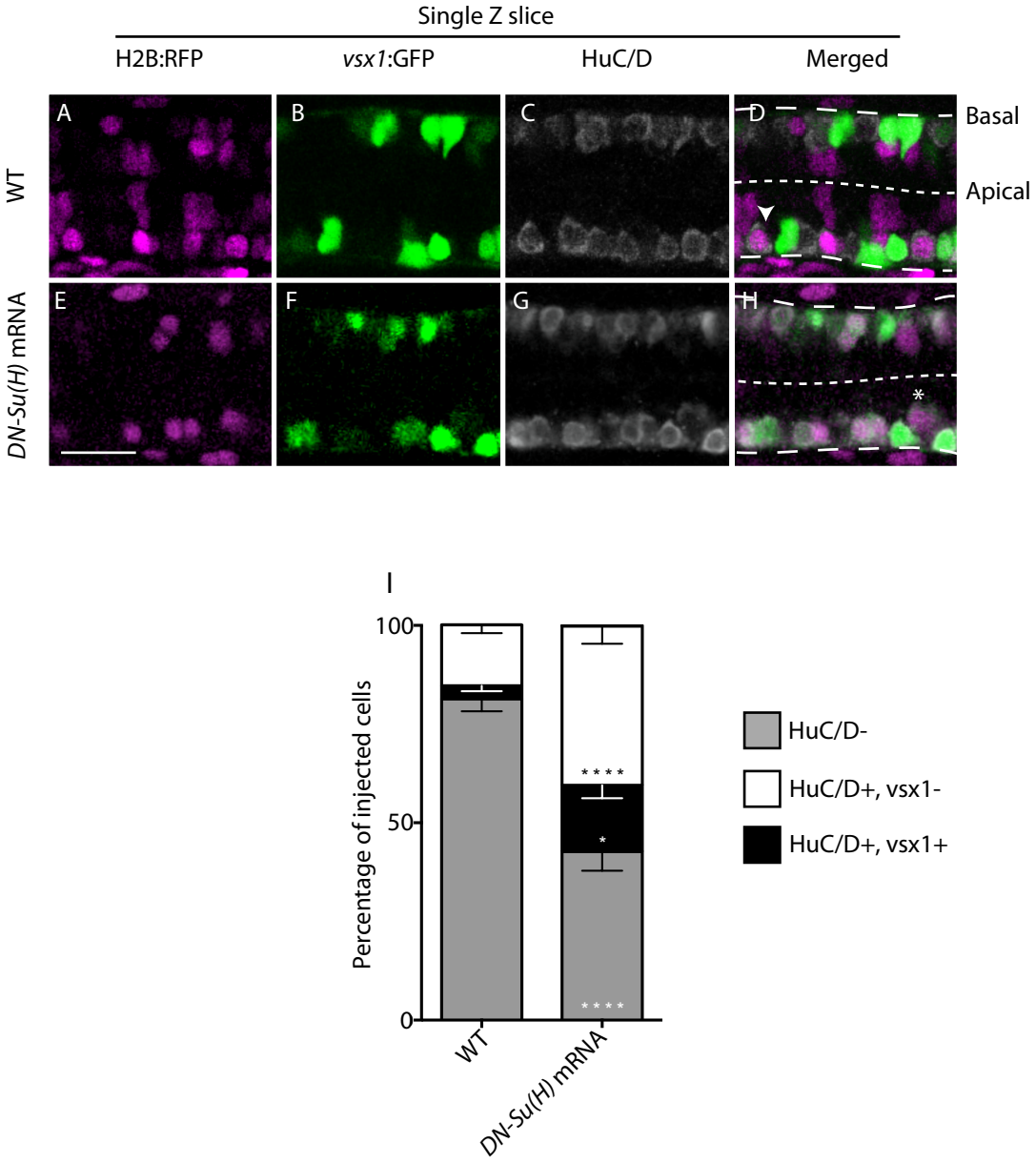
Single Z slice
H2B:RFP
vsx1:GFP
HuC/D
Merged
WT
DN-Su(H) mRNA
A
B
C
D
E
F
G
H
Basal
Apical
*
I
100
50
0
Percentage of injected cells
WT
DN-Su(H) mRNA
HuC/D-
HuC/D+, vsx1-
HuC/D+, vsx1+
* * * *
*
* * * *

Figure 6-7: DN-Su(H) drives differentiation of non-apical progenitors. Stills from a 3D render of a time-lapse movie of *vsx1*:GFP embryos with mosaically labelled cells expressing membrane-GFP, nuclear-RFP and DN-Su(H) (labelled 1-3). **Cell 1** initially has a T-shape morphology, with basal soma, extended basal arms (full arrowheads) and an apical process (empty arrowheads) (**A**). The cell retracts its basal arms (full arrowheads) and apical processes (empty arrowheads) (**C** and **D**) and begin to express *vsx1*:GFP (cytoplasmic) (**E**). **Cell 2** has already rounded up and is expressing cytoplasmic *vsx1*:GFP from **A** and can be seen dividing (asterisks in **B** and **C**). Scale bar = 25 μm. Apical surface shown by dotted line. Basal surface shown by dashed line. Time shown in minutes. N = 1 embryo.

Figure 6-7

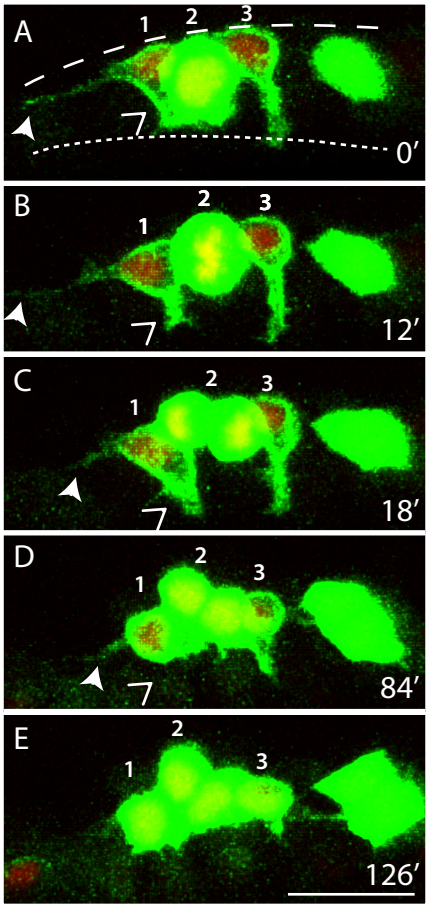
A
1
2
3
Basal
0′
Apical
B
1
2
3
12′
C
1
2
3
18′
D
1
2
3
84′
E
1
2
3
126′
Dorsal view
vsx1:GFP
membrane-GFP
nuclear-RFP

6.4 Discussion

In this chapter I have investigated the role of two pathways known to regulate neurogenesis on the production of non-apical progenitors in the zebrafish spinal cord.

6.4.1 Non-apical *vsx1* progenitors share some mechanisms that regulate their development with neurons

First, I investigated the affect of the loss of the apical protein aPKC on the production of non-apical progenitors. Previous work has shown that the apical domain, which includes aPKCλ, is inherited by the daughter of an apical progenitor that is biased to neuronal differentiation in the zebrafish neural tube and that aPKCλ is required for neuronal differentiation (Alexandre et al. 2010; Kressmann et al. 2015). In the data presented here, after formation of the apical domain and neural tube, depletion of aPKCλ results in the loss of *vsx1*:GFP non-apical progenitors during neurogenesis. Furthermore, I observed that loss of aPKCλ generated ectopic non-apical divisions (i.e. *vsx1*:GFP-negative) both before and after formation of the apical domain.

Next, I looked at the role of Notch signalling. Lateral inhibition, mediated by Notch signalling, is a well characterised mechanism of regulating neurogenesis (see section 1.3.1; reviewed in Louvi & Artavanis-Tsakonas 2006). DN-Su(H) is known to promote neurogenesis cell autonomously by inhibiting a cell's ability to transduce Notch signalling (Wettstein et al. 1997; Chapouton et al. 2010). Here I show that mosaic overexpression of DN-Su(H) in the zebrafish spinal cord results in an increased proportion of cells differentiating as *vsx1*:GFP interneurons. Therefore, the non-apical progenitor population responded in the same way to impair Notch signalling as neurons populations do, indicating that the Notch pathway regulates the development of both neurons and non-apical progenitors. Analysing the behaviour DN-Su(H) overexpressing cells by live imaging showed that DN-Su(H)-overexpressing *vsx1*:GFP cells undergo the T-shaped morphological transition and divide basally, as is seen in wild type embryos. These data show that blocking the Notch signalling pathway is able to drive non-apical progenitor production, without impairing the morphological changes that we know occur during neuronal differentiation in wild type embryos.

In summary, the results presented in this chapter show that the production of non-apical progenitors in the zebrafish spinal cord a) requires aPKCλ function and b) is regulated by activated Notch signals. Both of these regulatory mechanisms are known to act the same way in neuronal differentiation suggesting that both cell types share aspects of their differentiation programmes. This is supported by earlier observations that differentiating neurons and non-apical progenitors share a number of cell biological features (expression of HuC/D; Chapter 3), basal soma location and T-shaped morphological transition (see section 4.1.3.1, unpublished

data). From these data, we speculate that non-apical progenitors originate from the daughter of an asymmetric apical progenitor division biased towards neuronal differentiation in the zebrafish neural tube.

6.4.2 Effect of reduction of aPKC protein on early and late neurogenesis

Data presented in this chapter show opposing outcomes of depletion of aPKC protein at early and late stages of zebrafish neurogenesis. Analysis of aPKCλ-depleted embryos at 36 hpf, during mid-late stages of neurogenesis, suggests aPKCλ is required for neuronal differentiation, as has been reported for zebrafish neuroepithelial cells (Alexandre et al. 2010; Kressmann et al. 2015). In contrast, I observed an increase in the number of neurons in produced in early neurogenesis when aPKCλ is depleted, implicating aPKCλ in promoting the proliferation of progenitor cells prior to neural tube formation.

Before the formation of a morphologically and molecularly distinct apical domain, the neuroepithelium resembles a rod of non-polarised cells. At this stage aPKC has been reported to be expressed weakly and diffusely throughout the tissue (Geldmacher-Voss et al. 2003). It is possible that at this stage aPKCλ has a different role compared to when it is targeted to the apical cortex. In fact, aPKC has been observed in the nucleus of the non-polar cells in the inner layer of the *Xenopus* neural plate as well as cultured, non-polar mammalian cell lines (Sabherwal et al. 2009). In this context, nuclear aPKC was shown to promote proliferation (Sabherwal et al. 2009), which could explain the results I obtained on neurogenesis in aPKC depleted embryos at neural rod stages. However, this published study was based on the overexpression of constitutively active forms of aPKC and does not examine the effect of loss of endogenous proteins (Sabherwal et al. 2009). Furthermore, to my knowledge, aPKCλ has not been reported in the nucleus of zebrafish neuroepithelial cells. Nevertheless, this idea that aPKCλ is a protein with alternate functions in non-polarised and polarised cell types is interesting in this context and requires further experimental investigation to understand fully.

6.4.3 Ectopic non-apical divisions are likely an artefact of loss of aPKC

The injection of aPKCλ morpholino into Tg(*vsx1*:GFP) embryos results in no change in the total number of non-apical divisions in the zebrafish caudal hindbrain at 36 hpf. However, the population of *vsx1*:GFP-expressing non-apical progenitors is reduced and a population of non-apical divisions that do not express *vsx1*:GFP is generated. The identity of these *vsx1*:GFP-negative non-apical divisions and their progeny (neuron/progenitor) is currently unknown. However, the ectopic non-apical progenitors express HuC/D, which suggests they might be neurogenic divisions. These ectopic non-apical divisions are located dorsal to the *vsx1*:GFP

domain, so are unlikely to contribute to the production of *olig2*-expressing non-apical progenitor cells, which are located ventral to the expression *vsx1* domain.

The origin of the unidentified non-apical divisions is also not clear from this data. The loss of aPKCλ protein might start a programme to specify the production of non-apical progenitors, however is it more likely that the *vsx1*-negative non-apical divisions are generated through ectopic detachment of apical progenitors. Depletion of aPKCλ protein in the neural tube might lead to the ectopic detachment of daughters of apical progenitors in a number of ways, including: a) increasing the number of oblique and perpendicular divisions of apical progenitors (Roberts & Appel 2009); b) overcrowding of the ventricular zone, as aPKC depletion increases the apical progenitor pool (Roberts & Appel 2009; Alexandre et al. 2010); or c) weakening of the adherens junction contacts between neuroepithelial cells. In summary, the ectopic non-apical progenitors are likely to be an artefact of loss of aPKC.

6.4.4 Mosaic injection of DN-Su(H) could be used to further investigate the origins and behaviour of non-apical progenitor

There are still number of outstanding questions regarding the function and behaviour of these non-apical progenitors in the zebrafish neural tube. Many of these will be best answered using time-lapse imaging of the behaviour of these progenitors and their daughters on the single cell and subcellular level. The approach taken in the Clarke and Alexandre labs to observe cell behaviour is to mosaically label single cells in an embryo, as I have used here. This technique randomly labels a small number of cells within the embryo to allow the visualization of the morphology and behaviour of a single cell in an otherwise unlabelled embryo. The random element of this approach can make it challenging to observe a specific event or subtype of cells, particularly when the subtype you are interest in are rare (for example, non-apical progenitors). Therefore, it would be advantageous to be able to increase the chance of labelling the correct cell type. The data presented here shows that overexpressing DN-Su(H) increases the likelihood of a labelled cell undergoing a non-apical division during the imaging period. However, this approach would still be limited by the random element of the labelling technique, as the correct stem or progenitor population has to be labelled in order for that cell to be driven to differentiate. We might be able to overcome this using the transcriptional code that patterns the dorsoventral axis of the neural tube. The V2 progenitor domain is induced in the region in of the zebrafish neural tube in which the expression of transcription factors Irx3 and Nkx6.1 overlap (**Figure 3-1**; England et al. 2011). Therefore, it might be possible to label and/or manipulate the *vsx1* non-apical progenitor population specifically by driving the expression of factors (for example, DN-Su(H)) using the combination of Irx3 and Nkx6.1 promoters.

6.4.5 Conclusion

Data presented in this chapter demonstrates that the production of *vsx1*-expressing non-apical progenitors requires aPKCλ and is inhibited by Notch signalling. Taken together, these data indicate that neurons and non-apical progenitors are generated through similar developmental programmes in the zebrafish neural tube. This suggests that non-apical progenitors in the zebrafish spinal cord are derived from the daughter of an asymmetric apical progenitor division that is biased towards neuronal differentiation.

CHAPTER 7
GENERAL DISCUSSION

7 General discussion

This thesis examined the contribution of non-apical neuronal progenitors to zebrafish neurogenesis. Specifically, I characterised the distribution of non-apical neural progenitors during zebrafish embryonic development. This work identified a small population of non-apical neuronal progenitors in the neural tube up to 72 hpf (3 dpf) and found that the spatial and molecular characteristics of non-apical neuronal progenitors vary between brain regions. A large proportion of the non-apical progenitors in the hindbrain and spinal cord cells express *vsx1*. A smaller population in the spinal cord express *olig2*, while in the hindbrain and telencephalon there are a number of non-apical progenitors with unknown identity. In summary, non-apical progenitors represent a small population of progenitors in the zebrafish neural tube that changes through development. Further analysis of the mechanisms that regulate their production indicates that non-apical progenitors share several features of their differentiation programme with neurons.

I also quantified the spatiotemporal patterning of *vsx1* non-apical neuronal progenitors in the spinal cord and investigated the mechanisms that generate the pattern. These experiments showed that *vsx1*:GFP progenitors differentiate with a long distance spacing pattern in time and space. We hypothesise that this pattern is created by a long-range lateral inhibition signal from the transient basal arms of differentiating *vsx1* progenitors. We have observed the expression of deltaD protein on the basal arms, suggesting that the long distance inhibitory signal is mediated by Delta Notch signalling. The outcomes of a simple model of this hypothesis provide support to this idea and allowed us to refine the details of the mechanics this long-range pattern formation. Many of the remaining questions regarding the spatiotemporal differentiation pattern will be best answered using a computational model of this patterning process.

Here, I discuss the implications that these results have on our understanding of the role of non-apical progenitors on neurogenesis as well as the evolution of this cell type.

7.1 Why might long distance spacing of neurogenesis be important?

The T-shaped morphological transition (P. Alexandre, unpublished) and long distance spacing pattern of neuronal markers (this thesis and Thisse & Thisse 2004; Thisse et al. 2001; Hutchinson & Eisen 2006; Gribble et al. 2007; Kimura et al. 2008) is a common feature of neuron differentiation in the zebrafish spinal cord. We propose that differentiating cells extend long, transient protrusions over distances corresponding to multiple cell body lengths to inhibit other cells from progressing through the process of differentiation at the same time and in the

same place. This patterning event does not affect the fate choice of cells within the neuroepithelium and instead acts to delay the morphological differentiation of nascent neurons and, we assume, their ability to integrate into the assembling spinal cord circuitry.

The biological function of regulating neuronal differentiation in a spatiotemporal way is unknown. However, I speculate that the spatiotemporal 'spreading out' of differentiating cells means that fewer newborn neurons need to be wired into a circuit at any one time. This would allow circuits to first be constructed from a minimal number of neurons, with more neurons added through time to build complexity. This would make it easier and more efficient to form correct connections between partner neurons. Consider the opposite idea; it would be extremely challenging to form the correct connections between the hundreds of cells that make up an adult circuit if they are all generated at approximately the same time. There is functional and developmental *in vivo* evidence that suggests locomotor circuits are generated in this way through early development. Circuits required for fast, powerful swimming behaviour develop first, and neurons and circuits required for finer, more controlled swimming movements develop in a layered function on top of the initial system (McLean & Fetcho 2009).

Therefore, limiting the differentiation and circuit integration of neurons along the anteroposterior axis of the neural tube might increase the ease and sped with which the functional circuitry in the zebrafish spinal cord can be established. A similar differentiation pattern of initial long distance spacing of neurons followed by infilling has also been observed in *Xenopus* embryos (Roberts et al. 1987). This is likely to be particularly important in the zebrafish and amphibian embryos as they develop externally and therefore need to develop the ability to escape predators and hunt quickly.

7.1.1 Are the transient basal arms providing Delta Notch-mediated lateral inhibition?

The similarities between our model of T-shaped cells patterning *vsx1* cells in zebrafish and SOP patterning in *Drosophila* suggest that the inhibitory signal provided by the basal arms is Delta. Supporting this, I observed that inactivating Notch signalling cell autonomously by the overexpression of DN-Su(H) mosaically in the zebrafish spinal cord resulted in a cluster of three cells differentiating as *vsx1*:GFP progenitors (see section 6.3.2.2). Such a cluster is very rare in the normal spacing of *vsx1*:GFP cells (see Chapter 3). This suggests Notch signalling is required to generate the spatiotemporal pattern of newborn neurons. Further evidence can be found in the literature, as published data shows the loss of the initial spacing patterning and prematurely space filling when Notch signalling is abrogated (Batista et al. 2008; Okigawa et al. 2014). Furthermore, I have observed deltaD expression on the basal arms of T-shaped cells in

the Tg(*deltaD-GFP*) transgenic line, suggesting that these structures could be delivering delta over long distances. In fact, in this line only T-shaped cells express high levels of delta proteins (**Figure 4-10** and P. Alexandre, unpublished; see **Figure 4-2**). These observations require confirmation as this transgenic line contains a large number of BAC insertions so we might be observing events that are due to overexpression of Delta.

While the data presented here is consistent with our hypothesis, it does not confirm it. To test this idea directly we could interfere with Delta Notch signalling in *vsx1*:GFP embryos by injection of morpholinos for different Delta protein or mRNA encoding a Mindbomb dominant negative and then monitoring the resulting spatiotemporal pattern of *vsx1* progenitor divisions. Due to the multifunctional roles of Delta Notch signalling in neurogenesis, any experiments aiming to manipulate this pathway in order to test its potential role in generating the spacing pattern has to be able to disentangle the any effect on spacing with altered neurogenesis. I attempted to inhibit the activation of Notch signalling using the ϒ-secretase inhibitor DAPT, a drug that prevents the cleavage of NICD (data not shown). However, we found that the drug's solvent DMSO alone had an impact on neurogenesis and we so we were unable to observe a specific effect of DAPT on the pattern of differentiation. In future experiments involving the manipulation of Delta Notch signalling we will need to ensure that basal arm growth is not affected, as in *Drosophila* Delta is required to drive filopodial growth (De Joussineau et al. 2003).

Alternatively, we could use a computational model to address the potential role of Delta Notch signalling in this patterning process. Due to the important roles Delta Notch signalling plays in development of a number of species, this signalling pathway has been thoroughly characterised and described in both general and in-depth mathematic equations (for example: Collier et al. 1996; Sprinzak et al. 2010; Sprinzak et al. 2011) and some of these have been applied to long-range lateral inhibition (Cohen et al. 2010). It is possible to incorporate our quantitative data on the dynamics of basal arm behaviours into these equations to model the effect of basal arms on the spatiotemporal pattern of neuronal differentiation. Generating a computational model of this patterning event will allow us to critically test our hypothesis and statistically compare the outcomes of the simulations to our observations of *vsx1* spatiotemporal differentiation.

In summary, further experiments are required to identify and demonstrate the molecular mechanisms that form the signals that generate the spacing pattern see in spinal cord neurogenesis.

7.2 *Vsx1* non-apical progenitors might aid functional circuit assembly

The data presented here suggests that *vsx1* is expressed by most of the non-apical progenitors in the zebrafish embryonic spinal cord through the first three days of development. Therefore, in this tissue, the majority of non-apical progenitors are produced by a single progenitor domain, which suggests that the production of non-apical progenitors is not a commonly used feature of neurogenesis in the developing zebrafish spinal cord. Furthermore, as the zebrafish spinal cord undergoes restricted growth, this observation also indicates that it is unlikely that non-apical progenitors exist solely to greatly expand neuron numbers, as is thought to occur in the mammalian cortex. Instead, one putative function of the *vsx1*-expressing non-apical progenitors in the zebrafish spinal cord may be to generate equal numbers of specific types of excitatory and inhibitory interneurons to ensure the correct excitation/inhibition (E/I) balance from early stages of neuronal circuit formation. This might be particularly important for V2a and V2b interneurons as they form a part of the circuits required for locomotion (Kimura et al. 2006; Lundfald et al. 2007). As V2a and V2b interneurons in the avian and mammalian spinal cord are also generated in approximately equal numbers, it is possible that V2 neurons are generated by a (non-apical) intermediate progenitor in these species too (Karunaratne et al. 2002; Al-Mosawie et al. 2007; Kimura et al. 2008; Panayi et al. 2010).

It is not immediately obvious why this neuron pair-producing progenitor needs to divide in a non-apical location, as similar n – n divisions are observed at the ventricular surface in the zebrafish hindbrain (Lyons et al. 2003; Kressmann et al. 2015). One of the advantages of non-apical divisions is that the daughter cells are unaffected by the putative spacing effects of T-shaped cells. To elaborate, if an apical division generated the V2a and V2b interneurons, instead of the non-apical divisions described here, then it is likely that one daughter will begin the T-shaped transition before the other and the second cell would be delayed by the long distance spacing mechanism described in this thesis (**Figure 7-1**A). That would mean that one daughter neuron would integrate into the circuitry hours before the other (**Figure 7-1**A). This would nullify the effect of simultaneously generating daughters with an intrinsic E/I balance. On the other hand, if V2a/V2b interneuron pairs are generated after the progenitor has been spaced by basal arms then the relative numbers of excitatory and inhibitory neurons that integrate into the circuit at a given time are maintained (**Figure 7-1**B). In summary, I speculate that non-apical divisions provide a mechanism for pairs of newborn neurons to bypass the delaying or spacing effect regulated by the basal arms, allowing both daughters to become competent to integrate into the developing circuitry at approximately the same time.

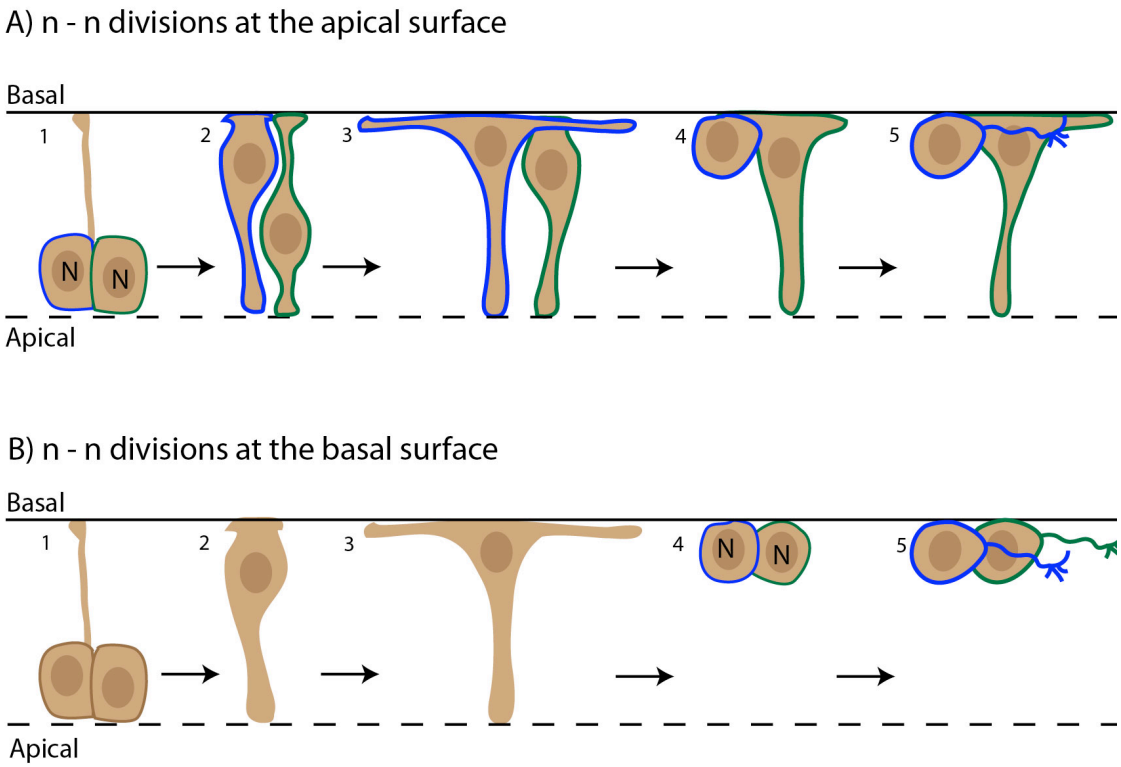

Figure 7-1: Non-apical progenitors allow daughter cells to bypass delaying effect of basal arms. **A**) If an n - n division occurs at the apical surface (1, one daughter outlined in blue and the other in green), both daughters will begin to differentiate by translocating to the basal surface (2). It is likely that one cell will begin the T-shaped transition before the other (3), generating a time delay between when each daughter elongates its axon. **B**) If an n – n division at the basal surface (4), it has already undergone the T-shaped morphological transition (3). Therefore, both of the nascent neuronal daughters will elongate axons at approximately the same time.

7.3 Insights into the evolution of non-apical progenitors

Data presented in this thesis strongly suggest that non-apical progenitors in the zebrafish spinal cord follow a similar differentiation programme, regulated by similar regulatory pathways, as differentiating neurons. From these data, we speculate that non-apical progenitors in zebrafish are derived from the daughter cell that is biased to differentiate after an asymmetric apical progenitor division. In this case, evolutionary origin of basal or non-apical progenitors involves the modification of the suite of transcriptional changes that occur during neuronal differentiation to allow further division after basal migration and detachment from the apical surface. It is possible that this idea can be extended to bIPs in the mammalian neocortex as Tbr2-expressing bIPs show characteristics similar to those seen in *vsx1*-expressing non-apical neuronal progenitors in the zebrafish neural tube, including: (1) limited proliferative potential and (2) the expression of 'neuronal' markers prior to mitosis (reviewed in Florio & Huttner

2014). This suggests that mammalian bIPs could also be derived from the daughter of an apical progenitor division more committed to neuronal differentiation. Nomura and colleagues reached a similar conclusion after they found that non-proliferative cells that are committed to neuronal differentiation express Tbr2 in the chicken pallium. (Nomura et al. 2016). They proposed that the proliferative capacity of the Tbr2 population was modified to generate bIPs in placental mammals (Nomura et al. 2016). As small populations of non-apical progenitors are present in different amniote species (Martínez-Cerdeño et al. 2006; Nomura et al. 2016), Nomura et al also posited that ancestral amniote species had "a vestigial population of non-surface mitotic cells" (Nomura et al. 2016). This thesis shows that "non-surface mitotic cells" are not limited to amniotes and therefore it is possible that non-apical progenitors arose much further back in evolutionary history, perhaps in early ancestral vertebrates.

Work from this thesis might also provides potential insight into the evolutionary history of the SVZ. In the zebrafish telencephalon and hindbrain, we found that subapical divisions are located just outside of the ventricular zone. Non-apically dividing cells are seen in a similar location in pallium of the turtle (Martínez-Cerdeño et al. 2006) and chicken (Nomura et al. 2016) and this is qualitatively similar to the location of bIPs in mammals (Miyata et al. 2004; Haubensak et al. 2004; Noctor et al. 2004). Therefore, the small population of subapical progenitors in the zebrafish pallium might represent an early evolutionary form of the SVZ. As the mammalian brain evolved, the growing numbers of basal progenitors produced during neurogenesis could have driven the formation of the SVZ as a morphologically distinct layer of the developing neocortex.

In summary, comparing the data presented here regarding non-apical progenitors in the zebrafish neural tube and what is known about basal progenitors in amniote species allows us to theorise about the evolutionary history of basal/non-apical neuronal progenitors. As the characteristics of these progenitors are similar across different species, studying the molecular regulation of non-apical progenitors in the zebrafish neural tube might provide us with insights into the developmental programmes that give rise to basal progenitors in other species.

7.4 Summary and conclusion

This main aim of this thesis was to increase our knowledge of non-apical progenitors in non-cortical tissues by studying non-apical mitoses in the zebrafish embryonic central nervous system.

This work shows that a complex population of non-apical progenitors exists in the developing zebrafish neural tube, similar to what is known in the mammalian neocortex. In the embryonic

hindbrain specifically, I identified three spatial populations of non-apical progenitors. I also found that the number of non-apical progenitors increases as the region undergoes a drastic expansion, suggesting that non-apical progenitors might aid in the growth of this region as is hypothesised for basal progenitors in mammals. Further work focusing characterising the morphologies of different sub groups of zebrafish non-apical neuronal progenitors will allow us to draw further comparisons between non-apical progenitors in this system and mammalian species.

This work represents the first thorough characterisation of non-apical neural progenitors in a vertebrate spinal cord. In the zebrafish, the major population of non-apical progenitors in the spinal cord express *vsx1* and give rise to V2a/V2b interneuron daughter pairs. I speculate that in this tissue non-apical progenitors might facilitate quick and efficient circuit formation by intrinsically controlling the excitation/inhibition balance of developing locomotor circuits. The characteristics of V2 interneurons are conserved between zebrafish, avian and mammalian species, suggesting this function might also be conserved. However, it is currently unknown whether a similar (non-apical) intermediate progenitor gives rise to V2 cells in other species.

Zebrafish non-apical neuronal progenitors share a number of cellular, molecular and developmental characteristics with neurons. For example, both cell types express the marker HuC/D and both cell types go through a T-shaped transition before morphological differentiation. Following from these observations, I show that similar mechanisms regulate the production of neurons and non-apical progenitors, specifically they both require aPKC to differentiate and are both affected by Notch signalling. These similarities lead us to postulate that non-apical progenitors evolved through alterations to the neuronal differentiation pathway, which allowed cells committed to differentiation to undergo a terminal division. As bIP populations in the mammalian neocortex also express markers that are traditionally thought of as 'neuronal', it is possible that these findings from the zebrafish could provide us with insights into the evolutionary origin and molecular regulation of basal progenitors in mammals.

Finally, I quantified the long distance spatiotemporal pattern of *vsx1* progenitor differentiation. We hypothesise that the basal arms of differentiating neurons and non-apical progenitors underlie the formation of this pattern. Specifically, we think that basal arms provide a signal that can act over multiple cell diameters to delay cells that are committed to neuronal differentiation from progressing through the differentiation pathway. Our current data seems to suggest that the inhibitory signal in this patterning process is mediated by Delta Notch signalling. Future work on this hypothesis will focus on testing the role of the Delta Notch pathway, through experiments and computational modelling.

BIBLIOGRAPHY

8 Bibliography

Al-Mosawie, A, J M Wilson, and R M Brownstone. 2007. 'Heterogeneity of V2-Derived Interneurons in the Adult Mouse Spinal Cord.' *The European Journal of Neuroscience* 26 (11): 3003–15. doi:10.1111/j.1460-9568.2007.05907.x.

Alexandre, Paula, Alexander M Reugels, David Barker, Eric Blanc, and Jonathan D W Clarke. 2010. 'Neurons Derive from the More Apical Daughter in Asymmetric Divisions in the Zebrafish Neural Tube.' *Nature Neuroscience* 13 (6). Nature Publishing Group: 673–79. doi:10.1038/nn.2547.

Amoyel, Marc, Yi-Chuan Cheng, Yun-Jin Jiang, and David G Wilkinson. 2005. 'Wnt1 Regulates Neurogenesis and Mediates Lateral Inhibition of Boundary Cell Specification in the Zebrafish Hindbrain.' *Development (Cambridge, England)* 132 (4): 775–85. doi:10.1242/dev.01616.

Anderson, Ryan M, Alison R Lawrence, Rolf W Stottmann, Daniel Bachiller, and John Klingensmith. 2002. 'Chordin and Noggin Promote Organizing Centers of Forebrain Development in the Mouse.' *Development (Cambridge, England)* 129 (21): 4975–87.

Appel, Bruce, Lee Anne Givan, and Judith S Eisen. 2001. 'Delta-Notch Signaling and Lateral Inhibition in Zebrafish Spinal Cord Development'. *BMC Developmental Biology* 1 (1): 13. doi:10.1186/1471-213X-1-13.

Arnold, Sebastian J, Guo-Jen Huang, Amanda F P Cheung, Takumi Era, Shin-Ichi Nishikawa, Elizabeth K Bikoff, Zoltán Molnár, Elizabeth J Robertson, and Matthias Groszer. 2008. 'The T-Box Transcription Factor Eomes/Tbr2 Regulates Neurogenesis in the Cortical Subventricular Zone.' *Genes & Development* 22 (18): 2479–84. doi:10.1101/gad.475408.

Artavanis-Tsakonas, S. 1999. 'Notch Signaling: Cell Fate Control and Signal Integration in Development'. *Science* 284 (5415): 770–76. doi:10.1126/science.284.5415.770.

Attardo, Alessio, Federico Calegari, Wulf Haubensak, Michaela Wilsch-Bräuninger, and Wieland B Huttner. 2008. 'Live Imaging at the Onset of Cortical Neurogenesis Reveals Differential Appearance of the Neuronal Phenotype in Apical versus Basal Progenitor Progeny'. Edited by Thomas A Reh. *PLoS ONE* 3 (6). Public Library of Science: 16.

Azevedo, Frederico A C, Ludmila R B Carvalho, Lea T Grinberg, José Marcelo Farfel, Renata E L Ferretti, Renata E P Leite, Wilson Jacob Filho, Roberto Lent, and Suzana Herculano-Houzel. 2009. 'Equal Numbers of Neuronal and Nonneuronal Cells Make the Human Brain an Isometrically Scaled-up Primate Brain.' *The Journal of Comparative Neurology* 513 (5): 532–41. doi:10.1002/cne.21974.

Bagnall, Martha W, and David L McLean. 2014. 'Modular Organization of Axial Microcircuits in Zebrafish.' *Science (New York, N.Y.)* 343 (6167): 197–200. doi:10.1126/science.1245629.

Balaskas, Nikolaos, Ana Ribeiro, Jasmina Panovska, Eric Dessaud, Noriaki Sasai, Karen M

Page, James Briscoe, and Vanessa Ribes. 2012. ‘Gene Regulatory Logic for Reading the Sonic Hedgehog Signaling Gradient in the Vertebrate Neural Tube.’ *Cell* 148 (1-2): 273–84. doi:10.1016/j.cell.2011.10.047.

Batista, Manuel F, Jeffrey Jacobstein, and Katharine E Lewis. 2008. ‘Zebrafish V2 Cells Develop into Excitatory CiD and Notch Signalling Dependent Inhibitory VeLD Interneurons.’ *Developmental Biology* 322 (2): 263–75. doi:10.1016/j.ydbio.2008.07.015.

Bernardos, Rebecca L, and Pamela A Raymond. 2006. ‘GFAP Transgenic Zebrafish.’ *Gene Expression Patterns : GEP* 6 (8): 1007–13. doi:10.1016/j.modgep.2006.04.006.

Bernhardt, R R, S Goerlinger, M Roos, and M Schachner. 1998. ‘Anterior-Posterior Subdivision of the Somite in Embryonic Zebrafish: Implications for Motor Axon Guidance.’ *Developmental Dynamics : An Official Publication of the American Association of Anatomists* 213 (3): 334–47. doi:10.1002/(SICI)1097-0177(199811)213:3<334::AID-AJA9>3.0.CO;2-4.

Betizeau, Marion, Veronique Cortay, Dorothée Patti, Sabina Pfister, Elodie Gautier, Angèle Bellemin-Ménard, Marielle Afanassieff, et al. 2013. ‘Precursor Diversity and Complexity of Lineage Relationships in the Outer Subventricular Zone of the Primate.’ *Neuron* 80 (2). Elsevier: 442–57. doi:10.1016/j.neuron.2013.09.032.

Bischoff, Marcus, Ana-Citlali Gradilla, Irene Seijo, Germán Andrés, Carmen Rodríguez-Navas, Laura González-Méndez, and Isabel Guerrero. 2013. ‘Cytonemes Are Required for the Establishment of a Normal Hedgehog Morphogen Gradient in Drosophila Epithelia.’ *Nature Cell Biology* 15 (11). Nature Publishing Group, a division of Macmillan Publishers Limited. All Rights Reserved.: 1269–81. doi:10.1038/ncb2856.

Boije, Henrik, Per-Henrik D Edqvist, and Finn Hallböök. 2009. ‘Horizontal Cell Progenitors Arrest in G2-Phase and Undergo Terminal Mitosis on the Vitreal Side of the Chick Retina.’ *Developmental Biology* 330 (1): 105–13. doi:10.1016/j.ydbio.2009.03.013.

Borrell, Víctor, and Magdalena Götz. 2014. ‘Role of Radial Glial Cells in Cerebral Cortex Folding.’ *Current Opinion in Neurobiology* 27C (March): 39–46. doi:10.1016/j.conb.2014.02.007.

Bouwmeester, T, S Kim, Y Sasai, B Lu, and E M De Robertis. 1996. ‘Cerberus Is a Head-Inducing Secreted Factor Expressed in the Anterior Endoderm of Spemann’s Organizer.’ *Nature* 382 (6592): 595–601. doi:10.1038/382595a0.

Bray, Sarah J. 2006. ‘Notch Signalling: A Simple Pathway Becomes Complex.’ *Nature Reviews. Molecular Cell Biology* 7 (9). Nature Publishing Group: 678–89. doi:10.1038/nrm2009.

Briscoe, James, and Pascal P Thérond. 2013. ‘The Mechanisms of Hedgehog Signalling and Its Roles in Development and Disease.’ *Nature Reviews. Molecular Cell Biology* 14 (7). Nature Publishing Group, a division of Macmillan Publishers Limited. All Rights Reserved.: 416–29. doi:10.1038/nrm3598.

Buckley, Clare, and Jon Clarke. 2014. 'Establishing the Plane of Symmetry for Lumen Formation and Bilateral Brain Formation in the Zebrafish Neural Rod.' *Seminars in Cell & Developmental Biology*, April. Elsevier Ltd, 6–11. doi:10.1016/j.semcdb.2014.04.008.

Buckley, Clare E, Xiaoyun Ren, Laura C Ward, Gemma C Girdler, Claudio Araya, Mary J Green, Brian S Clark, Brian A Link, and Jonathan D W Clarke. 2013. 'Mirror-Symmetric Microtubule Assembly and Cell Interactions Drive Lumen Formation in the Zebrafish Neural Rod.' *The EMBO Journal* 32 (1): 30–44. doi:10.1038/emboj.2012.305.

Campbell, Kenneth, and Magdalena Götz. 2002. 'Radial Glia: Multi-Purpose Cells for Vertebrate Brain Development.' *Trends in Neurosciences* 25 (5): 235–38.

Campos-Ortega, J A, and Y N Jan. 1991. 'Genetic and Molecular Bases of Neurogenesis in Drosophila Melanogaster.' *Annual Review of Neuroscience* 14 (January). Annual Reviews 4139 El Camino Way, P.O. Box 10139, Palo Alto, CA 94303-0139, USA: 399–420. doi:10.1146/annurev.ne.14.030191.002151.

Cappello, Silvia, Alessio Attardo, Xunwei Wu, Takuji Iwasato, Shigeyoshi Itohara, Michaela Wilsch-Bräuninger, Hanna M Eilken, et al. 2006. 'The Rho-GTPase cdc42 Regulates Neural Progenitor Fate at the Apical Surface'. *Nature Neuroscience* 9 (9). Nature Publishing Group: 1099–1107. doi:10.1038/nn1744.

Carreira-Barbosa, Filipa, Miguel L Concha, Masaki Takeuchi, Naoto Ueno, Stephen W Wilson, and Masazumi Tada. 2003. 'Prickle 1 Regulates Cell Movements during Gastrulation and Neuronal Migration in Zebrafish.' *Development (Cambridge, England)* 130 (17): 4037–46.

Chapouton, Prisca, Paulina Skupien, Birgit Hesl, Marion Coolen, John C Moore, Romain Madelaine, Elizabeth Kremmer, et al. 2010. 'Notch Activity Levels Control the Balance between Quiescence and Recruitment of Adult Neural Stem Cells.' *The Journal of Neuroscience : The Official Journal of the Society for Neuroscience* 30 (23): 7961–74. doi:10.1523/JNEUROSCI.6170-09.2010.

Chen, Jerry S, Abygail M Gumbayan, Robert W Zeller, and Joseph M Mahaffy. 2014. 'An Expanded Notch-Delta Model Exhibiting Long-Range Patterning and Incorporating MicroRNA Regulation.' *PLoS Computational Biology* 10 (6). Public Library of Science: e1003655. doi:10.1371/journal.pcbi.1003655.

Cheng, Yi-Chuan, Marc Amoyel, Xuehui Qiu, Yun-Jin Jiang, Qiling Xu, and David G Wilkinson. 2004. 'Notch Activation Regulates the Segregation and Differentiation of Rhombomere Boundary Cells in the Zebrafish Hindbrain'. *Developmental Cell* 6 (4): 539–50. doi:10.1016/S1534-5807(04)00097-8.

Chenn, A, and S K McConnell. 1995. 'Cleavage Orientation and the Asymmetric Inheritance of Notch1 Immunoreactivity in Mammalian Neurogenesis.' *Cell* 82 (4): 631–41.

Chenn, Anjen, and Christopher A Walsh. 2002. 'Regulation of Cerebral Cortical Size by Control of Cell Cycle Exit in Neural Precursors.' *Science (New York, N.Y.)* 297 (5580): 365–69.

doi:10.1126/science.1074192.

Chitnis, A, D Henrique, J Lewis, D Ish-Horowicz, and C Kintner. 1995. 'Primary Neurogenesis in Xenopus Embryos Regulated by a Homologue of the Drosophila Neurogenic Gene Delta.' *Nature* 375 (6534): 761–66. doi:10.1038/375761a0.

Ciani, Lorenza, and Patricia C. Salinas. 2005. 'Signalling in Neural Development: WNTS in the Vertebrate Nervous System: From Patterning to Neuronal Connectivity'. *Nature Reviews Neuroscience* 6 (5): 351–62. doi:10.1038/nrn1665.

Clarke, Jon. 2009. 'Role of Polarized Cell Divisions in Zebrafish Neural Tube Formation'. *Current Opinion in Neurobiology* 19 (2): 134–38. doi:10.1016/j.conb.2009.04.010.

Coffman, C R, P Skoglund, W A Harris, and C R Kintner. 1993. 'Expression of an Extracellular Deletion of Xotch Diverts Cell Fate in Xenopus Embryos.' *Cell* 73 (4): 659–71.

Cohen, Michael, James Briscoe, and Robert Blassberg. 2013. 'Morphogen Interpretation: The Transcriptional Logic of Neural Tube Patterning.' *Current Opinion in Genetics & Development* 23 (4): 423–28. doi:10.1016/j.gde.2013.04.003.

Cohen, Michael, Marios Georgiou, Nicola L Stevenson, Mark Miodownik, and Buzz Baum. 2010. 'Dynamic Filopodia Transmit Intermittent Delta-Notch Signaling to Drive Pattern Refinement during Lateral Inhibition.' *Developmental Cell* 19 (1): 78–89. doi:10.1016/j.devcel.2010.06.006.

Cohen, Michael, Karen M Page, Ruben Perez-Carrasco, Chris P Barnes, and James Briscoe. 2014. 'A Theoretical Framework for the Regulation of Shh Morphogen-Controlled Gene Expression.' *Development (Cambridge, England)* 141 (20): 3868–78. doi:10.1242/dev.112573.

Collier, J R, N A Monk, P K Maini, and J H Lewis. 1996. 'Pattern Formation by Lateral Inhibition with Feedback: A Mathematical Model of Delta-Notch Intercellular Signalling.' *Journal of Theoretical Biology* 183 (4): 429–46. doi:10.1006/jtbi.1996.0233.

Copp, Andrew J, and Nicholas DE Greene. 2009. 'Genetics and Development of Neural Tube Defects'. *The Journal of Pathology* 220 (2): n/a – n/a. doi:10.1002/path.2643.

Corriden, Ross, Tim Self, Kathryn Akong-Moore, Victor Nizet, Barrie Kellam, Stephen J Briddon, and Stephen J Hill. 2013. 'Adenosine-A3 Receptors in Neutrophil Microdomains Promote the Formation of Bacteria-Tethering Cytonemes.' *EMBO Reports* 14 (8): 726–32. doi:10.1038/embor.2013.89.

Cui, Shuang, Cécile Otten, Stefan Rohr, Salim Abdelilah-Seyfried, and Brian A Link. 2007. 'Analysis of aPKClambda and aPKCzeta Reveals Multiple and Redundant Functions during Vertebrate Retinogenesis.' *Molecular and Cellular Neurosciences* 34 (3): 431–44. doi:10.1016/j.mcn.2006.11.016.

D'Souza, B, A Miyamoto, and G Weinmaster. 2008. 'The Many Facets of Notch Ligands.' *Oncogene* 27 (38). Macmillan Publishers Limited: 5148–67. doi:10.1038/onc.2008.229.

Dale, N, A Roberts, O P Ottersen, and J Storm-Mathisen. 1987. 'The Development of a

Population of Spinal Cord Neurons and Their Axonal Projections Revealed by GABA Immunocytochemistry in Frog Embryos.' *Proceedings of the Royal Society of London. Series B, Biological Sciences* 232 (1267): 205–15.

Das, Raman M, Arwen C Wilcock, Jason R Swedlow, and Kate G Storey. 2012. 'High-Resolution Live Imaging of Cell Behavior in the Developing Neuroepithelium.' *Journal of Visualized Experiments : JoVE*, no. 62 (January).

De Joussineau, Cyrille, Jonathan Soulé, Marianne Martin, Christelle Anguille, Philippe Montcourrier, and Daniel Alexandre. 2003. 'Delta-Promoted Filopodia Mediate Long-Range Lateral Inhibition in Drosophila.' *Nature* 426 (6966): 555–59. doi:10.1038/nature02157.

Dehay, Colette, and Henry Kennedy. 2007. 'Cell-Cycle Control and Cortical Development.' *Nature Reviews. Neuroscience* 8 (6): 438–50.

Del Barrio, Marta G, Raquel Taveira-Marques, Yuko Muroyama, Dong-In Yuk, Shengguo Li, Mary Wines-Samuelson, Jie Shen, et al. 2007. 'A Regulatory Network Involving Foxn4, Mash1 and Delta-like 4/Notch1 Generates V2a and V2b Spinal Interneurons from a Common Progenitor Pool.' *Development (Cambridge, England)* 134 (19): 3427–36. doi:10.1242/dev.005868.

Del Bene, Filippo. 2011. 'Interkinetic Nuclear Migration: Cell Cycle on the Move.' *The EMBO Journal* 30 (9). European Molecular Biology Organization: 1676–77. doi:10.1038/emboj.2011.114.

Desai, A R, and S K McConnell. 2000. 'Progressive Restriction in Fate Potential by Neural Progenitors during Cerebral Cortical Development.' *Development (Cambridge, England)* 127 (13): 2863–72.

Diez del Corral, Ruth, and Kate G Storey. 2004. 'Opposing FGF and Retinoid Pathways: A Signalling Switch That Controls Differentiation and Patterning Onset in the Extending Vertebrate Body Axis.' *BioEssays : News and Reviews in Molecular, Cellular and Developmental Biology* 26 (8): 857–69. doi:10.1002/bies.20080.

Doe, Chris Q. 2008. 'Neural Stem Cells: Balancing Self-Renewal with Differentiation.' *Development (Cambridge, England)* 135 (9): 1575–87. doi:10.1242/dev.014977.

Dong, Zhiqiang, Nan Yang, Sang-Yeob Yeo, Ajay Chitnis, and Su Guo. 2012. 'Intralineage Directional Notch Signaling Regulates Self-Renewal and Differentiation of Asymmetrically Dividing Radial Glia.' *Neuron* 74 (1): 65–78. doi:10.1016/j.neuron.2012.01.031.

Dornseifer, Peter, Christina Takke, and José A Campos-Ortega. 1997. 'Overexpression of a Zebrafish Homologue of the Drosophila Neurogenic Gene Delta Perturbs Differentiation of Primary Neurons and Somite Development'. *Mechanisms of Development* 63 (2): 159–71. doi:10.1016/S0925-4773(97)00037-3.

Dorsky, R I, D H Rapaport, and W A Harris. 1995. 'Xotch Inhibits Cell Differentiation in the Xenopus Retina.' *Neuron* 14 (3): 487–96.

Dorsky, R. I. 2003. 'Two tcf3 Genes Cooperate to Pattern the Zebrafish Brain'. *Development* 130 (9): 1937–47. doi:10.1242/dev.00402.

Eiraku, Mototsugu, Kiichi Watanabe, Mami Matsuo-Takasaki, Masako Kawada, Shigenobu Yonemura, Michiru Matsumura, Takafumi Wataya, Ayaka Nishiyama, Keiko Muguruma, and Yoshiki Sasai. 2008. 'Self-Organized Formation of Polarized Cortical Tissues from ESCs and Its Active Manipulation by Extrinsic Signals.' *Cell Stem Cell* 3 (5): 519–32. doi:10.1016/j.stem.2008.09.002.

Eisen, J S, P Z Myers, and M Westerfield. 1986. 'Pathway Selection by Growth Cones of Identified Motoneurones in Live Zebra Fish Embryos.' *Nature* 320 (6059): 269–71. doi:10.1038/320269a0.

Eisen, Judith S., and Susan H. Pike. 1991. 'The Spt-1 Mutation Alters Segmental Arrangement and Axonal Development of Identified Neurons in the Spinal Cord of the Embryonic Zebrafish'. *Neuron* 6 (5): 767–76. doi:10.1016/0896-6273(91)90173-W.

England, S., M. F. Batista, J. K. Mich, J. K. Chen, and K. E. Lewis. 2011. 'Roles of Hedgehog Pathway Components and Retinoic Acid Signalling in Specifying Zebrafish Ventral Spinal Cord Neurons'. *Development* 138 (23): 5121–34. doi:10.1242/dev.066159.

Englund, Chris, Andy Fink, Charmaine Lau, Diane Pham, Ray A M Daza, Alessandro Bulfone, Tom Kowalczyk, and Robert F Hevner. 2005. 'Pax6, Tbr2, and Tbr1 Are Expressed Sequentially by Radial Glia, Intermediate Progenitor Cells, and Postmitotic Neurons in Developing Neocortex.' *The Journal of Neuroscience : The Official Journal of the Society for Neuroscience* 25 (1): 247–51. doi:10.1523/JNEUROSCI.2899-04.2005.

Esain, Virginie, John H Postlethwait, Patrick Charnay, and Julien Ghislain. 2010. 'FGF-Receptor Signalling Controls Neural Cell Diversity in the Zebrafish Hindbrain by Regulating olig2 and sox9.' *Development (Cambridge, England)* 137 (1): 33–42. doi:10.1242/dev.038026.

Fietz, Simone A, and Wieland B Huttner. 2011. 'Cortical Progenitor Expansion, Self-Renewal and Neurogenesis-a Polarized Perspective.' *Current Opinion in Neurobiology* 21 (1): 23–35. doi:10.1016/j.conb.2010.10.002.

Fietz, Simone A, Iva Kelava, Johannes Vogt, Michaela Wilsch-Bräuninger, Denise Stenzel, Jennifer L Fish, Denis Corbeil, et al. 2010. 'OSVZ Progenitors of Human and Ferret Neocortex Are Epithelial-like and Expand by Integrin Signaling.' *Nature Neuroscience* 13 (6): 690–99.

Fietz, Simone A, Robert Lachmann, Holger Brandl, Martin Kircher, Nikolay Samusik, Roland Schröder, Naharajan Lakshmanaperumal, et al. 2012. 'Transcriptomes of Germinal Zones of Human and Mouse Fetal Neocortex Suggest a Role of Extracellular Matrix in Progenitor Self-Renewal.' *Proceedings of the National Academy of Sciences of the United States of America* 109 (29): 11836–41. doi:10.1073/pnas.1209647109.

Fifadara, Nimita H, Freddy Beer, Shoichiro Ono, and Santa J Ono. 2010. 'Interaction between Activated Chemokine Receptor 1 and FcepsilonRI at Membrane Rafts Promotes

Communication and F-Actin-Rich Cytoneme Extensions between Mast Cells.' *International Immunology* 22 (2): 113–28. doi:10.1093/intimm/dxp118.

Fleming, Angeleen, Marcia G Kishida, Charles B Kimmel, and Roger J Keynes. 2015. 'Building the Backbone: The Development and Evolution of Vertebral Patterning.' *Development (Cambridge, England)* 142 (10). The Company of Biologists Limited: 1733–44. doi:10.1242/dev.118950.

Florio, M., M. Albert, E. Taverna, T. Namba, H. Brandl, E. Lewitus, C. Haffner, et al. 2015. 'Human-Specific Gene ARHGAP11B Promotes Basal Progenitor Amplification and Neocortex Expansion'. *Science* 347 (6229): 1465–70. doi:10.1126/science.aaa1975.

Florio, Marta, and Wieland B Huttner. 2014. 'Neural Progenitors, Neurogenesis and the Evolution of the Neocortex.' *Development (Cambridge, England)* 141 (11): 2182–94. doi:10.1242/dev.090571.

Folgueira, Mónica, Philippa Bayley, Pavla Navratilova, Thomas S Becker, Stephen W Wilson, and Jonathan D W Clarke. 2012. 'Morphogenesis Underlying the Development of the Everted Teleost Telencephalon.' *Neural Development* 7 (1): 32. doi:10.1186/1749-8104-7-32.

Furutachi, Shohei, Hiroaki Miya, Tomoyuki Watanabe, Hiroki Kawai, Norihiko Yamasaki, Yujin Harada, Itaru Imayoshi, et al. 2015. 'Slowly Dividing Neural Progenitors Are an Embryonic Origin of Adult Neural Stem Cells'. *Nature Neuroscience* 18 (5): 657–65. doi:10.1038/nn.3989.

Gal, Jonathan S, Yury M Morozov, Albert E Ayoub, Mitali Chatterjee, Pasko Rakic, and Tarik F Haydar. 2006. 'Molecular and Morphological Heterogeneity of Neural Precursors in the Mouse Neocortical Proliferative Zones.' *The Journal of Neuroscience : The Official Journal of the Society for Neuroscience* 26 (3): 1045–56.

Galkina, Svetlana I, Julia M Romanova, Vladimir I Stadnichuk, Julian G Molotkovsky, Galina F Sud'ina, and Thomas Klein. 2009. 'Nitric Oxide-Induced Membrane Tubulovesicular Extensions (Cytonemes) of Human Neutrophils Catch and Hold Salmonella Enterica Serovar Typhimurium at a Distance from the Cell Surface.' *FEMS Immunology and Medical Microbiology* 56 (2). The Oxford University Press: 162–71. doi:10.1111/j.1574-695X.2009.00560.x.

Ganz, Julia, Volker Kroehne, Dorian Freudenreich, Anja Machate, Michaela Geffarth, Ingo Braasch, Jan Kaslin, and Michael Brand. 2014. 'Subdivisions of the Adult Zebrafish Pallium Based on Molecular Marker Analysis.' *F1000Research* 3 (January): 308. doi:10.12688/f1000research.5595.1.

Gaspard, Nicolas, Tristan Bouschet, Raphael Hourez, Jordane Dimidschstein, Gilles Naeije, Jelle van den Ameele, Ira Espuny-Camacho, et al. 2008. 'An Intrinsic Mechanism of Corticogenesis from Embryonic Stem Cells.' *Nature* 455 (7211). Macmillan Publishers Limited. All rights reserved: 351–57. doi:10.1038/nature07287.

Gaspard, Nicolas, and Pierre Vanderhaeghen. 2010. 'Mechanisms of Neural Specification from Embryonic Stem Cells.' *Current Opinion in Neurobiology* 20 (1): 37–43. doi:10.1016/j.conb.2009.12.001.

Geldmacher-Voss, Benedikt, Alexander M Reugels, Stefan Pauls, and José A Campos-Ortega. 2003. 'A 90-Degree Rotation of the Mitotic Spindle Changes the Orientation of Mitoses of Zebrafish Neuroepithelial Cells.' *Development (Cambridge, England)* 130 (16): 3767–80.

Gonzalez-Quevedo, Rosa, Yoonsung Lee, Kenneth D Poss, and David G Wilkinson. 2010. 'Neuronal Regulation of the Spatial Patterning of Neurogenesis.' *Developmental Cell* 18 (1): 136–47. doi:10.1016/j.devcel.2009.11.010.

Götz, Magdalena, and Wieland B Huttner. 2005. 'The Cell Biology of Neurogenesis.' *Nature Reviews. Molecular Cell Biology* 6 (10). Nature Publishing Group: 777–88.

Gribble, Suzanna L, O Brant Nikolaus, and Richard I Dorsky. 2007. 'Regulation and Function of Dbx Genes in the Zebrafish Spinal Cord.' *Developmental Dynamics : An Official Publication of the American Association of Anatomists* 236 (12): 3472–83. doi:10.1002/dvdy.21367.

Gupta, Neetu, and Anthony L DeFranco. 2003. 'Visualizing Lipid Raft Dynamics and Early Signaling Events during Antigen Receptor-Mediated B-Lymphocyte Activation.' *Molecular Biology of the Cell* 14 (2): 432–44. doi:10.1091/mbc.02-05-0078.

Guthrie, S, M Butcher, and A Lumsden. 1991. 'Patterns of Cell Division and Interkinetic Nuclear Migration in the Chick Embryo Hindbrain.' *Journal of Neurobiology* 22 (7): 742–54. doi:10.1002/neu.480220709.

Haddon, C, L Smithers, S Schneider-Maunoury, T Coche, D Henrique, and J Lewis. 1998. 'Multiple Delta Genes and Lateral Inhibition in Zebrafish Primary Neurogenesis'. *Development* 125 (3): 359–70.

Hansen, David V, Jan H Lui, Philip R L Parker, and Arnold R Kriegstein. 2010. 'Neurogenic Radial Glia in the Outer Subventricular Zone of Human Neocortex.' *Nature* 464 (7288): 554–61.

Haubensak, Wulf, Alessio Attardo, Winfried Denk, and Wieland B Huttner. 2004. 'Neurons Arise in the Basal Neuroepithelium of the Early Mammalian Telencephalon: A Major Site of Neurogenesis.' *Proceedings of the National Academy of Sciences of the United States of America* 101 (9): 3196–3201. doi:10.1073/pnas.0308600100.

He, Ying, Xiaofeng Xu, Shufang Zhao, Shanshan Ma, Lei Sun, Zhenghua Liu, and Chen Luo. 2014. 'Maternal Control of Axial-Paraxial Mesoderm Patterning via Direct Transcriptional Repression in Zebrafish.' *Developmental Biology* 386 (1): 96–110. doi:10.1016/j.ydbio.2013.11.022.

Henrique, D, J Adam, A Myat, A Chitnis, J Lewis, and D Ish-Horowicz. 1995. 'Expression of a Delta Homologue in Prospective Neurons in the Chick.' *Nature* 375 (6534). Nature Publishing Group: 787–90. doi:10.1038/375787a0.

Hernandez, Rafael E, Aaron P Putzke, Jonathan P Myers, Lilyana Margaretha, and Cecilia B Moens. 2007. 'Cyp26 Enzymes Generate the Retinoic Acid Response Pattern Necessary for Hindbrain Development.' *Development (Cambridge, England)* 134 (1): 177–87. doi:10.1242/dev.02706.

Holzer, Tatjana, Katrin Liffers, Karolin Rahm, Benjamin Trageser, Suat Ozbek, and Dietmar Gradl. 2012. 'Live Imaging of Active Fluorophore Labelled Wnt Proteins.' *FEBS Letters* 586 (11): 1638–44. doi:10.1016/j.febslet.2012.04.035.

Hori, Kazuya, Anindya Sen, and Spyros Artavanis-Tsakonas. 2013. 'Notch Signaling at a Glance.' *Journal of Cell Science* 126 (Pt 10): 2135–40. doi:10.1242/jcs.127308.

Horne-Badovinac, S, D Lin, S Waldron, M Schwarz, G Mbamalu, T Pawson, Y Jan, D Y Stainier, and S Abdelilah-Seyfried. 2001. 'Positional Cloning of Heart and Soul Reveals Multiple Roles for PKC Lambda in Zebrafish Organogenesis.' *Current Biology : CB* 11 (19): 1492–1502.

Houart, Corinne, Luca Caneparo, Carl-Philipp Heisenberg, K.Anukampa Barth, Masaya Take-Uchi, and Stephen W. Wilson. 2002. 'Establishment of the Telencephalon during Gastrulation by Local Antagonism of Wnt Signaling'. *Neuron* 35 (2): 255–65. doi:10.1016/S0896-6273(02)00751-1.

Huang, Hai, and Thomas B Kornberg. 2015. 'Myoblast Cytonemes Mediate Wg Signaling from the Wing Imaginal Disc and Delta-Notch Signaling to the Air Sac Primordium.' *eLife* 4 (January). eLife Sciences Publications Limited: e06114. doi:10.7554/eLife.06114.

Hutchinson, Sarah A, and Judith S Eisen. 2006. 'Islet1 and Islet2 Have Equivalent Abilities to Promote Motoneuron Formation and to Specify Motoneuron Subtype Identity.' *Development (Cambridge, England)* 133 (11): 2137–47. doi:10.1242/dev.02355.

Ishibashi, M, K Moriyoshi, Y Sasai, K Shiota, S Nakanishi, and R Kageyama. 1994. 'Persistent Expression of Helix-Loop-Helix Factor HES-1 Prevents Mammalian Neural Differentiation in the Central Nervous System.' *The EMBO Journal* 13 (8): 1799–1805.

Jessell, T M. 2000. 'Neuronal Specification in the Spinal Cord: Inductive Signals and Transcriptional Codes.' *Nature Reviews. Genetics* 1 (1): 20–29. doi:10.1038/35049541.

Johnson, Jane E, and Raymond J Macdonald. 2011. 'Notch-Independent Functions of CSL.' *Current Topics in Developmental Biology* 97 (January): 55–74. doi:10.1016/B978-0-12-385975-4.00009-7.

Johnson, Matthew B, Peter P Wang, Kutay D Atabay, Elisabeth A Murphy, Ryan N Doan, Jonathan L Hecht, and Christopher A Walsh. 2015. 'Single-Cell Analysis Reveals Transcriptional Heterogeneity of Neural Progenitors in Human Cortex.' *Nature Neuroscience* 18 (5): 637–46. doi:10.1038/nn.3980.

Kang, Kyungjoon, Donghoon Lee, Seulgi Hong, Sung-Gyoo Park, and Mi-Ryoung Song. 2013. 'The E3 Ligase Mind Bomb-1 (Mib1) Modulates Delta-Notch Signaling to Control

Neurogenesis and Gliogenesis in the Developing Spinal Cord.' *The Journal of Biological Chemistry* 288 (4): 2580–92. doi:10.1074/jbc.M112.398263.

Karunaratne, Asanka, Murray Hargrave, Alisa Poh, and Toshiya Yamada. 2002. 'GATA Proteins Identify a Novel Ventral Interneuron Subclass in the Developing Chick Spinal Cord'. *Developmental Biology* 249 (1): 30–43. doi:10.1006/dbio.2002.0754.

Kawaguchi, Daichi, Takeshi Yoshimatsu, Katsuto Hozumi, and Yukiko Gotoh. 2008. 'Selection of Differentiating Cells by Different Levels of Delta-like 1 among Neural Precursor Cells in the Developing Mouse Telencephalon.' *Development (Cambridge, England)* 135 (23): 3849–58. doi:10.1242/dev.024570.

Kelava, Iva, Eric Lewitus, and Wieland B Huttner. 2013. 'The Secondary Loss of Gyrencephaly as an Example of Evolutionary Phenotypical Reversal.' *Frontiers in Neuroanatomy* 7 (January): 16. doi:10.3389/fnana.2013.00016.

Kiecker, C, and C Niehrs. 2001. 'A Morphogen Gradient of Wnt/beta-Catenin Signalling Regulates Anteroposterior Neural Patterning in Xenopus.' *Development (Cambridge, England)* 128 (21): 4189–4201.

Kiecker, Clemens, and Andrew Lumsden. 2005. 'Compartments and Their Boundaries in Vertebrate Brain Development'. *Nature Reviews Neuroscience* 6 (7): 553–64. doi:10.1038/nrn1702.

Kim, C H, T Oda, M Itoh, D Jiang, K B Artinger, S C Chandrasekharappa, W Driever, and A B Chitnis. 2000. 'Repressor Activity of Headless/Tcf3 Is Essential for Vertebrate Head Formation.' *Nature* 407 (6806): 913–16. doi:10.1038/35038097.

Kim, Cheol-Hee H, Young-Ki K Bae, Yojiro Yamanaka, Susumu Yamashita, Takashi Shimizu, Ritsuko Fujii, Hae-Chul C Park, et al. 1997. 'Overexpression of Neurogenin Induces Ectopic Expression of HuC in Zebrafish'. *Neuroscience Letters* 239 (2-3): 113–16. doi:10.1016/S0304-3940(97)00908-7.

Kim, Cheol-Hee, Emiko Ueshima, Osamu Muraoka, Hidekazu Tanaka, Sang-Yeob Yeo, Tae-Lin Huh, and Naomasa Miki. 1996. 'Zebrafish elav/HuC Homologue as a Very Early Neuronal Marker'. *Neuroscience Letters* 216 (2): 109–12. doi:10.1016/0304-3940(96)13021-4.

Kim, Ho, Jimann Shin, Suhyun Kim, Justin Poling, Hae-Chul Park, and Bruce Appel. 2008. 'Notch-Regulated Oligodendrocyte Specification from Radial Glia in the Spinal Cord of Zebrafish Embryos.' *Developmental Dynamics : An Official Publication of the American Association of Anatomists* 237 (8): 2081–89. doi:10.1002/dvdy.21620.

Kimura, Yukiko, Yasushi Okamura, and Shin-ichi Higashijima. 2006. 'Alx, a Zebrafish Homolog of Chx10, Marks Ipsilateral Descending Excitatory Interneurons That Participate in the Regulation of Spinal Locomotor Circuits.' *The Journal of Neuroscience : The Official Journal of the Society for Neuroscience* 26 (21): 5684–97. doi:10.1523/JNEUROSCI.4993-05.2006.

Kimura, Yukiko, Chie Satou, and Shin-Ichi Higashijima. 2008. 'V2a and V2b Neurons Are Generated by the Final Divisions of Pair-Producing Progenitors in the Zebrafish Spinal Cord.' *Development (Cambridge, England)* 135 (18): 3001–5. doi:10.1242/dev.024802.

Kirby, Brandon B, Norio Takada, Andrew J Latimer, Jimann Shin, Thomas J Carney, Robert N Kelsh, and Bruce Appel. 2006. 'In Vivo Time-Lapse Imaging Shows Dynamic Oligodendrocyte Progenitor Behavior during Zebrafish Development.' *Nature Neuroscience* 9 (12). Nature Publishing Group: 1506–11. doi:10.1038/nn1803.

Kondo, S., and T. Miura. 2010. 'Reaction-Diffusion Model as a Framework for Understanding Biological Pattern Formation'. *Science* 329 (5999): 1616–20. doi:10.1126/science.1179047.

Konno, Daijiro, Go Shioi, Atsunori Shitamukai, Asako Mori, Hiroshi Kiyonari, Takaki Miyata, and Fumio Matsuzaki. 2008. 'Neuroepithelial Progenitors Undergo LGN-Dependent Planar Divisions to Maintain Self-Renewability during Mammalian Neurogenesis.' *Nature Cell Biology* 10 (1). Nature Publishing Group: 93–101.

Kornberg, Thomas B, and Sougata Roy. 2014. 'Cytonemes as Specialized Signaling Filopodia.' *Development (Cambridge, England)* 141 (4): 729–36. doi:10.1242/dev.086223.

Kowalczyk, Tom, Adria Pontious, Chris Englund, Ray A M Daza, Francesco Bedogni, Rebecca Hodge, Alessio Attardo, Chris Bell, Wieland B Huttner, and Robert F Hevner. 2009. 'Intermediate Neuronal Progenitors (Basal Progenitors) Produce Pyramidal-Projection Neurons for All Layers of Cerebral Cortex.' *Cerebral Cortex (New York, N.Y. : 1991)* 19 (10): 2439–50. doi:10.1093/cercor/bhn260.

Kressmann, Sabine, Claudia Campos, Irinka Castanon, Maximilian Fürthauer, and Marcos González-Gaitán. 2015. 'Directional Notch Trafficking in Sara Endosomes during Asymmetric Cell Division in the Spinal Cord.' *Nature Cell Biology* 17 (3): 333–39. doi:10.1038/ncb3119.

Kriegstein, Arnold, Stephen Noctor, and Verónica Martínez-Cerdeño. 2006. 'Patterns of Neural Stem and Progenitor Cell Division May Underlie Evolutionary Cortical Expansion.' *Nature Reviews. Neuroscience* 7 (11): 883–90.

Kudoh, Tetsuhiro, Stephen W Wilson, and Igor B Dawid. 2002. 'Distinct Roles for Fgf, Wnt and Retinoic Acid in Posteriorizing the Neural Ectoderm.' *Development (Cambridge, England)* 129 (18): 4335–46.

Lancaster, Madeline A, Magdalena Renner, Carol-Anne Martin, Daniel Wenzel, Louise S Bicknell, Matthew E Hurles, Tessa Homfray, Josef M Penninger, Andrew P Jackson, and Juergen A Knoblich. 2013. 'Cerebral Organoids Model Human Brain Development and Microcephaly.' *Nature* 501 (7467). Nature Publishing Group, a division of Macmillan Publishers Limited. All Rights Reserved.: 373–79. doi:10.1038/nature12517.

Le Dréau, Gwenvael, and Elisa Martí. 2012. 'Dorsal-Ventral Patterning of the Neural Tube: A Tale of Three Signals.' *Developmental Neurobiology* 72 (12): 1471–81. doi:10.1002/dneu.22015.

Lee, Jeong-Soo, Arun Padmanabhan, Jimann Shin, Shizhen Zhu, Feng Guo, John P Kanki, Jonathan A Epstein, and A Thomas Look. 2010. 'Oligodendrocyte Progenitor Cell Numbers and Migration Are Regulated by the Zebrafish Orthologs of the NF1 Tumor Suppressor Gene.' *Human Molecular Genetics* 19 (23): 4643–53. doi:10.1093/hmg/ddq395.

Lee, S.-K. 2005. 'Olig2 and Ngn2 Function in Opposition to Modulate Gene Expression in Motor Neuron Progenitor Cells'. *Genes & Development* 19 (2): 282–94. doi:10.1101/gad.1257105.

Leone, Dino P, Karpagam Srinivasan, Bin Chen, Elizabeth Alcamo, and Susan K McConnell. 2008. 'The Determination of Projection Neuron Identity in the Developing Cerebral Cortex.' *Current Opinion in Neurobiology* 18 (1): 28–35. doi:10.1016/j.conb.2008.05.006.

Lewis, Katharine E, and Judith S Eisen. 2003. 'From Cells to Circuits: Development of the Zebrafish Spinal Cord.' *Progress in Neurobiology* 69 (6): 419–49.

———. 2004. 'Paraxial Mesoderm Specifies Zebrafish Primary Motoneuron Subtype Identity.' *Development (Cambridge, England)* 131 (4): 891–902. doi:10.1242/dev.00981.

Lewitus, Eric, Iva Kelava, and Wieland B Huttner. 2013. 'Conical Expansion of the Outer Subventricular Zone and the Role of Neocortical Folding in Evolution and Development.' *Frontiers in Human Neuroscience* 7 (January). Frontiers: 424. doi:10.3389/fnhum.2013.00424.

Li, Shengguo, Kamana Misra, Michael P Matise, and Mengqing Xiang. 2005. 'Foxn4 Acts Synergistically with Mash1 to Specify Subtype Identity of V2 Interneurons in the Spinal Cord.' *Proceedings of the National Academy of Sciences of the United States of America* 102 (30): 10688–93. doi:10.1073/pnas.0504799102.

Li, Shengguo, Kamana Misra, and Mengqing Xiang. 2010. 'A Cre Transgenic Line for Studying V2 Neuronal Lineages and Functions in the Spinal Cord.' *Genesis (New York, N.Y. : 2000)* 48 (11): 667–72. doi:10.1002/dvg.20669.

Litingtung, Y, and C Chiang. 2000. 'Specification of Ventral Neuron Types Is Mediated by an Antagonistic Interaction between Shh and Gli3.' *Nature Neuroscience* 3 (10): 979–85. doi:10.1038/79916.

Liu, Zijing, Xuemei Hu, Jun Cai, Ben Liu, Xiaozhong Peng, Michael Wegner, and Mengsheng Qiu. 2007. 'Induction of Oligodendrocyte Differentiation by Olig2 and Sox10: Evidence for Reciprocal Interactions and Dosage-Dependent Mechanisms'. *Developmental Biology* 302 (2): 683–93. doi:10.1016/j.ydbio.2006.10.007.

Lomax Boyd, J., Stephanie L. Skove, Jeremy P. Rouanet, Louis-Jan Pilaz, Tristan Bepler, Raluca Gordân, Gregory A. Wray, and Debra L. Silver. 2015. 'Human-Chimpanzee Differences in a FZD8 Enhancer Alter Cell-Cycle Dynamics in the Developing Neocortex'. *Current Biology* 25 (6). Elsevier: 772–79. doi:10.1016/j.cub.2015.01.041.

Louvi, Angeliki, and Spyros Artavanis-Tsakonas. 2006. 'Notch Signalling in Vertebrate Neural Development.' *Nature Reviews. Neuroscience* 7 (2): 93–102. doi:10.1038/nrn1847.

Lowery, Laura Anne, and Hazel Sive. 2004. 'Strategies of Vertebrate Neurulation and a Re-Evaluation of Teleost Neural Tube Formation'. *Mechanisms of Development* 121 (10): 1189–97. doi:10.1016/j.mod.2004.04.022.

Lui, Jan H, David V Hansen, and Arnold R Kriegstein. 2011. 'Development and Evolution of the Human Neocortex.' *Cell* 146 (1): 18–36. doi:10.1016/j.cell.2011.06.030.

Lukaszewicz, Agnès, Pierre Savatier, Véronique Cortay, Pascale Giroud, Cyril Huissoud, Michel Berland, Henry Kennedy, and Colette Dehay. 2005. 'G1 Phase Regulation, Area-Specific Cell Cycle Control, and Cytoarchitectonics in the Primate Cortex.' *Neuron* 47 (3): 353–64. doi:10.1016/j.neuron.2005.06.032.

Lumsden, A., and R. Krumlauf. 1996. 'Patterning the Vertebrate Neuraxis'. *Science* 274 (5290): 1109–15. doi:10.1126/science.274.5290.1109.

Lundfald, Line, C Ernesto Restrepo, Simon J B Butt, Chian-Yu Peng, Steven Droho, Toshiaki Endo, Hanns Ulrich Zeilhofer, Kamal Sharma, and Ole Kiehn. 2007. 'Phenotype of V2-Derived Interneurons and Their Relationship to the Axon Guidance Molecule EphA4 in the Developing Mouse Spinal Cord.' *The European Journal of Neuroscience* 26 (11): 2989–3002. doi:10.1111/j.1460-9568.2007.05906.x.

Lyons, David A, Adam T Guy, and Jonathan D W Clarke. 2003. 'Monitoring Neural Progenitor Fate through Multiple Rounds of Division in an Intact Vertebrate Brain.' *Development (Cambridge, England)* 130 (15): 3427–36.

Martínez-Cerdeño, Verónica, and Stephen C Noctor. 2016. 'Cortical Evolution 2015: Discussion of Neural Progenitor Cell Nomenclature.' *The Journal of Comparative Neurology* 524 (3): 704–9. doi:10.1002/cne.23909.

Martínez-Cerdeño, Verónica, Stephen C Noctor, and Arnold R Kriegstein. 2006. 'The Role of Intermediate Progenitor Cells in the Evolutionary Expansion of the Cerebral Cortex.' *Cerebral Cortex (New York, N.Y. : 1991)* 16 Suppl 1 (suppl_1): i152–61. doi:10.1093/cercor/bhk017.

Masahira, Noritaka, Hirohide Takebayashi, Katsuhiko Ono, Keisuke Watanabe, Lei Ding, Miki Furusho, Yasuhiro Ogawa, et al. 2006. 'Olig2-Positive Progenitors in the Embryonic Spinal Cord Give Rise Not Only to Motoneurons and Oligodendrocytes, but Also to a Subset of Astrocytes and Ependymal Cells.' *Developmental Biology* 293 (2): 358–69. doi:10.1016/j.ydbio.2006.02.029.

McLean, David L, and Joseph R Fetcho. 2009. 'Spinal Interneurons Differentiate Sequentially from Those Driving the Fastest Swimming Movements in Larval Zebrafish to Those Driving the Slowest Ones.' *The Journal of Neuroscience : The Official Journal of the Society for Neuroscience* 29 (43): 13566–77. doi:10.1523/JNEUROSCI.3277-09.2009.

Meinhardt, H, and A Gierer. 2000. 'Pattern Formation by Local Self-Activation and Lateral Inhibition.' *BioEssays : News and Reviews in Molecular, Cellular and Developmental Biology* 22 (8): 753–60. doi:10.1002/1521-1878(200008)22:8<753::AID-BIES9>3.0.CO;2-Z.

Menelaou, Evdokia, and David L McLean. 2012. ‘A Gradient in Endogenous Rhythmicity and Oscillatory Drive Matches Recruitment Order in an Axial Motor Pool.’ *The Journal of Neuroscience : The Official Journal of the Society for Neuroscience* 32 (32): 10925–39. doi:10.1523/JNEUROSCI.1809-12.2012.

Mione, Marina, Shantha Shanmugalingam, David Kimelman, and Kevin Griffin. 2001. ‘Overlapping Expression of Zebrafish T-Brain-1 and Eomesodermin during Forebrain Development’. *Mechanisms of Development* 100 (1): 93–97. doi:10.1016/S0925-4773(00)00501-3.

Miyasaka, Nobuhiko, Kozo Morimoto, Tatsuya Tsubokawa, Shin-ichi Higashijima, Hitoshi Okamoto, and Yoshihiro Yoshihara. 2009. ‘From the Olfactory Bulb to Higher Brain Centers: Genetic Visualization of Secondary Olfactory Pathways in Zebrafish.’ *The Journal of Neuroscience : The Official Journal of the Society for Neuroscience* 29 (15): 4756–67. doi:10.1523/JNEUROSCI.0118-09.2009.

Miyata, Takaki, Ayano Kawaguchi, Kanako Saito, Masako Kawano, Tetsuji Muto, and Masaharu Ogawa. 2004. ‘Asymmetric Production of Surface-Dividing and Non-Surface-Dividing Cortical Progenitor Cells.’ *Development (Cambridge, England)* 131 (13): 3133–45.

Miyata, Takaki, Daichi Kawaguchi, Ayano Kawaguchi, and Yukiko Gotoh. 2010. ‘Mechanisms That Regulate the Number of Neurons during Mouse Neocortical Development.’ *Current Opinion in Neurobiology* 20 (1): 22–28. doi:10.1016/j.conb.2010.01.001.

Mizutani, Ken-ichi, Keejung Yoon, Louis Dang, Akinori Tokunaga, and Nicholas Gaiano. 2007. ‘Differential Notch Signalling Distinguishes Neural Stem Cells from Intermediate Progenitors.’ *Nature* 449 (7160). Nature Publishing Group: 351–55. doi:10.1038/nature06090.

Molyneaux, Bradley J, Paola Arlotta, Joao R L Menezes, and Jeffrey D Macklis. 2007. ‘Neuronal Subtype Specification in the Cerebral Cortex.’ *Nature Reviews. Neuroscience* 8 (6): 427–37. doi:10.1038/nrn2151.

Morin, Xavier, Florence Jaouen, and Pascale Durbec. 2007. ‘Control of Planar Divisions by the G-Protein Regulator LGN Maintains Progenitors in the Chick Neuroepithelium.’ *Nature Neuroscience* 10 (11): 1440–48. doi:10.1038/nn1984.

Mueller, Thomas, and Mario F Wullimann. 2003. ‘Anatomy of Neurogenesis in the Early Zebrafish Brain.’ *Brain Research. Developmental Brain Research* 140 (1): 137–55.

Mueller, Thomas, Mario F Wullimann, and Su Guo. 2008. ‘Early Teleostean Basal Ganglia Development Visualized by Zebrafish Dlx2a, Lhx6, Lhx7, Tbr2 (Eomesa), and GAD67 Gene Expression.’ *The Journal of Comparative Neurology* 507 (2): 1245–57. doi:10.1002/cne.21604.

Myers, P Z. 1985. ‘Spinal Motoneurons of the Larval Zebrafish.’ *The Journal of Comparative Neurology* 236 (4): 555–61. doi:10.1002/cne.902360411.

Nelson, Branden R, Rebecca D Hodge, Francesco Bedogni, and Robert F Hevner. 2013. ‘Dynamic Interactions between Intermediate Neurogenic Progenitors and Radial Glia in

Embryonic Mouse Neocortex: Potential Role in Dll1-Notch Signaling.' *The Journal of Neuroscience : The Official Journal of the Society for Neuroscience* 33 (21): 9122–39. doi:10.1523/JNEUROSCI.0791-13.2013.

Noctor, Stephen C, Verónica Martínez-Cerdeño, Lidija Ivic, and Arnold R Kriegstein. 2004. 'Cortical Neurons Arise in Symmetric and Asymmetric Division Zones and Migrate through Specific Phases.' *Nature Neuroscience* 7 (2). Nature Publishing Group: 136–44.

Nomura, Tadashi, Chiaki Ohtaka-Maruyama, Wataru Yamashita, Yoshio Wakamatsu, Yasunori Murakami, Federico Calegari, Kunihiro Suzuki, Hitoshi Gotoh, and Katsuhiko Ono. 2016. 'The Evolution of Basal Progenitors in the Developing Non-Mammalian Brain.' *Development (Cambridge, England)* 143 (1): 66–74. doi:10.1242/dev.127100.

Nordström, Ulrika, Thomas M Jessell, and Thomas Edlund. 2002. 'Progressive Induction of Caudal Neural Character by Graded Wnt Signaling.' *Nature Neuroscience* 5 (6): 525–32. doi:10.1038/nn854.

Novitch, Bennett G, Hynek Wichterle, Thomas M Jessell, and Shanthini Sockanathan. 2003. 'A Requirement for Retinoic Acid-Mediated Transcriptional Activation in Ventral Neural Patterning and Motor Neuron Specification.' *Neuron* 40 (1): 81–95.

Ohata, Shinya, Ryo Aoki, Shigeharu Kinoshita, Masahiro Yamaguchi, Sachiko Tsuruoka-Kinoshita, Hideomi Tanaka, Hironori Wada, et al. 2011. 'Dual Roles of Notch in Regulation of Apically Restricted Mitosis and Apicobasal Polarity of Neuroepithelial Cells.' *Neuron* 69 (2): 215–30. doi:10.1016/j.neuron.2010.12.026.

Ohtsuka, T, M Sakamoto, F Guillemot, and R Kageyama. 2001. 'Roles of the Basic Helix-Loop-Helix Genes Hes1 and Hes5 in Expansion of Neural Stem Cells of the Developing Brain.' *The Journal of Biological Chemistry* 276 (32): 30467–74. doi:10.1074/jbc.M102420200.

Okigawa, Sayumi, Takamasa Mizoguchi, Makoto Okano, Haruna Tanaka, Miho Isoda, Yun-Jin Jiang, Maximiliano Suster, Shin-Ichi Higashijima, Koichi Kawakami, and Motoyuki Itoh. 2014. 'Different Combinations of Notch Ligands and Receptors Regulate V2 Interneuron Progenitor Proliferation and V2a/V2b Cell Fate Determination.' *Developmental Biology* 391 (2): 196–206. doi:10.1016/j.ydbio.2014.04.011.

Oppenheimer, Jane M. 1936. 'Transplantation Experiments on Developing Teleosts (Fundulus and Perca)'. *Journal of Experimental Zoology* 72 (3): 409–37. doi:10.1002/jez.1400720304.

Panayi, H., E. Panayiotou, M. Orford, N. Genethliou, R. Mean, G. Lapathitis, S. Li, et al. 2010. 'Sox1 Is Required for the Specification of a Novel p2-Derived Interneuron Subtype in the Mouse Ventral Spinal Cord'. *Journal of Neuroscience* 30 (37): 12274–80. doi:10.1523/JNEUROSCI.2402-10.2010.

Papan, Cyrus, and Jos$\diamondsuit$ A. Campos-Ortega. 1994. 'On the Formation of the Neural Keel and Neural Tube in the zebrafishDanio (Brachydanio) Rerio'. *Roux's Archives of Developmental Biology* 203 (4): 178–86. doi:10.1007/BF00636333.

Paridaen, Judith T M L, and Wieland B Huttner. 2014. 'Neurogenesis during Development of the Vertebrate Central Nervous System.' *EMBO Reports* 15 (4). EMBO Press: 351–64. doi:10.1002/embr.201438447.

Park, Hae-Chul, Amit Mehta, Joanna S. Richardson, and Bruce Appel. 2002. 'olig2 Is Required for Zebrafish Primary Motor Neuron and Oligodendrocyte Development'. *Developmental Biology* 248 (2): 356–68. doi:10.1006/dbio.2002.0738.

Park, Hae-Chul, Jimann Shin, and Bruce Appel. 2004. 'Spatial and Temporal Regulation of Ventral Spinal Cord Precursor Specification by Hedgehog Signaling.' *Development (Cambridge, England)* 131 (23): 5959–69. doi:10.1242/dev.01456.

Park, Hae-Chul, Jimann Shin, Randolph K Roberts, and Bruce Appel. 2007. 'An olig2 Reporter Gene Marks Oligodendrocyte Precursors in the Postembryonic Spinal Cord of Zebrafish.' *Developmental Dynamics : An Official Publication of the American Association of Anatomists* 236 (12): 3402–7. doi:10.1002/dvdy.21365.

Passini, M A, A L Kurtzman, A K Canger, W S Asch, G A Wray, P A Raymond, and N Schechter. 1998. 'Cloning of Zebrafish vsx1: Expression of a Paired-like Homeobox Gene during CNS Development.' *Developmental Genetics* 23 (2): 128–41. doi:10.1002/(SICI)1520-6408(1998)23:2<128::AID-DVG5>3.0.CO;2-8.

Peng, Chian-Yu, Hiroshi Yajima, Caroline Erter Burns, Leonard I. Zon, Sangram S. Sisodia, Samuel L. Pfaff, and Kamal Sharma. 2007. 'Notch and MAML Signaling Drives Scl-Dependent Interneuron Diversity in the Spinal Cord'. *Neuron* 53 (6): 813–27. doi:10.1016/j.neuron.2007.02.019.

Per, Brodal. 2010. *The Central Nervous System*. 4th ed. Oxford University Press, USA.

Persson, Madelen, Despina Stamataki, Pascal te Welscher, Elisabet Andersson, Jens Böse, Ulrich Rüther, Johan Ericson, and James Briscoe. 2002. 'Dorsal-Ventral Patterning of the Spinal Cord Requires Gli3 Transcriptional Repressor Activity.' *Genes & Development* 16 (22): 2865–78. doi:10.1101/gad.243402.

Piccolo, Stefano, Eric Agius, Luc Leyns, Subha Bhattacharyya, Horst Grunz, Tewis Bouwmeester, and E. M. De Robertis. 1999. 'The Head Inducer Cerberus Is a Multifunctional Antagonist of Nodal, BMP and Wnt Signals' 397 (6721): 707–10. doi:10.1038/17820.

Pierfelice, Tarran, Lavinia Alberi, and Nicholas Gaiano. 2011. 'Notch in the Vertebrate Nervous System: An Old Dog with New Tricks.' *Neuron* 69 (5): 840–55. doi:10.1016/j.neuron.2011.02.031.

Pilz, Gregor-Alexander, Atsunori Shitamukai, Isabel Reillo, Emilie Pacary, Julia Schwausch, Ronny Stahl, Jovica Ninkovic, et al. 2013. 'Amplification of Progenitors in the Mammalian Telencephalon Includes a New Radial Glial Cell Type.' *Nature Communications* 4 (January): 2125. doi:10.1038/ncomms3125.

Pinto, Luisa, Michael T Mader, Martin Irmler, Marco Gentilini, Federico Santoni, Daniela

Drechsel, Robert Blum, et al. 2008. ‘Prospective Isolation of Functionally Distinct Radial Glial Subtypes--Lineage and Transcriptome Analysis.’ *Molecular and Cellular Neurosciences* 38 (1): 15–42. doi:10.1016/j.mcn.2008.01.012.

Poluch, Sylvie, and Sharon L Juliano. 2007. ‘A Normal Radial Glial Scaffold Is Necessary for Migration of Interneurons during Neocortical Development.’ *Glia* 55 (8): 822–30. doi:10.1002/glia.20488.

Price, David, Andrew Jarman, John Mason, and Peter Kind. 2011. *Building Brains*. Chichester, UK: John Wiley & Sons, Ltd. doi:10.1002/9780470979624.

Qiu, Xuehui, Chiaw-Hwee Lim, Steven Hao-Kee Ho, Kian-Hong Lee, and Yun-Jin Jiang. 2009. ‘Temporal Notch Activation through Notch1a and Notch3 Is Required for Maintaining Zebrafish Rhombomere Boundaries.’ *Development Genes and Evolution* 219 (7): 339–51. doi:10.1007/s00427-009-0296-6.

Qiu, Xuehui, Haoying Xu, Catherine Haddon, Julian Lewis, and Yun-Jin Jiang. 2004. ‘Sequence and Embryonic Expression of Three Zebrafish Fringe Genes: Lunatic Fringe, Radical Fringe, and Manic Fringe.’ *Developmental Dynamics : An Official Publication of the American Association of Anatomists* 231 (3): 621–30. doi:10.1002/dvdy.20155.

Rakic, Pasko. 1995. ‘A Small Step for the Cell, a Giant Leap for Mankind: A Hypothesis of Neocortical Expansion during Evolution’. *Trends in Neurosciences* 18 (9): 383–88. doi:10.1016/0166-2236(95)93934-P.

———. 2008. ‘Confusing Cortical Columns.’ *Proceedings of the National Academy of Sciences of the United States of America* 105 (34): 12099–100. doi:10.1073/pnas.0807271105.

———. 2009. ‘Evolution of the Neocortex: A Perspective from Developmental Biology.’ *Nature Reviews. Neuroscience* 10 (10). Nature Publishing Group: 724–35. doi:10.1038/nrn2719.

Ramírez-Weber, F A, and T B Kornberg. 1999. ‘Cytonemes: Cellular Processes That Project to the Principal Signaling Center in Drosophila Imaginal Discs.’ *Cell* 97 (5): 599–607.

Reillo, Isabel, and Víctor Borrell. 2012. ‘Germinal Zones in the Developing Cerebral Cortex of Ferret: Ontogeny, Cell Cycle Kinetics, and Diversity of Progenitors.’ *Cerebral Cortex (New York, N.Y. : 1991)* 22 (9): 2039–54. doi:10.1093/cercor/bhr284.

Reillo, Isabel, Camino de Juan Romero, Miguel Ángel García-Cabezas, and Víctor Borrell. 2011. ‘A Role for Intermediate Radial Glia in the Tangential Expansion of the Mammalian Cerebral Cortex.’ *Cerebral Cortex (New York, N.Y. : 1991)* 21 (7): 1674–94. doi:10.1093/cercor/bhq238.

Renaud, O, and P Simpson. 2001. ‘Scabrous Modifies Epithelial Cell Adhesion and Extends the Range of Lateral Signalling during Development of the Spaced Bristle Pattern in Drosophila.’ *Developmental Biology* 240 (2): 361–76. doi:10.1006/dbio.2001.0482.

Ribes, Vanessa, and James Briscoe. 2009. ‘Establishing and Interpreting Graded Sonic

Hedgehog Signaling during Vertebrate Neural Tube Patterning: The Role of Negative Feedback.' *Cold Spring Harbor Perspectives in Biology* 1 (2): a002014. doi:10.1101/cshperspect.a002014.

Roberts, A, N Dale, O P Ottersen, and J Storm-Mathisen. 1987. 'The Early Development of Neurons with GABA Immunoreactivity in the CNS of Xenopus Laevis Embryos.' *The Journal of Comparative Neurology* 261 (3): 435–49. doi:10.1002/cne.902610308.

———. 1988. 'Development and Characterization of Commissural Interneurones in the Spinal Cord of Xenopus Laevis Embryos Revealed by Antibodies to Glycine.' *Development (Cambridge, England)* 103 (3): 447–61.

Roberts, Randolph K, and Bruce Appel. 2009. 'Apical Polarity Protein PrkCi Is Necessary for Maintenance of Spinal Cord Precursors in Zebrafish.' *Developmental Dynamics : An Official Publication of the American Association of Anatomists* 238 (7): 1638–48. doi:10.1002/dvdy.21970.

Roy, Sougata, Hai Huang, Songmei Liu, and Thomas B Kornberg. 2014. 'Cytoneme-Mediated Contact-Dependent Transport of the Drosophila Decapentaplegic Signaling Protein.' *Science (New York, N.Y.)* 343 (6173): 1244624. doi:10.1126/science.1244624.

Sabherwal, Nitin, Akiko Tsutsui, Sarah Hodge, Jun Wei, Andrew D Chalmers, and Nancy Papalopulu. 2009. 'The Apicobasal Polarity Kinase aPKC Functions as a Nuclear Determinant and Regulates Cell Proliferation and Fate during Xenopus Primary Neurogenesis.' *Development (Cambridge, England)* 136 (16): 2767–77. doi:10.1242/dev.034454.

Sahara, Setsuko, and Dennis D M O'Leary. 2009. 'Fgf10 Regulates Transition Period of Cortical Stem Cell Differentiation to Radial Glia Controlling Generation of Neurons and Basal Progenitors.' *Neuron* 63 (1): 48–62.

Sakamoto, Masami, Hiromi Hirata, Toshiyuki Ohtsuka, Yasumasa Bessho, and Ryoichiro Kageyama. 2003. 'The Basic Helix-Loop-Helix Genes Hesr1/Hey1 and Hesr2/Hey2 Regulate Maintenance of Neural Precursor Cells in the Brain.' *The Journal of Biological Chemistry* 278 (45): 44808–15. doi:10.1074/jbc.M300448200.

Salta, Evgenia, Pierre Lau, Carlo Sala Frigerio, Marion Coolen, Laure Bally-Cuif, and Bart De Strooper. 2014. 'A Self-Organizing miR-132/Ctbp2 Circuit Regulates Bimodal Notch Signals and Glial Progenitor Fate Choice during Spinal Cord Maturation.' *Developmental Cell*, August. doi:10.1016/j.devcel.2014.07.006.

Sanders, Timothy A, Esther Llagostera, and Maria Barna. 2013. 'Specialized Filopodia Direct Long-Range Transport of SHH during Vertebrate Tissue Patterning.' *Nature* 497 (7451). Nature Publishing Group, a division of Macmillan Publishers Limited. All Rights Reserved.: 628–32. doi:10.1038/nature12157.

Sato-Maeda, Mika, Masuo Obinata, and Wataru Shoji. 2008. 'Position Fine-Tuning of Caudal Primary Motoneurons in the Zebrafish Spinal Cord.' *Development (Cambridge, England)* 135

(2): 323–32. doi:10.1242/dev.007559.

Sato-Maeda, Mika, Hiroshi Tawarayama, Masuo Obinata, John Y Kuwada, and Wataru Shoji. 2006. 'Sema3a1 Guides Spinal Motor Axons in a Cell- and Stage-Specific Manner in Zebrafish.' *Development (Cambridge, England)* 133 (5): 937–47. doi:10.1242/dev.02268.

Saúde, L, K Woolley, P Martin, W Driever, and D L Stemple. 2000. 'Axis-Inducing Activities and Cell Fates of the Zebrafish Organizer.' *Development (Cambridge, England)* 127 (16): 3407–17.

Schmidt, Rebecca, Uwe Strähle, and Steffen Scholpp. 2013. 'Neurogenesis in Zebrafish - from Embryo to Adult.' *Neural Development* 8 (1): 3. doi:10.1186/1749-8104-8-3.

Schwanbeck, Ralf. 2015. 'The Role of Epigenetic Mechanisms in Notch Signaling during Development.' *Journal of Cellular Physiology* 230 (5): 969–81. doi:10.1002/jcp.24851.

Sessa, Alessandro, Chai-An Mao, Anna-Katerina Hadjantonakis, William H Klein, and Vania Broccoli. 2008. 'Tbr2 Directs Conversion of Radial Glia into Basal Precursors and Guides Neuronal Amplification by Indirect Neurogenesis in the Developing Neocortex.' *Neuron* 60 (1): 56–69.

Shen, Qin, Yue Wang, John T Dimos, Christopher A Fasano, Timothy N Phoenix, Ihor R Lemischka, Natalia B Ivanova, Stefano Stifani, Edward E Morrisey, and Sally Temple. 2006. 'The Timing of Cortical Neurogenesis Is Encoded within Lineages of Individual Progenitor Cells.' *Nature Neuroscience* 9 (6). Nature Publishing Group: 743–51. doi:10.1038/nn1694.

Shih, J, and S E Fraser. 1996. 'Characterizing the Zebrafish Organizer: Microsurgical Analysis at the Early-Shield Stage.' *Development (Cambridge, England)* 122 (4): 1313–22.

Shin, Jimann, Hae-Chul Park, Jolanta M Topczewska, David J Mawdsley, and Bruce Appel. 2003. 'Neural Cell Fate Analysis in Zebrafish Using olig2 BAC Transgenics.' *Methods in Cell Science : An Official Journal of the Society for In Vitro Biology* 25 (1-2): 7–14. doi:10.1023/B:MICS.0000006847.09037.3a.

Smart, I H. 1972a. 'Proliferative Characteristics of the Ependymal Layer during the Early Development of the Spinal Cord in the Mouse.' *Journal of Anatomy* 111 (Pt 3): 365–80.

———. 1972b. 'Proliferative Characteristics of the Ependymal Layer during the Early Development of the Mouse Diencephalon, as Revealed by Recording the Number, Location, and Plane of Cleavage of Mitotic Figures.' *Journal of Anatomy* 113 (Pt 1): 109–29.

———. 1973. 'Proliferative Characteristics of the Ependymal Layer during the Early Development of the Mouse Neocortex: A Pilot Study Based on Recording the Number, Location and Plane of Cleavage of Mitotic Figures.' *Journal of Anatomy* 116 (Pt 1): 67–91.

Smart, I. H.M. 2002. 'Unique Morphological Features of the Proliferative Zones and Postmitotic Compartments of the Neural Epithelium Giving Rise to Striate and Extrastriate Cortex in the Monkey'. *Cerebral Cortex* 12 (1): 37–53.

Soroldoni, D, DJ Jörg, and LG Morelli. 2014. 'A Doppler Effect in Embryonic Pattern

Formation'. *Science*.

Spear, Philip C, and Carol A Erickson. 2012. 'Interkinetic Nuclear Migration: A Mysterious Process in Search of a Function.' *Development, Growth & Differentiation* 54 (3): 306–16. doi:10.1111/j.1440-169X.2012.01342.x.

Sprinzak, David, Amit Lakhanpal, Lauren LeBon, Jordi Garcia-Ojalvo, and Michael B Elowitz. 2011. 'Mutual Inactivation of Notch Receptors and Ligands Facilitates Developmental Patterning.' *PLoS Computational Biology* 7 (6). Public Library of Science: e1002069. doi:10.1371/journal.pcbi.1002069.

Sprinzak, David, Amit Lakhanpal, Lauren Lebon, Leah A Santat, Michelle E Fontes, Graham A Anderson, Jordi Garcia-Ojalvo, and Michael B Elowitz. 2010. 'Cis-Interactions between Notch and Delta Generate Mutually Exclusive Signalling States.' *Nature* 465 (7294). Macmillan Publishers Limited. All rights reserved: 86–90. doi:10.1038/nature08959.

Stahl, Ronny, Tessa Walcher, Camino De Juan Romero, Gregor Alexander Pilz, Silvia Cappello, Martin Irmler, José Miguel Sanz-Aquela, et al. 2013. 'Trnp1 Regulates Expansion and Folding of the Mammalian Cerebral Cortex by Control of Radial Glial Fate'. *Cell* 153 (3): 535–49. doi:10.1016/j.cell.2013.03.027.

Stancik, Elizabeth K, Ivan Navarro-Quiroga, Robert Sellke, and Tarik F Haydar. 2010. 'Heterogeneity in Ventricular Zone Neural Precursors Contributes to Neuronal Fate Diversity in the Postnatal Neocortex.' *The Journal of Neuroscience : The Official Journal of the Society for Neuroscience* 30 (20): 7028–36. doi:10.1523/JNEUROSCI.6131-09.2010.

Stenzel, D., M. Wilsch-Brauninger, F. K. Wong, H. Heuer, and W. B. Huttner. 2014. 'Integrin v3 and Thyroid Hormones Promote Expansion of Progenitors in Embryonic Neocortex'. *Development* 141 (4): 795–806. doi:10.1242/dev.101907.

Stephan, H, H Frahm, and G Baron. 1981. 'New and Revised Data on Volumes of Brain Structures in Insectivores and Primates.' *Folia Primatologica; International Journal of Primatology* 35 (1): 1–29.

Stern, C. D. 2005. 'Neural Induction: Old Problem, New Findings, yet More Questions'. *Development* 132 (9): 2007–21. doi:10.1242/dev.01794.

Streit, Andrea, and Claudio D Stern. 1999. 'Neural Induction: A Bird's Eye View'. *Trends in Genetics* 15 (1): 20–24. doi:10.1016/S0168-9525(98)01620-5.

Tarabykin, Victor, Anastassia Stoykova, Natalia Usman, and Peter Gruss. 2001. 'Cortical Upper Layer Neurons Derive from the Subventricular Zone as Indicated by Svet1 Gene Expression'. *Development* 128 (11): 1983–93.

Taverna, Elena, and Wieland B Huttner. 2010. 'Neural Progenitor Nuclei IN Motion.' *Neuron* 67 (6): 906–14.

Tawk, Marcel, Claudio Araya, Dave A Lyons, Alexander M Reugels, Gemma C Girdler, Philippa R Bayley, David R Hyde, Masazumi Tada, and Jonathan D W Clarke. 2007. 'A

Mirror-Symmetric Cell Division That Orchestrates Neuroepithelial Morphogenesis.' *Nature* 446 (7137): 797–800. doi:10.1038/nature05722.

Terriente, Javier, Sebastian S Gerety, Tomomi Watanabe-Asaka, Rosa Gonzalez-Quevedo, and David G Wilkinson. 2012. 'Signalling from Hindbrain Boundaries Regulates Neuronal Clustering That Patterns Neurogenesis.' *Development (Cambridge, England)* 139 (16): 2978–87. doi:10.1242/dev.080135.

Thisse, B, V Heyer, A Lux, A Alunni, A Degrave, I Seiliez, J Kirchner, J-P Parkhill, and C Thisse. 2005. 'High Throughput Expression Analysis of ZF-Models Consortium Clones'. *Meth. Cell. Biol*. https://zfin.org/cgi-bin/webdriver?MIval=aa-pubview2.apg&OID=ZDB-PUB-051025-1.

Thisse, B, and C Thisse. 2004. 'No TitleFast Release Clones: A High Throughput Expression Analysis.' *ZFIN Direct Data Submission (Http://zfin.org)*.

Thisse, B., S. Pflumio, M. Fürthauer, B. Loppin, V. Heyer, A. Degrave, R. Woehl, et al. 2001. 'Expression of the Zebrafish Genome during Embryogenesis'. *ZFIN Direct Data Submission, (Http://zfin.org)*.

Tiberi, Luca, Pierre Vanderhaeghen, and Jelle van den Ameele. 2012. 'Cortical Neurogenesis and Morphogens: Diversity of Cues, Sources and Functions.' *Current Opinion in Cell Biology* 24 (2): 269–76. doi:10.1016/j.ceb.2012.01.010.

Trevarrow, B, D L Marks, and C B Kimmel. 1990. 'Organization of Hindbrain Segments in the Zebrafish Embryo.' *Neuron* 4 (5): 669–79.

Turing, A M. 1952. 'The Chemical Basis of Morphogenesis'. *Philosophical Transactions of the Royal Society of London* 237 (641): 37–72.

Tyler, William A, and Tarik F Haydar. 2013. 'Multiplex Genetic Fate Mapping Reveals a Novel Route of Neocortical Neurogenesis, Which Is Altered in the Ts65Dn Mouse Model of Down Syndrome.' *The Journal of Neuroscience : The Official Journal of the Society for Neuroscience* 33 (12): 5106–19. doi:10.1523/JNEUROSCI.5380-12.2013.

van Eeden, F J, M Granato, U Schach, M Brand, M Furutani-Seiki, P Haffter, M Hammerschmidt, et al. 1996. 'Mutations Affecting Somite Formation and Patterning in the Zebrafish, Danio Rerio.' *Development (Cambridge, England)* 123 (December): 153–64.

Vasistha, Navneet A, Fernando García-Moreno, Siddharth Arora, Amanda F P Cheung, Sebastian J Arnold, Elizabeth J Robertson, and Zoltán Molnár. 2015. 'Cortical and Clonal Contribution of Tbr2 Expressing Progenitors in the Developing Mouse Brain.' *Cerebral Cortex (New York, N.Y. : 1991)* 25 (10): 3290–3302. doi:10.1093/cercor/bhu125.

Vilas-Boas, Filipe, Rita Fior, Jason R Swedlow, Kate G Storey, and Domingos Henrique. 2011. 'A Novel Reporter of Notch Signalling Indicates Regulated and Random Notch Activation during Vertebrate Neurogenesis.' *BMC Biology* 9 (1): 58.

Wang, Lynn, Krista K Bluske, Lauren K Dickel, and Yasushi Nakagawa. 2011. 'Basal

Progenitor Cells in the Embryonic Mouse Thalamus - Their Molecular Characterization and the Role of Neurogenins and Pax6.' *Neural Development* 6 (1): 35. doi:10.1186/1749-8104-6-35.

Wang, Xiaoqun, Jin-Wu Tsai, Bridget LaMonica, and Arnold R Kriegstein. 2011. 'A New Subtype of Progenitor Cell in the Mouse Embryonic Neocortex.' *Nature Neuroscience* 14 (5). Nature Publishing Group, a division of Macmillan Publishers Limited. All Rights Reserved.: 555–61. doi:10.1038/nn.2807.

Weber, Isabell P., Ana P. Ramos, Paulina J. Strzyz, Louis C. Leung, Stephen Young, and Caren Norden. 2014. 'Mitotic Position and Morphology of Committed Precursor Cells in the Zebrafish Retina Adapt to Architectural Changes upon Tissue Maturation'. *Cell Reports* 7 (2): 386–97. doi:10.1016/j.celrep.2014.03.014.

Wettstein, D A, D L Turner, and C Kintner. 1997. 'The Xenopus Homolog of Drosophila Suppressor of Hairless Mediates Notch Signaling during Primary Neurogenesis.' *Development (Cambridge, England)* 124 (3): 693–702.

Wilson, Leigh, and Malcolm Maden. 2005. 'The Mechanisms of Dorsoventral Patterning in the Vertebrate Neural Tube'. *Developmental Biology* 282 (1): 1–13. doi:10.1016/j.ydbio.2005.02.027.

Wodarz, Andreas. 2002. 'Establishing Cell Polarity in Development.' *Nature Cell Biology* 4 (2). Nature Publishing Group: E39–44. doi:10.1038/ncb0202-e39.

Wodarz, Andreas, and Wieland B. Huttner. 2003. 'Asymmetric Cell Division during Neurogenesis in Drosophila and Vertebrates'. *Mechanisms of Development* 120 (11): 1297–1309. doi:10.1016/j.mod.2003.06.003.

Zannino, D. A., and B. Appel. 2009. 'Olig2+ Precursors Produce Abducens Motor Neurons and Oligodendrocytes in the Zebrafish Hindbrain'. *Journal of Neuroscience* 29 (8): 2322–33. doi:10.1523/JNEUROSCI.3755-08.2009.

Zhou, Qiao, Songli Wang, and David J Anderson. 2000. 'Identification of a Novel Family of Oligodendrocyte Lineage-Specific Basic Helix–Loop–Helix Transcription Factors'. *Neuron* 25 (2): 331–43. doi:10.1016/S0896-6273(00)80898-3.